FISCHER-TROPSCH SYNTHESIS: TOWARDS UNDERSTANDING

XIAOJUN LU

PH.D. Thesis

2011

FISCHER-TROPSCH SYNTHESIS: TOWARDS UNDERSTANDING

By

Xiaojun Lu

A thesis submitted to the Faculty of Engineering and Built Environment, University of the Witwatersrand, Johannesburg, in fulfilment of the requirements for the degree of Doctor of Philosophy.

Johannesburg 2011

DECLARATION

I declare that this thesis is my own, unaided work under the supervision of Professor Diane Hildebrandt and Professor David Glasser. It is being submitted for the Degree of Doctor of Philosophy to the University of the Witwatersrand, Johannesburg. It has not been submitted before for any degree or examination in any other University.

_____

Signature of candidate

Signed this_____day of _____year_____

ABSTRACT

A series of experiments in different types of reactors were performed with TiO_2 supported cobalt catalyst to gain a better understanding of the phenomena related to Fischer-Tropsch Synthesis (FTS) reaction. The performance of FTS was investigated during unsteady state and steady state. The experiments were conducted firstly to investigate the effect of external mass transfer on the performance of FTS, and the results suggested that it has effects only in short term but not long term. During the beginning period of the experiment conducted in the CSTR, two steady stages in terms of reaction rate and product selectivity could be observed and large changes were found in-between them. In order to reveal the precise reason(s) for causing these observed phenomena, flushing experiments were designed after the reactor system reached the secondary steady stage by means of changing the feed from synthesis gas to inert gas, argon. By comparing the results in the reactions before and after flushing, we can conclude that those observed large changes were mainly caused by the deposit of liquid phase products on the catalyst. The information of the materials in the stream out of reactor during flushing was also collected. The dynamic concentration of C_1-C_8 in the flushed out gas suggested that reaction among the light products might take place under a moderate FT reaction condition. To present another way to look at the reaction behaviour of FTS, a number of experiments were conducted in a batch reactor with different reaction durations. An unusual behaviour of the product distribution when compared to the typical ASF model was observed. The pressure in the reactor during the reaction was monitored, and the comparison of the pressure readings of the reactor system at different reaction durations with the pressure derived from the mass balance suggested that a considerable proportion of the water produced was in the liquid phase under reaction conditions. The study of FTS under steady state was carried out in a tubular fixed bed reactor. The olefin

to paraffin ratios for different carbon numbers and the relationship of C_2 and C_3 both in olefins and total amount under various reaction conditions were mainly investigated. A detailed explanation was presented to describe the behaviour of olefin to paraffin ratios with the change of the space velocity. The relationships of C_3H_6/C_2H_4 and C_3/C_2 were also summarised respectively. On the analysis of the experimental data both from CSTR and PFR, we found that the ratios of neighbouring light olefins kept constant although there were large alterations on the ratio of olefin to paraffin. Based on the implication from flushing experiments that light hydrocarbons may react with each other, an equilibrium was proposed for the olefin product distribution of FTS.

ACKNOWLEDGEMENTS

First and foremost I would like to sincerely thank my supervisors, Professor Diane Hildebrandt and Professor David Glasser for their guidance, inspiration and sound advice throughout the period of my study. It has been a privilege for me to study under their supervision.

I am very grateful to the staff and post grad students at COMPS, past and present, for providing a stimulating and fun environment in which to learn and grow. Especially, thanks to Dr. Brendon Hausberger, Dr. Xingyin Liu, and Dr. Kalala Jalama for their kind advice and discussions.

I extremely thank to Mr. Basil Chassoulas and the staff of physics work shop to help me for technical support in the laboratory

I also really appreciate Pippa Lange's assistance with my English.

Most importantly I wish to thank all my family, particularly my mum, dad and my son, without their support this work would not have been possible. Special thanks to my wife, whenever I met any problems, she always stands my side to use her knowledge and endless love to help, support and courage me.

Finally, I would like to thank the National Research Foundation (NRF), the University of the Witwatersrand, the school of chemical and metallurgical, the centre of Materials and Process Synthesis, and Golden Nest for financial support and facilities

LIST OF PUBLICATIONS AND PRESENTATIONS

Publications:

1. Lu, X.; Hildebrandt, D.; Liu, X.; Glasser, D. Making Sense of the Fischer-Tropsch Synthesis Reaction: Start-up. *Industrial & Engineering Chemistry Research* **2010**, *49*, 9753–9758.
2. Zhu, X.; Lu, X.; Liu, X.; Hildebrandt, D.; Glasser, D. Study of Radial Heat Transfer in a Tubular Fischer-Tropsch Synthesis Reactor. *Industrial & Engineering Chemistry Research* **2010**, 49, 10682–10688.
3. Lu, X.; Zhu, X.; Hildebrandt, D.; Liu, X.; Glasser, D. A new way to look at FTS using flushing experiments. *Industrial & Engineering Chemistry Research* **2011**, 50, 4359–4365.

Conference Presentations:

1. Lu, X.; Hildebrandt, D.; Glasser, D. External Mass Transfer in F-T Reactions? World Congress of Chemical Engineering, 2009.
2. Lu, X.; Hildebrandt, D.; Glasser, D. A Thermodynamic Approach for the Olefin Products Distribution in Fischer-Tropsch Synthesis. AIChE 2010 Spring Meeting.
3. Lu, X.; Hildebrandt, D.; Liu, X.; Glasser, D. Fischer-Tropsch Synthesis: an investigation of the phase of the water in the low temperature synthesis reactor. SACI 2011.
4. Lu, X.; Hildebrandt, D.; Liu, X.; Glasser, D. A Study of Fischer-Tropsch Synthesis in a Batch Reactor with a TiO_2 Supported Cobalt Catalyst. AIChE 2011 Spring Meeting.

CONTENTS

DECLARATION I

ABSTRACT II

ACKNOWLEDGEMENTS IV

LIST OF PUBLICATION AND PRESENTATIONS V

LIST OF FIGURES XI

LIST OF TABLES XVIII

ABBREVIATIONS AND ACRONYMS XIX

CHAPTER 1 1

INTRODUCTION 1

1.1 Overall Introduction 1

1.2 Aims of Thesis 2

1.3 Thesis Overview 2

1.4 Reference 5

CHAPTER 2 7

LITERATURE REVIEW 7

2.1 History of the Fischer-Tropsch Synthesis 7

2.2 Chemistry of FTS 9

2.3 Reaction Mechanism 10

2.4 Fischer-Tropsch Catalysts 14

2.4.1 Catalysts 14

2.4.2 Active Sites and Catalyst Reduction 15

2.5 Kinetics 16

2.6 Product Selectivity 19

2.6.1 One parameter, ideal distribution model

(Anderson-Schulz-Flory distribution) 19
2.6.2 Deviations from ideal distributions 21
2.7 FTS reaction system and the reactors 23
2.8 Syngas production and product upgrading 27
2.8.1 Synthesis Gas Production 27
2.8.2 Product Upgrading and Separation 28
2.9 Applications (the characteristics of commercial FT processes) 29
2.10 References 31

CHAPTER 3 44
EXPERIMENTAL 44
3.1 Introduction 44
3.2 Experimental Set-up and Reactors 45
3.2.1 Experimental Set-up 45
3.2.2 Reactors 47
3.3 Catalyst 55
3.3.1 Catalyst Preparation 55
3.3.2 Catalyst Characterization 56
3.4 Product Analysis 58
3.5 Mass balance calculation 62
3.6 Reference 67

CHAPTER 4 68
MAKING SENSE OF THE FISCHER-TROPSCH SYNTHESIS: START-UP IN A CSTR ... 68
4.1 Introduction 69
4.2 Experimental 70
4.3 Results and Discussion 74
4.3.1 Short term FT runs 74

4.3.2 Long term FT runs 78
4.3.3 Time on Stream Runs at Constant SS 80
4.4 Conclusion 90
4.5 References 91

CHAPTER 5 93
A NEW WAY TO LOOK AT FISCHER-TROPSCH USING FLUSHING EXPERIMENTS . 93
5.1 Introduction 95
5.2 Experimental 98
5.2.1 FTS Experiments 98
5.2.2 Reactor system flushing experiments 99
5.2.3 FTS experiments after the flushing 100
5.3 Results and Discussion 101
5.3.1 FTS Behaviour after Flushing 101
5.3.2 Reactants and Products in the Flushed-Out Gas during Flushing 106
5.5 Conclusion 121
5.6 Reference 123

Chapter 6 126
A STUDY OF FISCHER-TROPSCH SYNTHESIS IN A BATCH REACTOR ON A TIO_2 SUPPORTED COBALT CATALYST 126
6.1 Introduction 128
6.2 Experimental Section 130
6.3 Results and Discussion 133
6.3.1 Conversion and Reaction Rate 133
6.3.2 Product Selectivity and Distribution 137
6. 3.3 The Phase of the Product Water 144

6.4 Conclusion 146

6.5 References 148

CHAPTER 7 151

BEHAVIOUR OF LOWER HYDROCARBONS IN FISCHER-TROPSCH SYNTHESIS ... 151

7.1 Introduction 153

7.2 Experimental 155

7.3 Results and Discussion 157

7.3.1 Reactant conversions and reaction rates 157

7.3.2 Methane selectivity 160

7.3.3 Olefin to paraffin ratios for light hydrocarbons 162

7.3.4 Chain growth probability α 166

7.3.5 The distribution of C_2 and C_3 168

7.4 Conclusion 181

7.5 Reference 183

CHAPTER 8 185

A THERMODYNAMIC APPROACH TO OLEFIN PRODUCT DISTRIBUTION IN FISCHER-TROPSCH SYNTHESIS 185

8.1 Introduction 186

8.2 Experimental 189

8.2.1 Fischer-Tropsch experiments in a CSTR 189

8.2.2 Fischer-Tropsch experiments in a PFR 190

8.3 Results and Discussion 190

8.3.1 Olefin to paraffin ratio 190

8.3.2 Normalized molar fraction for C_nH_{2n}, C_nH_{2n+2}, and $C_{n+1}H_{2(n+1)}$ 194

8.3.3 Olefin equilibrium for C_3 and above 200

8.3.4 Olefin equilibrium when C_2 is included 203

8.4 Conclusion 206

8.5 References 207

CHAPTER 9 210

CONCLUSIVE REMARKS 210

Appendix A 214

LIST OF FIGURES

Fig. 1-1 The scheme of a Fischer-Tropsch process 1

Fig. 2-1 Schematic of chain growth, readsorption, and secondary reactions of olefins in FTS 14

Fig. 2-2 Hydrocarbon selectivity as function of the chain growth probability factor α 20

Fig. 3-1 The experiment set-up with a continuous stirred basket reactor 46

Fig. 3-2 The experimental set-up with a tubular fixed bed reactor 47

Fig. 3-3 The layout of the continuously stirred tank reactor 48

Fig. 3-4 The layout of the stirrer 49

Fig. 3-5 The structure of the catalyst basket 49

Fig. 3-6 RTD curve when stirring speed is 65rpm 52

Fig. 3-7 RTD curve when stirring speed is 0 52

Fig. 3-8 The tubular fixed bed reactor used in the experiments 53

Fig. 3-9 Central temperature profile of the reactor for the part for the catalyst bed 55

Fig. 3-10 TRP result for the prepared catalyst 57

Fig. 3-11 Scheme of the liquid and gaseous streams for analysis 58

Fig. 3-12 An online GC trace for hydrocarbons in tail gas 61

Fig. 3-13 A GC trace for analysis of oil from cool trap 61

Fig. 3-14 A GC trace for analysis of wax from hot trap 62

Fig. 4-1 $\ln(C_{Hydrogen})$-Time curve in RDT test for CSTR when SS = 65rpm 72

Fig. 4-2 The experiment set-up with a continuous stirred basket reactor 72

Fig. 4-3 CO conversion at fixed SS (100rpm) and varied SS (100-1500-0rpm) (T = 190 ^{o}C, P = 20 bar (g), FR = 0.6Nlh^{-1}(gcat)$^{-1}$; numbers above data

points are the corresponding SS applied) 75

Fig. 4-4 CH_4 selectivity at fixed SS (100rpm) and varied SS (100-1500-0rpm) (T = 190 ^oC, P = 20 bar (g), FR = 0.6$Nlh^{-1}(gcat)^{-1}$; numbers above data points are the corresponding SS applied) 75

Fig. 4-5 Olefin/paraffin ratios with TOS when SS fixed (100rpm) (T = 190 ^oC, P = 20 bar (g), FR = 0.6$Nlh^{-1}(gcat)^{-1}$; numbers above data points are the corresponding SS applied) 77

Fig. 4-6 Olefin/paraffin ratios with TOS when SS varied SS (100-1500-0rpm) (T = 190 ^oC, P = 20 bar (g), FR = 0.6$Nlh^{-1}(gcat)^{-1}$; numbers above data points are the corresponding SS applied) 77

Fig. 4-7 CO conversion and CH_4 selectivity at different SSs during the entire TOS (T = 190^oC, P = 20 bar (g), FR = 1.2$NLh^{-1}(gcat)^{-1}$; numbers above data points are the corresponding SS applied) 79

Fig. 4-8 Olefin/paraffin ratios at different SS during the entire TOS (T = 190 ^oC, P = 20 bar (g), FR = 1.2$NLh^{-1}(gcat)^{-1}$; numbers above data points are the corresponding SS applied) 80

Fig. 4-9 CO conversion, CH_4 selectivity and O/P ratio at 190^oC with respect to TOS while SS remained constant (P = 20 bar (g), FR = 1.2$NLh^{-1}(gcat)^{-1}$ SS=100rpm) 82

Fig. 4-10 CO conversion, CH_4 selectivity and O/P ratio at 210 ^oC with respect to TOS while SS remained constant (P = 20 bar (g), FR = 1.2$NLh^{-1}(gcat)^{-1}$ SS=100rpm) 83

Fig. 4-11 The O/P ratio (C_3 and C_4) at different temperatures 84

Fig. 4-12 C_2-C_5 selectivity at 210 ^oC in respect of TOS while SS remained constant (P = 20 bar (g), FR = 1.2$NLh^{-1}(gcat)^{-1}$ SS=100rpm) 85

Fig. 4-13 C_2-C_5 paraffins selectivity at 210^oC with respect to TOS while SS remained constant (P = 20 bar (g), FR = 1.2$NLh^{-1}(gcat)^{-1}$ SS=100rpm) 86

Fig. 4-14 C_1, C_2-C_5, and C_6+ selectivity at 210 ^oC with respect to TOS while

SS remained constant (P = 20 bar (g), FR = 1.2NLh^{-1}(gcat)$^{-1}$ SS=100rpm) 87

Fig. 5-1 CO conversion, CH_4 selectivity at 210 ^{o}C during the entire TOS when stirring speed (SS) remained constant (P = 20 bar (g), FR = 1.2Nlh^{-1}(gcat)$^{-1}$ SS=100rpm) 96

Fig. 5-2 O/P ratio at 210 ^{o}C during the entire TOS when SS remained constant (P = 20 bar (g), FR = 1.2Nlh^{-1}(gcat)$^{-1}$ SS=100rpm) 96

Fig. 5-3 Demonstration of the switch between the FTS and flushing experiments 101

Fig. 5-4 The CO conversion during FT reactions (the same reaction conditions) before and after flushing with different flushing temperatures 102

Fig. 5-5 Methane selectivity during reactions (the same reaction conditions) before and after flushing with different flushing temperatures 102

Fig. 5-6 O/P ratios for C_2–C_4 during reactions (the same reaction conditions) before and after flushing with different flushing temperatures 103

Fig. 5-7 Molar fraction of reactants in the flushed-out stream during the flushing period 109

Fig. 5-8 The molar percentage of CH_4 in the flushed-out gas during the entire flushing period at two flushing temperatures..... 114

Fig. 5-9 The molar percentage of C_2–C_4 alkenes in the flushed-out gas during the entire flushing period with $T_{Flushing}$ = 210 ^{o}C 115

Fig. 5-10 The molar percentage of C_2–C_4 alkanes in the flushed-out gas during the entire flushing period with $T_{Flushing}$ = 210 ^{o}C 115

Fig. 5-11 The molar percentage of C_4–C_8 alkanes in the flushed-out gas in the entire flushing period with $T_{Flushing}$ = 210 ^{o}C 119

Fig. 5-12 The molar percentage of C_4–C_8 alkanes in the flushed-out gas during the entire flushing period with $T_{Flushing}$ = 230 ^{o}C 119

Fig. 5-13 Total flushed-out amounts of C_1–C_8 hydrocarbons 120

Fig. 6-1 CO conversion for various reaction durations..... 133

Fig. 6-2 H_2 conversion for various reaction durations 134

Fig. 6-3 The reaction rates in the CSTR and batch operation modes as a function of CO conversion and TOS (Time on Stream)..... 135

Fig. 6-4 Partial pressures of the reactants in the reactor for different reaction durations 136

Fig. 6-5 Logarithmic plot of H_2 concentration as a function of the reaction duration..... 137

Fig. 6-6 Logarithmic plot of CO concentration as a function of the reaction duration..... 137

Fig. 6-7 CH_4 selectivity at different reaction durations 138

Fig. 6-8 The olefin/paraffin ratios starting at CSTR mode and with different subsequent durations of batch operation mode..... 140

Fig. 6-9 The FT product distribution in the batch reactor..... 142

Fig. 6-10 The FT product distribution in the CSTR 142

Fig. 6-11 The FT product distribution in the batch reactor for different reaction durations 143

Fig. 6-12 The pressures in the reactor at different reaction times 145

Fig. 7-1 The reaction rates with different space velocities and H_2/CO ratios when the temperature was at 210^{o}C and P at 20 bar(g)..... 159

Fig. 7-2 The reaction rates with different space velocities and H_2/CO ratios when the temperature was at 230^{o}C and P at 20 bar(g)..... 160

Fig. 7-3 The Olefin/Paraffin ratios for C_2–C_5 at their corresponding CO conversions when H_2/CO=3:1 (The change of CO conversion at each reaction temperature was caused by the variation of FR from 1.8 to 7.2 NL/h/gcat)..... 163

Fig. 7-4 The Olefin/Paraffin ratios for C_2–C_5 at their corresponding CO conversions when H_2/CO=2:1(The change of CO conversion at each reaction temperature was caused by the variation of FR from 1.8 to 7.2 NL/h/gcat) 163

Fig. 7-5 The Olefin/Paraffin ratios for C_2–C_5 at their corresponding CO conversions when H_2/CO=1:1(The change of CO conversion at each reaction temperature was caused by the variation of FR from 1.8 to 7.2 NL/h/gcat) 164

Fig. 7-6 Product distribution in a full mass balance run 167

Fig. 7-7 C_4H_8/C_3H_6 as a function of CO conversion (PFR: H_2/CO = 2:1 T = 190-230 ^oC, FR=1.8-7.2 NL/(h-gcat); CSTR: H_2/CO = 2:1 T = 210 ^oC, FR=1.2 NL/(h-gcat)) 170

Fig. 7-8 C_5H_{10}/C_4H_8 as a function of CO conversion (PFR: H_2/CO = 2:1 T = 190-230 ^oC, FR=1.8-7.2 NL/(h-gcat); CSTR: H_2/CO = 2:1 T = 210 ^oC, FR=1.2 NL/(h-gcat)) 171

Fig. 7-9 The C_3H_6/C_2H_4 ratio versus CO conversion with H_2/CO=1:1 in the feed 172

Fig. 7-10 The C_3H_6/C_2H_4 ratio versus CO conversion with H_2/CO=2:1 in the feed 172

Fig. 7-11 The C_3H_6/C_2H_4 ratio versus CO conversion with H_2/CO=3:1 in the feed 173

Fig. 7-12 The C_3H_6/C_2H_4 ratio versus CO conversion in a CSTR run (H_2/CO=2:1, T=190 ^oC) 174

Fig. 7-13 The C_3H_6/C_2H_4 ratio versus CO conversion in a CSTR run (H_2/CO=2:1, T=210 ^oC) 175

Fig. 7-14 The C_3H_6/C_2H_4 ratio versus CO conversion in a Batch run (H_2/CO=2:1, T=210 ^oC) 175

Fig. 7-15 The C_3H_6/C_2H_4 ratio as a function of CO conversion in all the

experimental runs including PFR, CSTR, and BR..... 176

Fig. 7-16 The chain growth probabilities (α values) at various reaction conditions in respect of the CO conversion (T= 210, 230, and 250 ^{o}C; P = 20 bar; H_2/CO = 2:1) 178

Fig. 7-17 The relative molar amount for C_3/C_2 versus CO conversion at different reaction temperatures (when H_2/CO=1:1 in the feed)..... 179

Fig. 7-18 The relative molar amount for C_3/C_2 versus CO conversion at different reaction temperatures (when H_2/CO=2:1 in the feed)..... 179

Fig. 7-19 The relative molar amount for C_3/C_2 versus CO conversion at different reaction temperatures (when H_2/CO=3:1 in the feed)..... 180

Fig. 7-20 The C_3/C_2 ratio at various H_2/CO ratios and operation temperatures (the equation for the fit lines follows the same sequence as the data groups from top to the bottom) 181

Fig. 8-1 Olefin/Paraffin ratios for C_2–C_5 at various TOS in a CSTR when all the conditions were fixed (P=20bar, T=210^{o}C, FR=1.2NL/h/gcat, SS=100rpm) 191

Fig. 8-2 Olefin/Paraffin ratios versus carbon monoxide conversion for C_2–C_5 at various conditions in a PFR (P=20bar, T=210-250^{o}C, FR=1.8-5.4NL/h/gcat H_2/CO=2)..... 192

Fig. 8-3 Olefin to paraffin ratios for C_2–C_4 during reaction before and after flushing with different flushing temperatures..... 194

Fig. 8-4 Demonstration of triangular plot for normalized molar fractions of C_nH_{2n}, C_nH_{2n+2}, and $C_{n+1}H_{2(n+1)}$ 195

Fig. 8-5 The normalized mole fraction for C_3H_6, C_3H_8, and C_4H_8 from the experimental results in the CSTR..... 195

Fig. 8-6 The normalized mole fraction for C_4H_8, C_4H_{10}, and C_5H_{10} from the experimental results in the CSTR..... 197

Fig. 8-7 The normalized mole fraction for C_3H_6, C_3H_8, and C_4H_8 from the

experimental results in the PFR 197

Fig. 8-8 The normalized mole fraction for C_4H_8, C_4H_{10}, and C_5H_{10} from the experimental results in the PFR 198

Fig. 8-9 The normalized mole fraction for C_3H_6, C_3H_8, and C_4H_8 from the experimental results of the CSTR during reaction before and after flushing with different flushing temperatures..... 199

Fig. 8-10 The normalized mole fraction for C_3H_6, C_4H_8, and C_5H_{10} from the experimental results of the CSTR 202

Fig. 8-11 The normalized mole fraction for C_2H_4, C_2H_6, and C_3H_6 from the experimental results in the CSTR..... 203

Fig. 8-12 The normalized mole fraction for C_2H_4, C_2H_6, and C_3H_6 from the experimental results in the PFR 204

LIST OF TABLES

Table 2-1 Major reactions of Fischer-Tropsch Synthesis 10

Table 2-2 Proposed mechanism of the hydrocarbon synthesis from CO and H_2 12

Table 2-3 Representative reaction rate equations for CO consumption in FTS on Co and Fe catalysts 18

Table 2-4 Major reaction during coal gasification 27

Table 2-5 Major reactions during reforming of natural gas 27

Table 2-6 The characteristics of commercial FT processes 30

Table 3-1 The specification of the tubular fixed bed reactor used in the experiments 53

Table 3-2 Properties of the catalyst 57

Table 3-3 Parameters of online GC 60

Table 3-4 Response factors for hydrocarbons (C_2 as reference) 63

Table 7-1 The CO conversion under different operation conditions with three feed gas compositions 158

Table 7-2 The CH_4 selectivity under different operation conditions with three feed gas compositions 161

Table 7-3 The chain growth probability under various operation conditions when the H_2/CO=1:1 in the feed 168

Table 8-1 Thermodynamic equilibrium constants when n=3,4,5 201

Table 8-2 Thermodynamic equilibrium constants when n=3,4,5 205

ABBREVIATIONS AND ACRONYMS

AES	Auger electron spectroscopy
AFROX	African Oxygen
ASF	Anderson-Schulz-Flory
BET	Brunauer-Emmett-Teller
BR	Batch reactor
CFB	Circulated Fluidized Bed reactor
C	Concentration
Co	Cobalt
CO_2	Carbon dioxide
CO	Carbon monoxide
Hr	Enthalpy of reaction [kJ/mol]
CSTR	Continuously stirred tank reactor
CTL	Coal to liquid
Cp	Heat capacity [J/mol/k]
Cu	Copper
ER	Eley-Rideal
Fe	Iron
FBR	Fixed bed reactor
FFB	Fixed Fluidized Bed
FID	Flame ionization detector
FR	Flow rate[$NLh^{-1}(gcat)^{-1}$]
FT	Fischer-Tropsch
FTS	Fischer-Tropsch Synthesis
GC	Gas chromatograph
GTL	Gas to liquid
H	Height

H_2	Hydrogen
HRTEM	High Resolution Transmission Electron Microscopy
ID	Internal diameter
LHHW	Langmuir-Hinshelwood-Hougen-Watson
k	Reaction rate constant
LTFT	Low-temperature Fischer Tropsch
LPG	Light petroleum gas(C_1-C_4 hydrocarbons)
n	Carbon number
N	Molar amount [mol]
Ni	Nickel
N_2	Nitrogen
NMF	Normalized molar fraction
OD	Out diameter
O/O	Olefin to olefin ratio (the neighbouring)
O/P	Olefin to paraffin ratio (the same carbon number)
P	Pressure (bar)
PFR	Plug flow reactor
PG	Pressure gage
PSV	Pressure safety valve
rpm	Round per minute
RTD	Residence time distribution
Ru	Ruthenium
SA	Surface area [m^2/g]
SAM	Steam methane reforming
SBCR	Slurry bubble column reactor
sel	Selectivity [%]
SMDS	Shell Middle Distillate Synthesis
SSs	Stirring speeds [rpm]
SV	Space velocity [$NLh^{-1}(gcat)^{-1}$]

T	Temperature [^{o}C]
TCD	Thermal conductivity detector
TFBR	Tubular fixed bed reactor
TPR	Temperature programmed reduction
TOS	Time on stream
UHP	Ultra high purity
V_r	Volume of the reactor [ml]
VLE	Vapour liquid equilibrium
WGS	Water-gas-shift
XRD	X-ray Diffraction

Greek Letters

τ	Residence time
η_{pore}	Pore effectiveness factor
α	Chain growth probability

CHAPTER 1

INTRODUCTION

1.1 Overall Introduction

Fischer-Tropsch Synthesis (FTS) is a catalyzed chemical reaction in which synthesis gas (syngas), a mixture of carbon monoxide (CO) and hydrogen (H_2), is converted into gaseous, liquid and solid hydrocarbons [1-12] and an appreciable amount of oxygenates [13-18].This process is highly-promising, developing option for environmentally-sound production of chemicals and fuels from biomass, coal and natural gas. In view of large coal and natural gas reserves, dwindling petroleum reserves, and significant, projected increases in demand for liquid fuels, it is expected to play an ever increasing role in coming decades. FTS can be based on several synthesis gas feedstocks including those from coal gasification, natural gas, and biomass. Currently, a promising topic in the energy industry is the conversion of remote-located, underutilized or flared natural gas to premium, sulphur-free diesel fuels, specialty chemicals and waxes.

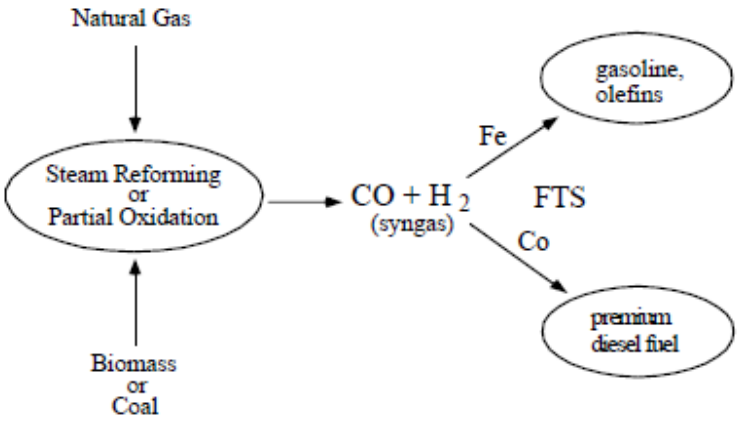

Fig. 1-1 The scheme of a Fischer-Tropsch process

1.2 Aims of Thesis

Despite many years of extensive study on FTS, there remains deeper insights to the fundamental reaction behaviours of FTS such as what are the main reasons for causing the large changes in the reaction performance in the early stage, why FTS has a very unique product distribution, what is the role of the products (hydrocarbons and water) in the performance of the FTS, and et al. The aim of this thesis is to try to understand the phenomena related to Fischer-Tropsch found in the experiments. The FTS reaction was performed in different type of reactors and operation modes to collect comprehensive experimental results. The results for the reaction rate and product selectivity from different experimental designs were mainly investigated and synthesised, so that the fundamental behaviours of the FTS could be suggested.

1.3 Thesis Overview

The Chapters in the thesis have been written in the style of journal articles. Each of the Chapters has been published, submitted for publication, or prepared for submission in a reputable international journal, except chapters 2 and 3 (Literature Review and Experimental). The current status of the each paper is given at the beginning of each chapter. As the chapters were written independently of each other, repetition of the basics and some experimental results occur from one chapter to the other. However, this does allow each chapter to be read independently, with each having its own abstract, introduction, approaching and conclusion. The outline of this thesis is given as following:

Chapter 2

In this chapter we give a review of the published literature related to Fischer-Tropsch Synthesis. The review covers major aspects of FTS including the reaction mechanism, kinetics, catalysts, and reactors.

Chapter 3

In this chapter we describe all the experimental techniques and procedures that were used to carry out the experiments on which the thesis is based. We also explain the methodology used to analyse and calculate the experimental data.

Chapter 4

The study in this chapter was started with the investigation of the effect of external mass transfer on reaction rate and product selectivity of FTS on a TiO_2 supported Cobalt catalyst. Short term and long term FT experiments were carried out in a continuous stirring tank reactor (CSTR). The results suggest that the external mass transfer only have effects on short term but not long term. Time on stream experiments were then designed and performed and large changes were observed on the reaction rate and product selectivity. Two possible explanations for this behaviour were proposed and more experiment was suggested to reveal the exact reason.

Chapter 5

Based upon the experimental phenomena found in Chapter 4, the flushing treatment experiments were designed in Chapter 5 to reveal the possible explanation(s). The FT reaction was resumed after each flushing treatment to the reactor system. Conclusively, the large changes observed in chapter 4 were proven to be caused by the liquid deposit. The information for the reactants and

C_1-C_8 products collected during flushing offered more insight for understanding the FTS. Additionally, a model was developed to describe the change of the reaction rate with the increase of the liquid layer on the catalyst.

Chapter 6

In this Chapter, the FT reaction was carried out in batch operation mode using the same reactor in Chapters 4 and 5. The FT reaction behaviour under even distribution of the reactants was investigated in a wide partial pressure of the reactants. The phase of the product water under reacting conditions is suggested by means of comparing the pressure reading of the reactor and the calculated system pressure at different reaction extent.

Chapter 7

In this chapter, quite a number of FTS experimental runs were conducted in a tubular fixed bed reactor on the same TiO_2 supported cobalt catalyst. How the reaction behaves with different H_2/CO ratio in the feed is investigated. The olefin to paraffin ratio is presented with different gas ratios. The distribution for C_2 and C_3 in terms of the both olefins and paraffins are mainly discussed and summarized based on the experimental results derived in Chapters 4 to 7.

Chapter 8

Based on the experimental result derived from the CSTR and PFR and the analysis of data, the olefin product distribution for FTS is approached from the thermodynamic point of view. A thermodynamic equilibrium model is proposed for the olefin products, the results derived from the model is compared to the experimental results.

1.4 Reference

1. Anderson, R. B. *The Fischer-Tropsch Synthesis.* Academic Press: Orlando, 1984.
2. Bromfield, T. *The effect of low-level sulfide addition on the performance of precipitated-iron Fischer-Tropsch catalysts*, PhD Thesis, University of the Witwatersrand, Johannesburg, 1997.
3. Bond, G. C. *Catalysis by Metals*. Academic Press: London, 1962.
4. Guczi, L. *Stud. Surf. Sci. Catal. 64 Series: New Trends in CO Activation*, Elsevier: Amsterdam, 1991.
5. Storch, H. H.; Golumbic, N.; Anderson, R. B. *The Fischer-Tropsch and related syntheses: including a summary of theoretical and applied contact catalysis,* John Wiley: New York, 1951.
6. Davis, B. H. Final Report, *Technology development for iron Fischer-Tropsch catalysis*, Contract No. DE-AC22-94PC94055-13. 1999.
7. Dry, M. E. Practical and Theoretical Aspects of the Catalytic Fischer-Tropsch Process. *Appl. Catal. A: Gen.* **1996**, *138*, 319-344.
8. Price, J. G. *An investigation into novel bimetallic catalysts for use in the Fischer-Tropsch reaction*, PhD Thesis, University of the Witwatersrand, Johannesburg, 1994.
9. Dry, M. E. *The Fischer-Tropsch Synthesis, in Catalysis Science and Technology*, Anderson, J. R.; Boudart, M.; Eds. Springer-Verlag: New York, 1981.
10. Iglesia, E. Fischer-Tropsch Synthesis on Cobalt Catalysts: Structural Requirements and Reaction Pathways. *Stud. Surf. Sci. Catal.* **1997**, *107*, 153.
11. Dry, M. E. Present and Future Applications of the Fischer–Tropsch Process. *Appl. Catal. A: Gen.* **2004**, *276*, 1.
12. Dry, M. E. The Fischer-Tropsch Process: 1950-2000. *Catal. Today* **2002**, *71*, 227.
13. Blyholder, G.; Shihabi, D.; Wyatt, W. V.; Bartlett, R. Adsorption and Interaction of C_2H_4, H_2, CO, and Organic Acids on Fe, Co, and Ni. *J. Catal.* **1976**, *43*, 122.

14. Henrici-Olivé, G.; Olivé, S. Hydroformylation and Fischer—Tropsch Reaction — Analogies and Discrepancies. *J. Mol. Catal.* **1977/78**, *3*, 443.
15. Kummer, J. T.; Emmett, P. H. Fischer—Tropsch Synthesis Mechanism Studies. The Addition of Radioactive Alcohols to the Synthesis Gas. *J. Am. Chem. Soc.* **1953**, *75*, 5177.
16. Kummer, J. T.; Podgurski, H. H.; Spencer, W. B.; Emmett, P. H. Mechanism Studies of the Fischer—Tropsch Synthesis. The Addition of Radioactive Alcohol. *J. Am. Chem. Soc.*, **1951**, *73*, 564.
17. Overett, M. J.; Hill, R.; Moss, J. Organometallic Chemistry and Surface Science: Mechanistic Models for the Fischer-Tropsch Synthesis. *Coordination Chemistry Reviews* **2000**, *206-207*, 581-605.

CHAPTER 2

LITERATURE REVIEW

This chapter introduces the important Fischer-Tropsch process in the following aspects: the history of the Fischer-Tropsch synthesis, the chemistry of Fischer-Tropsch, reaction mechanism, catalysts, kinetics, product selectivity, reaction systems and reactors, FT process, and commercial applications.

2.1 History of the Fischer-Tropsch Synthesis

The Fischer-Tropsch Synthesis (FTS) is essentially a polymerization reaction in which carbon bonds are formed from carbon atoms derived from carbon monoxide, under the influence of hydrogen in the presence of a metal catalyst. The reaction leads to a range of products which depend on the reaction conditions and catalysts employed. [1] The history of this important synthesis process can be traced back to the beginning of 20^{th} century. It has been more than 100 years since Sabatier and Senderens hydrogenated CO to methane over a nickel catalyst (1902). [2] In 1913 and 1914 Badische Anilin and Soda Fabrik (BASF) were awarded patents for the production of hydrocarbons and mainly oxygenated derivatives (Synthol) from syngas using alkali promoted osmium and cobalt catalysts at high pressure. [3 a-c] It has been more than 80 years since Franz Fischer and Hans Tropsch synthesized hydrocarbons from syngas on Co catalysts (1923). [4] In the 1920's Fischer and Tropsch [4] reported the formation of a product similar to the synthol product over alkalized iron shavings at 100 atm and 400 ^{o}C. They also synthesized small amounts of ethane and higher hydrocarbons at atmospheric pressure and at 370 ^{o}C over Fe_3O_4-ZnO catalysts. [5, 6] Because of the rapid

deactivation exhibited by iron-based catalysts, further studies focused on the use of cobalt and nickel catalysts. Fischer and Meyer developed Ni-ThO_2-Kieselguhr and Co-ThO_2-Kieselguhr catalysts in the early 1930's. [7] Due to limited supply of cobalt, initial studies used nickel catalyst but the high yields of methane over the latter catalyst shifted the attention to cobalt. It has been more than 70 years since the first commercial plant began operation in Germany (1936). The application of FTS at an industrial level started in Germany and by 1938 nine plants with a combined production capacity of about 660 x 10^3 tons per year were in operation using cobalt catalysts at medium pressures. [7] From 1937 research focused on use of iron as FTS catalyst and Fischer and Pichler found improved product yields and longer catalyst lifetime when using alkalized iron catalysts at medium pressures (5-30 atm). [1] The use of ruthenium based catalysts was also reported in 1938 by Pichler who observed the formation of high boiling waxes over these catalysts. [8] Even though the nine FT plants in Germany ceased to operate after World War II, the fear of an impending shortage of petroleum kept the interest in the FT process alive. It has been more than 50 years since continuous commercial operations commenced in South Africa (1955). Based on the world-wide prediction of increasing crude oil prices, the South Africa Coal Oil and Gas Cooperation (SASOL) commissioned an FT plant based on coal in Sasolburg in South Africa. Research on FTS has continued ever since at SASOL. [9] Due to the oil crises of the mid 1970s, Sasol constructed two, much larger, coal-based FT plants which came on-line in 1980 and 1982 respectively. The combined capacity of the three Sasol plants was about 6 x 10^6 tons per year.

After 1950's, except for the commercial operations in South Africa, the FTS, as an alternative route to produce fuels, became attractive anytime when the price of the crude oil increased significantly, and conversely lost it appeal when its profits became unattractive. Although the projects for commercialization of the FTS process came and went, the research on this continued and boomed especially in

the countries which had massive reserves of coal. With the discovery of stranded natural gas reserves, the interest of converting natural gas to liquid fuel by applying FTS became strong in late 1980's. The birth of modern-day GTL industry began in 1993 with the commissioning of two new plants, the first by Shell of a 10,000 bbl/day wax-cracking plant in Bintulu, Malaysia [10] using a Co catalyst and the second by PetroSA of a 25,000 bbl/day natural gas to gasoline plant (Mossgas) in Mossel Bay, South Africa using an Fe catalyst. The Mossgas plant in South Africa and the Shell plant at Bantuli, Malaysia, came on stream in 1992 and 1993, respectively. [11] In the last few years the interest for FTS has significantly grown due to the increase in oil prices as well as the high demand for energy. Recent commercial ventures include the development of a GTL plant, Oryx GTL, in a joint venture of Sasol with Qatar Petroleum at Ras Laffan in Qatar. Sasol is also developing a GTL plant at Escravos in Nigeria. With demand for energy expected to grow 5 % a year to 2020 (according to the Carbon Sequestration Leadership Forum: www.cslforum.org/china.htm), China has been looking at exploiting its abundant coal reserves to meet its energy requirements. Pre-feasibility studies focusing on exploring the potential of developing two Coal-To-Liquid (CTL) plants, using Sasol's low temperature Fischer-Tropsch technology, each with a capacity of about 80000 barrels per day were concluded in November 2005. Three demonstration plants (two has a capacity of 160,000 t/a and one has a capacity of 180,000 t/a) are currently being commissioning and operated.

2.2 Chemistry of FTS

The Fischer-Tropsch product spectrum consists of a complex multicomponent mixture of linear and branched hydrocarbons and oxygenated products. Main products are linear paraffins and α-olefins. The hydrocarbon synthesis is catalyzed by metals such as nickel, cobalt, iron, and ruthenium. Both iron and cobalt are

used commercially these days at a temperature of 200 to 350 °C (cobalt catalyst is normally used under a temperature of 240 °C) and at 10 to 60 bar pressure. [12, 13] The chemistry of FTS process can be described by the following set of reactions, summarized in Table 2.1: [7, 14]

Table 2-1 Major reactions of Fischer-Tropsch Synthesis

1. Paraffins	$(2n+1)H_2 + nCO \rightarrow C_nH_{2n+2} + nH_2O$	(2.1)
2. Olefins	$2nH_2 + nCO \rightarrow C_nH_{2n} + nH_2O$	(2.2)
3. Water gas shift reaction	$CO + H_2O \rightarrow CO_2 + H_2$	(2.3)
4. Alcohols	$2nH_2 + nCO \rightarrow C_nH_{2n+2}O + (n-1)H_2O$	(2.4)
5. Boudouard reaction	$2CO \rightarrow C + CO_2$	(2.5)

Generally, four types of catalysts are used to catalyze the FT reaction and they are Ni, Co, Fe, and Ru. They each have different abilities to favour certain reactions listed in Table 2-1, although the reaction conditions also have a strong effect on them. Ni catalyst are highly selective to methane compared to Co, Fe, and Ru catalysts; under typical conditions (e.g. 180-270 ^{o}C, H_2/CO=1-2) the last three types catalysts promote paraffins and olefins reactions. The selectivity of olefins of these catalysts is of the sequence: Ru>Fe>Co>Ni. Fe gives the highest alcohols selectivity among them. Of these four metals, only Fe catalyzes the WGS under typical reaction conditions, thereby enabling operation at a lower H_2/CO ratio.

2.3 Reaction Mechanism

Mechanisms of FTS on Co, Fe, and Ru catalysts have been the topic of numerous studies (reported in > 1000 papers [14]) and reviews. [7, 15-29] In a broad sense, for the formation of the products, the FTS is a polymerization reaction with the following steps: [22] 1, reactant adsorption; 2, chain initiation; 3, chain growth; 4, chain termination; 5, product desorption; 6, readsorption and further reaction.

Quite a number of mechanistic schemes have been developed for the FTS over the past 80 years; these can be grouped into three principle types, which vary in their approach to explain activation of CO, formation of monomer species, and addition of monomers to growing chains, i.e. [14]

First, the carbene mechanism entailing CO adsorption and dissociation to adsorbed C and O atoms, hydrogenation of C atoms to CH_x species, and insertion of CH_x monomers into the metal-carbon bond of an adsorbed alkyl chain. A similar mechanism, entailing reaction of CO with the metal to form a bulk carbide followed by hydrogenation if the carbide to hydrocarbons, was first proposed by Fischer and Tropsch in 1926. [30]

Secondly, the hydroxy-carbene mechanism involving partial hydrogenation of adsorbed CO to an adsorbed hydroxycarbene (enol) –CHOH species; condensation of two –CHOH species with elimination of water to form an adsorbed –COH-CH_3 species, and hydrogenation to an alkene and water.

The third mechanism is the carbonyl insertion mechanism which proceeds via the insertion of adsorbed CO into the metal-alkyl bond as proposed by Pichler and Schulz (1970).

The carbene mechanism is supported by the vast majority of studies [28, 31-36] while evidence for production of hydrocarbons via the second and third mechanisms is weak, although these latter two mechanisms are likely routes to alcohols and aldehydes. But, for the carbene mechanism, it is still uncertain if the monomer formation proceeds via hydrogenation of dissociated or undissociated CO.

A sequence of elementary steps consistent with the carbene mechanism [14, 17, 37-40] is shown in Table 2-2. This mechanism involves: (1) the adsorption and

dissociation of CO (Eq. 2.6 and 2.7) and dissociative adsorption of H_2 (Eq. 2.8) all in a quasi-equilibrium; (2) surface reaction of O atoms and H to form water and of O atoms and CO to form CO_2 (Eq. 2.9 and 2.10); (3) reaction of adsorbed carbon and hydrogen atoms to form adsorbed CHx species (Eq. 2.11 to 2.13); (4) the hydrogenation of adsorbed methyl radicals to form methane (Eq. 2.14); (5) chain growth through the addition of methylene groups to methyl, ethyl, and n-alkyl radicals (Eq. 2.15 and 2.16); and (6) the termination of an alkyl radical to form an alkene (reversible) or irreversible hydrogenation to form an alkane (Eq. 2.17 and 2.18). It does not include mechanistic steps for the water gas shift reaction or formation of polycarbon species (e.g. amorphous or graphitic carbons).

Table 2-2 Proposed mechanism of the hydrocarbon synthesis from CO and H_2

$CO + s \rightarrow COs$	2.6
$COs + s \rightarrow Cs + Os$	2.7
$H_2 + 2s \rightarrow 2Hs$	2.8
$Os + 2Hs \rightarrow H_2O + 3s$	2.9
$Os + COs \rightarrow CO_2 + 2s$	2.10
$Cs + Hs \rightarrow CHs + s$	2.11
$CHs + Hs \rightarrow CH_2s + s$	2.12
$CH_2s + Hs \rightarrow CH_3s + s$	2.13
$CH_3s + Hs \rightarrow CH_4s + s$	2.14
$CH_3s + CH_2s \rightarrow CH_3CH_2s + s$	2.15
$CH_3(CH_2)_{n-1}CH_2s + CH_2s \rightarrow CH_3(CH_2)_nCH_2s + s$	2.16
$CH_3(CH_2)_nCH_2s \rightarrow CH_3(CH_2)_{n-1}HC = CH_2 + Hs$	2.17
$CH_3(CH_2)_nCH_2s + Hs \rightarrow CH_3(CH_2)_nCH_3 + 2s$	2.18

Secondary reactions occur when primary products desorb from a site and interact with another catalytic site before leaving the reactor. Novak et al. [41, 42] listed possible secondary reactions of α-olefins: (i) hydrogenation to give n-paraffins, (ii) isomerization, (iii) cracking and hydrogenolysis, (iv) insertion into growing chains, mostly effective for C_2H_4 and C_3H_6, and (v) readsorption and initiation of hydrocarbon chains. Schulz et al. [43, 44] showed a possible reaction mechanism for the readsorption of olefins followed by hydrogenation to paraffins or isomerization to internal olefins via double bond shift reactions. Secondary reactions can influence the type and molecular weight of the hydrocarbon products as will be proved later.

Possible chain growth pathways, olefin readsorption, and secondary olefin reactions consistent with the carbene mechanism are illustrated in Figure 2-1 [37]. chain growth occurs by addition to adsorbed alkyl groups of surface methylene (CH_2,ad) species (rate constant, k_p); alkyl species can undergo β-hydrogen abstraction to form linear α-olefins (k_o) or hydrogen addition (k_h) to form n-paraffins with desorb. Readsorption of olefins (k_f) may lead to the reinitiation of the adsorbed alkyl chain to produce large hydrocarbons or to secondary reactions, including olefin hydrogenation (k_s), hydrogenolysis or cracking (k_c), or CO insertion to form an alcohol (k_a).

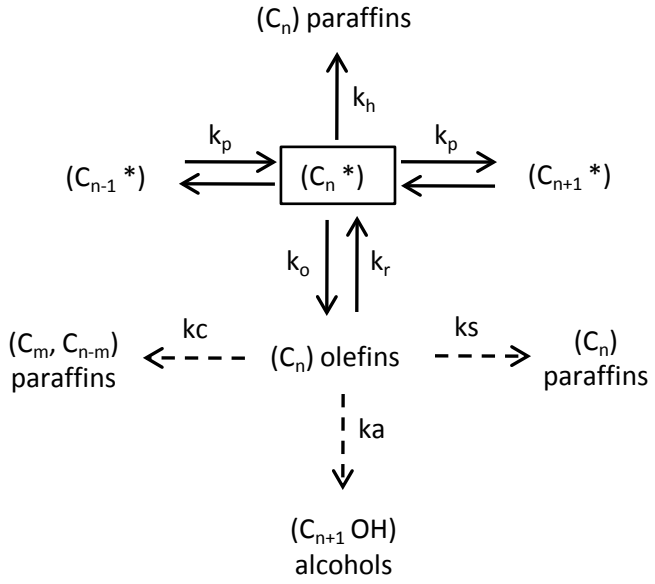

Fig. 2-1 Schematic of chain growth, readsorption, and secondary reactions of olefins in FTS

2.4 Fischer-Tropsch Catalysts

2.4.1 Catalysts

A variety of catalysts can be used for the Fischer-Tropsch process, but the most common are the transition metals (group 8-10 metals) since they can dissociatively adsorb H_2 and CO [37]. Fe, Ni, Co and Ru are the only metals that have the required FT activity for commercial application [45]. Ni has been reported to produce too much methane under FT conditions [2, 9, 45-48]. On the other hand, Ru has been found to be less selective to methane and more selective to the C_{5+} hydrocarbon fraction than other metals [47]. However, Ru is the most expensive of these four metals and the available amount in the world is insufficient for large scale application. For these reasons Fe and Co are viable catalysts for industrial applications. Fe catalysts are used in the major FTS operation at Sasol and Mossgas projects in South Africa [21, 49]. Extensive reviews of the use of Fe for FTS are reported in the literature [19, 49-53]. Low temperature FT process Fe-based catalysts used for wax production are currently

prepared by precipitation methods and are promoted with Cu and K_2O and bound with SiO_2 (5g K_2O, 5 g Cu and 25 g SiO_2 per 100g Fe) while the high-temperature FT Fe-based catalyst is prepared by fusing magnetite together with the required chemical (usually K_2O) and structural promoters such as Al_2O_3 or MgO [17]. Cobalt based catalysts are only used in the LTFT process where they possess high activity and selectivity for heavy waxy product and a lower water-gas-shift reaction activity compared to Fe catalysts [52, 54]. A high operating temperature results in production of excess methane. The catalytic behaviour of cobalt for FTS is influenced by many factors such as type of support, Co dispersion and particle size, catalyst preparation method, type of promoters, pre-treatment conditions, etc.

2.4.2 Active Sites and Catalyst Reduction

Within the catalysts introduced above for FTS, Co and Fe are the two studied the most and used in commercial plants. For Co catalyst, the active sites for FTS consist of metal atoms on the surface of Co metal crystallites. The studies have documented that cobalt metal surface, rather than cobalt oxides or carbides, catalyze FTS [55-57]. However, in the case of Fe catalysts, assignments of active phase and active sites is less definitive due to the rapid inter-conversion of Fe carbides, Fe_3O_4, and Fe metal in FT catalysts under reaction conditions [58], although substantial evidence implicates surface defect carbides, $Fe_5C_2(\chi)$, $Fe_{2.2}C(\varepsilon')$, and Fe_7C_3, as active phases [59-62]. In fact, Kerbs and Bonzel [59] found that the FTS activity of an iron foil was associated with surface carbides species observed by AES. Moreover, in an HRTEM/XRD/Mössbauer study, Datye et al. [62] observed in used Fe catalysts an active carbonaceous layer on the surface of metal carbode crystallies which was absent on fine magnetite crystals. In general, it is widely accepted that Co metal is the active phase in FTS on Co catalysts, and Fe carbides (Fe_xC, $x < 2.5$) and oxycarbides are active phases on Fe catalysts.

The catalysts, synthesized in the form of a metal oxide, are subjected to an activation treatment to become active for FT synthesis. Cobalt is almost always reduced in H_2 at temperatures between 473 and 723 K and remains in the metallic state under process conditions [7]. Ernst et al. [63] reported the behaviour of a cobalt silica catalyst both during reduction and for Fischer-Tropsch reaction. Before reduction the cobalt is present as Co_3O_4 spinel phase. A two-step reduction by H_2 at 673 K of Co_3O_4 to CoO and to Co^0 was observed. The pretreatment for iron is, on the other hand, not as straightforward. The common activation treatments for iron catalysts are H_2 reduction, CO reduction or reduction in synthesis gas (induction). Reduction of Fe_3O_4 by hydrogen to the zero-valent state is reported by, for example, Rao et al. [64] and Bukur et al. [65]. Lox et al. [66] reported that H_2 reduction at 220 °C results in 20 % metallic iron. After pretreatment of Fe-SiO_2 with CO or synthesis gas, the χ-carbide is the dominant iron phase [64, 65, 67, 68]. Pretreatment with synthesis may also result in formation of ε'-carbide [67].

2.5 Kinetics

Kinetic models of FTS on cobalt and iron and ruthenium catalysts have received considerable attention from researchers. [20, 21, 24, 69-71] The major problem in describing the FT reaction kinetics is the complexity of the reaction mechanism and the large number of species involved. The mechanistic proposals for the FTS used a variety of surface species and different elementary reaction steps, resulting in empirical power law expressions for the kinetics. [72, 73] However, the Langmuir–Hinshelwood–Hougen–Watson (LHHW) and Eley–Rideal (ER) type of rate equations based on a reaction mechanism for the hydrocarbon forming reactions, [74, 75] which are typically useful models for surface reaction, are capable of representing data over a wider range of variable space than power law expressions. In most cases the rate-determining step was assumed to be the

formation of the monomer. [74, 76-78]. These rate expressions for the consumption of synthesis gas differ mainly on the nature of the monomer, and on the adsorption of CO, H_2 and products (H_2O and CO_2) on the catalyst surface.

Rate is generally a function of both CO and H_2 partial pressures. Most rate expressions include P_{CO} in the denominator or, in the case of power law expressions, advise a reaction order less than zero, indicating that CO is adsorbed strongly at high coverage and inhibits the reaction rate. Predicted reaction orders for CO and H_2 are in the range of -1.0–0.5 and 0.5–2 respectively; activation energies cover a range of 80–130 kJ/mol. [14].

Representative rate equations based to some degree on well-known mechanistic models and fitted to rate data from kinetic studies of Co and Fe FTS catalysts are summarized in Table 2-3. There are some important differences between the data for cobalt and iron catalysts: (a) experimental temperatures are lower for cobalt, which is consistent with its higher activity; (b) H_2/CO ratios are generally lower for Fe because it catalyses the WGS reaction and hence produces H_2 internally; (c) the rate expression for cobalt is most likely to have been derived from an LHHW mechanism, which explains why the denominator is squared, whereas for Fe, the majority of expressions tend to favour an ER mechanism and so the denominator is not squared; and (d) inhibition by water is observed for Fe but not for Co. [14]

Table 2-3 Representative reaction rate equations for CO consumption in FTS on Co and Fe catalysts

Kinetic expression	References
Cobalt Catalysts	
$-r_{CO} = kP_{CO}^{-0.2}P_{H_2}^{0.7}$	[70, 79]
$-r_{CO} = \frac{aP_{CO}P_{H_2}}{(1+bP_{CO})^2}$	[79-81]
$-r_{CO} = \frac{aP_{CO}^m P_{H_2}^n}{1+bP_{CO}}, m = 0.5-0.6, n = 0.6-0.9$	[35, 82]
$-r_{CO} = \frac{aP_{CO}^{0.5}P_{H_2}^{0.5}}{(1+bP_{CO}^{0.5})^2}$	[83-85]
Iron catalyst	
$-r_{CO} = kP_{H_2}$	[7, 71, 86]
$-r_{CO} = aP_{CO}^m P_{H_2}^n$	[87]
$-r_{CO} = \frac{aP_{CO}P_{H_2}}{1+bP_{CO}+cP_{H_2O}}$	[74, 88-91]
$-r_{CO} = \frac{aP_{CO}P_{H_2}}{(1+bP_{CO}+cP_{H_2O})^2}$	[91]

When we look at the kinetic studies in the literature, we find that there is a variety of rate expressions and a wide range of activation energies for both Co and Fe catalysts. This raises questions about which of these data, kinetic parameters and rate expressions can be relied on for estimating reaction rates and/or conducting preliminary reactor design. This problem has also been pointed out by Bartholomew *et al*., [14] who have summarized the reasons for the inconsistencies in the kinetic expressions. These include the omission of pore diffusional restrictions; the derivation of kinetic parameters from data that have not been

obtained under isothermal experimental conditions; and fitting the data to different, complex rate expressions derived under limited operational conditions.

2.6 Product Selectivity

A huge variety of products of different chain length and different functionality is formed in FTS. The actual product distribution of a FT process depends on many reaction variables such as reaction conditions (temperature and partial pressures of the reactants and product water), the reactor system used, as well as the catalyst formulation and physical properties of a catalyst. The main products of Fischer-Tropsch synthesis are n-olefins and n-paraffins, and the side-products are oxygenates (1-alcohols, aldehydes, ketones, carboxylic acids), and branched compounds.

The high degree of order with repeating selectivity patterns in different carbon number fractions suggests a strict kinetic basis of this surface polymerization with stepwise addition of a C_1 monomer species, which is well suited for selectivity modelling. Many mathematical models have been developed to describe FT product distributions.

2.6.1 One parameter, ideal distribution model (Anderson-Schulz-Flory distribution)

Approximately, the molar amount of the sums of products in individual carbon number fractions declines exponentially with carbon number. This behaviour, which is indicative of a polymerization reaction that proceeds stepwise from a C_1 monomer, was originally noticed by Herrington [92] and Friedel and Anderson [93]. In the ideal case where the carbon number is independent chain growth

probability (Pg) of surface species, the molar product distribution may be presented as:

$$x_n = (1 - p_g)\, p_g^{n-1} \tag{2-19}$$

The complete derivation of this equation was first developed by Schulz [94] and Flory [95]. The only parameter in Eq. 2-19 is the chain growth probability Pg, which is also often referred to as α. When the molar fractions of the products plotted logarithmically with corresponding carbon number and a straight line is observed, the chain growth probability can be determined from the slope:

$$\lg x_n = \lg \frac{(1 - p_g)}{p_g} + n \lg p_g \tag{2-20}$$

This plot is generally called Anderson-Schulz-Flory (ASF) distribution and is commonly used to characterize FT synthesis products. The achievable selectivity of product weight fractions is shown in Figure 2-2 below when assuming ideal ASF kinetics places constraints on [96, 97].

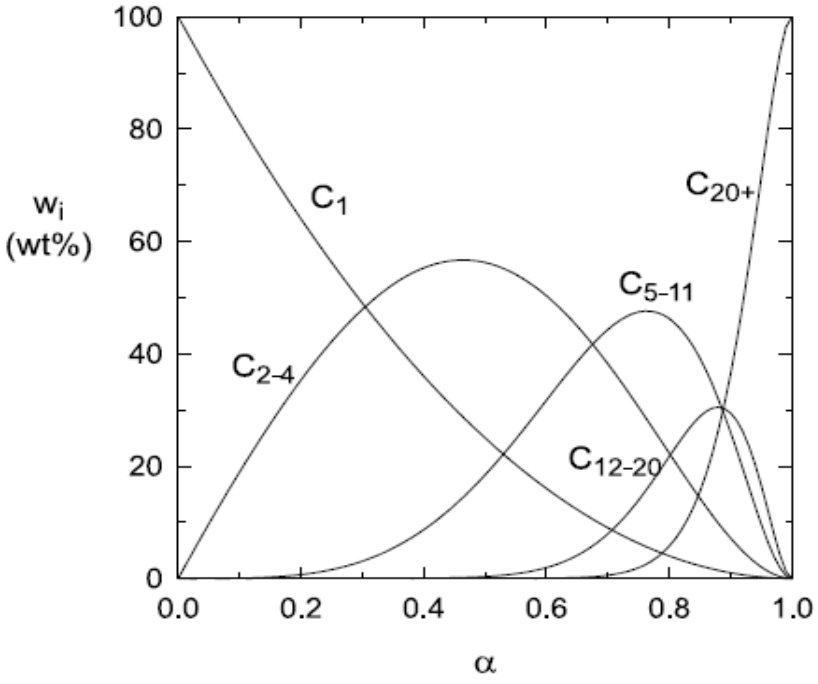

Fig. 2-2 Hydrocarbon selectivity as function of the chain growth probability factor α

The range of α is dependent on the reaction conditions and catalyst type. Dry [49] reported typical ranges of α on Ru, Co, and Fe of: 0.85-0.95, 0.70-0.80, and 0.50-0.70, respectively. The chain growth probability α decreases with an increase of the reactor temperature [49, 98-101]. A large variation in α is observed at temperatures higher than 280 °C [49, 100, 101]. A decrease of α is observed at higher H_2/CO ratios [198-100].

2.6.2 Deviations from ideal distributions

Significant deviations from the Anderson-Schulz-Flory distribution are reported in literature. The deviations were sometimes assigned to analytical difficulties [102] and non-steady state conditions of the reactor system [103]. However, novel analytical techniques usually rule out these explanations as the major source for the observed deviations. Commonly observed deviations from ideal distributions are:

a) a relatively high molar methane content.

   Wojciechowski [104] and Sarup and Wojciechowski [105] modeled the distribution of linear and branched paraffins with the use of termination probabilities. This way, the excess methane yield was described with a separate parameter for the increased termination probability of C_1 precursors. The methane termination probability parameter appears to be between 5 to 20 times larger than the termination probability to paraffins [105]. Schulz et al. [106] assumed a different catalytic site for the methanation reaction for the description of excessive methane formation on a cobalt catalyst in a slurry reactor. Heat and mass transfer limitations are reported in literature as possible reasons for high methane yields. Dry [49] reported that mass transfer limitations will result in an increase of the thermodynamically favoured

products, which is methane. The existence of hot spots, due to high reaction heats, may result in a decrease of the chain growth parameter and a higher yield of methane [49, 98].

b) a relatively low molar contents of C_2 in the ASF diagram and low olefin contents in the C_2 fraction.

Secondary reactions are often reported as the most probable reason for the anomalies of C_2 products: i) incorporation of ethene in growing chains [41, 42], ii) rapid readsorption of ethene [34, 106, 107]. iii) hydrogenolysis of ethene [43], and iv) hydrogenation of ethene to ethane [108-110]. Komaya and Bell [107] modeled the elementary reactions in FTS over a Ru/TiO_2 catalyst. Ethene could be hydrogenolyzed to methyl and methylene (monomer), with the readsorption constant of ethene approximately four orders of magnitude larger than higher olefins. Iglesia et al. [34] showed that ethene and propene obtain a higher reactivity and larger readsorption constants (factor 10) than other olefins.

c) a curvature of the ASF distribution at low carbon numbers, chain length dependent Pg reaching asymptotic values;

At a carbon number of about 10, the slope of the semi-logarithmic mole fractions of hydrocarbons against carbon number increases. This phenomenon has been observed on iron [98, 111-113], cobalt [104, 105, 111, 114], and ruthenium catalysts [111, 115, 116]. Suggestions for the increased chain growth parameter or two probabilities of chain growth are the occurrence of different catalytic sites [98, 117, 118] or the existence of different chain termination reactions [105, 106]. It is widely considered that the occurrence of secondary reactions (hydrogenation, reinsertion, hydrogenolysis, isomerization) gives the most reasonable explanation for these deviations of

the ASF distribution [35, 43, 108, 110, 119]. If a product is terminated by a reaction on an FT growth site to a paraffin or olefin it is called a primary product. Readsorption of olefins on growth sites may also lead to primary products whereas adsorption on other sites will produce secondary products due to hydrogenation or isomerization reactions. Secondary reactions as well as readsorption are directly influenced by space velocity. It is generally accepted that secondary reactions of olefins depend on the chain length, resulting in a decrease of the (O_n/P_n) ratio and increase of the growth probability α_n with chain length.

2.7 FTS reaction system and the reactors

The Fischer-Tropsch Synthesis is a process with a high, exothermic reaction enthalpy. Any practical application of this process when a reasonable reaction rate was desired, the reactor system, including the catalyst inside, should have a function of removing the heat generated by the reaction rapidly. Fischer and Pichler [120] indicated that four approaches were suitable for removing the heat of reaction and for maintaining a uniform temperature in the reactor: (1) circulating oil outside the tube with the catalyst, (2) suspending the catalyst in oil, (3) circulating superheated water outside the catalyst apace, and (4) the suspension of the catalyst in the superheated water. This is also recorded by Steynberg and Dry [121].

Among all the proposed reaction systems, three of them with corresponding reactor types have been proved useful, both practically and commercially [14, 121]: (1) fixed bed reactor (e.g. Sasol ARGE reactor and Shell Middle Distillate Synthesis reactor), (2) fluidized bed reactor (e.g. Sasol Synthol reactor and Sasol Advanced Synthol reactor), and (3) slurry bed reactor (e.g. Sasol-Chevron slurry reactor in Qatar (Orxy)). Because of the high exothermic nature of the FT reaction

and an adiabatic temperature rise that can be as high as 1750 K (simply estimated by $\Delta Hr/C_{p,\ products}$), rapid removal of heat from the catalyst bed is essential [122-124], and all three of the aforementioned reactor types are designed for rapid heat removal using a combination of heat exchangers, recycles, and staged systems. However, heat transfer rates are substantially higher for fluidized bed and slurry bed reactors. Fluidized bed reactors are operated at high temperatures to ensure the absence of liquid phases that would cause agglomeration. This is a specific application in conversion of coal to light hydrocarbon liquids including gasoline and important chemicals. Low temperature fixed bed and slurry bed reactors find application in both coal to liquid (CTL) and gas to liquid (GTL) processes with the production of waxes, diesel fuel and lubricants. Some attributes, advantages and limitations of each of the aforementioned reactors are described below.

(1) The fixed bed reactor. The representatives for the fixed bed reactor (FBR) are the ARGE reactor in SASOL, which is currently operated in SASOL I located in Sasolburg, South Africa, and the Shell Middle Distillate Synthesis (SMDS) reactor in Shell, which is currently operated in Bintulu, Malaysia and the fixed bed reactors in the Pearl project in Qatar.

In a typical fixed bed reactor, heat is removed by circulating water/steam coolant over catalyst tubes; for example, each Sasol ARGE FBR operates as a tube-shell heat exchanger, a 3 m diameter shell containing 2050 tubes, each 5.5 cm in diameter and 12 m in length, into which catalyst is packed and where heat is removed by producing high-pressure steam. In this type reactor, operation temperature is normally at 210-225 ^{o}C for a Co catalyst and 230-245 ^{o}C for a Fe catalyst. A single pass conversion is maintained below 50%, or even lower to avoid temperature overshooting in the catalyst bed. To facilitate temperature control while maximizing conversion, a portion of tail gas is

recycled when only one reactor or the feed is passed through a train of reactors. The advantages of this type reactor in FTS relative to slurry phase reactor are: (i) higher conversion due to near plug flow of the fluid, (ii) no catalyst loss due to attrition, (iii) longer catalyst life because of low susceptibility to poisons, and (iv) greater operational flexibility; however, its application has serious limitations which include: (i) low heat transfer characteristics and marginal temperature control, (ii) limited productivity since catalyst activity is limited by a relative lower average bed temperature, (iii) significantly more complex construction causing substantial capital cost, (iv) higher pressure drop leading to higher operating cost, and (v) inability to shut down to change catalyst. The design of the fixed bed reactor has been addressed by many researchers in the literature; however, only limited (around 7) serious modelling studies on FT fixed bed reactors have been reported in the (open) literature [125-132].

(2) The fluidized bed reactor. The representatives in this case are the Circulated Fluidized Bed reactor (CFB) in SASOL II, SASOL III and Petro SA (SASOL Synthol Reactor), and the Fixed Fluidized Bed (FFB) in SASOL II and III (the Advanced Synthol Reactor). In order to fluidize the catalyst and prevent any agglomeration, no liquid phase is allowed in this type of reactor.

Fluidized beds are generally of two types, circulating and fixed. The main difference between the two types of reactor is that in the fixed fluidized bed reactor (FFD) the catalyst bed remains stationary and the gases pass upward through the bed while in the circulating fluidised bed reactor (CFB) the catalyst is entrained in the fast moving stream. The FT plant in the Brownsville, TX [133] which was later shut down for economic reasons, used the FFB reactor while the CFB reactor was developed by The Kellogg Company and was used in the first Sasol plant at Sasolburg [134]. The

fluidized bed reactors such as the SAS reactor provide more efficient heat removal; nearly isothermal operation and higher throughput per volume of reactor relative to the fixed bed. The main advantages of FFB over CFB reactors include simplicity, low construction cost, ease of operation, low overall catalyst consumption because of a lower rate of on-line catalyst removal and replacement with fresh catalyst to maintain high conversions.

(3) The slurry phase rector. The representatives are the SASOL Chevron slurry reactor in Qatar (Oryx project) operated at low temperature FTS conditions with a cobalt catalyst, and the three demonstration plants in Shenhua, Yitai, and Luan in China operated at low temperature FTS conditions with iron catalysts.

Slurry bed reactors are three phase systems in which gas is bubbled through a suspension of finely divided catalyst in a liquid which has a low vapour pressure at the temperature of operation. In the 1970s Sasol tests indicated that similar conversions and selectivity could be obtained when comparing the performance of fixed bed reactors under same operation conditions [17, 135, 136]. Relative to a fixed bed reactor, slurry reactor has advantages of (i) low cost to construct, (ii) very efficient heat transfer and uniform temperature, (iii) lower catalyst consumption per ton of product, (iv) ability to operate at a higher average temperature resulting in higher conversions, and (v) on-line removal/addition of catalyst allows longer reactor runs. Slurry reactor design has been reported by researchers [126, 135, 137-141] and a typical SBCR design and operating conditions are described by Maretto and Krishna[141]: diameter: 6-10 m, height: 30-40 m, operation pressure: 20-40 bar; temperature: 230-250 ^{o}C, superficial gas velocity: 0.1-0.4 m/s depending upon catalyst activity and concentration, slurry volume fraction: 0.3-0.4, and vertical cooling tubes: 5,000-8,000, 5 cm in diameter and 15 cm pitch.

2.8 Syngas production and product upgrading

The commercial FT process involves three main sections, namely: synthesis gas production and purification, Fischer-Tropsch synthesis, and product grade-up. The syngas production and product upgrading are described in more detail below.

2.8.1 Synthesis Gas Production

As the feed for the FTS process, synthesis gas can be obtained from the gasification of coal, refinery residues, biomass and even city wastes; or by steam reforming or (catalytic) partial oxidation of natural gas, coal bed gas, and industrial off-gases.

The most important reactions for the gasification process are listed in Table 2-4:

Table 2-4 Major reaction during coal gasification

$C + O_2 \rightarrow CO_2$	2-21
$2C + O_2 \rightarrow 2CO$	2-22
$C + H_2O \rightarrow CO + H_2$	2-23
$CO + H_2O \rightarrow CO_2 + H_2$	2-24

Synthesis gas can also be obtained from reforming natural gas with either steam or carbon dioxide, or by partial oxidation. The most important reactions are:

Table 2-5 Major reactions during reforming of natural gas

Steam reforming	$CH_4 + H_2O \rightarrow CO + 3H_2$	2-25
CO_2 reforming	$CH_4 + CO_2 \rightarrow 2CO + 2H_2$	2-26
Partial oxidation	$CH_4 + 1/2O_2 \rightarrow CO + 2H_2$	2-27
Water gas shift reaction	$CO + H_2O \rightarrow CO_2 + H_2$	2-28

Usually, a combination of synthesis gas production processes is used to obtain synthesis gas with a stoichiometric ratio of hydrogen and carbon monoxide. Synthesis gas produced in modern coal gasifiers (vendors: Shell/Koppers or Texaco gasifiers, Lurgi) and from heavy oil residues has a high CO content in comparison with synthesis gas from natural gas. If synthesis gas with a H_2/CO ratio below 2 is used, the composition is not stoichiometric for the FT reactions. In that case, the WGS reaction has the important function to change the H_2/CO ratio to 2. Iron catalysts (which are inexpensive in comparison to cobalt) can convert low H_2/CO ratio synthesis gas directly without an external shift reaction. [142-144] Given its availability, methane is usually preferred to coal for syngas production. When using natural gas as the feedstock, many authors [145-150] have recommended autothermal reforming or autothermal reforming in combination with steam reforming as the best option for syngas generation. This is primarily attributable to the resulting H_2/CO ratio and the fact that there is a more favourable economy of scale for air separation units than for tubular reactors.

2.8.2 Product Upgrading and Separation

Conventional refinery processes can be used for upgrading of Fischer-Tropsch liquid and wax products. A number of possible processes for FT products are: wax hydrocracking, distillate hydrotreating, catalytic reforming, naphtha hydrotreating, alkylation and isomerization [151, 152]. Fuels produced with the FT synthesis are of a high quality due to a very low aromaticity and zero sulfur content. The product stream consists of various fuel types: LPG, gasoline, diesel fuel, jet fuel, etc. The diesel fraction has a high cetane number resulting in superior combustion properties and reduced emissions. New and stringent regulations may promote replacement or blending of conventional fuels by sulfur and aromatic free FT products [153, 154]. Also, other products besides fuels can be manufactured with

Fischer-Tropsch in combination with upgrading processes, for example, ethene, propene, α-olefins, alcohols, ketones, solvents, specialty waxes, and so forth. These valuable by-products of the FT process have higher added values, resulting in an economically more attractive process.

2.9 Applications (the characteristics of commercial FT processes)

The applications of FT processes with different reactors have been introduced in section 2.1 and 2.9. This section summarizes the characteristics of typical, commercial FT processes. The related information is given in Table 2-6 below.

Table 2-6 The characteristics of commercial FT processes

Characteristic	TFBR (Co) Shell MTFB	TFBR (Fe) Sasol Arge TFB	SBCR (Fe) Sasol SSPD
Reactor Characteristic			
Reactor productivity, bbl/d	6700	1500	2500
Diameter (ID), m	6.2	3	5
Height, m	20	12	22
Reactor weight, tons	865		
Reactor tubes/Cooling tubes	8000	2050	
Heat removal/temperature control	fair	fair	Excellent
Thermal efficiency, %		85	91
Volume (active volume), m^3	600(310)	85	432
Production, tons/m^3 rctr -d	1.14	1.8	0.59
Capital cost, $1000/inst-bbl/d	31	68	31
Operation conditions			
Pressure, bar	40	27	25
Pressure drop, bar		4	<1
Temperature, ^oC	237	230	236
H_2/CO ratio	2.15	1.25-2.0	
H_2 fresh feed conversion, %	73	46	49
Gas velocity, m/s	0.18	0.36	0.36
Recycle/feed ratio		1.9	1.9
Catalyst properties/performance			
Catalyst	$Co/ZrO_2/SiO_2$	$Fe/Cu/K/SiO_2$	$Fe/Cu/K/SiO_2$
Catalyst charge, ton	310	38	121
Catalyst particle size	2 mm	2.5 mm	40-140 um
Propagation probability, alpha	0.96	0.95	0.95
C_{5+} selectivity, % C	90	84	84.5
CH_4 selectivity, % C	4	7	5
CO_2 selectivity, % C	1	2.5	
Productivity, kg-C_{5+}/kg cat/h	0.092	0.14	0.087
Catalyst life, month	60	9 to 12	
Catalyst consumption (19000 bpd), m^3/a	50	9 to 12	

2.10 References

1. Olive-Henrichi, G.; Olive, S. In *The chemistry of the metal-carbon bond – vol 3*, Hertley and Patai (Eds.). John Wiley and Sons: New York, 1985.
2. Sabatier, P.; Senderens, J. B. *Hebd. Seances Acad. Sci.* **1902**, *134*, 514, 680.
3. a, BASF, *German Patent*, (1913) 293, 787.; b, BASF, *German Patent*, (1914) 295, 202.; c, BASF, *German Patent*, (1914) 295, 203.
4. Fischer, F.; Tröpsch, H. *Brennstoff. Chem.* **1923**, *4*, 276.
5. Fischer, F.; Tröpsch, H. *German Patent*, (1925) 484,337.
6. Fischer, F.; Tröpsch, H. *Brennstoff. Chem*. **1926**, *7*, 97.
7. Anderson, R. B. In *Catalysis* Vol. 4, Emmet, P.H.; Ed. Von Norstand –Reinhold: New Jersey, 1956.
8. Pichler, H. *Brennstoff. Chem*. **1938**, *19*, 226.
9. Dry, M. E. in *Applied Industrial Catalysis* - Vol. 2, Samuel, K.M. et al., (Eds.) 1983.
10. Post, M.F.M. *Shell International Research, Eur Pat*, EP 0,174,696 (1985).
11. Dry, M. E. The Fischer–Tropsch process: 1950–2000. *Catal. Today*. **2002**, *71*, 227.
12. Jager, B.; Espinoza, R. Advances in Low-Temperature Fischer-Tropsch Synthesis. *Catal. Today* **1995**, *23*, 17–28.
13. Sie, S.T. Process Development and Scale up: IV Case History of the Development of a Fischer-Tropsch Synthesis Process. *Rev. Chem. Eng.* **1998**, *14*, 109–157.
14. Bartholomew, C. H.; Farrauto, R. J. Fundamentals of industrial catalytic processes. Wiley: New Jersey, 2006.
15. Anderson, R. B. *Catalysts for the Fischer-Tropsch synthesis*, vol. 4, Van Nostrand Reinhold: New York, 1956.
16. Ponec, V. Some Aspects of the Methanation and Fischer-Tropsch Synthesis. *Catal. Rev.-Sci. Eng.* **1978**, *18*, 151–171.
17. Dry, M.E. The Fischer-Tropsch Synthesis, in Anderson; J. R. M. Boudart, eds., *Catalysis-Science and technology*, vol. 1, Springer-Verlag, New York, 1981.

18. Bell, A. T. Catalytic Synthesis of Hydrocarbons over Group VIII Metals: A Discussion of the Reaction Mechanism. *Catal. Rev.-Sci. Eng.* **1981**, *23*, 203-232.
19. Hindermann, J. P.; Hutchings, G. J.; Kiennermann, A. Mechanistic Aspects of the Formation of Hydrocarbons and Alcohols from CO Hydrogenation. *Catal. Rev.- Sci. Eng.* **1993**, *35*, 1–127.
20. Dry, M. E. Conversion of Syngas to Fuels and Chemicals, in *Int. Conf. on Catal.& Catal. Proc.* Cape Town, South Africa, 1993, 57–66.
21. Dry, M. E. Practical and Theoretical Aspects of the Catalytic Fischer-Tropsch Process. *Appl. Catal. A* **1996**, *138*, 319–344.
22. Adesina, A. A., Hydrocarbon Synthesis via Fischer-Tropsch Reaction: Travails and Triumphs. *Appl. Catal. A* **1996**, *138*, 345–367.
23. van de Laan, G. P.; Beenackers, A. A. C. M. Kientics and Selectivity of the Fischer-Tropsch Synthesis: A literature Review. *Catal. Rev.- Sci. Eng.* **1999**, 41, 255-318.
24. Maitilis, P. M.; Quyoum, R.; Long, H. C.; Turner, M. L. Towards a Chemical Understanding of the Fischer-Tropsch Reaction: Alkene Formation. Applied Catalysis: A. **1999**, *186*, 363-374.
25. Overett, M. J.; Hill, R.; Moss, J. Organometallic Chemistry and Surface Science: Mechanistic Models for the Fischer-Tropsch Synthesis. *Coordination Chemistry Reviews* **2000**, *206-207*, 581-605.
26. Davis, B. H. Fischer-Tropsch Synthesis: Current Mechanism and Futuristic Needs. *Fuel Processing Technology* **2001**, *71*, 157-166.
27. Temkin, O. N. Zeigarnik, A. V.; Kuz'min, A. E. Bruk, L. G.; Slivinskii, E. V.; Lomonosov, M. V. Construction of the Reaction Networks for Heterogeneous Catalytic Reactions: Fischer-Tropsch Synthesis and Related Reactions. *Russian Chemical Bulletin* **2002**, *51*, 1-36.
28. van Dijk, H.; Hoebink, J.; Schouten, J. A Mechanistic Study of the Fischer-Tropsch Synthesis Using Transient Isotopic Tracing. Part 1: Model Identification and Discrimination, Part 2: Model Quantification. *Topics in Catalysis* **2003**, *26*, 111-119, 163-171.
29. Yang, J.; Liu, Y.; Chang, J.; Wang, Y.-N.; Bai, L.; Xu, Y.-Y.; Xiang, H.-W.;

Li, Y.-W.; Zhong, B. Detailed Kinetics of Fischer-Tropsch Synthesis on an Industrial Fe-Mn Catalyst. *Industrial & Engineering Chemistry Research* **2003**, *42*, 5066-5090.

30. Fischer, F.; Tropsch, H. Synthesis of Petroleum from Gasification Products of Coal at Normal Pressure. *Ber.* 49, 830, 832, 923.
31. Biolen, P.; Helle, J. N.; Sachtler, W. M. H. Incorporation of Surface Carbon into Hydrocarbons during Fischer-Tropsch Synthesis: Mechanistic Implications. *J. Catal.* **1979**, *58*, 95.
32. Brady, R. C.; Pettit, R. On the Mechanism of the Fischer-Tropsch Reaction: The Chain Propagation Step. *J. Am. Chem. Soc.* **1981**, *103*, 1287-1289.
33. Iglesia, E.; Reyes, S. C.; Madon, R. J. Transport-Enhanced α-Olefin Readsorption Pathways in Ru-Catalyzed Hydrocarbon Synthesis. *J. Catal.* **1991**, *129*, 238-256.
34. Iglesia, E.; Reyes, S. C.; Madon, R. J.; Soled, S. L. Selectivity Control and Catalyst Design in the Fischer-Tropsch Synthesis: Sites, Pellets, and Reactors. *Advances in Catalysis* **1993**, *39*, 221-302.
35. Madon, R. J.; Iglesia, E. The Importance of Olefin Readsorption and H_2/CO Reactant Ratio for Hydrocarbon Chain Growth on Ruthenium Catalysts. *J. Catal.* **1993**, *139*, 576-590.
36. van Dijk, H. A. J. The Fischer-Tropsch Synthesis: A Mechanistic Study using Transient Isotopic Tracing. PhD Dissertation, 2001, Eindhoven University of Technology, Netherlands.
37. Biloen, P.; Sachtler, W.M.H. Mechanism of Hydrocarbon Synthesis over Fischer-Tropsch Catalysts. *Adv. Catal.* **1981**, *30*, 165–216.
38. Lox, E. S.; Froment, G. F. Kinetics of the Fischer-Tropsch Reaction on a Precipitated Promoted Iron Catalyst. 2. Kinetic Modeling. *Ind. Eng. Chem. Res.* **1993**, *32*, 71–82.
39. Hovi, J.-P.; Lahtinen, J.; Liu, Z. S.; Nieminen, R.M. Monte Carlo Study of CO Hydrogenation on Cobalt Model Catalysts. *J. Chem. Phys.* **1995**, *102*, 7674–7682.
40. Ndlovu, S. B.; Phala, N. S.; Hearshaw-Timme, M.; Beagly, P.; Moss, J. R.; Claeys, M.; van Steen, E. Some Evidence Refuting the Alkenyl Mechanism

for Chain Growth in Iron-based Fischer-Tropsch Synthesis. *Catal. Today* **2002**, *71*, 343-349.

41. Novak, S.; Madon, R. J.; Suhl, H. Models of Hydrocarbon Product Distributions in Fischer-Tropsch Synthesis. *J. Chem. Phys.* **1981**, *74*, 6083–6091.
42. Novak, S.; Madon, R. J.; Suhl, H. Secondary Effects in the Fischer-Tropsch Synthesis. *J. Catal.* **1982**, *77*, 141–151.
43. Schulz, H.; Beck, K.; Erich, E. Mechanism of the Fischer-Tropsch Process, in D. M. Bibby; C. D. Chang; R. F. Howe; S. Yurchak, eds., *Methane Conversion*, Elsevier Science, 1988.
44. Schulz, H.; Beck, K.; Erich, E. Kinetics of Fischer-Tropsch selectivity. *Fuel Process. Technol.* **1988**, *18*, 293–304.
45. Hexane, W. M. A systematic study of the effect of chemical promoters on the precipitated Fe-based Fischer-Tropsch Synthesis catalyst. PhD Thesis, University of the Witwatersrand, Johannesburg, South Africa, 2009.
46. Chai, G.Y.; Falconer, J. L. Alkali Promoters on Supported Nickel: Effect of Support, Preparation, and Alkali Concentration. *J. Catal.* **1985**, *93*, 152.
47. Vannice, M. A. The Catalytic Synthesis of Hydrocarbons from H_2/CO Mixtures over the Group VIII Metals: I. The Specific Activities and Product Distributions of Supported Metals. *J. Catal.* **1975**, *37*, 449.
48. Vannice, M. A. The Catalytic Synthesis of Hydrocarbons from H_2/CO Mixtures over the Group VIII Metals: V. The Catalytic Behaviour of Silica-Supported Metals. *J. Catal.* **1977**, *50*, 228.
49. Dry, M. E. Catalytic Aspects of Industrial Fischer-Tropsch Synthesis. *J. Mol. Catal.* **1982**, *17*, 133.
50. Caesar, P. D.; Brennan, J. A.; Garwood, W. E.; Ciric, J. Advances in Fischer-Tropsch Chemistry. *J. Catal.* **1979**, *56*, 274.
51. Dry, M. E.; Erasmus, H.B. *Ann. Rev. Energy* **1987**, 1.
52. Jonardanarao, M. Direct Catalytic Conversion of Synthesis Gas to Lower Olefins. *Ind. Eng. Chem. Res.* **1990**, *29*, 1735.
53. Rao, V. U. S.; Stiegel, G. J.; Cinquegrane, G. J.; Strvastava, R. D. Iron-Based Catalysts for Slurry-Phase Fischer-Tropsch Process: Technology Review.

Fuel Processing Technology **1992**, *30*, 83.

54. Schulz, H. Short History and Present Trends of Fischer–Tropsch Synthesis. *Appl. Catal. A: General* **1999**, *186*, 3.
55. Johnson, B. G.; Bartholomew, C. H.; Goodman, D. W. The Role of Surface Structure and Dispersion in CO Hydrogenation on Cobalt. *J. Catal.* **1991**, *128*, 231-247.
56. Beitel, G. A.; de Groot, C.; Oosterbeek, H.; Wilson, J. A Combined *in-situ* PM-RAIRS and Kinetic Study of Single-Cristal Cobalt Catalysts under Synthesis Gas at Pressures up to 300Mbar. *J. Phys. Chem. B.* **1997**, *101*, 4035-4043.
57. Geerkings, J.; Wilson, J.; Kramer, G.; Kuipers, H.; Hoek, A.; Huisman, H. Fischer-Tropsch Technology – from Active Site to Commercial Process. *Applied Catalysis: A.* **1999**, *186*, 27-40.
58. Li, S.; Ding, W.; Meitzner, G.; Eglesia, E. Spectroscopic and Transient Kinetics Studies of Site Requirements in Iron-Catalyzed Fischer-Tropsch Synthesis. *J. Phys. Chem. B.* **2002**, *106*, 85-91.
59. Krebs, H. J.; Bonzel, H. P. Evidence for Adsorbed Hydrocarbon Intermediates during the Initial Stage of Carbon Monoxide Hydrogenation on Iron. *ACS Spring Meeting, Div. Fuel Chemistry.* **1980**, *25*, 19-26.
60. Dictor, R. A.; Bell, A. T. Studies of Fischer-Tropsch Synthesis over a Fused Iron Catalyst. *Appl. Catal.* **1986**, *20*, 145-162.
61. Jung, H.; Thomson, W. Dynamic X-Ray Diffusion Study on an Unsupported Iron Catalyst in Fischer-Tropsch Synthesis. *J. Catal.* **1992**, *134*, 654-667.
62. Datye, A.; Jin, Y.; Mansker, L; Motjope, R. T.; Dlamini, T. H.; Colville, N. The Nature of the Active Phase in Iron Fischer-Tropsch Catalysts, Corma, A. et al. eds. *Stud. Surf. Sci. Catal.* **2000**, *130*, 1139-1144.
63. Ernst, B.; Bensaddik, A.; Jilaire, L.; Chaumette, P.; Kienemann, A. Study on Cobalt Silica Catalyst During Reduction and Fischer- Tropsch Reaction: In-situ EXAFS Compared to XPS and XRD. *Catal. Today* **1998**, *39*, 329–341.
64. Rao, K.R.P.M.; Huggins, F.E.; Mahajan, V.; Huffman, G.P.; Rao, V.U.S.; Bhatt, B.L.; Bukur, D.B.; Davis, B.H.; O'Brien, R.J. M¨ossbauer

Spectroscopy Study of Iron-based Catalysts Used in Fischer-Tropsch Synthesis. *Top. Catal.* **1995**, *2*, 71–78.

65. Bukur, D. B.; Koranne, M.; Lang, X.; Rao, K.R.P.M.; Huffman, G. P. Pretreatment Effect Studies with a Precipitated Iron Fischer-Tropsch Catalyst, *Appl. Catal. A* **1995**, *126*, 85–113.
66. Lox, E. S.; Marin, G. B.; de Graeve, E.; Bussiere, P. Characterization of a Promoted Precipitated Iron Catalyst for Fischer-Tropsch Synthesis. *Appl. Catal. A* **1988**, *40*, 197–218.
67. Rao, K.R.P.M.; Huggins, F.E.; Huffman, G.P.; Gormley, R.J.; O'Brien, R.J.; Davis, B.H. Mössbauer Spectroscopy Study of Iron Fischer-Tropsch Catalysts During Activation and Synthesis. *Energy Fuels* **1996**, *10*, 546–551.
68. Rao, K.R.P.M.; Huggins, F. E.; Mahajan, V.; Huffman, G. P.; Davis, B.; O'Brien, R.J.; Xu, L.; Rao, V.U.S. Effect of Pre-Heat Treatment on a Fischer-Tropsch Iron Catalyst. *Hyperfine Interact.* **1994**, *93*, 1755–1758.
69. Ribeiro, F. H.; Schach vonWittenau, A. E.; Bartholemew, C. H.; Somorjai, G. A. Reproducibility of Turnover Rates in Heterogeneous Metal Catalysis: Compilation of Data and Guidelines for Data analysis. *Catal. Rev.-Sci. Eng.* **1997**, *39*, 49–76.
70. Huff, Jr., G. A.; Satterfield, C. N. Intrinsic Kinetics of the Fischer-Tropsch Synthesis on a Reduced Fused-Magnetite Catalyst. *Ind. Eng. Chem. Process Des. Dev.* **1984**, *23*, 696–705.
71. Zimmerman, W. H.; Bukur, D. B. Reaction Kinetics over Iron Catalysts Used for the Fischer-Tropsch Synthesis. *Can. J. Chem. Eng.* **1990**, *68*, 292–301.
72. Vannice, M. A. The Catalytic Synthesis of Hydrocarbons from H_2/CO Mixtures over the Group VIII Metals. II. The Kinetics of the Methanation Reaction over Supported Metals. *J. Catal.* **1975**, *37*, 462–473.
73. Bub, G.; Baerns, M. Prediction of the Performance of Catalytic Fixed Bed Reactors for Fischer-Tropsch Synthesis. *Chem. Eng. Sci.* **1980**, *35*, 348–355.
74. Wojciechowski, B. W. The Kinetics of the Fischer Tropsch Synthesis. *Catal. Rev.-Sci. Eng.* **1988**, *30*, 629–702.

75. Dixit, R. S.; Tavlarides, L. L. Kinetics of the Fischer-Tropsch Synthesis. *Ind. Eng. Chem. Process Des. Dev.* **1983**, *22*, 1–9.
76. Sarup, B.; Wojciechowski, B.W. Studies of the Fischer-Tropsch Synthesis on a Cobalt Catalyst. II. Kinetics of Carbon Monoxide Conversion to Methane and to Higher Hydrocarbons. *Can. J. Chem. Eng.* **1989**, *67*, 62–74.
77. Nettelhoff, H.; Kokuun, R.; Ledakowicz, S.; Deckwer, W.-D. Studies on the Kinetics of Fischer-Tropsch Synthesis in Slurry Phase. *Ger. Chem. Eng.* **1985**, *8*, 177–185.
78. Huff, Jr., G. A.; Satterfield, C. N., Stirred Autoclave Apparatus for Study of the Fischer-Tropsch Synthesis in a Slurry Bed. 2. Analytical Procedures. *Ind. Eng. Chem. Fundam.* **1983**, *22*, 258–263.
79. Zennaro, R.; Bartholomew, C. H.; Tagliabue, M. Kinetics of Fischer-Tropsch Synthesis on Titania-Supported Cobalt Catalyst. *Catalyst Today* **2000**, *58*, 309-319.
80. Whiters, Jr., H. P.; Eleizer, K. F.; Mitchell, J. W. Slurry-phase Fischer-Tropsch Synthesis and Kinetic Studies over Supported Cobalt Carbonyl Derived Catalysts, *Ind. Eng. Chem. Res.* **1990**, *29*, 1807–1814.
81. Yates, I. C.; Satterfield, C. N. Intrinsic Kinetics of the Fischer-Tropsch Synthesis on a Cobalt Catalyst. *Energy Fuels* **1991**, *5*, 168–173.
82. Peluso, E.; Galarraga, C.; Lasa, H. Eggshell Catalyst in Fischer-Tropsch Synthesis Intrinsic Reaction Kinetics. *Chemical Engineering Science* **2001**, *56*, 1239-1245.
83. Sarup, B.; Wojciechowski, B.W. Studies of the Fischer-Tropsch Synthesis on a Cobalt Catalyst. II. Kinetics of Carbon Monoxide Conversion to Methane and to Higher Hydrocarbons. *Can. J. Chem. Eng.* **1989**, *67*, 62–74.
84. Keyser, M. J.; Everson, R. C.; Espinoza, R. L. Fischer-Tropsch Kinetic Studies with Cobalt-manganese Oxide Catalysts. *Industrial and Engineering Chemistry Research* **2000**, *39*, 48-54.

85. Huber, G. W. Intrinsic Kinetics of Pt-Promoted Co/SiO_2 Fischer-Tropsch Synthesis Catalysts. M. S. Thesis, Brigham Young University, United States.
86. Dry, M. E.; Shingles, T.; Boshoff, L. J.; Oosthuizen, G. J. Rate of the Fischer-Tropsch Reaction over Iron Catalysts. *J. Catal.* **1972**, *25*, 99–104.
87. Eliason, S. A.; Bartholomew, C. H. Reaction and Deactivation Kinetics for Fischer-Tropsch Synthesis on Unpromoted and Potassium-promoted Iron Catalysts. *Applied Catalysis* **1999**, *186*, 229-243.
88. Atwood, H. E.; Bennett, C. O. Kinetics of The Fischer-Tropsch Reaction over Iron. *Ind. Eng. Chem. Process Des. Dev.* **1979**, *18*, 163–170.
89. Nettelhoff, H.; Kokuun, R.; Ledakowicz, S.; Deckwer, W.-D. Studies on the Kinetics of Fischer-Tropsch Synthesis in Slurry Phase. *Ger. Chem. Eng.* **1985**, *8*, 177–185.
90. Deckwer, W.-D.; Kokuun, R.; Sanders, E.; Ledakowicz, S. Kinetic Studies of Fischer-Tropsch Synthesis on Suspended Fe/K Catalyst. Rate Inhibition by CO_2 and H_2O. *Ind. Eng. Chem. Process Des. Dev.* **1986**, *25*, 643–649.
91. van der Laan, G. P.; Beenackers, A. A. C. M. Intrinsic Kinetics of the Gas-Solid Fischer-Tropsch and Water Gas Shift Reactions over a Precipitated Iron Catalyst. *Applied Catalysis* **2000**, *193*, 39-53.
92. Herrington, E. F. G. *Chemical Industries*. **1946**, *65*, 346.
93. Friedel, R. A.; Anderson, R. B. Composition of Synthetic Liquid Fuels. I. Product Distribution and Analysis of C_5—C_8 Paraffin Isomers from Cobalt Catalyst. *Journal of American Chemical Society*. **1950**, *72*, 1212.
94. Schulz, G. V. Z. *Physik. Chem.* **1935**, *B30*, 379.
95. Flory, P. Molecular Size Distribution in Linear Condensation Polymers. *Journal of American Chemical Society* **1936**, *58*, 1877.
96. Dry, M. E. The Fischer-Tropsch Process - Commercial Aspects. *Catalysis Today* **1990**, *6*,183.
97. van der Laan, G. P. Kinetics, Selectivity and Scale Up of the Fischer-Tropsch Synthesis. PhD thesis, University of Groningen, Netherlands, 1999.

98. Dictor, R. A.; Bell, A. T. Fischer-Tropsch Synthesis over Reduced and Unreduced Iron Oxide Catalysts. *J. Catal.* **1986**, *97*, 121–136.

99. Lox, E. S.; Froment, G. F. Kinetics of the Fischer-Tropsch Reaction on a Precipitated Promoted Iron Catalyst. 1. Experimental Procedure and Results. *Ind. Eng. Chem. Res.* **1993**, *32*, 61–70.

100. Donnelly, T. J.; Satterfield, C. N. Product Distributions of the Fischer-Tropsch Synthesis on Precipitated Iron Catalysts. *Appl. Catal. A* **1989**, *52*, 93–114.

101. Everson, R. C.; Woodburn, E. T.; Kirk, A. R. M. Fischer-Tropsch Reaction Studies with Supported Ruthenium Catalysts. I. Product Distributions at Moderate Pressures and Catalyst Deactivation. *J. Catal.* **1978**, *53*, 186–197.

102. Puskas, I.; Hurlbut, R. S.; Pauls, R. E. Telomerization Model for Cobalt Catalyzed Fischer-Tropsch Products. *J. Catal.* **1993**, *139*, 591–601.

103. Huff, Jr., G. A.; Satterfield, C. N. Liquid Accumulation in a Fischer-Tropsch Fixed-bed Reactor. *Ind. Eng. Chem. Process Des. Dev.* **1985**, *24*, 986–995.

104. Wojciechowski, B. W. The Kinetics of the Fischer Tropsch Synthesis. *Catal. Rev.-Sci. Eng.* **1988**, *30*, 629–702.

105. Sarup, B.; Wojciechowski, B. W. Studies of the Fischer-Tropsch Synthesis on a Cobalt Catalyst. I. Evaluation of Product Distribution Parameters from Experimental Data. *Can. J. Chem. Eng.* **1988**, *66*, 831–842.

106. Schulz, H.; Van Steen, E.; Claeys, M., Olefin Formation, Hydrogenation and Isomerisation in the Kinetic Regime of Fischer-Tropsch Synthesis, in *Selective hydrogenation and dehydrogenation*, DGMK, Kassel, Germany, 1993 .

107. Komaya, T.; Bell, A. T., Estimates of Rate Coefficients for Elementary Processes Occurring during Fischer-Tropsch Synthesis over Ru/TiO_2. *J. Catal.* **1994**, *146*, 237–248.

108. Jordan, D. S.; Bell, A. T. Influence of Ethene on the Hydrogenation of CO

over Ruthenium. *J. Phys. Chem.* **1986**, *90*, 4797–4805.

109. Kuipers, E. W.; Scheper, C.; Wilson, J. H.; Oosterbeek, H. Non-ASF Product Distributions due to Secondary Reactions During Fischer-Tropsch Synthesis. *J. Catal.* **1996**, *158*, 288–300.

110. Kuipers, E. W.; Vinkenburg, I. H.; Oosterbeek, H. Chain Length Dependence of α-olefin Readsorption in Fischer-Tropsch Synthesis. *J. Catal.* **1995**, *152*, 137– 146.

111. Madon, R. J.; Iglesia, E.; Reyes, S. C. Non-Flory Product Distributions in Fischer-Tropsch Synthesis Catalyzed by Ruthenium, Cobalt, and Iron. *ACS Symposium Series, American Chemical Society* **1993**, *517*, 383–396.

112. Huff, Jr., G. A.; Satterfield, C. N. Intrinsic Kinetics of the Fischer-Tropsch Synthesis on a Reduced Fused-Magnetite Catalyst. *Ind. Eng. Chem. Process Des. Dev.* **1984**, *23*, 696–705.

113. Egiebor, N. O.; Cooper, W. C.; Wojciechowski, B. W. Carbon Number Distribution of Fischer-Tropsch CO-Hydrogenation Products from Precipitated Iron Catalysts. *Can. J. Chem. Eng.* **1985**, *63*, 826–834.

114. Yates, I. C.; Satterfield, C. N. Hydrocarbon Selectivity from Cobalt Fischer-Tropsch Catalysts. *Energy & Fuels* **1992**, *6*, 308–314.

115. Inoue, M.; Miyake, T.; Inui, T. Alcohol Synthesis from Syngas on Ruthenium Based Composite Catalysts. *J. Catal.* **1987**, *105*, 266.

116. Iglesia, E.; Vroman, H.; Soled, S. L.; Baumgartner, J. E.; Fiato, R. A. Selective Catalysts and Their Preparation for Catalytic Hydrocarbon Synthesis, US Patent 5,036,032 1991.

117. Huff, Jr., G. A.; Satterfield, C. N. Some Kinetic Design Considerations in the Fischer-Tropsch Synthesis on a Reduced Fused-Magnetite Catalyst. *Ind. Eng. Chem. Process Des. Dev.* **1984**, *23*, 851–854.

118. Stenger, H. G.; Satterfield, C. N. Effect of Liquid Composition on the Slurry Fischer-Tropsch Synthesis. 1. Rate of Reaction. *Ind. Eng. Chem. Process Des.*

Dev. **1985**, *24*, 407–411.

119. Bianchi, C. L.; Ragaini, V. Experimental Evidence of α-olefin Readsorption in Fischer-Tropsch Synthesis on Ruthenium-Supported ETS-10 Titanium Silicate Catalysts, *J. Catal.* **1997**, *168*, 70–74.
120. Fischer, F.; Pichler, H. *Brennstoff-Chemie.* **1939**, *20*, 247.
121. Steynberg, A.; Dry, M. E. Study in Surface Science and Catalysis. *Fischer-Tropsch Technology*; Elsevier: Boston, 2004, Vol. 152.
122. Davis, B. H. Overview of Reactors for Liquid Phase Fischer–Tropsch Synthesis. *Catal. Today.* **2002**, *71*, 249.
123. Jager, B. Developments in Fischer-Tropsch Technology. *Stud. Surf. Sci. Catal.* **1997**, *107*, 219.
124. Espinoza, R. L. Steynberg, A. P. Jager, B. Vosloo, A. C. Low Temperature Fischer–Tropsch Synthesis from a Sasol Perspective. *Appl. Catal. A: Gen.* **1999**, *186*, 13.
125. Atwood, H. E.; Bennett, C. O. Kinetics of the Fischer-Tropsch Reaction over Iron. *Ind. Eng. Chem. Process. Des. Dev.* **1979**, *18*, 163.
126. Bub, G.; Baerns, M. Prediction of the Performance of Catalytic Fixed Bed Reactors for Fischer-Tropsch Synthesis. *Chem. Eng. Sci.* **1980**, *35*, 348.
127. Jess, A. Popp, R. Hedden, K. Fischer-Tropsch-Synthesis with Nitrogen-rich Syngas: Fundamentals and Reactor Design Aspects. *Appl. Cat. A: Gen.* **1999**, *186*, 321.
128. Wang, Y. N. Xu, Y. Y.; Li, Y. W.; Zhao, Y. L.; Zhang, B. J. Heterogeneous Modeling for Fixed-Bed Fischer–Tropsch Synthesis: Reactor Model and Its Applications. *Chem. Eng. Sci.* **2003**, *58*, 867.
129. De Swart, J. W. A. Scale-Up of a Fischer-Tropsch Slurry Reactor. Ph.D. Thesis, University of Amsterdam, Netherlands, 1996.
130. De Swart, J. W. A.; Krishna, R.; Sie, S. T. Selection, Design and Scale Up of the Fischer-Tropsch reactors. *Studies in Surface Science and Catalysis* **1997**, *107*, 213-218.
131. Güttel, R.; Turek, T. Comparison of Different Reactor Types for Low Temperature Fischer–Tropsch Synthesis: A simulation Study. *Chem. Eng. Sci.* **2009**, *64*, 955.

132. Jess, A.; Kern, C. Modeling of Multi-Tubular Reactors for Fischer-Tropsch Synthesis. *Chem. Eng. Technol.* **2009**, *32*, 1164.

133. Keith, P. C. *Oil Gas J.* **1946**, *45*, 102.

134. Dry, M. E. Fischer-Tropsch synthesis over iron catalysts. *Cat. Lett.* **1990**, *7*, 241-251.

135. Dry, M. E. The Sasol Fischer-Tropsch Processes. In *Applied Industrial Catalysis*; Leach, B. E.; Ed. Academic Press, Vol. 2, 1983.

136. Dry, M. E. Industrials Chemicals via C_1 Processes. *ACS Symposium Series*, 328, 18-33.

137. Decker, W. D.; Fields, R. W. *Bubble Column Reactors*; Wiley: New York, 1992.

138. Jager, B.; Kelfkens, R. C.; Steynberg, A. P. A Slurry Bed Reactor for Low-Temperature Fischer-Tropsch. *Stud. Surf. Sci.* **1994**, *81*, 419-425.

139. Saxena, S. C. Bubble Column Reactors and Fischer-Tropsch Synthesis. *Catal. Rev. Sci. Eng.* **1995**, *37*, 227-309.

140. Krishna, R.; Ellenberger, J.; Sie, S. T. Reactor Development for Conversion of Natural Gas to Liquid Fuels: A Scale-up Strategy Relying on Hydrodynamic Analogies. *Chem. Eng. Sci.* **1996**, *51*, 2041-2050.

141. Maretto, C.; Krishna, R. Modeling of a Bubble Column Slurry Reactor for Fischer-Tropsch Synthesis. *Catalysis Today* **1999**, *52*, 279-289.

142. Rao, V. U. S.; Stiegel, G. J.; Cinquegrane, G. J.; Srivastave, R. D. Iron-Based Catalysts for Slurry-Phase Fischer-Tropsch Process: Technology Review. *Fuel Process. Technol.* **1992**, *30*, 83–107.

143. Xu, L.; Bao, S.; O'Brien, R. J.; Raje, A.; Davis, B. H. Don't Rule out Iron Catalysts for Fischer-Tropsch synthesis. *CHEMTECH.* **1998**, *8*, 47–53.

144. Raje, A. P.; Davis, B. H. Fischer-Tropsch Synthesis: Process Considerations Based on Performance of Iron-Based Catalysts. *Fuel* **1997**, *76*, 273–280.

145. Rider, D. K. *Energy: Hydrocarbon Fuels and Chemical Resources*; John Wiley: New York, 1981.

146. Jager, B.; Dry, M. E.; Shingles, T. Steynberg, A. P. Experience with a New Type of Reactor for Fischer-Tropsch Synthesis. *Catal. Lett.* **1990**, *7*, 293.

147. Vernon, P. D. F.; Green, M. L. H.; Cheetham, A. K.; Ashcroft, A. T. Partial Oxidation of Methane to Synthesis Gas. *Catal. Lett.* **1990**, *6*, 181.

148. Abbott, J.; Crewdson, B. Oil & Gas J. **2002**, *100*, 70.

149. Choudhary, V. R.; Mondal, K. C.; Mamman, A. S. High-Temperature Stable and Highly Active/Selective Supported Ni/Co/Mg/CeOx Catalyst Suitable for Autothermal Reforming of Methane to Syngas. *J. Catal.* **2005**, *233*, 36.

150. Biesheuvel, P. M.; Kramer, G. J. Two-section Reactor Model for Autothermal Reforming of Methane to Synthesis Gas. *AIChE J.* **2003**, *49*, 1827.

151. Choi, G. N.; Kramer, S. J.; Tam, S. T.; Fox, J. M., Design/Economics of a Natural Gas Based Fischer-Tropsch Plant, in *Spring National Meeting*, American Institute of Chemical Engineers, Houston, 1996 .

152. Choi, G. N.; Kramer, S. J.; Tam, S. T.; Fox, J. M.; Carr, N. L.; Wilson, G. R. Design/Economics of a Once-Through Natural Gas Based Fischer-Tropsch Plant with Power Co-production, in *Coal Liquefaction and Solid Fuels*, Pittsburgh, 1997 .

153. Fox, J. M. The Different Catalytic Routes for Methane Valorization: An Assessment of Processes for Liquid Fuels. *Catal. Rev.-Sci. Eng.* **1993**, *35*, 169–212.

154. Gregor, J. H. Fischer-Tropsch Products as Liquid Fuels or Chemicals: An Economical Evaluation. *Catal. Lett.* **1990**, *7*, 317–332.

CHAPTER 3

EXPERIMENTAL

3.1 Introduction

The performance of the FT reaction at the laboratory scale demands a cautious handling of various parameters which can affect the final outcome of the experiment. The system is complex as it involves a large spectrum of products usually distributed in the gas, liquid and solid phases. The performance of the FTS could be affected by a variety of factors including the operation conditions and the reactor system. The main motivation of the work is to get a better understanding for Fischer-Tropsch Synthesis, and thus only a simple and typical catalyst namely a TiO_2 supported Co catalyst (without any promoter) was used for all the experiments. Three types of reactors, namely tubular fixed bed (TFBR), continuous stirred tank reactor (CSTR), and batch reactor (BR) are used in this work so that the data collected in the experiments are comprehensive. All the FT experiments in all these three reactors were carried out in a gas-solid regime so that the influence of the products could be investigated and again, the results from different types of reactors offered us more insights into FTS. Some novel experiments such as flushing treatments to the reactor system, when the steady state of the reaction was accomplished, were designed over and above the FTS experiments and extra and valuable information was collected from these tests. The data for the experiments were collected both at transient (the early stage after the reaction started) and steady state stages of the experiment.

In this section, we describe the general procedure that was followed to carry out the FT experiments. As many experiments were performed using different

systems in this study, this section only presents a general procedure and description of equipment. The specific details on the experimental data measurement will be described for each system used and experimental design in the appropriate chapter. We also describe the principles and methods that were used to characterize the catalysts and process the original data.

3.2 Experimental Set-up and Reactors

3.2.1 Experimental Set-up

In this study, a continuously stirred tank reactor (CSTR) (Autoclave Engineers) and a tubular fixed bed reactor (TFBR) (Autoclave Engineers) are used to run Fischer-Tropsch synthesis experiments. They were set up in two individual rigs but share the same feed and the analysis system. The set-ups of these two rigs are illustrated in Figures 3-1 and 3-2 respectively. The details of the rig, taking the one contains TFBR, are described below.

Syngas was supplied by a synthesis cylinder (Afrox UHP) and its flow rate controlled by a Mass Flow Controller (Brooks Instrument 5850，max. pressure: 100bar). It was preheated to the required experimental temperature by hot ceramic balls located at the top part of the reactor. The products and reactants that had not been consumed were sent from the bottom of the reactor to the product traps. To prevent condensation, the product tubes leading from the reactor down to the high-pressure hot trap (P=pressure of the reactor, T = 150°C) were heated and insulated to maintain a temperature of 200°C. Condensed wax products were removed before and after each mass balance run. The uncondensed stream was fed to the high-pressure cool trap (P=PR, T=25°C) to separate oil and aqueous products, which were removed at the same time when wax was collected. The pressure of the reactor and the two traps was controlled by a back pressure

regulator (Swagelok 0-34.4bar), which was placed next to the cool trap. The back pressure regulator reduced the pressure of the gaseous stream containing the gas phase products and unreacted feed to atmospheric level, after which the stream passed through the sampling loops mounted on an online gas chromatograph (GC) (Agilent 6890A) with a thermal conductive detector (TCD) and flame ionization detector (FID). The gaseous stream was then sent from the sampling loops to a bubble meter and finally to a vent. Two samples from the gaseous stream were taken via sample valves from the sampling loops every 2.35 hours, and analysed by the online GC. The product tubes in between the wax trap and the GC were heated to 150°C to prevent product condensation. One piece of 1/16" OD thermocouple (ANATECH) with 1/8" OD thermocouple wells was placed vertically in the centre of the reactor tube, to monitor the bed centre temperature during the FTS reaction.

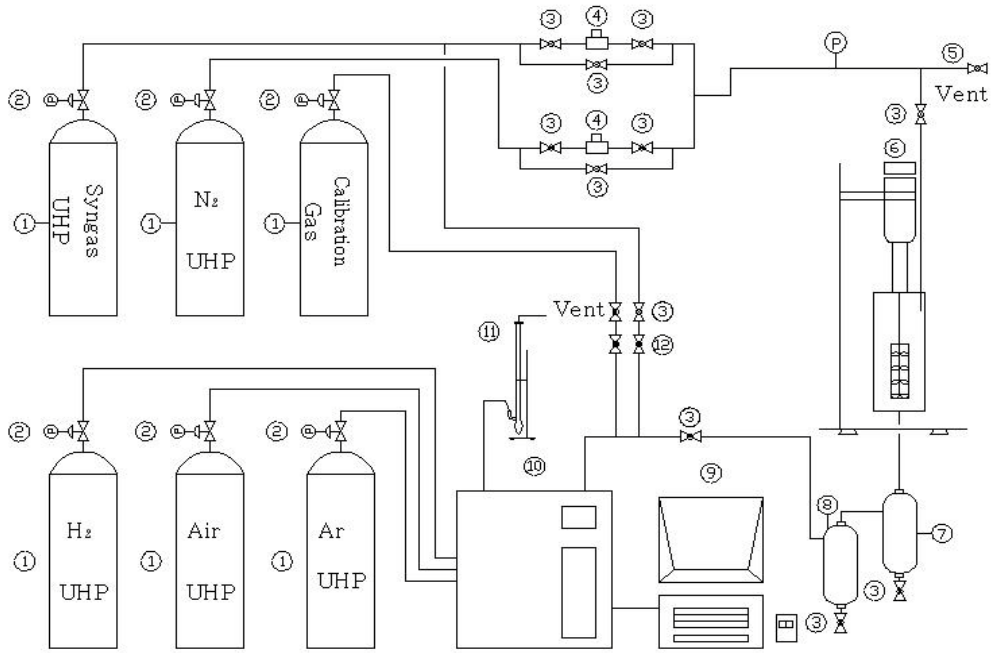

1. gas cylinders; 2. regulators; 3. shut-off valves; 4. mass flow controllers; 5. vent valve; 6. continuous stirring tank reactor; 7. wax trap; 8. liquid trap; 9. data collection; 10. gas chromatograph; 11. Flow meter; 12. non-return valve

Fig. 3-1 The experiment set-up with a continuous stirred basket reactor

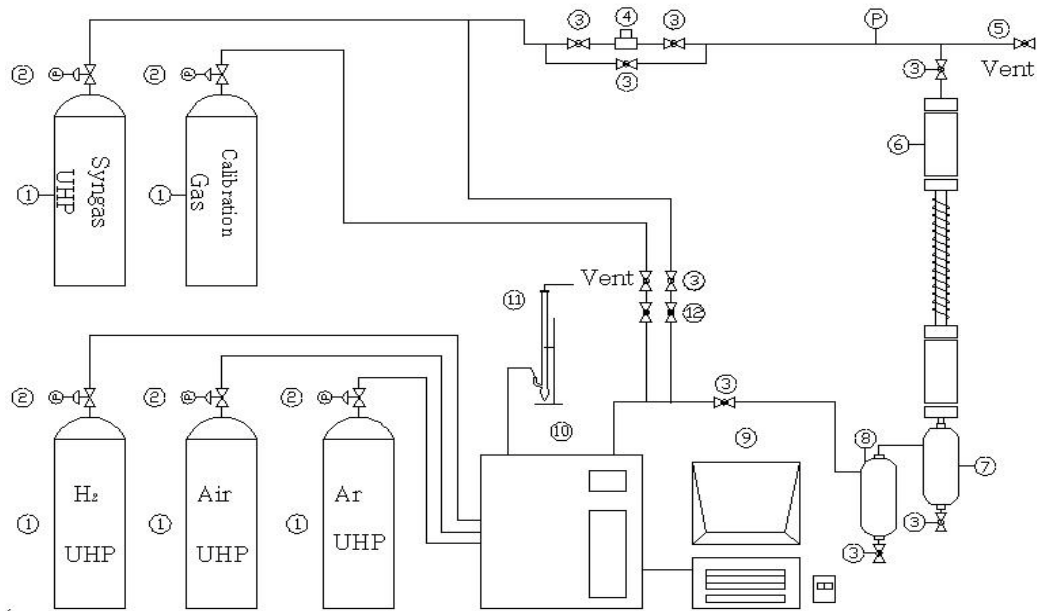

1. gas cylinders; 2. regulators; 3. shut-off valves; 4. mass flow controllers; 5. vent valve; 6. continuous stirring tank reactor; 7. wax trap; 8. liquid trap; 9. data collection; 10. gas chromatograph; 11. flow meter; 12 non-return valve

Fig. 3-2 The experimental set-up with a tubular fixed bed reactor

3.2.2 Reactors

The Continuous Stirred Tank Reactor

The CSTR is supplied by *Autoclave Engineers*, the layout of the reactor is presented in Figure 3-3. The volume of the cylindrical tank is 100 ml and its dimension is as follows: H = 9.8 cm, OD = 4.6 cm. During all the experimental runs (CSTR mode or Batch mode), the feed material was fed to the reactor from the feed port on top of the tank and all the products and un-reacted feed materials left the reactor continuously from the product outlet at the bottom of the tank. The reactor was heated by a heating jacket covered on the tank and temperature of the reactor was controlled by a separated control module.

There is a stirrer in the geometrical centre of the tank to supply a mixing force to the material in the reactor. It is connected to the magnetic motor above the tank and its stirring speed is controllable in a range of 0-3200 rpm. A representation of the stirrer is given in Figure 3-4 below.

The catalyst for the experiment is loaded in a basket, which is supplied with the reactor. The structure of the basket is illustrated in Figure 3-5. The cage was made by dual-layer stainless steel wires and the size of the holes on it is around 0.3 mm, which can prevent the leaking of the catalyst from the basket to the product stream. The fins on the side of the basket is designed to contact with the inner wall of the tank to ensure that there is no shaking or movement for the basket and the catalyst inside when the stirrer stirs.

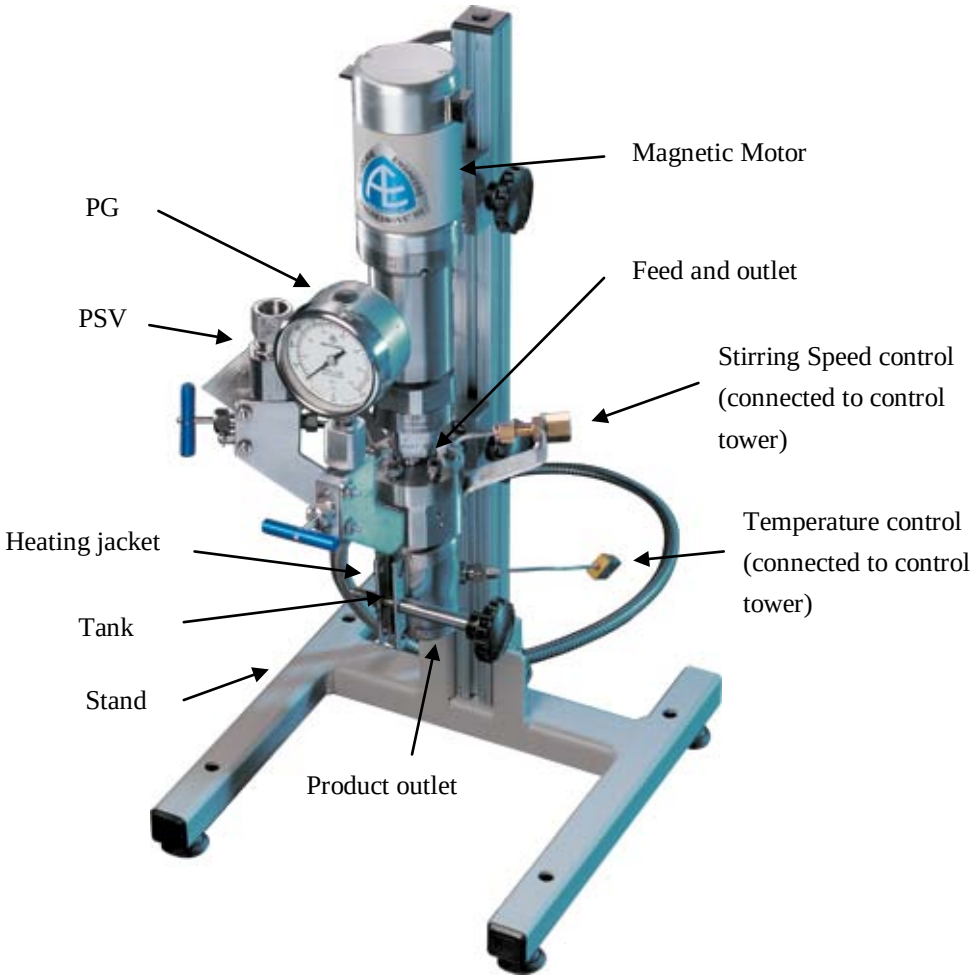

Fig. 3-3 The layout of the continuously stirred tank reactor

Fig. 3-4 The layout of the stirrer

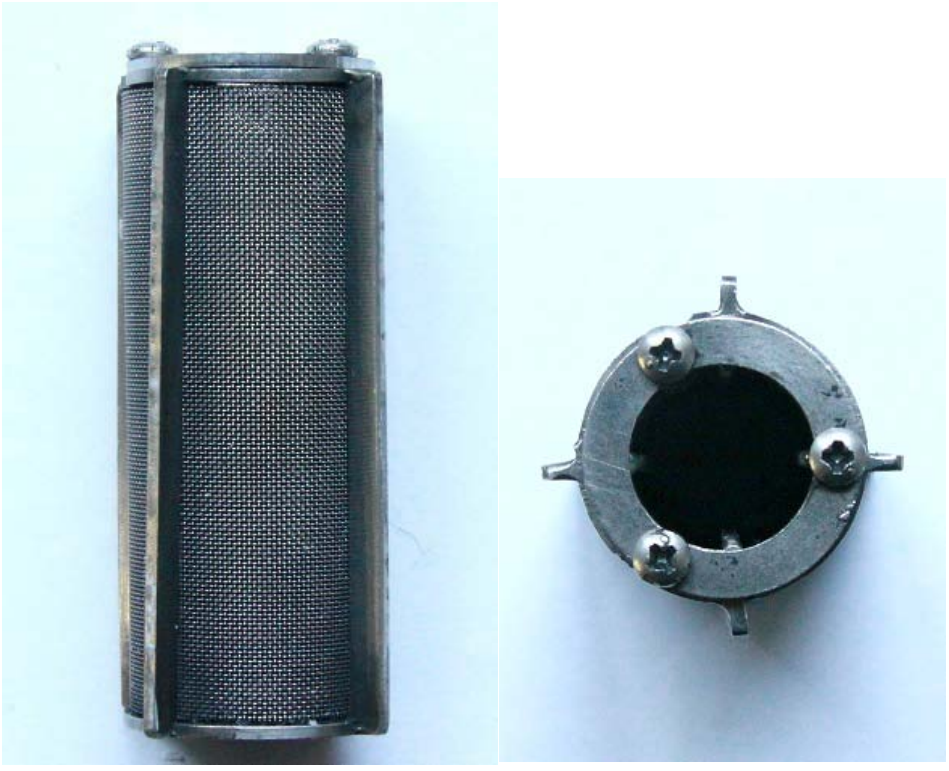

Side view **Top view**

Fig. 3-5 The structure of the catalyst basket

Residence time distribution test for the CSTR

When we use a tank reactor, we would like to eliminate any influence from the reactor itself to the result of the FT reaction. Therefore, we tested the residence time distribution (RTD) of the reactor to confirm with what operation parameter of the reactor (mainly the stirring speed for the mixing) it would perform as a real CSTR before conducting any reaction in it. As the reactor was going to be used for a gas-solid reaction system, the test was conducted at FT reaction conditions (temperature and pressure) with gas only. H_2 was used as the test gas because of two reasons: a, one of the reactants in the future experiments, and b, short retention time in the GC analysis so that as many as possible data points could be acquired. Argon gas was chosen as the dilution medium as it was the reference gas of the GC so that no peak will be shown for argon to disturb the H_2 peak. The details of the test for the CSTR are described below.

For a CSTR, the volume is V, assuming perfect mixing, at time 0, the tracer is injected into the reactor very rapidly. There is no reaction in the reactor, thus the inlet flow rate F equals to the outlet flow rate. The concentration of the tracer in the tank is $C_{A,0}$ at time 0 and C_A at time t. The mass balance for the tracer can be written as Eq. 3-1[1]:

$$-V\frac{dC_A}{dt} = FC_A \tag{3-1}$$

Integrate from time 0 to time t in Eq. 3-1, we can get Eq. 3-2:

$$LnC_A = -\frac{F}{V}t + LnC_{A,0} \tag{3-2}$$

Mean residence time can be written as: $\tau = \frac{V}{F}$, Eq. 3-2 therefore can be written as Eq. 3-3:

$$LnC_A = -\frac{1}{\tau}t + LnC_{A,0} \tag{3-3}$$

The mean residence time can be calculated from the slope of the Eq. 3-3 and the volume of the reactor over the flow rate of the stream, which is written in Eq. 3-4,

$$\tau_{\text{theoretial}} = \frac{V}{F} = \frac{P_{CSTR} \times \frac{T_{out}}{T_{CSTR}}}{P_{out}} \times \frac{V_{CSTR}}{F_{out}} \tag{3-4}$$

Once the $Ln(C_A) - t$ is a straight line and the mean residence time calculated from the slope of this straight line matches well with the result derived by Eq. 3-3, we then can tell that the mixing in the CSTR is ideal and the reactor can be regarded as a real CSTR.

During RDT tests, the reactor was operated at reaction temperatures and pressures (T = 190-250, P = atmospheric to 25 bar) with argon feed to the reactor continuously. At time 0, a small amount of H_2 from another cylinder was injected into the argon feed line quickly (the injection time is less than 1 second). In the mean time the online GC started to take samples continuously from the outlet of the reactor and performed an analysis every 2 minutes. For each individual test, a certain SS was applied and the SS was varied from 0 to 1100 rpm. One of the test results is given in Figure 3-7. The results showed that the mixing inside the reactor was ideal when SS was higher than around 65 rpm. From Figure 3-6 we can see that $\ln(C_A) - Time$ curve is a straight line which tells us that the behaviour of the mixing is satisfactory and the reactor can be considered to be a real CSTR.

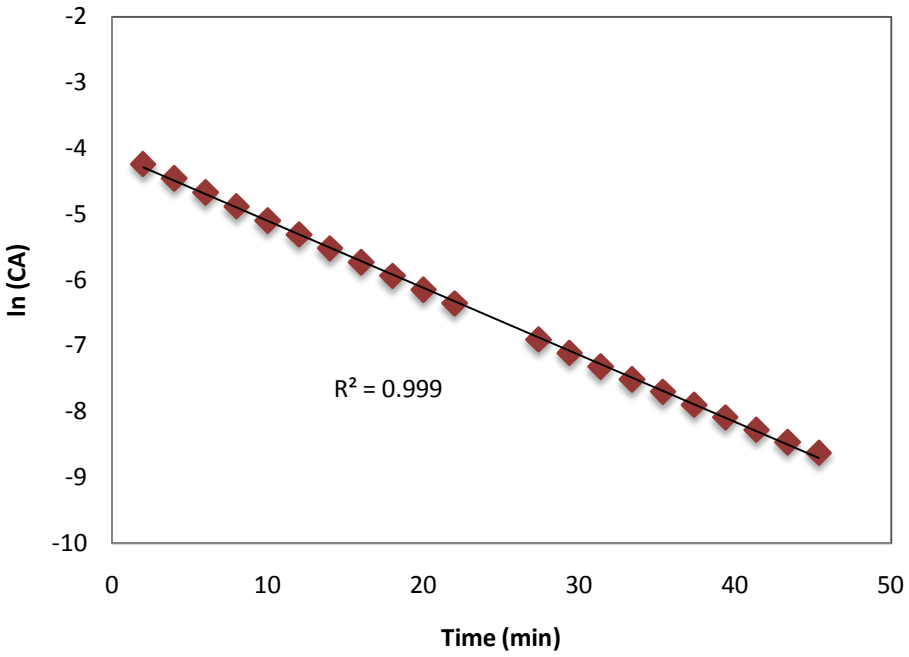

Fig. 3-6 RTD curve when stirring speed is 65rpm

The RTD test result when the stirring speed was 0 is given in Figure 3-7. The curve behaviour shows that at these conditions, the reactor is very far from behaving like a real CSTR since the curve isn't linear.

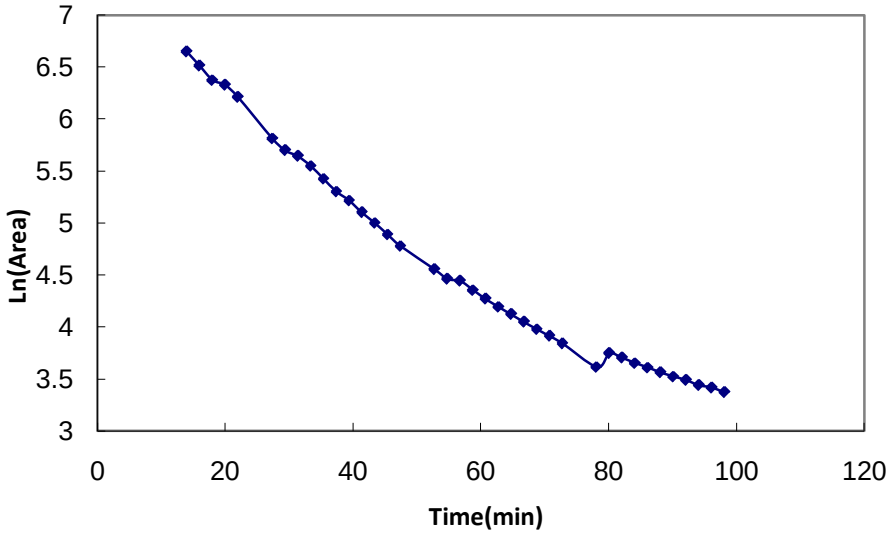

Fig. 3-7 RTD curve when stirring speed is 0

This reactor is going to be used as a CSTR and a batch reactor depends on the demands of the experimental work. The details of the reactor running mode and related operations are going to be described in the corresponding chapters that follow.

Tubular Fixed Bed Reactor

The tubular fixed bed reactor is supplied by Autoclave Engineers. The dimensions and the specifications of the reactor are given in Figure 3-8 and Table 3-1 respectively.

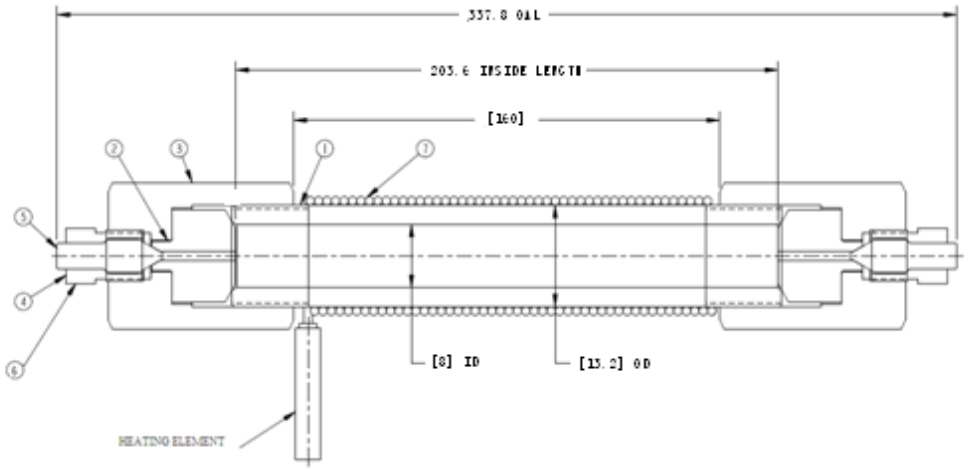

1. Body; 2. Cover; 3. Coupling; 4. Gland; 5. Plug; 6. Collar; 7. Cable heater

Fig. 3-8 The tubular fixed bed reactor used in the experiments

Table 3-1 The specification of the tubular fixed bed reactor used in the experiments

Parameters	Value
Full length (mm)	337.8
Tube length (mm)	203.6
Inner diameter (mm)	8.0
Outer diameter (mm)	13.2
Maximum allowable working pressure (bar)	379bar at 400^{o}C
Minimum design metal temperature (^{o}C)	-29^{o}C at 379bar

This reactor is placed vertically on the rig and used as an integral reactor. In the experiments, around 1 g catalyst was loaded in the central part of the tube, while the remaining space was filled with stainless steel balls with a diameter of 2-3 mm. A thin layer of quartz wool was put at either end of the catalyst bed to prevent the loss of the catalyst. The reactor was heated by three independent heating jackets along the axial direction to make sure the temperature profile of the catalyst bed was flat. The reactor was covered by a thermal blanket to prevent heat loose.

Isothermal test for the tubular fixed bed reactor

Because of the high exothermic nature of the FT reaction, a proper diameter for a fixed bed reactor is necessary to prevent the temperature overshooting in the catalyst bed. In this research, care has to be taken that the catalyst bed is operated isothermally, as non-isothermal operation could make the results obscure and thus making correlation of the results to the operation conditions difficult. The ID of the reactor was 8mm, which is quite small for a fixed bed reactor used for the study of FTS. The temperature profiles of the centre of the bed without and with reaction were measured. An example is presented in Figure 3-9. The difference between the central and wall control temperatures along the catalyst loaded part of the reactor was only 0.3 ^{o}C (the catalyst bed took less than 15 mm in the middle part of the reactor) so that the reactor could be regarded as isothermal.

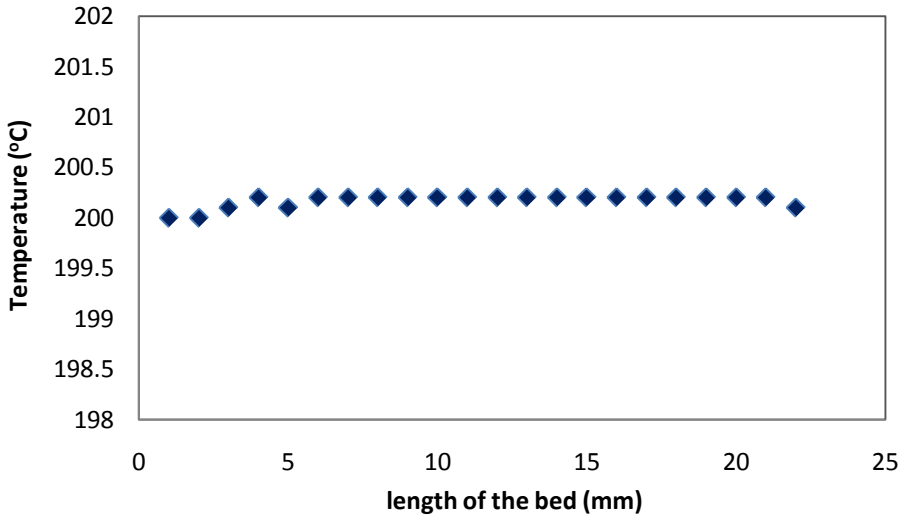

Fig. 3-9 Central temperature profile of the reactor for the part for the catalyst bed

3.3 Catalyst

As this work is not particularly focused on developing and testing any new catalysts but more on investigating the reaction behaviour of Fischer-Tropsch, a basic supported cobalt without any promoter was prepared and used for all the work conducted in this thesis. The preparation of the catalyst follows a classic impregnation procedure, and basic characterizations were performed, which include the temperature programmed reduction (TPR) and Brunauer-Emmett-Teller (BET) test.

3.3.1 Catalyst Preparation

The catalyst used in this thesis is supported cobalt catalyst with 10% Cobalt / 90% TiO_2. Cobalt: Sigma-Aldrich $Co(NO_3)_2.6H_2O$; TiO_2: Degussa Titania (TiO_2) P25, Surface area (SA) = 50 m^2g^{-1}.

Catalyst preparation procedure:

a. Mix TiO_2 with distilled water in a mass ratio of 1:1 to make a paste. Make

sure the paste is well mixed;

b. Dry paste at 120°C for 2 hours;
c. Move this dried paste to a crucible and calcine it in a Muffle oven at the following temperature program. The oven temperature was ramped at 5°C/min until it reached 400°C, and kept at this temperature for 6 hours. It was left to cool down overnight;
d. Crush the support after it cools down; choose the particle size between 0.5mm and1mm for catalyst preparation;
e. Take 1g support; use distilled water to evaluate the pore volume of the support;
f. Weigh $Co(NO_3)_2.6H_2O$ after calculating the 10% metal loading according to the mass of the support;
g. Dissolve $Co(NO_3)_2.6H_2O$ in distilled water in a volume calculated based on the result of step e.;
h. Mix the support and $Co(NO_3)_2.6H_2O$ solution well and dry at 120°C for 2 hours;
i. Repeat step c and seal the catalyst in vials for later experiments.

3.3.2 Catalyst Characterization

Temperature Programmed Reduction (TPR)

In this work, the TPR test of the catalyst was mainly for confirming a suitable reduction temperature and period for the catalyst. The TPR analysis was performed in the TPR apparatus where 0.1 g of catalyst sample (the same size as it used for the experiments) was placed in a U-shaped quartz tube reactor and exposed to a flow of pure nitrogen at 150°C for 30 min prior to the catalyst reduction. The reduction was done using a 5% H_2 in Ar gas mixture at a flow rate of 5 ml/min. The temperature was increased at 10 ^{o}C/min for 35 min and then

maintained at 350°C for 60 minutes. The hydrogen uptake was measured using a TCD at the exit of the reactor. The TPR result for the catalyst is shown in Fig. 3-10.

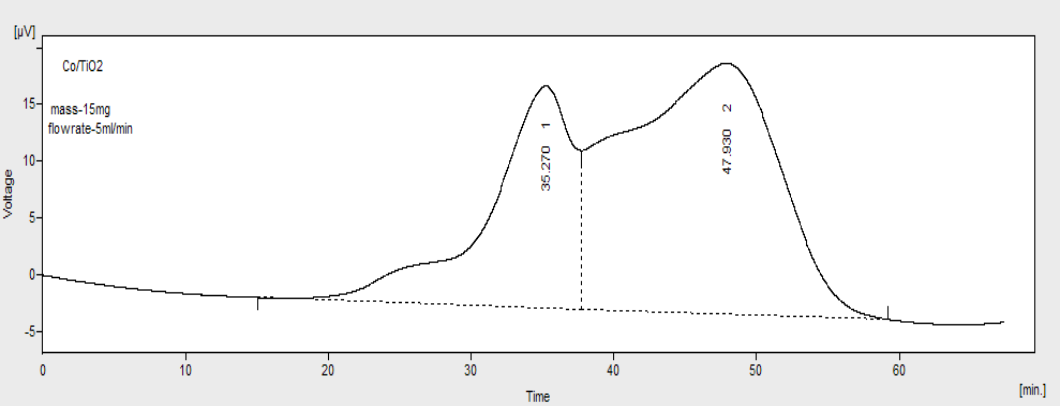

Fig. 3-10 TPR result for the prepared catalyst

The TPR result shows that the signal started to deviate from the base line at a time of around 20min, which corresponded to 200°C, which tells us that the reduction of Co_3O_4 started.

BET analysis

N_2 physisorption was employed for surface-area determination and pore volume measurements of the calcined catalysts. The samples were degassed using N_2 at 150ºC for 2 hours before being measured. N_2 adsorption-desorption isotherms at the N_2 boiling point (-196ºC) were measured on a Micromeritics TRISTAR 3000 analyser. The surface areas were determined by the Brunauer-Emmett-Teller (BET) method. The result of this test is given in Table 3-2 below.

Table 3-2 Properties of the catalyst

Catalyst	Co/TiO_2
Catalyst particle size (mm)	0.5-1
Catalyst surface area (m^2/g)	28.6
Catalyst pore volume (cm^3/g)	0.26
Average pore diameter (nm)	35.8

3.4 Product Analysis

The system of analysis used in this study is illustrated in Figure 3-11 below. The total product stream was split into three phases: a wax phase (high pressure hot trap), an oil phase (high pressure cool trap), and a low pressure gaseous phase.

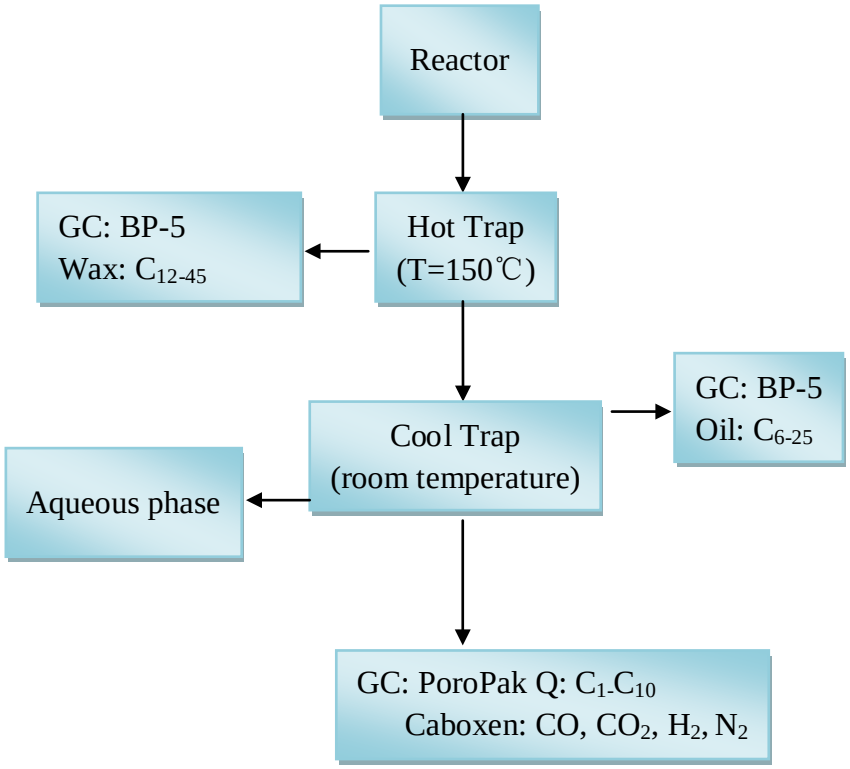

Fig. 3-11 Scheme of the liquid and gaseous streams for analysis

The gaseous phase was analysed with a Hewlett-Packard 6980A gas chromatograph (GC). The gaseous components were CO, H_2, N_2, CO_2, linear paraffins C_1-C_{10}, and α-olefins C_2-C_5. The GC was equipped with two series of sampling loops and sample valves. Two samples were taken simultaneously and each was injected into a parallel column. The H_2, CO, CO_2, and N_2 components were separated on a Carboxen packed column (support: Carboxen 1000; support size: 80/100 mesh; length/OD: 1.5m×1/8” and analysed by means of aTCD; and the hydrocarbon products were separated onto a Poropak-Q packed column (support: Porapak Q; support size: 80/100 mesh; length/OD: 2m×1/8”) and

detected with an FID. Argon (Afrox 99.99%) was used as carrier gas for both of the detectors.

The initial temperature of the oven (35°C) was maintained for 5 minutes, after which it was increased to 200°C at the rate of 3°C/min. Once it had reached 200°C, that temperature was maintained for 60 minutes. The total online analysis time was 120 minutes. During this two-hour period, all the components of interest were eluted.

The GC was connected to a personal computer on which all the information provided by the GC was captured and stored, using the GC software ChemStation. The GC-related parameters are listed in Table 3-3, and a typical online gas chromatogram is shown in Figure 3-12.

The GC was calibrated with a premixed gas in which all the molar fractions for the gases were known. This mixture contained H_2, CO, CO_2, N_2, CH_4, C_2H_4, and C_2H_6, which covered the entire range of permanent gases that might appear in the experiments. The composition of the calibration gas is given in Table 3-4. The C_1 and C_2 hydrocarbons were calibrated directly, and the remaining hydrocarbons in the gas phase were calculated using the calibration for C_2 and the corresponding response factors. The details of the mass balance calculation will be described in the section that follows.

The analysis of the oil and wax products was carried out using an off-line GC with an FID on a DB-5 capillary column. For the analysis of these condensed phases, a mass composition was directly obtained from the GC peak area percentages, as the mass response factors were around one. Peak identification was performed using an injection of pure components. The typical GC analysis shows traces of oil and wax products as shown in Figures 3-13 and 3-14 respectively.

Table 3-3 Parameters of online GC

Detector	TCD	FID
Column	Carboxen	Poropak Q
Temp, sample valve (^oC)	180	180
Temp, inlet (^oC)	120	120
Temp, detector (^oC)	200	230
Temp, oven program		
Initial temp (^oC)	35	35
Hold time (min)	5	5
Ramping rate (^oC /min)	3	3
Final Temp (^oC)	220	220
Hold Time (min)	60	60
Gas flow rate (ml/min)		
Carrier gas (Ar)	30	20
Reference gas (Ar)	15	-
H_2	-	20
Air	-	200
Inlet pressure (kPa)	120	120

Table 3-4 Components and compositions of the calibration gas

Component	Mole percentage (%mol)
H_2	52.83
CO	29.1
CO_2	5.0
N_2	9.9
CH_4	2.5
C_2H_4	0.19
C_2H_6	0.48

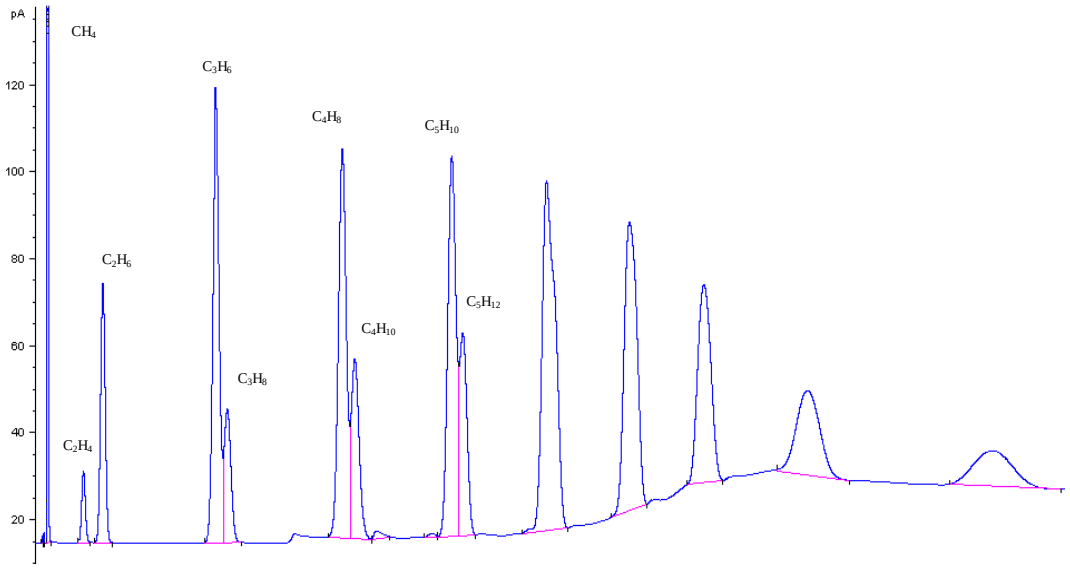

Fig. 3-12 An online GC trace for hydrocarbons in tail gas

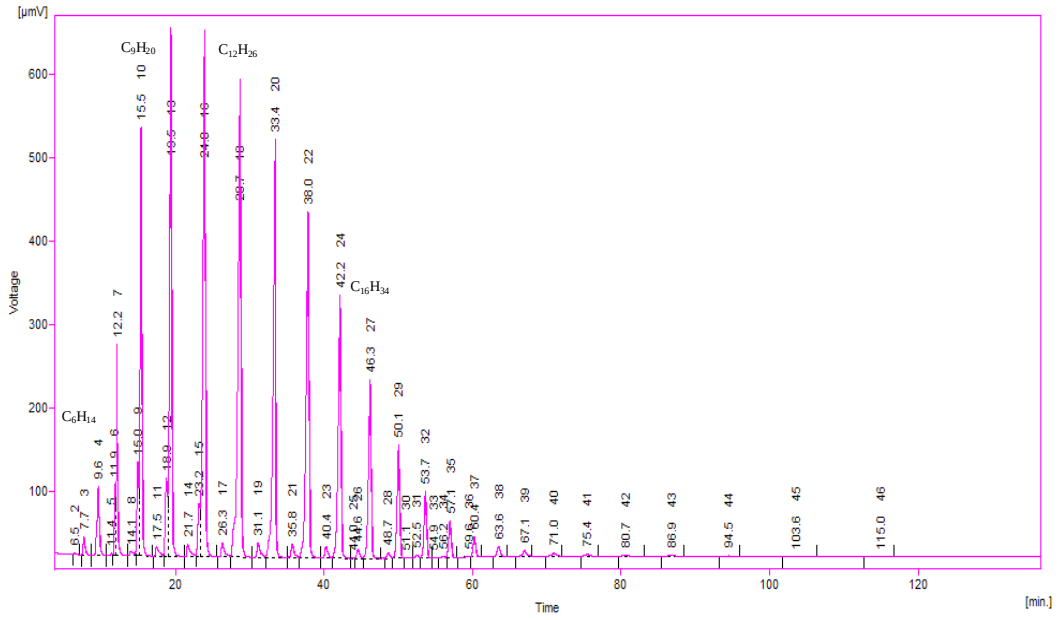

Fig. 3-13 A GC trace for analysis of oil from cool trap

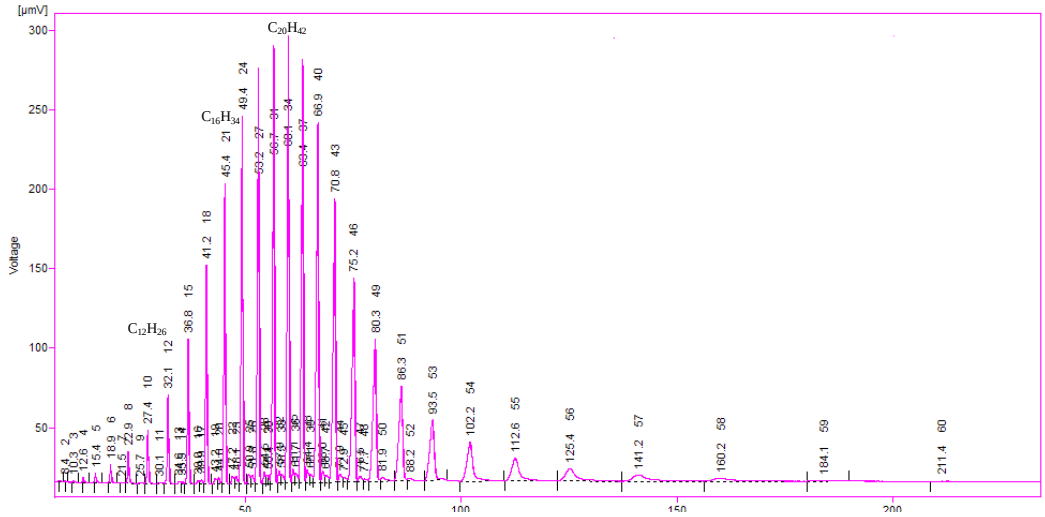

Fig. 3-14 A GC trace for analysis of wax from hot trap

3.5 Mass balance calculation

The calculations used to determine the mass balance are similar to those used by Duvenhage [2], Mokoena [3], Bahome [4], Phadi [5], and Price [6].

The molar percentage of a compound in the gas was calculated as:

$$\%\theta_{gas} = \left(\frac{A_{\theta,gas}}{A_{\theta,cal}} \right) \times \%\theta_{cal} \qquad (3\text{-}5)$$

where: $\%\theta_{gas}$ = molar percentage of compound θ in the analysed gas;

$A_{\theta,\ gas}$ = integrated area of the GC peak corresponding to the compound θ in the analysed gas;

$A_{\theta,\ cal}$ = integrated area of the GC peak corresponding to the compound θ in the calibration mixture;

$\%\theta_{cal.}$ = molar percentage of compound θ in the calibration mixture.

For compounds for which calibration data could not be obtained directly from the calibration mixture, calibration data of a reference compound and relative molar response factors were used. The following expression was used:

$$\%\theta_{gas} = \left(\frac{A_{\theta,gas}}{A_{\alpha,cal}} \right) \times \%\alpha_{cal} \times RF_{\theta,\alpha} \quad (3\text{-}6)$$

where: $\%\alpha_{cal.}$ = molar percentage of the reference compound θ in the calibration mixture; $A_{\alpha,cal}$ = integrated area of the GC peak corresponding to the reference compound α in the calibration mixture and $RF_{\theta,\alpha}$ = relative response factor of the compound θ with respect to the reference compound α. C_2H_4 was used as reference for olefins, and C_2H_6 was used as reference for paraffins. Molar response factors for hydrocarbon products are presented in Table 3-5.

Table 3-5 Response factors for hydrocarbons (C_2 as reference)

Carbon Number	Olefin	Paraffin
2	1	1
3	0.7	0.74
4	0.55	0.55
5	0.47	0.47
6	0.4	0.4
7	0.35	0.35
8	0.32	0.32
9	0.28	0.28
10	0.24	0.24
11	0.21	0.21
12	0.19	0.19
13	0.18	0.18
14	0.17	0.17
15	0.15	0.15

Mass balance calculations.

The configuration of the experimental set-up used in this study (Figures 3-1 and 3-2) allows setting the inlet volumetric flowrate, from which the outlet flow rate can be calculated. N_2 was used in the reactor feed to serve as an internal standard. As it is an inert gas during the FT reaction, N_2 is present only in the feed stream and in the reactor outlet gas stream. The N_2 balance across the reactor is therefore expressed as:

$$F_{in} \times X_{N_2,in} = F_{out} \times X_{N_2,out} \tag{3-7}$$

where: F_{in} = total molar flowrate [mol/min] of the reactor feed;

F_{out} = total molar flowrate [mol/min] of the reactor outlet gas stream;

$X_{N2,\,in}$ = molar fraction of nitrogen in the reactor feed;

$X_{N2,\,out}$ = molar fraction of nitrogen in the reactor outlet gas.

The rate of CO conversion can be calculated as follows (restricted to CSTR and PFR; reaction rate for batch experiments will be explained in Chapter 6):

$$-r_{CO} = \frac{F_{CO,in} - F_{CO,out}}{m_{cat}} \tag{3-8}$$

Where: $F_{CO,in}$ = molar flowrate [mol/min] of CO in the reactor feed;

$F_{CO,out}$ = molar flowrate [mol/min] of CO in the reactor outlet gas;

$m_{cat.}$ = mass [gram] of catalyst;

r_{CO} = rate of CO conversion [mol/min/g$_{cat}$].

$$F_{CO,in} = F_{in} \times X_{CO,in} \tag{3-9}$$

$$F_{CO,out} = F_{out} \times X_{CO,out} \tag{3-10}$$

Where $X_{CO,in}$ and $X_{CO,out}$ are the CO molar fraction in the reactor feed and outlet gas respectively.

After introducing expressions (3-9) and (3-10) in expression (3-8) and after expressing F_{in} as a function of F_{out} using equation (3-7), the rate of CO consumption rate was expressed as:

$$-r_{CO} = \frac{F_{out} \times [X_{CO.in} \times (\frac{X_{N_2,out}}{X_{N_2,in}}) - X_{CO,out}]}{m_{cat}} \quad (3\text{-}11)$$

In this thesis, Equation (3-12), given below, was used to calculate the rate of CO conversion directly, as $X_{CO,in}$ and $X_{N2,\,in}$ were known from the premixed gas cylinder and $X_{CO,\,out}$ and $X_{N2,\,out}$ were derived from the reactor outlet gas analysis. F_{out} was also calculated from the total gas volumetric flow rate at the reactor exit by assuming the ideal gas law.

The CO conversion was calculated as follows:

$$\%CO_{conv} = \frac{[X_{CO,in} - X_{CO.out} \times (\frac{X_{N_2,in}}{X_{N_2,out}})] \times 100}{X_{CO,in}} \quad (3\text{-}12)$$

The rate of formation of a gas product θ_i was calculated as follows:

$$r_{\theta_i} = \frac{F_{out} \times X_{\theta_i.in}}{m_{cat}} \quad (3\text{-}13)$$

where $r_{\theta i}$ is the rate in mole/min/gcat and $X_{\theta}\,i$ the molar fraction of product θ_i in the reactor outlet gas.

The carbon balance was checked as follows:

$$[nC]_{gas,\,product} + [nC]_{liquid,\,product} + [nC]_{wax,\,product} = -r_{CO} \times t \times m_{CO} \quad (3\text{-}14)$$

where *nC* represents the total number of moles of carbon contained in a product fraction (gas, liquid or wax) at the end of the mass balance period, *t.*

The error on the carbon balance was calculated as:

$$\%error = \frac{\left\{-r_{CO} \times t \times m_{CO} - [nC]_{gas,\,product} - [nC]_{liquid,\,product} - [nC]_{wax,\,product}\right\}}{-r_{CO} \times t \times m_{CO}} \quad (3\text{-}15)$$

The carbon balance was considered satisfactory when the % error was < 5%.

The product selectivity was calculated on moles of carbon basis, as follows:

$$Sel(\theta) = \frac{[nC]_{\theta}}{-r_{CO} \times t \times m_{cat}} \quad (3\text{-}16)$$

where *Sel(θ)* represents the selectivity of product θ and $[nC]_{\theta}$ represents the moles of carbon contained in the product θ.

Olefin/paraffin ratio

Olefin/paraffin (O/P) ratio considered the relative molar amount for the same carbon number in the outlet stream, which was calculated as follows:

$$O_n / P_n = \frac{N_{C_nH_{2n}}}{N_{C_nH_{2n+2}}} \quad (3\text{-}17)$$

Olefin/olefin ratio

Olefin/olefin (O_n/O_{n-1}) ratio looked at the relative molar amount for the neighbouring olefins in the outlet stream, which was calculated as follows:

$$O_n / O_{n-1} = \frac{N_{C_nH_{2n}}}{N_{C_{n-1}H_{2(n-1)}}} \quad (3\text{-}18)$$

Normalized molar fraction for C_nH_{2n}, C_nH_{2n+2}, and $C_{n+1}H_{2(n+1)}$

Normalized molar fraction (NMF) looked at the relative molar fraction for C_nH_{2n}, C_nH_{2n+2}, and $C_{n+1}H_{2(n+1)}$, which was calculated with the following equation:

$$NMF = \frac{N_i}{\sum N_i} \quad (3\text{-}19)$$

In which N_i represents the molar amount of C_nH_{2n}, C_nH_{2n+2}, and $C_{n+1}H_{2(n+1)}$.

3.6 Reference

1. Denbigh, K. G.; Turner, J. C. R. Chemical Reactor Theory, Third Edition. Cambridge University Press, Cambridge. 1984.
2. Duvenhage, D.J. The Preparation, Characterization and Evaluation of Titania Supported Fe:Co Bimetallic Catalysts for the Hydrogenation of CO, PhD Thesis, University of the Witwatersrand, Johannesburg (1994).
3. Mokoena, E.M. Synthesis and use of silica materials as support for the Fischer-Tropsch reaction, PhD Thesis, University of the Witwatersrand, Johannesburg (2005).
4. Bahome, M.C. Synthesis and use of carbon nanotubes as a support for the Fischer-Tropsch Synthesis, PhD Thesis, University of the Witwatersrand, Johannesburg (2007).
5. Phadi, T.T. Titanates and titania coated titanates as supports in the Fischer-Tropsch synthesis, MSc Dissertation, University of the Witwatersrand, Johannesburg (2008).
6. Price, J.G. An investigation into novel bimetallic catalysts for use in the Fischer-Tropsch reaction, PhD Thesis, University of the Witwatersrand, Johannesburg (1994).

CHAPTER 4

MAKING SENSE OF THE FISCHER-TROPSCH SYNTHESIS: START-UP IN A CSTR

The material in this chapter has been published in Industrial and Engineering Chemistry Research. Reference: Lu, X; Hildebrandt, D; Liu, X; Glasser, D. Making Sense of the Fischer-Tropsch Synthesis Reaction: Start-Up. *Ind. Eng. Chem. Res.* **2010**, *49*, 9753–9758.

Abstract

Conventional Fischer-Tropsch experiments were designed to investigate the effect of external mass transfer on reaction rate and product selectivity on a TiO_2 supported Cobalt catalyst in a CSTR. Short term and long term experiments were performed with fresh catalysts respectively. The experiments results showed that stirrer speed had an influence on the Fischer-Tropsch performance to some extent only in short term but not in long term. This suggested that the Fischer-Tropsch reaction does not seem to be external mass transfer controlled under typical reaction conditions in a gas-solid system. Large changes on reaction rate and product selectivity were observed and time on stream experiments showed that these changes were caused neither by reaction conditions nor the external mass transfer. Two probable explanations were proposed but more research is needed to reveal the reason causing these clear and huge changes in experiments.

4.1 Introduction

Fischer-Tropsch Synthesis (FTS) is presumed to be a network of parallel and consecutive reactions that take place within catalyst pores that are believed to be filled with waxy liquid hydrocarbon products[1-3]. In complex catalytic processes such as FTS, the diffusion limitations of reactants and products often influence reaction rates and product selectivity. It is often assumed that FTS rates are proportional to hydrogen concentration[4,5] and independent of CO concentration. Such assumptions have led to simple models that take H_2 to be the diffusion-limited reactant. Zimmerman and Bukur[4] posited first-order kinetics with respect to hydrogen, and proved that transport limitation of H_2 occurs at particle diameters greater than 0.2 mm (T >235 ^{o}C) with a fused iron ammonia synthesis catalyst. Post et al.[5] also used first-order behavior parameters, and observed transport limitations of hydrogen at high temperatures (T>220 ^{o}C; d_P>0.4 mm) with a number of iron- and cobalt-based catalysts in a fixed bed microreactor. Iglesia et al.[6, 7] confirmed an intuitive conclusion derived from their experimental results: that CO exhibits the more severe intrapellet concentration gradients, and is the diffusion-limiting reactant under FTS conditions. Experimental findings recorded by Erkey and his colleagues[8] showed that the H_2 diffusion coefficient was around three times that of the CO in FT wax at the temperature range 450–540K. The mass transfer characteristics of reactants can be modified by an external force, which is mainly provided by the application of different impeller stirring speeds (SSs). Ledakowicz et al.[9] investigated the influence of SS on the gas transfer coefficient in gas-liquid systems. Their results showed that the volumetric mass transfer coefficients for gases have a large degree of dependency on the SS. Similar results have been achieved by other researchers[10].

Researchers into FTS found that, in addition to affecting the rate of transport of reactants to catalytic sites, the waxy liquid inside the pores also influences the removal rate and secondary reactions of FTS products. The re-adsorption and secondary reactions of olefins play an important role in product distribution. For example, they may create more opportunities for reactive FTS products such as α-olefins to produce a longer chain hydrocarbon, and/or hydrogenate; or they may modify the product distribution and cause a deviation from the Anderson-Schulz-Flory (ASF) model[6].

This study investigates the FTS reaction rate and product selectivity in a gas-solid system under typical (low temperature) FTS reaction conditions. Short- term and long-term Fischer-Tropsch (FT) experiments were performed, during which external mass transfer was shown to have an effect only in the short term. Time on stream (TOS) experiments were then conducted, and obvious changes in reaction rate and product selectivity were observed. Two probable explanations are proposed and discussed.

4.2 Experimental

The experiments were carried out in a 100 ml CSTR (*Autoclave Engineers*) in a gas-solid system without adding any solvent. Residence time distribution (RTD) experiments showed that the reactor can be considered to be an ideal mixed reactor when the SS is higher than around 65 rpm. During RTD tests, the reactor was operated at reaction temperatures and pressures with Argon feed at a flow rate of $2.7 NLh^{-1}$. At time 0, a small amount of H_2 was quickly injected into the Argon feed line (the time taken was less than one second). In the meantime the online gas chromatograph (GC) started to take samples from the reactor outlet every two minutes, and analyze them. For each individual RTD test, a certain SS, which varied from 0 to 1500 rpm, was applied. In Figure 4-1 we can see that the

ln($C_{Hydrogen}$)-Time curve is a straight line. The mean residence time (τ ,derived from the slope of the straight line in the figure) matches the volumetric residence time (volume of the reactor/feed gas flow rate) well. These tell us that the behaviour of the mixing is satisfactory, and the reactor can be regarded as a real CSTR for SSs above 65 rpm.

Premixed syngas (10% N_2/30% CO/60% H_2) was fed from top of the reactor at 20 bar (g), with the flow rate controlled by a *Brooks 5850* Mass Flow Controller. The product was drained from the bottom of the tank on line to ensure that the entire contents, including condensed products, could be fully taken out of the reactor To prevent product condensation in the outlet lines, these lines were heated at 200 ^oC down to the two product traps, which were kept at reactor pressure and at 150 ^oC and 30 ^oC, to collect wax and liquid products respectively. The gaseous stream was then reduced to atmospheric pressure and connected to an on-line GC (*Agilent 6890A* with a thermal conductivity detector-TCD and a flame ionization detector-FID). The experimental set-up is shown in Figure 4-2.

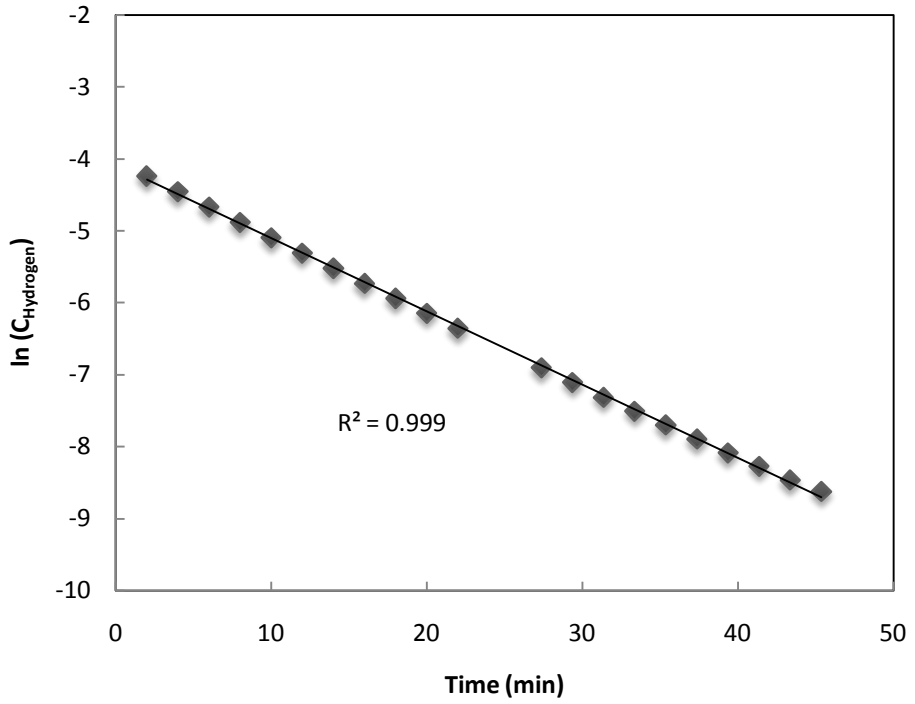

Fig. 4-1 ln($C_{Hydrogen}$)-Time curve in RDT test for CSTR when SS = 65rpm

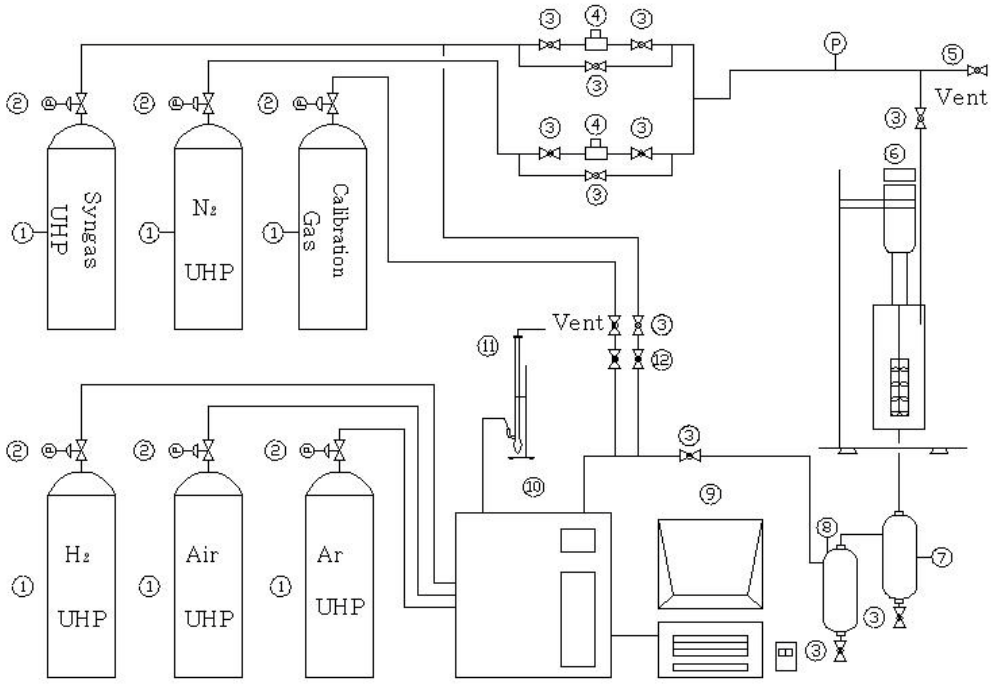

1. Gas cylinders; 2. Regulators; 3. Shut-off valves; 4. Mass flow controllers;
5. Vent valve; 6. Continuous stirring tank reactor; 7. Wax trap;
8. Liquid trap; 9. Data collection; 10. Gas chromatograph; 11. Flow meter

Fig. 4-2 The experiment set-up with a continuous stirred basket reactor

A supported cobalt catalyst （BET area 28.6 m^2/g, average pore diameter 35.8 nm） with 10% Co / 90% TiO_2 was used in the experiments. TiO_2 (*Degussa P-25*) was mixed with distilled water in a 1:1 ratio to prepare a paste, which was dried at 120 ^oC for two hours, calcined at 400 ^oC for six hours and then cooled overnight. The calcined paste was crushed and sieved to a particle size between 0.5 and 1 mm to serve as the support for the catalyst. An amount of $Co(NO_3)_3$ $6H_2O$ (*Sigma Aldrich*), that was calculated on the mass of the support, was dissolved in distilled water to form a solution, which was then mixed with the support and allowed to absorb uniformly into it by impregnation. The wet catalyst pellets were dried at 120 ^oC for two hours and then calcined at 400 ^oC for six hours.

Approximately 3g of prepared cobalt catalyst was loaded into a catalyst basket (provided with the reactor). The frame of the basket was fixed to the inner wall of the tank but the basket itself did not extend over the whole diameter. A stirrer in the inner radius was used to stir the gas and force it through the catalyst held in the basket. The catalyst basket together with the catalyst inside was suspended in the tank, without shaking during the experiment.

The catalyst was reduced with H_2 at 1.8 $NLh^{-1}(gcat)^{-1}$ at ambient pressure. The gas space velocity was based on the total mass of the unreduced catalyst. The temperature was increased from room temperature to 120 ^oC, first at a ramping rate of 60 ^oC h^{-1}, and held for two hours before being increased to 280 ^oC at the same ramping rate, and maintained at this temperature for 24 hours. After reduction, the reactor was cooled to below 100 ^oC.

The feed gas was switched from H_2, which had been used for the reduction, to syngas. The pressure of the reactor was stabilized at 20 bar(g) by a back pressure regulator (*Swagelok*), and the flow rate of the feed was controlled at 1.2$NLh^{-1}(gcat)^{-1}$ by a mass flow controller (*Brooks 5850*). The temperatures used

in the experiments were 190^{o}C and 210^{o}C. The initial SS inside the reactor was set at 100 rpm.

4.3 Results and Discussion

4.3.1 Short term FT runs

The initial experiments were performed to investigate the effect of SS on CO conversion, CH_4 selectivity and the production of hydrocarbons. In the experiments, the reactor was operated at 190 ^{o}C and 20 bar(g), while the SS was kept constant at 100 rpm in one run; and changed from 100 to 1500 rpm and then to 0 rpm during the other, at 12-hour intervals. Both of these runs were started using fresh catalysts. The CO conversion and CH_4 selectivity with TOS for fixed and varied SS's, are shown in Figures 4-3 and 4-4 respectively. There was an obvious consistency in result when the SS was fixed: the CO conversion and CH_4 selectivity remained constant. However, when the SS was varied, the results were quite different. Higher CO conversions were achieved at greater SS, and reduced when the SS was decreased to 0 rpm. Researchers commonly agree that the SS in a reactor affects the external mass transfer characteristics of reactants on the catalyst's surface, and that intense agitation would help bring about reduced external mass transfer resistance in the system. It therefore follows that better external mass transfer improves the mass transfer characteristics of reactants, and subsequently increases the reaction rate of FTS to a certain extent. Unlike the small changes in CO conversion, CH_4 selectivity was more strongly influenced by SS, increasing from about 4% at 100 rpm to about 16% at 1500 rpm. The reasons for this large increase in CH_4 selectivity at different SSs are not clear, but as a higher H_2 concentration on the active sites favours CH_4 selectivity, it may suggest that the influence of SS on the diffusion of H_2 is greater than that on the CO in the

catalyst. The CH_4 selectivity dropped when the SS was reduced to 0 rpm, as did the CO conversion.

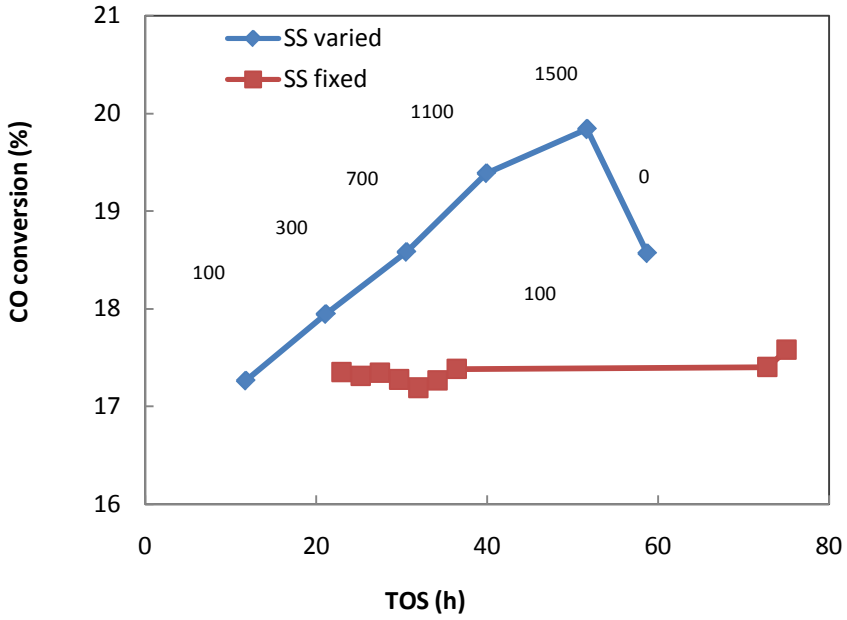

Fig. 4-3 CO conversion at fixed SS (100rpm) and varied SS (100-1500-0rpm) (T = 190 ^{o}C, P = 20 bar (g), FR = 0.6Nlh^{-1}(gcat)$^{-1}$; numbers above data points are the corresponding SS applied)

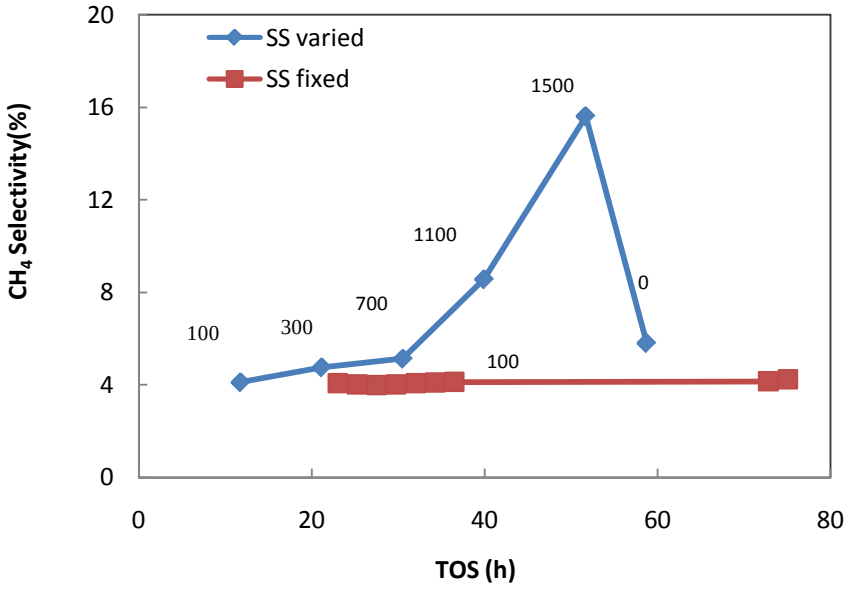

Fig. 4-4 CH_4 selectivity at fixed SS (100rpm) and varied SS (100-1500-0rpm) (T = 190 ^{o}C, P = 20 bar (g), FR = 0.6Nlh^{-1}(gcat)$^{-1}$; numbers above data points are the corresponding SS applied)

The olefin to paraffin (O/P) ratios, based on the same carbon number for light hydrocarbons at fixed and varied SSs with TOS, are given in Figures 4-5 and 4-6 respectively. Light hydrocarbons were chosen because the product composition of the heavier hydrocarbon products changed continually until the reaction had reached a final steady state (which will be discussed below), and the system of analysis used in the study was unable to monitor this continuous change. However, the information derived from the experimental use of light hydrocarbons is very informative. From the results obtained it was observed that the O/P ratios for C_2, C_3, and C_4 remained almost unchanged when the SS was kept constant, while a marked difference could be clearly seen when the SS was varied. Although a clear relationship cannot be determined between the SS and the O/P ratios, an ascending trend was observed for the C_3 and C_4 O/P ratios when the SS was increased from 100 to 700 rpm, but then dropped dramatically at a higher SS. It was also noticeable that for C_2, the O/P ratio behaved differently from that of C_3 and C_4, although all of them fell to very low values when the SS was at 1500 rpm. These extreme changes are quite similar to those seen in CH_4 selectivity when higher SSs were applied.

A common feature that can be observed in Figures 4-3, 4-4 and 4-6 is that when the SS was reduced to 0 rpm from its higher values during the experiment, the values of CO conversion, CH_4 selectivity and O/P ratios reverted to values close to what they were initially at a low SS and the beginning of TOS. The recovery of CO conversion, CH_4 selectivity and O/P ratios to the original levels when the SS was dropped to 0 rpm further supports the assumption that external mass transfer does have an effect on the performance of FTS.

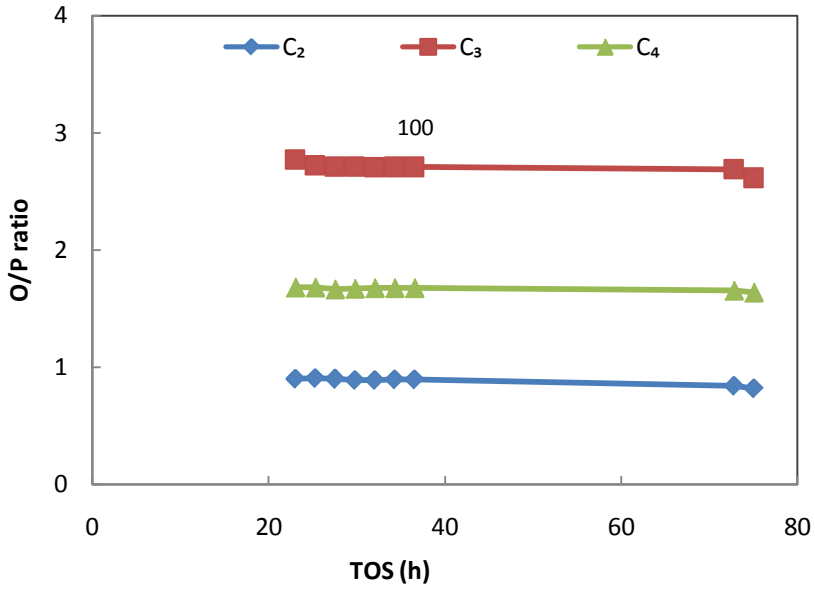

Fig. 4-5 Olefin/paraffin ratios with TOS when SS fixed (100rpm) (T = 190 ^{o}C, P = 20 bar (g), FR = 0.6Nlh^{-1}(gcat)$^{-1}$; numbers above data points are the corresponding SS applied)

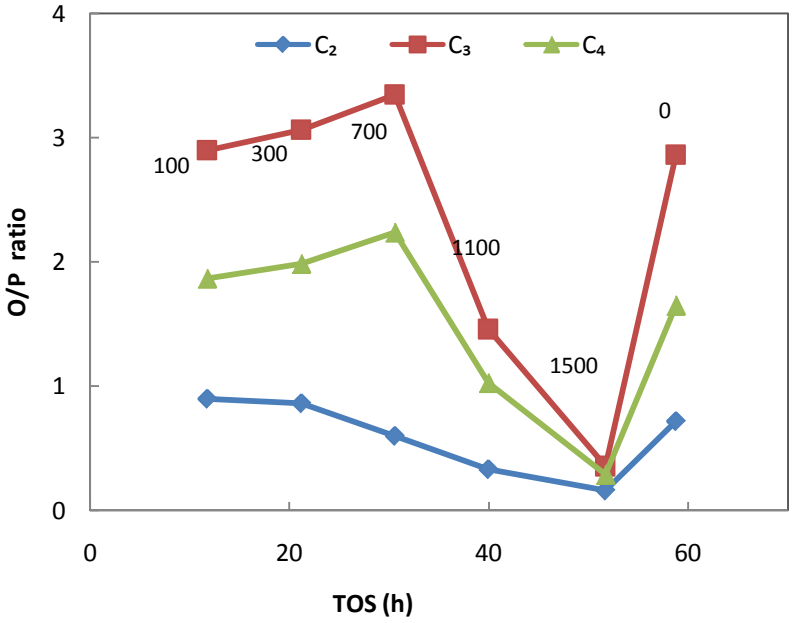

Fig. 4-6 Olefin/paraffin ratios with TOS when SS varied SS (100-1500-0rpm) (T = 190 ^{o}C, P = 20 bar (g), FR = 0.6Nlh^{-1}(gcat)$^{-1}$; numbers above data points are the corresponding SS applied)

4.3.2 Long term FT runs

In addition to the short-term experiments discussed above, which were run only for around 75 hours TOS, the researchers performed long-term experiments with the same amount of fresh catalyst as used in the previous runs to investigate further what occurs in a long-term FTS reaction. In these experiments, the reactor was operated at 190 ^{o}C and 20 bar(g), as in the short-term experiments, while the SS was kept constant for the first 100 hours, then increased stepwise to 1500 rpm, and finally reduced stepwise to 100 rpm (the initial SS). The SS was kept constant for a certain TOS after it had been set to a new value, the total TOS lasting about 600 hours. The changes observed in CO conversion, CH_4 selectivity and O/P ratios with SS are displayed in Figures 4-7 and 4-8.

The SS was operated at 100 rpm in the first 100 hours of TOS. The results in Figures 4-7 and 4-8 show that stable CO conversion, CH_4 selectivity and O/P ratios were noted in the first 80 hours of reaction. Sudden changes in the values of these parameters were observed from 80 to 120 hours TOS, after which these parameters again reached stable values, although these were very different from their initial values.

The relationship between the CO conversion and CH_4 selectivity as a function of SS at different TOS is shown in Figure 4-7. It can be seen that the values of CO conversion and CH_4 selectivity started to change when SS was still being maintained at 100 rpm, and that they reached their new stable values at about 120 hours. The CO conversion dropped from 17.5% to about 12.5%, and CH_4 selectivity increased from around 4% to about 26%. When they attained their new steady values, both parameters remained steady, that is without significant

changes, except in the case of CH_4 selectivity, which appeared to increase slightly at high SSs (1100 and 1500 rpm).

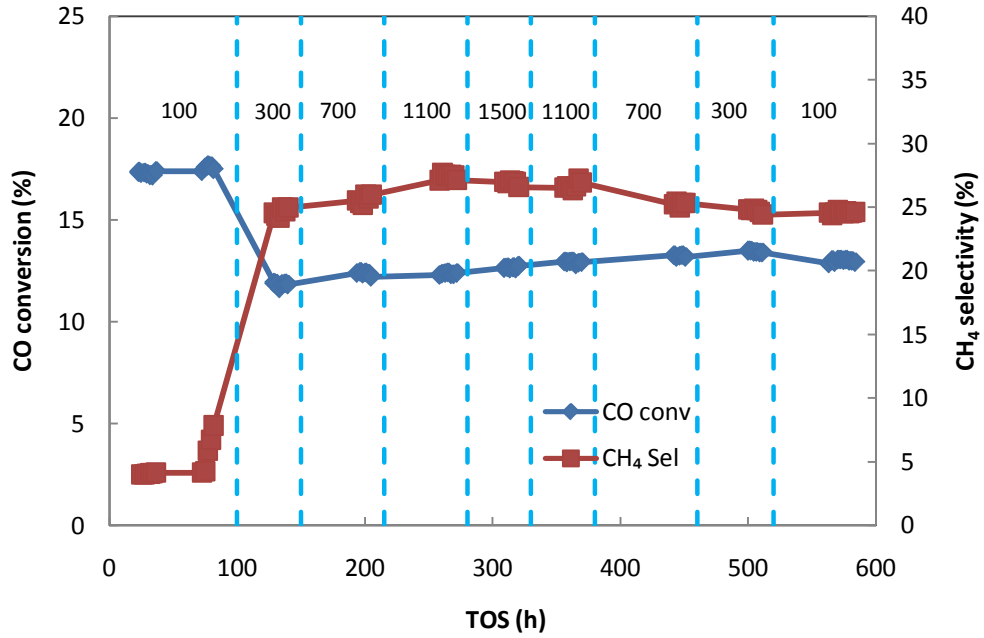

Fig. 4-7 CO conversion and CH_4 selectivity at different SSs during the entire TOS (T = 190°C, P = 20 bar (g), FR = 1.2NLh^{-1}(gcat)$^{-1}$; numbers above data points are the corresponding SS applied)

Olefin and paraffin products were monitored during reaction as well. It was found that the O/P ratio for C_2–C_5 also started to change significantly, dropping from their original high values to low values at about 80 hours, when the SS was still at 100 rpm, as can be seen in Figure 4-8. This change is similar to that observed in the plots of CO conversion and CH_4 selectivity with respect to SS at different TOSs. Another similarity was that after 600 hours TOS of FT reaction, when the SS had been returned to 100 rpm, the CO conversion, CH_4 selectivity and O/P ratios did not revert to their initial values. However, these results differ from what was shown in the earlier, short TOS run (Figures 4-3, 4-4, and 4-6).

It is therefore clear that in this 600-hour TOS run, the large variation in reaction rates and product selectivity was not mainly caused by SS, which in this experiment had almost no effect on these parameters after 120 hours. It seems that

for FTS, the external mass transfer does have some effect during the start-up period, but almost none after a certain period, when the FTS reaction continued. Reasoning that the cause might be related to the catalyst or the reaction environment, we designed a group of TOS experiments to carry the investigation further.

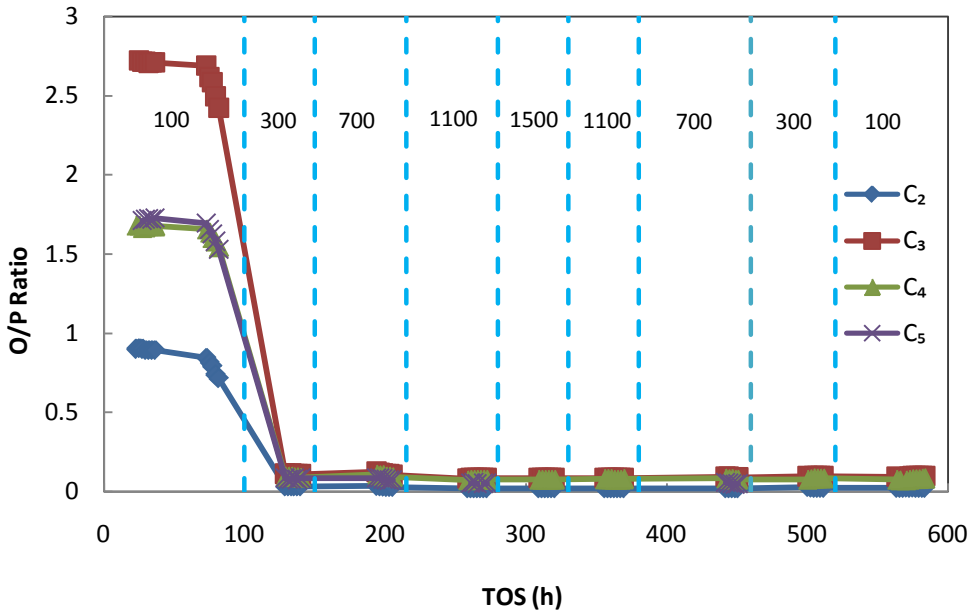

Fig. 4-8 Olefin/paraffin ratios at different SS during the entire TOS (T = 190 ^{o}C, P = 20 bar (g), FR = 1.2NLh^{-1}(gcat)$^{-1}$; numbers above data points are the corresponding SS applied)

4.3.3 Time on Stream Runs at Constant SS

The TOS experiment was designed to investigate the effects of TOS, but without the influence of different SSs. The same amount of fresh catalyst was loaded into the reactor for each of two runs, and the reactor was operated at 20 bar(g) and 190^{o} for the first run and 210 ^{o}C for the other run, with the SS kept at 100 rpm during the entire TOS. The CO conversion, CH_4 selectivity and O/P ratios recorded for these two runs at different temperatures versus TOS are plotted in Figures 4-9 and 4-10 respectively. We can clearly see from both figures that marked changes occurred in CO conversion, CH_4 selectivity and O/P ratios, even

at a constant SS. Further, these changes took place at almost the same TOS at one particular temperature run, although the time when the changes began differed at the different reaction temperatures. According to the characteristics of CO conversion, CH_4 selectivity and O/P ratios at different TOS during the reaction, we could divide the entire TOS of the experiment into four stages.

- Stage A (the first 12 hours in Figure 4-9 and 7 hours in Figure 4-10) is the period during which the reaction starts with fresh reduced catalyst. The reaction rate and light products formation increases gradually until pseudo-steady values are reached, after which Stage B begins.

- Stage B (from 12 to 80 hours in Figure 4-9 and from 7 to 22 hours in Figure 4-10) denotes the period during which the pseudo-steady state is maintained in terms of reaction rate and the formation of light hydrocarbons.

- Stage C commences from 80 to 150 hours of TOS in Figure 4-9 and from 22 to 80 hours in Figure 4-10. During this stage, the pseudo-steady state is destroyed as reaction rates and product selectivity start to change.

- Stage D occurs after 150 hours of TOS in Figure 4-9 and 80 hours in Figure 4-10, when a new steady state for the performance of FTS was reached and remained unchanged for the rest of the time during which the reaction conditions were constant.

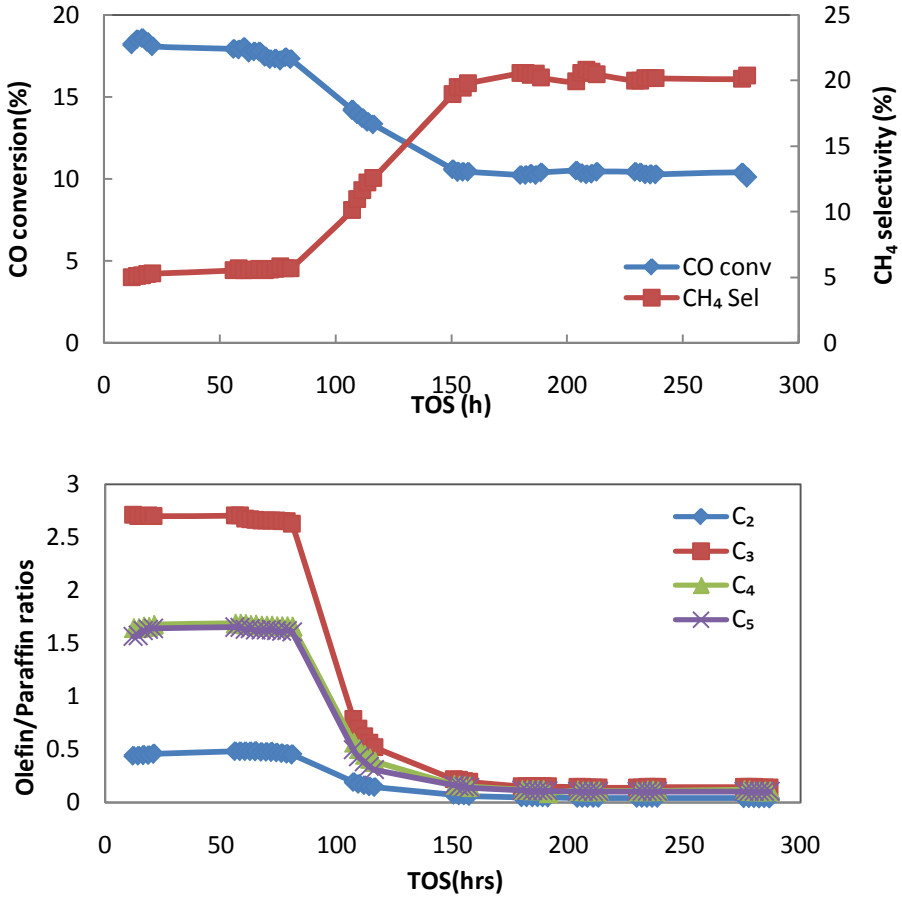

Fig. 4-9 CO conversion, CH_4 selectivity and O/P ratio at 190^{o}C with respect to TOS while SS remained constant (P = 20 bar (g), FR = 1.2NLh^{-1}(gcat)$^{-1}$ SS=100rpm)

As can be seen the length of time required for the change in values of CO conversion, CH_4 selectivity and O/P ratios was affected by temperature. The higher the reaction temperature, the shorter the period needed to accomplish the first three stages. Thus the obvious differences between the two plots illustrated in Figures 4-9 and 4-10 concern the length of time during which the results remain steady at high values, and the time taken to reach their new lower values. At the higher reaction temperature, 210 ^{o}C, CO conversion, CH_4 selectivity and O/P ratios remained steady at higher values for about 25 hours, while at the reaction temperature of 190^{o}C they stabilized at higher values for about 80 hours. Once they started to change, the variation occurred more rapidly when the reaction temperature was at 210 ^{o}C than at 190 ^{o}C.

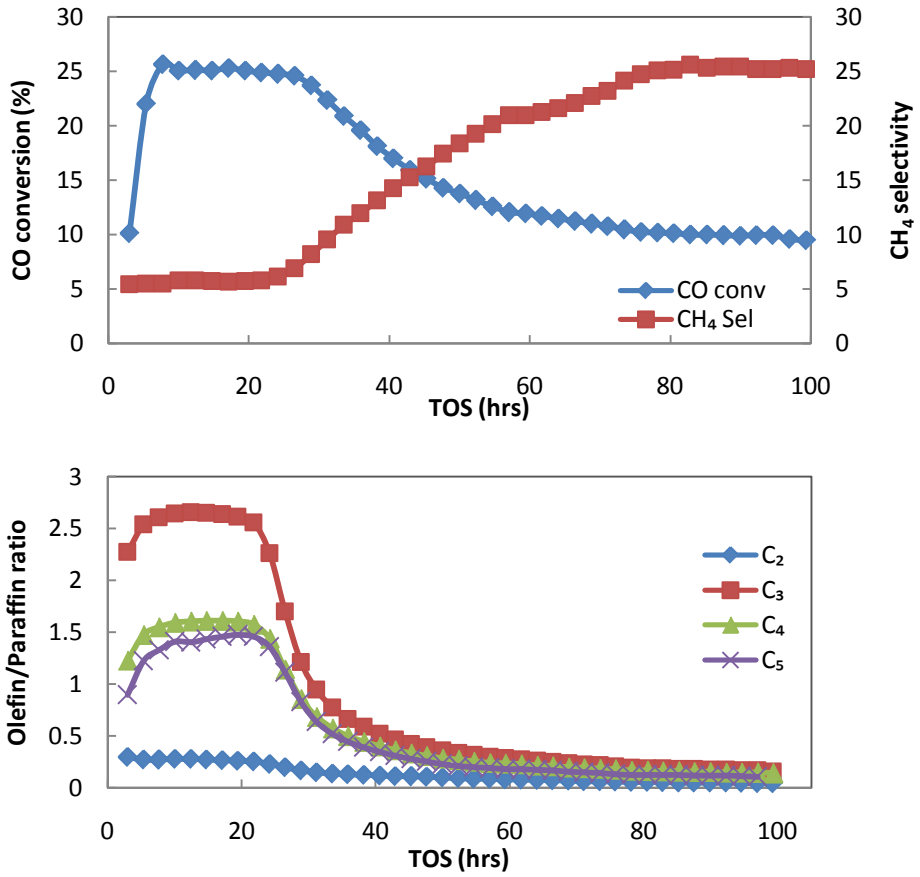

Fig. 4-10 CO conversion, CH_4 selectivity and O/P ratio at 210 ^{o}C with respect to TOS while SS remained constant (P = 20 bar (g), FR = 1.2NLh^{-1}(gcat)$^{-1}$ SS=100rpm)

The O/P ratios for different carbon numbers were observed to be very different during the entire TOS, with C_2 O/P ratios during the two different temperature runs the lowest and C_3 O/P ratios always the highest of the light hydrocarbons that we investigated. This is probably mainly attributable to their different hydrogenation capacities: propene is believed to be the least convertible. Although the two experiments were carried out at two different temperatures, for C_3 C_4 and C_5 the olefin to paraffin ratios started from, and ended up at, more or less the same values. However, C_2 is different from the other three, as it achieved a higher O/P ratio at a lower temperature. It seems that the starting and final values of O/P ratios are not sensitive to the reaction temperature for C_3-C_5, but are sensitive in the case of C_2.

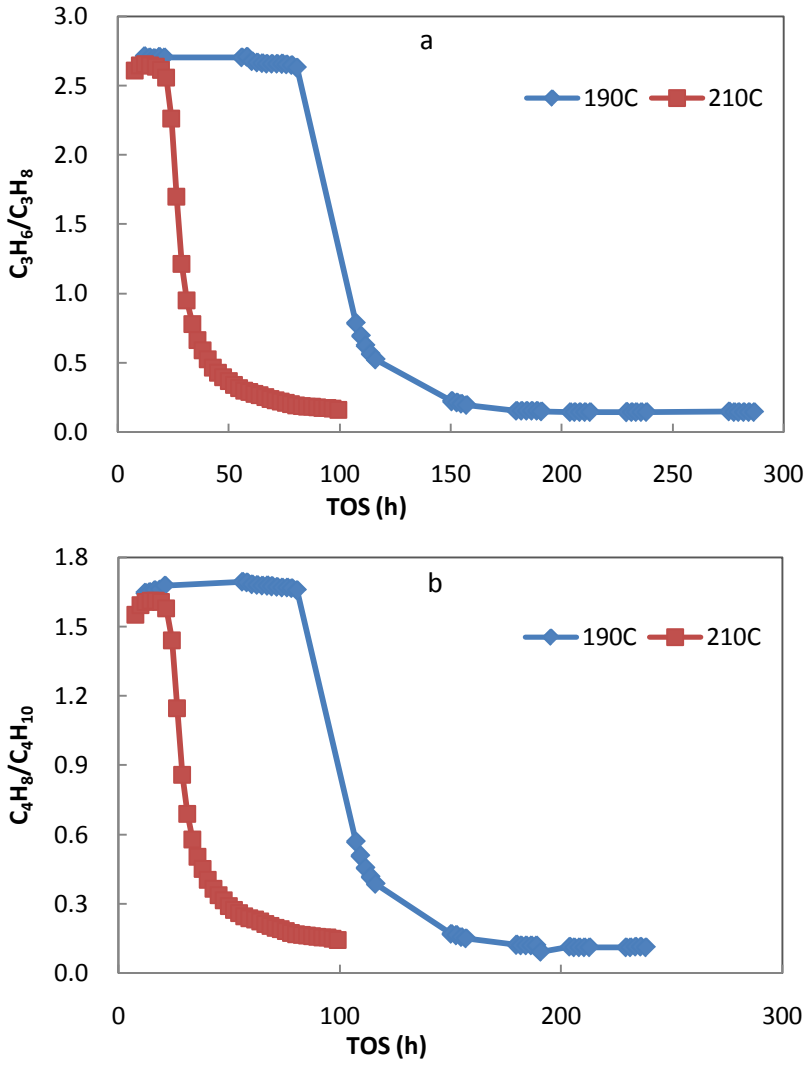

Fig. 4-11 The O/P ratio (C_3 and C_4) at different temperatures

With correspondence to the changing period discussed above, the product selectivity of C_2-C_5 and C_{6+} are investigated. The results in respect of TOS while operating conditions remained constant are presented in Figures 4-12 to 4-14.

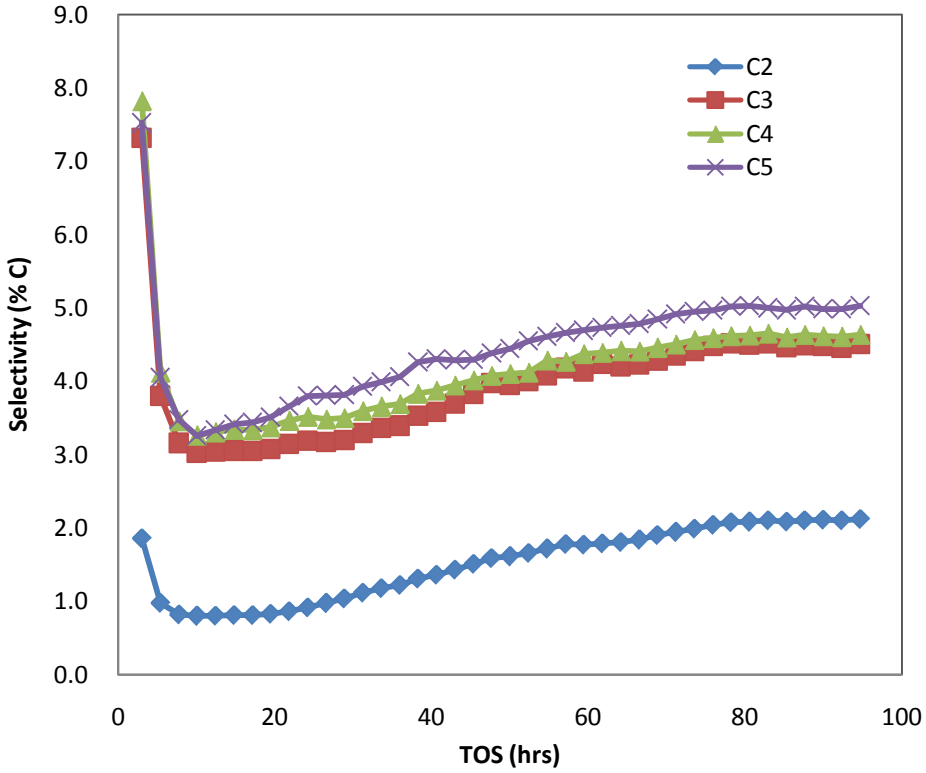

Fig. 4-12 C_2-C_5 selectivity at 210 ^oC in respect of TOS while SS remained constant (P = 20 bar (g), FR = 1.2NLh^{-1}(gcat)$^{-1}$ SS=100rpm)

In Figure 4-12, we can see that at the very early TOS, corresponding to Stage A mentioned above, the selectivity of C_3-C_5 could be as high as around 7.5 % and C_2 around 1.9 %. This suggests that the short chain hydrocarbons (except for CH_4, see Figures 4-8 and 4-10) are dominant in the product spectrum in the very early period after the reaction was initiated. This high level of the selectivity of short chain hydrocarbons dropped sharply to slightly higher than 3 % for C_3-C_5 and around 0.8 for C_2 with the formation of the long chain hydrocarbons via the chain growth process. The selectivity of C_2-C_5 held relatively stable (C_4 and C_5 look not stable especially C_5) at Stage B and started to increase at TOS of 22 hours, which corresponded to the commencement of Stage C. In Stage C, the selectivity climbed gradually form 0.85 to 2.1 % for C_2, from 3.0 to 4.5 % for C_3, from 3.5 to 4.6 % for C_4, and from 3.6 to 5.0 % for C_5. The selectivity of C_2-C_5 was observed clearly to increase in this transient period although the reason causing this is not clear, but the increment of selectivity is not as large as that of CH_4, which showed

a variation from around 5 % to 25 % at the same operation conditions. After the gradual increase, the selectivity of C_2-C_5 reached stable values and this corresponded to Stage D. The dynamic increase on the selectivity of the short chain hydrocarbons (C_2-C_5 in Figure 4-11 and C_1 in Figure 4-10) from stage C showed that the formation of short chain hydrocarbons are strengthened.

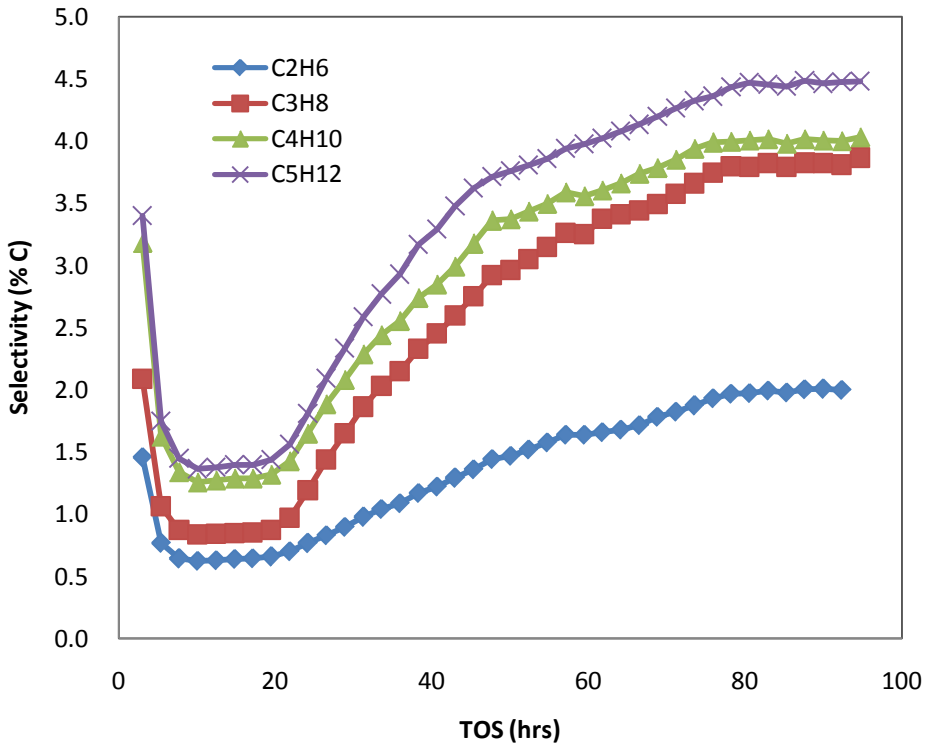

Fig. 4-13 C_2-C_5 paraffins selectivity at 210°C with respect to TOS while SS remained constant (P = 20 bar (g), FR = 1.2NLh^{-1}(gcat)$^{-1}$ SS=100rpm)

In Figure 4-13, the selectivity of C_2-C_5 paraffins with respect to TOS are given. The behaviour of the selectivity in this TOS is similar to that of the C_2-C_5 presented in Figure 4-11. The differences in this Figure when compared to Figure 4-11 are that (a), in Stage C, the selectivity of C_2-C_5 paraffins, especially C_3-C_5, increased rapidly during the first half period and the increasing rate dropped gradually until no more increment was observed for them; (b), the increment of the paraffins selectivity are higher than the selectivity of hydrocarbons for C_2-C_5. The larger margin of the increment of the selectivity of C_2-C_5 paraffin was due to

the enhanced secondary reaction of olefins to paraffins and the increased selectivity of the paraffins (see Figures 4-9 and 4-10).

The selectivity of C_6+, sum of C_2-C_5, and CH_4 is given in Figure 4-14. After passing stage A, the selectivity of C_6+ stayed at a relatively high level, i.e. around 83.5 %, but in stage C, it dropped to 58.5 %, which decreased by 25 %. Among the changes of the three groups of products, the sum of C_2-C_5 is the least one to be affected by the transient period, and CH_4 was the most one and so that the C_6+.

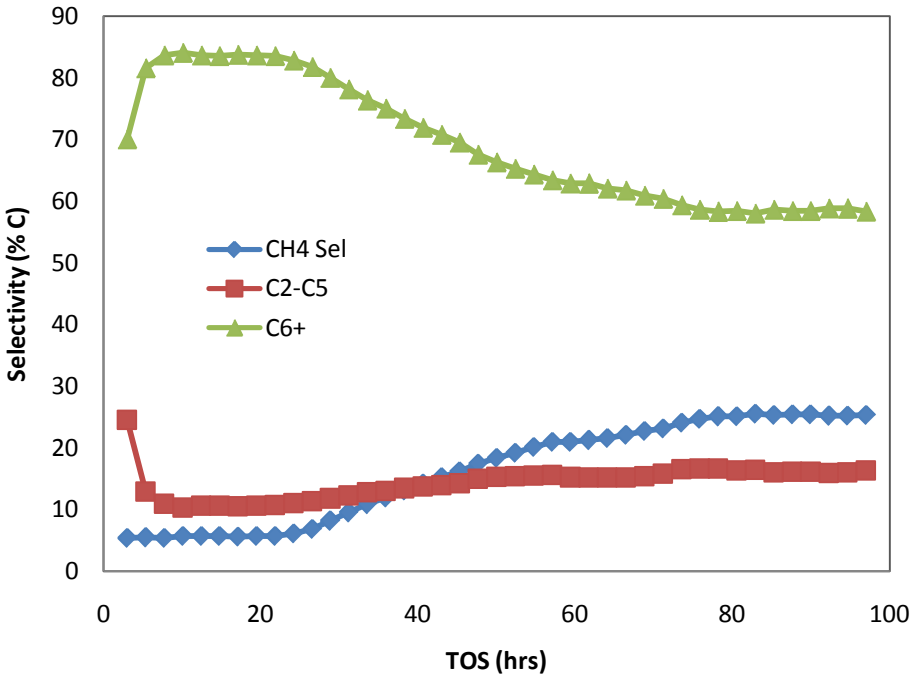

Fig. 4-14 C_1, C_2-C_5, and C_6+ selectivity at 210 ^{o}C with respect to TOS while SS remained constant (P = 20 bar (g), FR = 1.2NLh^{-1}(gcat)$^{-1}$ SS=100rpm)

There may be several reasons for the significant changes shown in the above figures that could occur during reaction even taking into account that all the reaction conditions are fixed.

The first possible reason is deactivation of the catalyst. The changing behaviour of CO during conversion suggests one could analyze the result from a catalyst deactivation point of view. However, the two pseudo-steady states imply that this result is unlikely to be caused by deactivation, as in most cases deactivation is a

sustained process, and the reaction conditions and feed are insufficient to bring about catalyst deactivation. The huge change in product selectivity and the fact that no CO_2 was detected during the entire TOS also indicate that the behaviour is most likely not deactivation-related.

A second possible reason is the changing of the catalyst's surface properties or the reconstruction of the catalyst in a syngas environment. Schulz[11,12] and his co-workers reported that the change in product selectivity and increase of activity during reaction were caused by the "catalyst construction". CO chemisorbs strongly on cobalt (as well as on Ni and Ru) and it has been pointed out by Pichler[13] that FT synthesis performs under conditions not so far from those which allow (thermodynamically) carbonyl formation from these metals. Then the reaction of CO with the metal surface can be assumed to induce surface restructuring [11]. Images of a cobalt metal surface which had been used for FT synthesis were obtained by Wilson and de Groot[14] through scanning tunnelling electron microscopy. These pictures led to the deduction that segregation produces an ordered surface structure in a syngas atmosphere. If the phenomena observed in the experiments discussed in this paper were caused by changes in catalyst's surface properties, this property alteration should be extensive, as the methane selectivity and olefin to paraffin ratios changed dramatically during the experiments.

The third possible reason is the formation and deposit of the liquid phase products in the catalyst. It is generally agreed that FTS can be described as a polymerization reaction[15]. At the beginning of the reaction, short chain hydrocarbons are dominant in the product spectrum. Long chain hydrocarbons start to form as the TOS increases. The catalyst surface is initially "dry", that is without liquid accumulation on its surface and pores at the start of the reaction, but as the FT reaction continues, the pores in the catalyst could begin to

accumulate liquid phase product. This would occur gradually, as long chain hydrocarbons are formed. The liquid products deposited in the catalyst could therefore change the mass transfer (diffusivity) of reactants and products, and consequently affect both the reaction rate and product selectivity.

The second and third possible reasons sound reasonable, but based upon the experiments conducted, we cannot say with certainty whether the extreme changes in reaction rate and product selectivity that were observed were caused by changes in catalyst's surface properties or by the liquid products deposited in the catalyst pores. Either one or both of these explanations might be applicable. More research would be needed to determine the reason(s) for the observed phenomena. Characterizations of the catalyst during the early stage after the FT reaction is initiated on a fresh catalyst may be necessary to investigate the effect of possible re-construction of the catalyst due to the performance of the FT reaction. An in-situ characterization would be more favourable as the properties of the catalyst when it is being used during the reaction might be different from when it is taken out from the reactor. A liquid deposit in the catalyst causing the observed phenomena is presumed. A novel experiment to give a direct evidence for this postulate has been designed and the results from it will be presented in a subsequent paper.

The results of the product selectivity presented in this work were only for the gas-phase hydrocarbons from C_1 to C_5 instead of for the full product spectrum because the changes we saw happened relatively quickly and one would not be able to collect sufficient liquid for analysis in time to follow these changes. For instance the mean residence time for gases in the CSTR is around 30min (from the slope of the curve of RTD test for the reactor at the operating conditions). The information for gas phase products (C_1-C_5) could be collected by an online GC, while the time taken for collecting sufficient liquid will be of orders of magnitude

larger than this. Thus in the reactor used in our experiments for the liquid all the dynamic effects we wished to study will tend to be obscured.

4.4 Conclusion

A study of external mass transfer on a TiO_2-supported cobalt catalyst was carried out in a CSTR. The experiments were performed under low-temperature FTS conditions in a gas-solid system. The experimental results suggested that external mass transfer has an effect on the reaction rate and product selectivity for short TOSs, but very little after a certain longer TOSs. Therefore, the long term FTS is not an entirely external mass transfer controlled reaction system. Dramatic changes in the reaction rate and product selectivity of FTS, which happened almost simultaneously, were observed in the experiments. The TOS experiments were interpreted as showing that these changes were attributable either to the changing of catalyst surface properties or the liquid products deposit in the catalyst pores. The TOS time at which these changes occurred depended on the reaction temperature. It was also found that the higher temperature resulted in a shorter initiation time. No conclusive explanation for the observed phenomena could be reached on the basis of the experiments, and therefore we recommend that further research be carried out.

4.5 References

1. Anderson, R. B. *The Fischer-Tropsch Synthesis*. Harcourt, Brace & Jovanovich: New York, 1984.
2. Donnelly, T. J.; Yates, I. C.; Satterfield, C. N. Analysis and Prediction of Product Distributions of the Fischer-Tropsch Synthesis. *Energy & Fuels.* **1988**, *2*, 734.
3. Madon, R. J.; Reyes, S. C.; Iglesia, E. Primary and Secondary Reaction Pathways in Ruthenium-Catalyzed Hydrocarbon Synthesis. *The Journal of Physical Chemistry*. **1991**, *95*, 7795.
4. Zimmerman, W. H.; Bukur, D. B. Effect of Particle Size on the Activity of a Fused Iron Fischer-Tropsch Catalyst. *Industrial & Engineering Chemistry Research*. **1989**, *28*, 406.
5. Post, M. F. M.; van't Hoog, A. C.; Sie, S. T. Diffusion limitations in Fischer-Tropsch catalysts. *AIChE Journal*. **1989**, *35*, 1107.
6. Madon, R. J.; Iglesia, E. Hydrogen and CO Intrapellet Diffusion Effects in Ruthenium-Catalyzed Hydrocarbon Synthesis. *Journal of Catalysis.* **1994**, *149*, 428.
7. Iglesia, E.; Reyes, S. C.; Soled, S. L. *Reaction-Transport Selectivity Models and the Design of Fischer-Tropsch Catalysts*: in E.R. Becker; C.J. Pereira, eds., Computer-Aided Design of Catalysts. Marcel Dekker: New York, 1993.
8. Erkey, C.; Rodden, J. B.; Akgerman, A. Diffusivities of Synthesis Gas and n-Alkanes in Fischer-Tropsch Wax. *Energy & Fuels*. **1990**, *4*, 275.
9. Ledakowicz, S.; Nettelhoff, H.; and Deckwer, W.-D. Gas-Liquid Mass Transfer Data in a Stirred Autoclave Reactor. *Industrial and Engineering Chemistry Fundamentals*. **1984**, *23*, 510.
10. Meille, V.; Pestre, N.; Fongarland, P.; de Bellefon, C. Gas/Liquid Mass Transfer in Small Laboratory Batch Reactors: Comparison of Methods. *Industrial & Engineering Chemistry Research*. **2004**, *43*, 924.

11. Schulz, H.; Nie, Z.; Ousmanov, F. Construction of the Fischer–Tropsch Regime with Cobalt Catalysts. *Catalysis Today*. **2002**, *71*, 351.
12. Schulz, H., Major and Minor Reactions in Fischer–Tropsch Synthesis on Cobalt Catalysts. *Topics in Catalysis*. **2003**, *26*, 73.
13. Pichler, H.; Frankenburg, W. *Advances in Catalysis*. Academic Press: New York, 1952; Vol. IV.
14. Wilson, J.; de Groot, C. Atomic-Scale Restructuring in High-pressure Catalysis. *The Journal of Physical Chemistry*. **1995**, *99*, 7860.
15. Herington, E. F. G. The Fischer-Tropsch Synthesis Considered as a Polymerization Reaction. *Chemical Industries*. **1946**, *65*, 346.

CHAPTER 5

A NEW WAY TO LOOK AT FISCHER-TROPSCH USING FLUSHING EXPERIMENTS

The material in this chapter has been accepted by the editorial office for publication in Industrial and Engineering Chemistry Research. The paper is currently available in the internet. The current Reference is: Lu, X; Zhu, X.; Hildebrandt, D; Liu, X; Glasser, D. A New Way to Look at Fischer-Tropsch Synthesis Using Flushing Experiment. *Ind. Eng. Chem. Res.* **2011**, 50, 4359–4365.

Abstract

When Fischer-Tropsch Synthesis (FTS) reaction experiments were conducted in a gas-solid system with a TiO_2 supported cobalt catalyst in a continuous stirred tank reactor (CSTR), we observed significant changes in the reaction rate and product selectivity at early stage of time on stream (TOS) when all the reaction conditions were kept constant as has been presented in Chapter 4. We designed flushing experiments with an inert gas that started when the FTS reaction had reached steady state. After the completion of flushing, the FTS reaction was resumed with syngas feed. We then compared the results of the FTS reaction rate and product selectivity both before and after flushing. Obvious differences were observed and the results are discussed. The flushing experimental results suggested that the marked variations we had observed were caused (either wholly or mainly) by

liquid products deposited in the catalyst rather than by the change in the properties of the catalyst surface. The concentrations and the relative amount of the reactant were looked at and the implications of the high H_2/CO ratio in the liquid in the catalyst to the reaction kinetics and product selectivity are discussed. Based upon the dynamic concentration of C_1-C_8 in the flushed out gas, we proposed that reaction among the products might take place under a moderate FT reaction condition. The product distribution (C_1-C_8) in the catalyst is also presented. A model for the change of the reaction rate during the period of liquid build-up is proposed with a simple reaction A to B. The result of the simulation shows similar behaviour to the phenomena that we observed in the experiment.

5.1 Introduction

Our previous paper [1] showed that rapid and substantial changes occurred in the FTS reaction rate and product selectivity at a certain time on stream (TOS) when low-temperature FTS was conducted on a TiO_2-supported cobalt catalyst (10%Co/90%TiO_2) in a CSTR. These changes can be clearly seen in Figures 1 and 2. In these examples, considerable changes were observed to start at around 25 hours of TOS. The time at which these changes occurred varied with the reaction temperature [1]. As discussed previously, these phenomena are unlikely to have been caused by deactivation of the catalyst, as two pseudo-steady states (from around 8–25 hours and after 85 hours in Figures 5-1 and 5-2) were observed, and the secondary steady state could be maintained without any further change in the TOS that we had investigated. The probable reasons we suggested for these large and sudden changes were: alterations in catalyst surface properties in a syngas environment; or the deposit of liquid phase products in the catalyst. The latter of these would affect the mass transfer of reactants and products, and consequently alter the reaction rate and product selectivity.

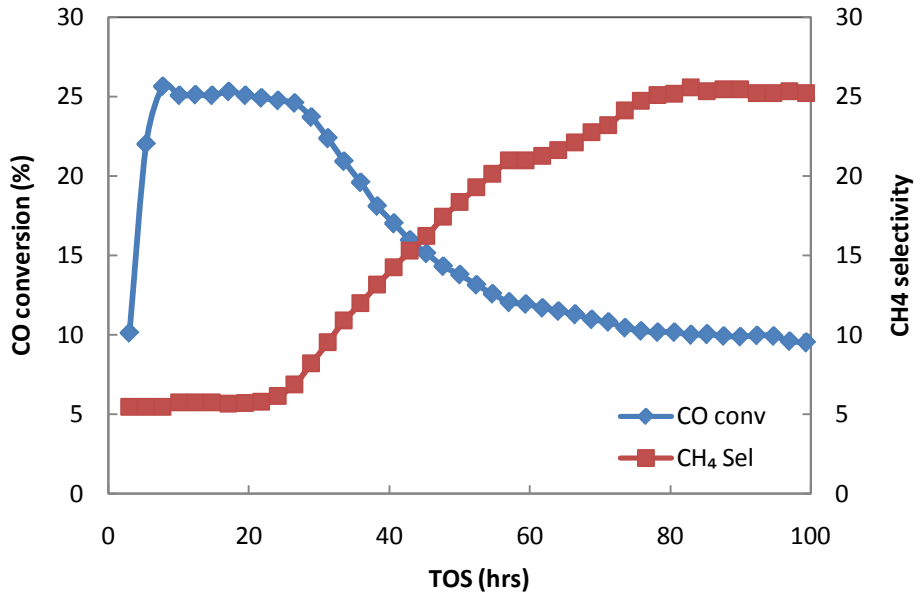

Fig. 5-1 CO conversion, CH_4 selectivity at 210 ^{o}C during the entire TOS when stirring speed (SS) remained constant (P = 20 bar (g), FR = 1.2Nlh^{-1}(gcat)$^{-1}$ SS=100rpm)

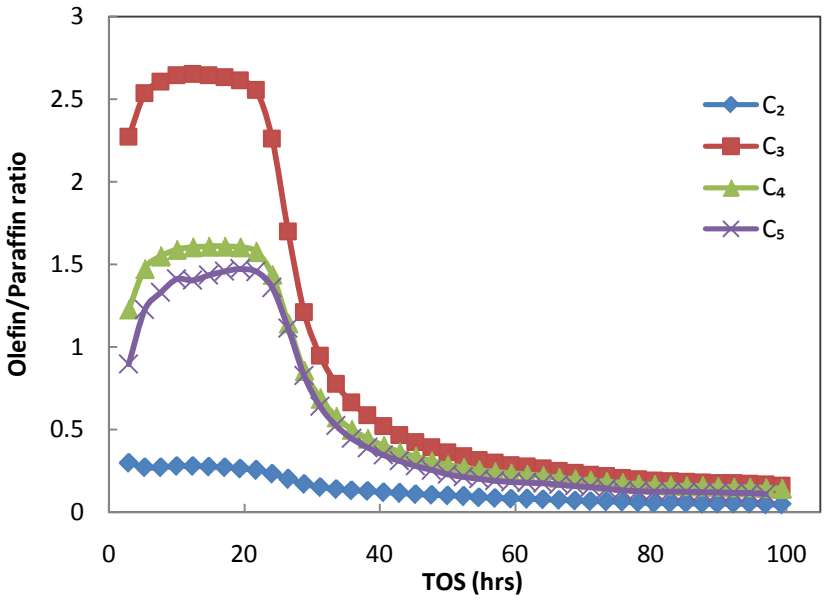

Fig. 5-2 O/P ratio at 210 ^{o}C during the entire TOS when SS remained constant (P = 20 bar (g), FR = 1.2Nlh^{-1}(gcat)$^{-1}$ SS=100rpm)

These transient related phenomena are believed to partly due to the accumulation of the liquid in the catalyst. [2, 3] Anderson *et al.* [4] first reported that intraparticle diffusional restrictions on the rate of reactant arrival to hydrocarbon

synthesis sites controlled the CO conversion rate of Fe-based catalysts. Post *et al.* [5] report a simplified transport-reaction model that describes only H_2 transport limitations, although CO is the more probable diffusion-limited reactant, in Fe and Co catalysts; they address only rate effectiveness factors for the primary CO hydrogenation reaction and do not discuss transport effects on synthesis selectivity or on secondary reaction. Iglesia *et al*. [6] report a transport-reaction model of hydrocarbon synthesis selectivity that describes intraparticle (diffusion) transport processes; these processes control the rate of arrival of CO and H_2 and the rate of removal of reactive products within catalyst pellets and reactors. The transport limitation enhanced the secondary reaction of the α-olefins. However there was no experimental evidence to prove the effect is from the liquid products in the catalyst directly, or to explain the extent to which the performance of the FTS could be affected.

On the other hand, a supported Co FT catalyst is believed to reconstruct in a syngas atmosphere, and alter the surface properties of the catalyst, which in turn will affect its performance, such as reaction rate and product selectivity. Schulz[7,8] and his co-workers reported that the change in product selectivity and increase of activity during reaction were caused by the "catalyst construction". CO chemisorbs strongly on cobalt (as well as on Ni and Ru) and it has been pointed out by Pichler [9] that FT synthesis performs under conditions not so far from those which allow (thermodynamically) carbonyl formation from these metals. Then the reaction of CO with the metal surface can be assumed to induce surface restructuring [7]. Images of a cobalt metal surface which had been used for FT synthesis were obtained by Wilson and de Groot [10] through scanning tunnelling electron microscopy. It is deduced from those pictures that segregation produces an ordered surface structure under syngas atmosphere. For any explanation for these large changes, it should be able to explain the all observed

phenomena simultaneously as the sudden changes for the reaction rate, CH_4 selectivity, and the O/P ratios occurred at the same time.

As a precise explanation for these phenomena could not be given on the basis of the experiments and the subsequent analysis we performed, we concluded further experiments need to be designed and carried out. [1] A group of flushing experiments with inert gas (argon) at various temperatures, plus FTS runs with syngas after flushing, were designed and conducted. The reactants and hydrocarbons from the reactor system during and after flushing were analyzed. The results are discussed below.

5.2 Experimental

5.2.1 FTS Experiments

The experiments were carried out in a 100 ml continuous stirred tank reactor (CSTR) (*Autoclave Engineers*) in a gas-solid system without adding any solvent. The experimental set up has been described in Chapter 4. Residence Time Distribution (RTD) experiments proved the reactor can be regarded as an ideal mixed reactor and the mean residence time (τ) showed a good match with the result of the volume of the reactor (V_r) over the volumetric flow rate (FR) of the feed gas when the stirring speed (SS) was higher than around 65 rpm. A supported cobalt catalyst with 10% Co / 90% TiO_2 (BET area 28.6 m^2/g, average pore diameter 35.8 nm) was used. Approximately 3g of prepared cobalt catalyst was loaded into a catalyst basket (provided with the reactor). The frame of the basket was fixed to the inner wall of the tank but the basket itself did not extend over the whole diameter. A stirrer in the inner radius was used to stir the gas and force it through the catalyst held in the basket. The catalyst basket together with the catalyst inside was suspended in the tank, without shaking during the experiment.

The catalyst was reduced with H_2 at 1.8Nlh^{-1}gcat^{-1} at ambient pressure. The gas space velocity was based on the total mass of the unreduced catalyst. The temperature was increased from room temperature to 120 ^{o}C initially at a ramping rate of 60 ^{o}Ch^{-1} and held for 2 hours; then it was increased to 280 ^{o}C at the same ramping rate, and held at this temperature for 24 hours. After reduction, the reactor was then cooled to below 100 ^{o}C for the experiment.

The feed gas was switched from H_2, which was used for reduction, to syngas (10% N_2/30% CO/ 60% H_2). The pressure of the reactor was stabilized at 2.0 MPa(g) by a back pressure regulator. The space velocity of the reactants was controlled at 1.2Nlh^{-1}(gcat)$^{-1}$ by a mass flow controller (*Brooks 5850*). The temperature used for reaction in the experiments was 190^{o}C. The applied stirring speed (SS) was varied according to the requirements of different experiments, but kept above 100 rpm in all cases to ensure that ideal mixing could be achieved.

5.2.2 Reactor system flushing experiments

When the reaction reached steady state (that is, the reaction rate and production of product were stable) the pressure of the reactor system was reduced to 0.3 Mpa(g), and the feed gas was switched from syngas to argon (Afrox, UHP, 99.999% in purity) at the reaction temperature. The gaseous products and un-reacted reactants were replaced rapidly by argon at a relatively high flow rate, 400ml/min, in around 3 minutes, and thereafter continuous flushing was carried out with argon at a lower flow rate of around 4 ml/min. That the replacement had taken place could be confirmed by the analysis of the stream from the reactor at the end of the replacement phase. For the continuous flushing stage that followed, the argon gas flow rate was reduced and the temperature of the reactor was set to flush temperature (a sequence of 190, 230 and 210 ^{o}C) very rapidly, with a ramping rate of 10 ^{o}C/min. The ramping period lasted only a few minutes. During the flushing,

a 300 rpm SS was applied. The product traps (one for wax products at the higher temperature and the other for oil and aqueous products at the low temperature) were bypassed so that all the material carried out of the reactor by the argon gas could be sent directly to the on-line gas chromatograph (GC) (Agilent 6890A, equipped with a TCD and an FID) for analysis. All the tail gas lines were maintained at 180 ^{o}C to prevent condensation for the light hydrocarbons.

Both the composition and the concentration of each component could be monitored by the on-line GC. As the flushing proceeded, the components became undetectable in the flushed-out stream as the peaks on the GC trace of sample were indistinguishable from the noise of the base line, after which the flushing experiment was considered complete. The duration of the flushing period depended on the argon gas flow rate and the amount of catalyst loaded in the reactor. In the experiments we performed, the length of time required was around 30 hours.

5.2.3 FTS experiments after the flushing

Once the flushing was completed, the feed for the reactor was switched back to syngas to allow the FT reaction to resume. The conditions for the FT reaction after flushing were the same as they had been before the flushing. Further flushing at different temperatures could be performed once the reaction had reached steady state again. Figure 5-3 below illustrates the switch between FT reaction and flushing operations.

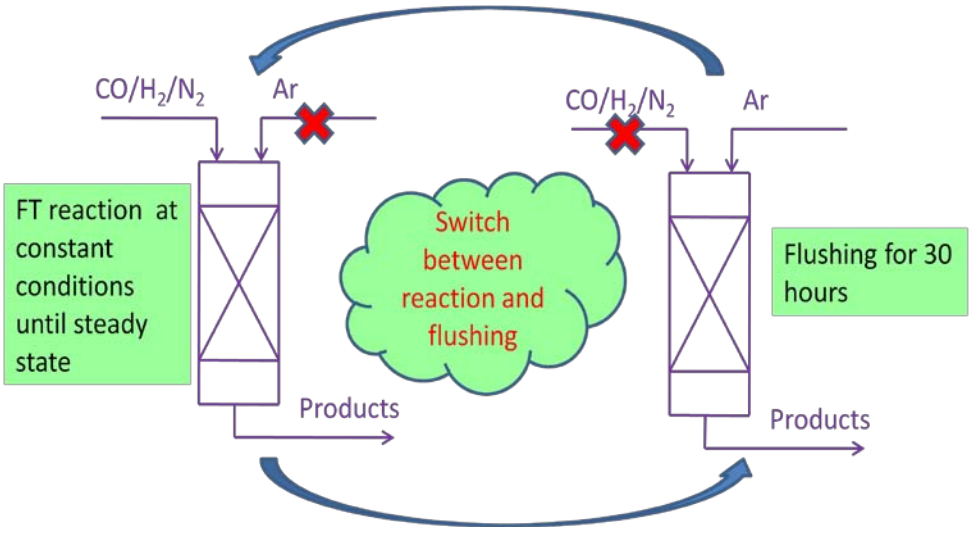

Fig. 5-3 Demonstration of the switch between the FTS and flushing experiments

5.3 Results and Discussion

5.3.1 FTS Behaviour after Flushing

The CO conversion, CH_4 selectivity, and O/P ratios for light hydrocarbons during the reaction after flushing are plotted with TOS in Figures 5-4, 5-5 and 5-6. The corresponding information before flushing is also presented in the plots to provide a basis for comparison. The flushing temperature sequence 190, 230, and 210 ^{o}C is also presented in these diagrams.

In Figure 5-4, the CO conversion decreased from around 17.5% when the catalyst was fresh, to around 10% when the secondary steady state had been achieved. The CO conversion increased after each flushing, but to different extents. The 190 ^{o}C flushing lifted the CO conversion only very slightly; 230 ^{o}C flushing made the CO conversion increase from around 10% to approximately 14%; and 210 ^{o}C flushing increased the CO conversion to about 12%, which is intermediate between the CO conversion increments that the 190 ^{o}C flushing and the 230 ^{o}C flushing could achieve.

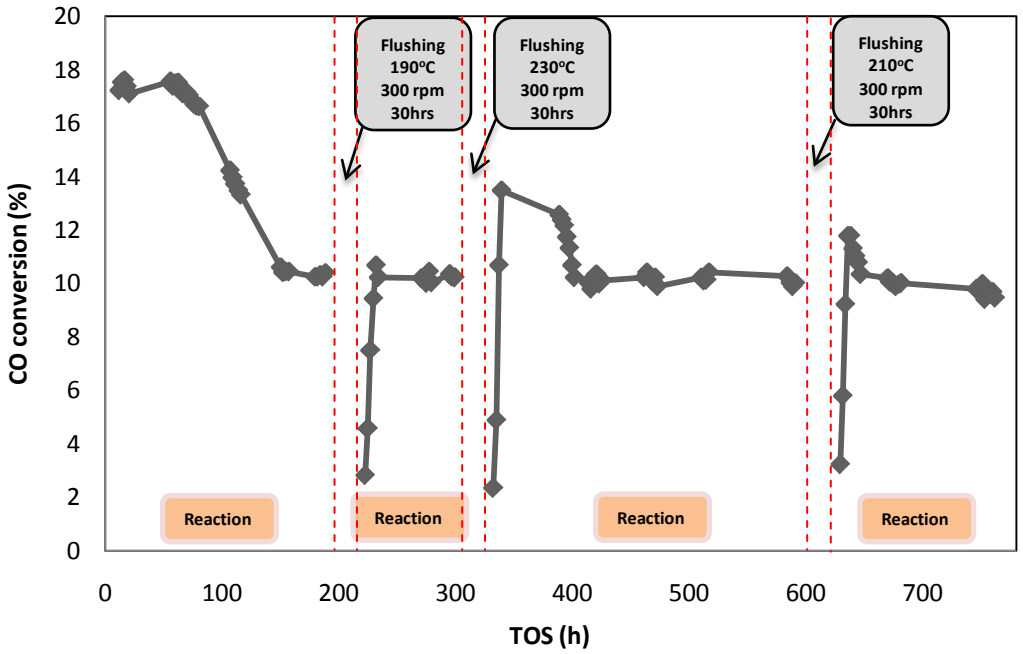

Fig. 5-4 The CO conversion during FT reactions (the same reaction conditions) before and after flushing with different flushing temperatures

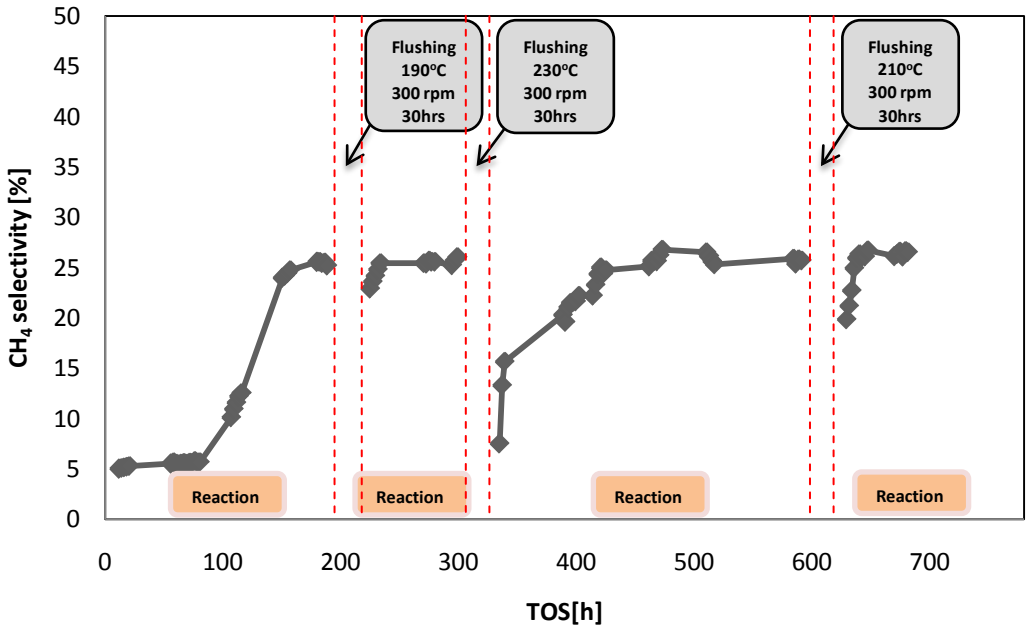

Fig. 5-5 Methane selectivity during reactions (the same reaction conditions) before and after flushing with different flushing temperatures

The CH_4 selectivity increased to a large extent, from around 5% with fresh catalyst to about 25% when the secondary steady state (TOS =140–180 hrs) was achieved, as can be seen in Figure 5-5. The 190 ^{o}C flushing reduced the CH_4

selectivity by a small margin; 230 ^{o}C flushing made the CH_4 selectivity drop dramatically to around 7%, which was very close to the level at which it had been when the catalyst was fresh; and 210 ^{o}C flushing decreased the CH_4 selectivity to around 19%, which was in between the CH_4 selectivity reduction that the 190 ^{o}C flushing and the 230 ^{o}C flushing brought about.

Figure 5-6 gives the changes for olefin to paraffin (O/P) ratios of light hydrocarbons (C_2–C_4) during the reaction periods before and after the flushing experiments were conducted. The results displayed show substantial reduction in olefin to paraffin ratios when the FTS was carried on for around 80 hours. These low O/P ratios can be improved after flushing, with the extent of the change dependent on the flushing temperature. Higher temperatures produced higher increases. Flushing at 230 ^{o}C could raise these ratios close to their original values at the beginning of the experiment, as is shown in the plot during the first 80 hours TOS.

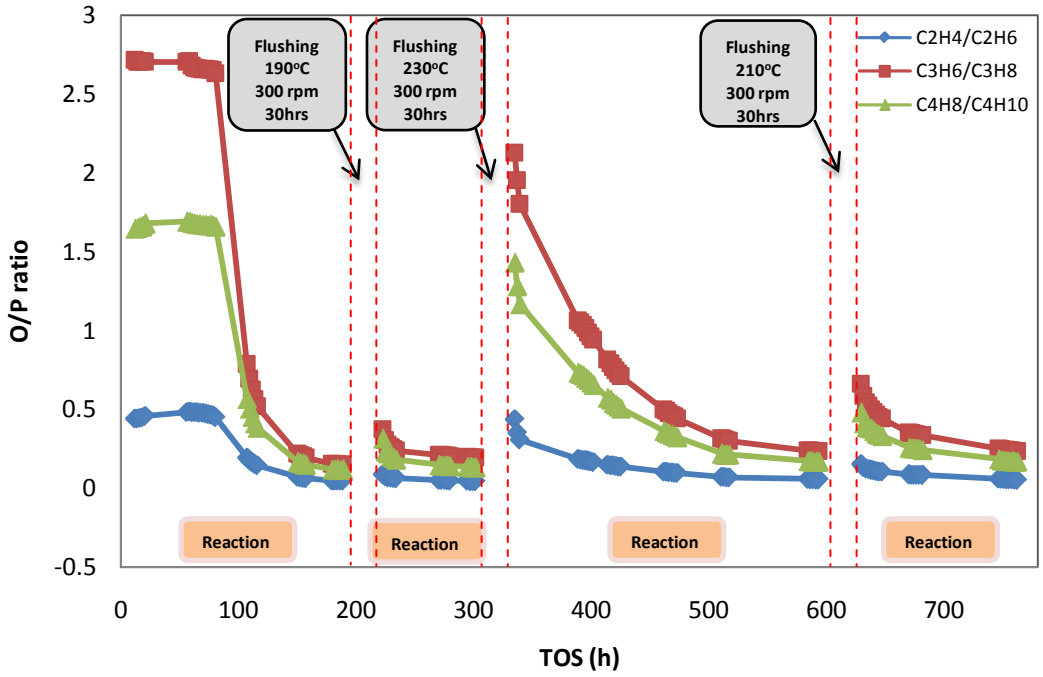

Fig. 5-6 O/P ratios for C_2–C_4 during reactions (the same reaction conditions) before and after flushing with different flushing temperatures

When we look at these three figures, some common phenomena can be observed. First, the values for CO conversion, CH_4 selectivity, and O/P ratios of C_2–C_4 changed after each flushing when compared with their values at the end part of the reaction (before flushing). Second, the values for those parameters at the tails of reactions after flushing could arrive more or less the levels just before flushing, regardless of the flushing temperature that had been applied. Third, the recovery of these parameters to their initial levels (before 80 hours of TOS) depended on the applied flushing temperature, with the higher temperature favoring more recoveries.

When flushing at these three different temperatures, we varied only the temperature. The other conditions, such as pressure, feed gas flow rate, and stirring speed, were the same. The only gas used in the flushing was argon, an inert gas, and there was no evidence to suggest that chemical or structural changes had taken place on the catalyst and had subsequently affected the performance of the FTS after each flushing. The changes in the values of the parameters therefore suggest that the flushing temperature has certain effects on the catalyst system. After flushing at the lower temperature (190 ^oC), the CO conversion, CH_4 selectivity and O/P ratios fell back to their levels before flushing very quickly, whereas flushing at higher temperatures held them at relatively higher levels for a longer time. This obvious difference suggests that the flushing temperature is a critical factor that changes the properties of the catalyst system.

As argon was used for flushing, the changes in the parameters after each flushing were probably attributable to physical alterations in either the catalyst or the catalyst regime rather than on the catalyst surface. In a gas-solid FTS system, liquid could be formed as a result of the reaction conditions and the volatility of long chain hydrocarbons. The liquid phase product was found in the reactor and on the catalyst surface occurred under conditions similar to those in the

experimental runs here. During flushing, the temperature and inert gas flow would drive off the liquid on and in the catalyst, which would bring about an alteration in the catalyst regime. As the flushing treatment in the reactor could be regarded as a mainly stripping process for the catalyst, the higher flushing temperature would drive more liquid from the catalyst, which in turn would mean that less liquid would remain when the FTS reaction was resumed. Both the amount and the composition of the liquid in the catalyst would be changed by the various flushing temperatures, and these proved to affect the conversion and product selectivity. Therefore, because the liquid deposit in the catalyst is responsible for the changes of conversion and product selectivity before and after flushing, it is a key factor in FTS performance.

As already noted, a higher flushing temperature resulted in a reduced amount of liquid in the catalyst when the FT reaction was resumed. The amount of liquid in the catalyst has an obvious inhibiting effect on the transportation of reactants to the active sites of the catalyst, and obstructs the mass transfer of the formed products out of the catalyst. The reaction rate therefore slowed down, as seen in Figures 5-1 and 5-4; and the O/P ratios increased, as illustrated in Figures 5-2 and 5-6, owing to the secondary reaction of olefins, as the slower rate of mass transfer provides greater opportunities for their re-adsorption. Therefore, when a higher temperature was applied for flushing, more liquid was driven off from the catalyst, and the recoveries of reaction rate and product selectivity were seen to be closer to the initial values (as shown in Figures 4–6) than when the catalyst was “dry” at the very beginning of the flushing experiment.

Although the liquid in the catalyst affects both the reaction rate and product selectivity, the extent of these effects differs. When we compare Figures 5-4, 5-5 and 5-6, we can see that product selectivity (Figures 5-5 and 5-6) is more sensitive to the liquid deposit than it is to the reaction rate (Figure 5-4). When the 230 ^{o}C

flushing temperature was applied, the CH_4 selectivity and O/P ratios were led back to levels close to those at the very beginning of the run, when the catalyst was fresh. However, the CO conversion was lifted by only about half of the difference between the initial and the final levels. This may be attributable to the characteristic difference in mass transfer of reactants and products in the liquid phase products.

5.3.2 Reactants and Products in the Flushed-Out Gas during Flushing

The on-line GC can detect the reactants and short chain hydrocarbon products (C_1–C_8) in the flushed-out gas. Their contents in the flushed-out stream are illustrated in the diagrams below (Figures 5-7 to 5-12). However, before going on to a detailed discussion of the contents, we consider it crucial to confirm the source of these reactants and hydrocarbons, that is, whether it is in the catalyst or in the reactor (in this case excluding the catalyst). Based upon the flushing experiment procedure and the analysis for the stream out of the reactor at the end of the quick replacement, we believe that these reactants and products in the flushed-out stream come from the catalyst and not the reactor system (excluding the catalyst). Our reasons are set out below.

a. In the transition between the FT and flushing experiments, we rapidly replaced the gas phase material in the reactor system with argon gas under reaction conditions, as described in the Experimental section. When the stream out of the reactor at the end of the rapid replacement phase was sent to the GC for analysis, the trace showed no detectable reactants or C_1–C_8 products in that stream. (We could not collect any information on higher molecular weight materials as the online GC in the experimental set-up was unable to analyze them.)

b. According to predictions based on the vapor liquid equilibrium (VLE) and the mean residence time of the reactor at flushing conditions, if the reactants and products detected in the flushed-out gas had come from reactor system (excluding the catalyst), these materials would have been taken out by the inert gas and become undetectable in less than 1.5 hours. Yet in our experiments the reactants could be detected in the flushed-out stream for about 20 hours and the products for more than 28 hours.

Therefore, the results collected during the flushing period are attributable to the catalyst and not the reactor, we can use the information we have obtained about the reactants and some of the products to gain more insight into FTS. We did this by investigating and comparing the concentration of hydrocarbons in the flushed-out stream.

If we assume that the reactor system (including the catalyst) can be regarded as a VLE-governed system, we can use Raoult's Law [11] to calculate the percentage of each type of hydrocarbon in the flushed-out gas stream, which will indicate the amount of hydrocarbons inside the reactor system:

$$y_A P = x_A P_A^{Vap} \qquad (5\text{-}1),$$

in which y_A is the hydrocarbon content in the vapor phase; x_A is the hydrocarbon content in the liquid phase; P is the pressure of the system; and P_A^{Vap} is the vapour pressure of the hydrocarbons.

Following the VLE theory, for an ideal stripping process in a system we assume the volume of the liquid is V; the flow rate of the stripping stream is F; the molar concentration of material A in the liquid phase is x_A and in the gas phase is y_A; the change in the concentration of A in the liquid phase over time can be written as the equation below: [11]

$$V\frac{dx_A}{dt} = F(x_A - y_A) \qquad (5\text{-}2).$$

In our reactor system, the stripping process did not follow an ideal VLE model, as some other factors such as diffusion and the change in volume of the liquid had to be taken into consideration. However, we considered it reasonable to study the alteration in the concentrations of the hydrocarbons in this way when we compared their relative stripping rates.

The ratio of y_A over x_A can be defined as k_A:

$$k_A = \frac{y_A}{x_A} \tag{5-3}.$$

Therefore, x_A can be expressed by y_A and k_A

$$x_A = \frac{y_A}{k_A} \tag{5-4}.$$

Replacing x_A in Eq. 5-2 by Eq. 5-4, Eq. 5-2 can be written as Eq. 5-5 and then Eq. 5-6:

$$V\frac{d(y_A / k_A)}{dt} = Fy_A(\frac{1}{k_A} - 1) \tag{5-5},$$

$$\frac{dy_A}{dt} = \frac{F}{V}y_A(1 - k_A) \tag{5-6}.$$

The relative change rate for the hydrocarbons in our reactor system was decided by their k_A values, while the k_A is determined by the volatility of the component. So the k value of C_n is greater than that of C_{n+1} (n>1) (the lower the boiling point, the higher the k value). This means that the change of the concentration over time dy_A/dt in a system is more rapid for material with a lower boiling point, which in our case are shorter chain hydrocarbons.

Reactants in the Flushed-Out Gas

Result The concentrations of H_2 and CO in the flushed-out gas during one continuous flushing are shown in Figure 5-7. The mean residence time for argon gas under flushing conditions (210 ^oC, 3 bar) was about 90 minutes. CO and H_2

were found in the flushed-out gas even after 20 hours, which indicated that both came from the catalyst. In Figure 5-7 we can clearly see that the concentration of H_2 is higher than that of CO throughout the flushing period, and the ratio of H_2/CO is higher than 2 (the ratio in the feed gas).

The amounts of H_2 and CO in the flushed-out stream during the entire flushing period were calculated by means of Eq. 5-7: [12]

$$n_A = F\int_{t=0}^{t=t_{end}} C_A dt \qquad (5\text{-}7),$$

in which n_A is the total amount of one reactant flushed out of the reactor system; F is the outlet molar flow rate, which can be taken to be equal to the inlet flow rate; C_A is the molar fraction of one reactant in the flushed-out stream; and t is the time taken for flushing. The total amount of flushed-out H_2 is around 4 times that of the flushed-out CO. This result shows that the ratio of H_2 to CO in the liquid-filled pores of the catalyst is far higher than in both the feed gas and the gas in the reactor.

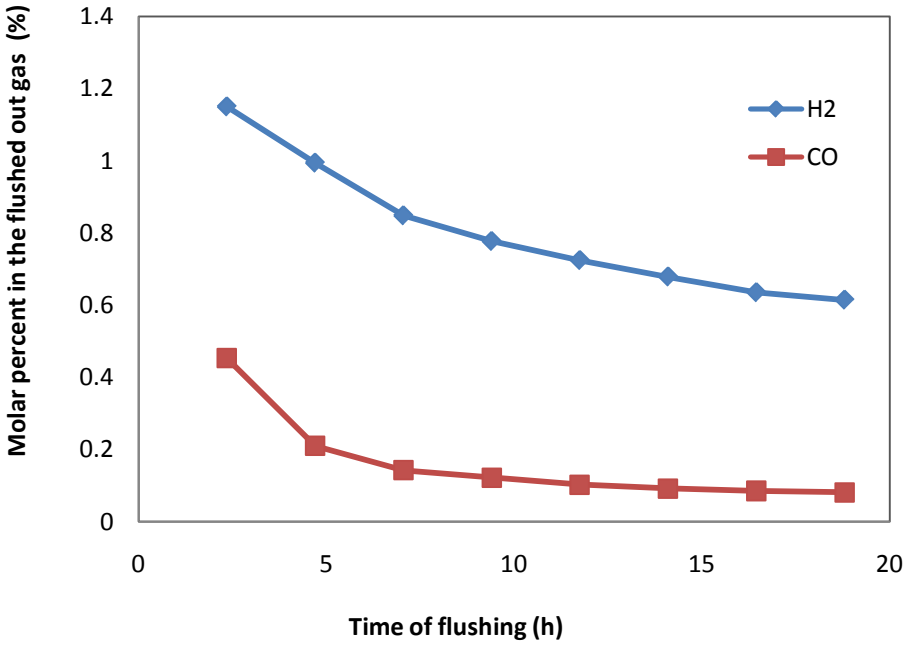

Fig. 5-7 Molar fraction of reactants in the flushed-out stream during the flushing period

Implications for the kinetics and product selectivity Some researchers have investigated the solubility of H_2 and CO in the liquid products. [13-15] For example, Chou *et al* [16] carried out experiments to measure the solubility of hydrogen, carbon monoxide, methane, carbon dioxide, ethane and ethylene in FT SASOL wax, which is primarily a mixture of n-paraffins, at pressures from 10-50 atm and at temperatures from 200-300℃. The results showed that the solubility of CO is around 1.46 times that of H_2 at 200℃ and 20 atm, which is very similar to the reaction conditions in our experiments. Various other scientists have published findings on the diffusion of the synthesis gas and products in the liquid produced. [17, 18] The experimental results reported by Erkey *et al* [18] showed that the diffusion coefficient of H_2 is around 2.4 times that of CO in FT wax at 220℃ and 14 bar.

Generally speaking, CO has a better solubility but poorer diffusivity than H_2 in Sasol wax under FTS conditions. However, the composition of the material in the catalyst is likely to consist of more than a mixture of n-paraffins, which challenges the assumption itself. The information obtainable from the literature deals with the diffusion properties and solubility of H_2 and CO separately, but the situation where H_2 and CO are both present inside the liquid-filled pores may be better described as a combination of their diffusion and solubility characteristics. This raises further questions. For example, one of them may dominate. Another question is to what degree these two factors decide the real H_2/CO ratio around the catalyst active sites. The results of the flushing experiments we performed contribute to an understanding of the reactants inside the catalyst pores because they provide information from: (a) a combined situation instead of isolated one, which means solubility only or diffusivity only; and (b) an FTS environment instead of merely FT wax. The results derived from flushing experiments show an entirely different H_2/CO ratio from what would normally be expected, and as these reactants (CO and H_2) are crucial to the performance of FTS, both for the

reaction rate and the product distribution, this interesting result may help us to understand FTS better.

In the research that has already been carried out on FTS, the kinetics of FTS on Co and Fe catalysts has been extensively investigated. It is noticeable that there is a variety of kinetic expressions, which covers not only the expressions themselves but the partial pressures of the reactants and even the products, and a similarly extensive span for the activation energies for both Co and Fe catalysts. Some of these studies are comprehensive, and offer separate complex expressions for the production of alkanes, alkenes, and CO_2 derived from mechanistic sequences and fitted to large data sets over wide ranges of operating conditions. This raises questions about which of these data, parameters and rate expressions can be relied upon for estimating reaction rates and/or conducting preliminary reactor design. This problem has also been pointed out by Bartholomew et al. [19], who have summarized the reasons of the inconsistency of the kinetic expressions, including the absence of considering of pore diffusional restrictions; derivations of kinetic parameters using data that are not obtained under isothermal experimental conditions; and fitting the data to different, complex rate expressions derived under limited operation conditions.

The results shown in this paper suggest that it is also important to understand the situation of the reactants in the liquid-filled catalyst as the dramatic alteration of the H_2/CO ratio from the gas to the liquid phases. A typical reaction rate expression for FTS on a cobalt catalyst can be expressed in the following equation (Eq. 5-8): [20, 21]

$$-r_{CO} = \frac{kp_{H_2} p_{CO}}{(1+bp_{CO})^2} \qquad (5\text{-}8).$$

As can be seen from the kinetic expression, the reaction rate is a function of the partial pressure of the reactants. In a kinetic study, one always derives the kinetic equation from the corresponding information on the reactants in the gas phase in

the reactor. But it is limited as the composition of the reactants inside the liquid is unknown, and the FT reaction happens on the active sites, which are submerged in the liquid phase products. Also, the composition of the liquid in the catalyst pores and on the surface may change when the catalyst type and reaction conditions are varied. Therefore, the H_2/CO ratio around the catalyst active sites, which are covered by the liquid, may differ from case to case, although the gas composition in the reactor does not change. Our later set of experiments showed that the product water might be in liquid phase under typical low temperature FTS conditions, and this makes the situation on the surface of the catalyst even more complicated.

The author does not want to discuss too much on how the extent to which the liquid deposited in the catalyst affects the kinetic expression and the rate itself. Instead, we would like to point out: (a) in the FT kinetic studies, it is a considerable factor to be noticed that the FTS that liquid deposit in the catalyst and the subsequent changes in the relative amounts of H_2 and CO on the active sites; and (b) the entirely different H_2/CO ratio in the catalyst and the reason for this discrepancy could offer another way of understanding the variety of the kinetic expressions for the FTS.

The results given above also indicate that when the liquid plays an important role in influencing the reaction rate as a consequence of gas-liquid diffusion, the CO becomes the limited reactant, as it is below the stoichiometric requirements of the reaction.

In terms of product selectivity, the O/P ratios or the selectivity of olefins decreased when the liquid phase products were deposited in the catalyst. A typical explanation of this behaviour offered in the literature (and by the authors named above) is that the liquid inside the catalyst pores strengthens the resistance to mass

transfer, in this way enhancing the secondary reaction of olefins to form paraffins. But we also noticed that the CH_4 selectivity had also been improved. As the H_2/CO ratio is important in deciding the extent of hydrogenation of olefins in FTS, the high H_2/CO ratio in the liquid in the catalyst may also explain why the CH_4 selectivity increased dramatically, from around 5% when the catalyst was fresh to around 25% when liquid products were deposited on the catalyst. Therefore, when the liquid builds up in the catalyst, the selectivity of paraffins increases substantially owing to at least two factors: the secondary reaction of olefins is strengthened by the diffusional resistance from the liquid phase products; and the hydrogenation reaction of olefins is favoured among the secondary reactions (such as hydrogenation of olefins to paraffins, chain growth reaction of C_n to C_{n+1}, and isomerisation), as the H_2/CO is extremely high in the liquid.

Products in the flushed-out gas

The short chain hydrocarbon products (C_1-C_8) can be detected in the flushed-out gas almost throughout the flushing period. For convenience of interpretation, the hydrocarbons in the flushed- out gas can be grouped into three: CH_4; C_2-C_4; and C_4-C_8. Their contents in the flushed-out gas at different time of flushing are given in Figures 5-8 to 5-12. As C_4 was the common thread for group C_2-C_4 and C_4-C_8, it appeared in Figures 5-9 to 5-10 and 5-11 to 5-12.

As is illustrated in Figure 8, the general trend for CH_4 content in the flushed-out gas was to decrease as the flushing progressed. It started at a relatively high concentration when compared with the other hydrocarbons detected in the flushed-out gas, and diminished rapidly until about 15 hours of flushing had been completed. From that point it remained at a very low but still detectable concentration until the end of the flushing experiment.

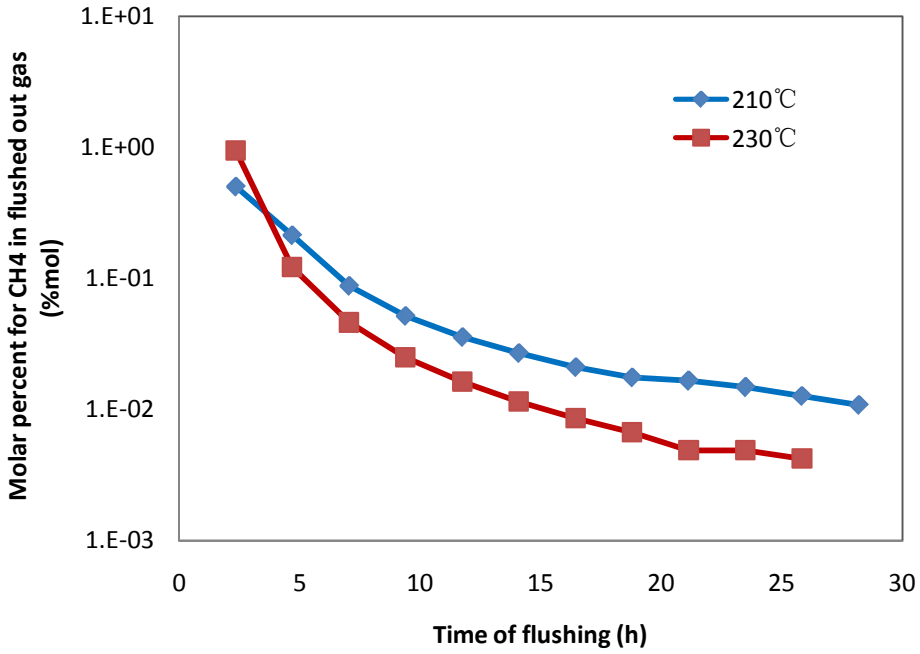

Fig. 5-8 The molar percentage of CH_4 in the flushed-out gas during the entire flushing period at two flushing temperatures

Both olefins and paraffins for C_2-C_4 were found in the flushed-out gas, and their concentrations over the time of flushing are plotted in Figures 9 and 10. The general trend of their concentration in the flushed-out gas was similar to that of CH_4. However the rate of their disappearance has yet to be explained. In the normal stripping process for a group of hydrocarbons, the lightest component will be most easily and hence the first to be stripped off, and the disappearance rate of the hydrocarbons in the solution decreases as the molecular weight increases because of the volatile properties of the hydrocarbons.

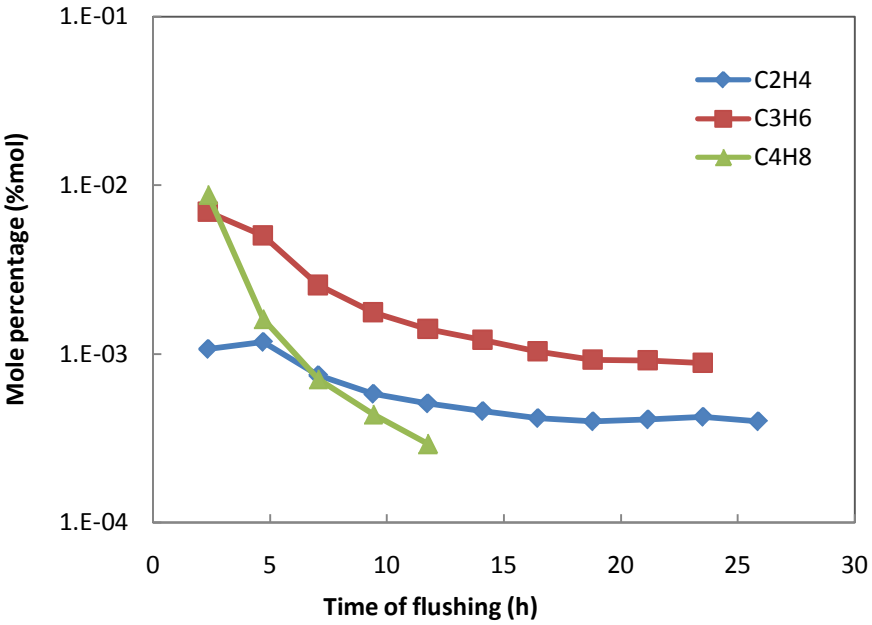

Fig. 5-9 The molar percentage of C_2–C_4 alkenes in the flushed-out gas during the entire flushing period with $T_{Flushing}$ = 210 °C

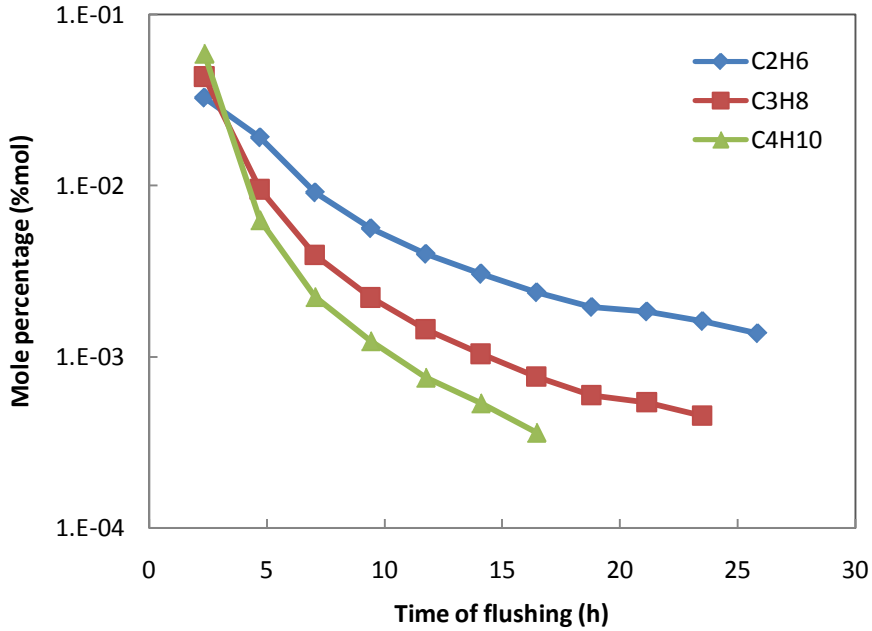

Fig. 5-10 The molar percentage of C_2–C_4 alkanes in the flushed-out gas during the entire flushing period with $T_{Flushing}$ = 210 °C

In both the olefin (Figure 5-9) and paraffin (Figure 5-10) groups, we can clearly see that although C_4 was present in the highest concentration, followed by C_3 and

then C_2 at the beginning of the flush, it had the fastest disappearance rate during the flushing period. As the duration of flushing continued, C_4H_8 and C_4H_{10} were the first in their own groups to become undetectable by the online GC, while C_2H_4 and C_2H_6 were found to change the least in comparison with the other hydrocarbons. All of these results are in conflict with those expected in a normal stripping procedure. This indicates that these phenomena cannot be explained by stripping alone.

Furthermore, if we compare Figures 5-9 and 5-10 based on the same carbon number, we can see that the disappearance rate of alkane is much more rapid than that of alkene as can be judged by the slopes of the curves. The flushing experiment was initiated when the liquid build-up was complete, so that the amount of alkene was supposed to be far lower than that of alkane. This can be confirmed by the first data points in Figures 5-9 and 5-10. Thus the alkenes will be undetectable sooner than alkanes owing to their slightly higher volatility and smaller amount when compared to alkanes, which are based on the same carbon number. But it was not the case in our experimental results. This leads to the conclusion that reaction(s) might have occurred during the flushing.

CO and H_2 were found in the liquid in the catalyst, and the flushing conditions were at typical reaction temperature and moderate pressure for FTS, so we assume that an FTS reaction occurred involuntarily. As discussed above, the liquid inside the catalyst pores would favour the formation of alkanes instead of alkenes, for three reasons: (a), there were more alkanes than alkenes in the liquid in the catalyst pores; (b), more alkanes were formed by the FTS reaction during flushing than alkenes; and (c), because the volatilities for alkenes and alkanes are similar for the same carbon number, it is therefore believed that the disappearance rate for alkane should be slower than that of alkenes. But our results showed an opposite trend. It is therefore quite possible that the FT reaction assumption alone is not

adequate to explain this. The experimental results show clearly that more alkenes were formed than could be thought possible. In the mean time, if we compare the O/P ratios during flushing with them in the reaction after flushing, we can see the ratios at the second half of the flushing period (taking C_3H_6/C_3H_8 for an example derived from the result in Figures 5-9 and 5-10, the ratios are bigger than 1) are higher than those at the initial stage of the reaction when it is resumed from the flushing with 210℃ (see Figure 5-6, C_3H_6/C_3H_8 was only around 0.6). Therefore, some of the olefins are not from the reaction from reactants for sure. This provides a clue that leads us to propose that reaction between the products may happen inside the catalyst under flushing conditions.

At FTS reaction conditions, secondary reactions of primary olefins include hydrogenation, chain growth, isomerisation, hydrogenolysis, cracking. The first three are widely accepted by the researchers while the last two remain points of argument. No cracking or hydrogenolysis reactions of co-fed olefins (ethene, 1-butene, 1- hexene, 1-decene) was observed by Hanlon and Satterfield [22]. Also Dwyer and Somorjai [23] did not observe any cracking products from added ethene or propene. Schulz et al. [24] reported less than 1% cracking of added ethene or propene on an iron catalyst. However, cracking of added olefins was observed by Jordan and Bell [25-27] on a ruthenium catalyst at low total pressure. Cracking is promoted by high hydrogen pressures and high temperatures (T > 300℃) and is strongly inhibited by CO pressure [28, 29] and H_2O pressures [30].

The results shown here in our work suggests that reactions might take place under the condition similar to FTS (typical temperature but lower pressure especially far lower partial pressure of reactants). The fact shown by the results in Figures 5-9 and 5-10 suggest that the reaction took place during flushing and the discussion above concluded that the reactions include reactions between products especially

olefins other than FT. The reaction we think is not necessarily to be cracking but reaction like the way written as Eq. 5-9 below.

$$C_{n-1}H_{2(n-1)} + C_{n+1}H_{2(n+1)} = 2C_nH_{2n} \qquad (5\text{-}9).$$

The molar percentages of flushed-out C_4-C_8 paraffins in the outlet stream are shown with flush time at 210 ^oC in Figure 5-11 and 230 ^oC in Figure 5-12. The concentrations of C_4-C_8 in the flushed out gas at the beginning of the flush were similar, as can be seen from the data points at a flushing time of 2.35 hours. At the end of the flushing experiment, the concentrations of C_4-C_8 were markedly different. This tells that the disappearance rate for lighter hydrocarbons is far more rapid than for heavier hydrocarbons. Also, the concentration of heavier hydrocarbons remained at a higher level than that of the lighter hydrocarbons, which suggests that there are more of the heavier hydrocarbons than of the lighter ones in the liquid in the catalyst.

The amount of C_1-C_8 hydrocarbons flushed out from the catalyst during the entire flushing period was calculated based on Eq. 5-7. As the inlet argon flow rate was constant, the outlet flow rate can be assumed to be constant and equal to the inlet argon flow rate, since the amount of material stripped from the catalyst was small when compared with the amount of argon. The total flushed- out amounts of C_1-C_8 hydrocarbons at two flushing temperatures are given in Figure 5-13.

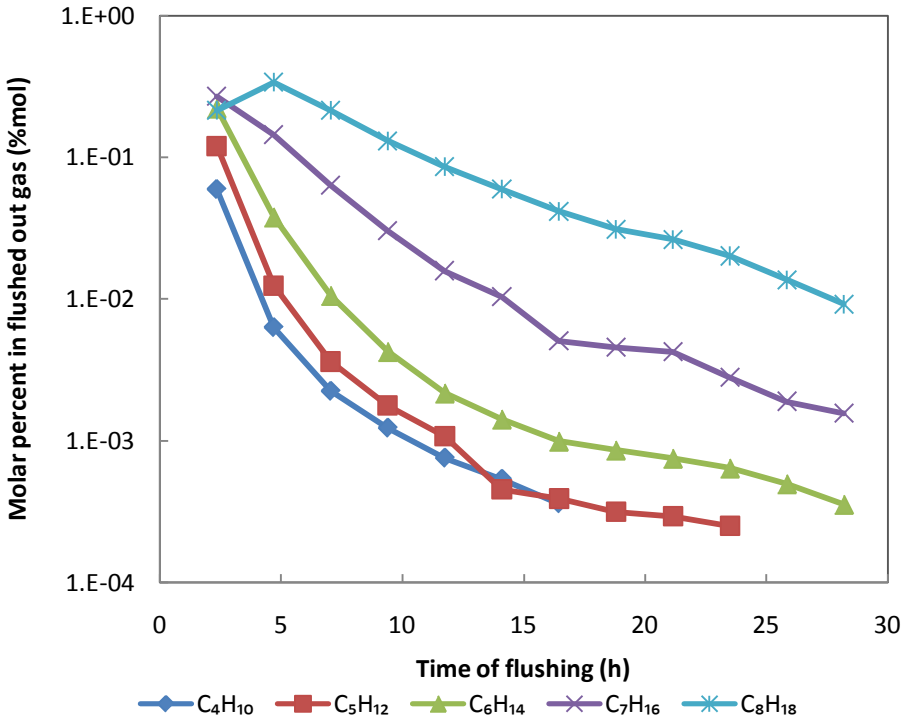

Fig. 5-11 The molar percentage of C_4–C_8 alkanes in the flushed-out gas in the entire flushing period with $T_{Flushing}$ = 210 ^{o}C

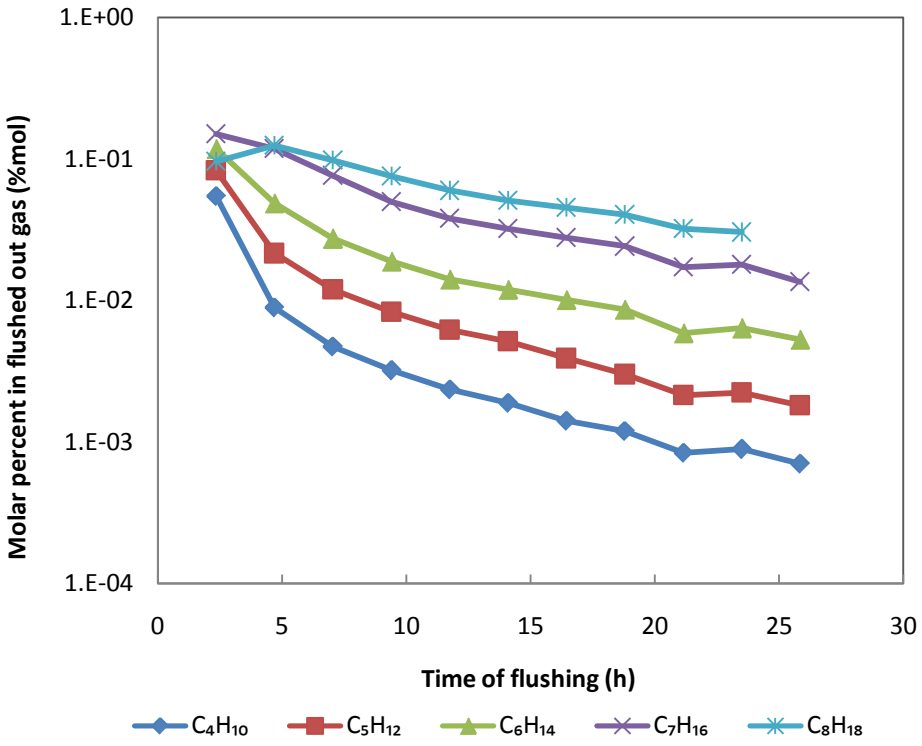

Fig. 5-12 The molar percentage of C_4–C_8 alkanes in the flushed-out gas during the entire flushing period with $T_{Flushing}$ = 230 ^{o}C

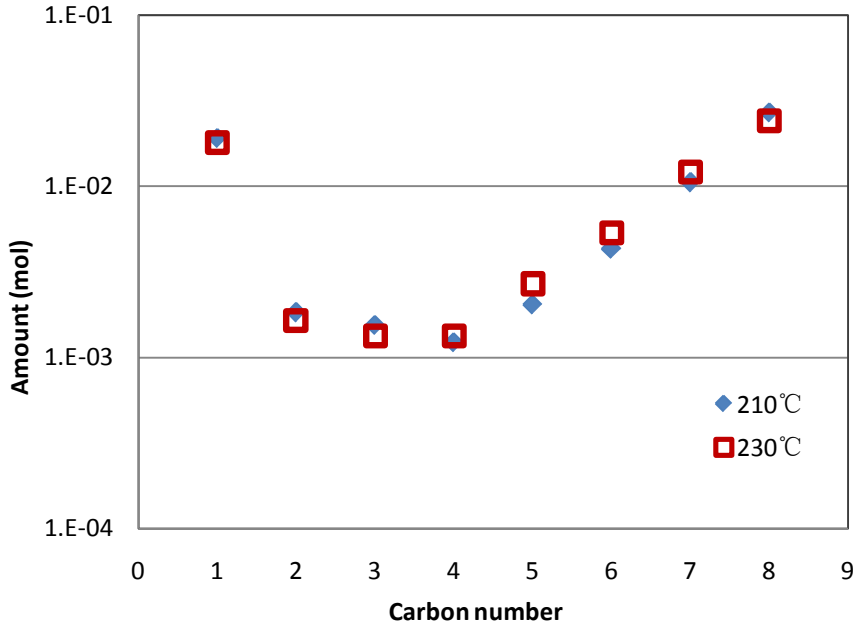

Fig. 5-13 Total flushed-out amounts of C_1–C_8 hydrocarbons

In Figure 5-13, we can see that throughout the flushing periods at two different temperatures, the amounts of hydrocarbons flushed out are comparable for each carbon number. This factor might tell us that during the flushes at applied temperatures and pressure, the light hydrocarbons in the catalyst have been stripped out fully.

The distribution of the products from catalyst shows a clear trend. The amount of CH_4 is outstanding when compared with that of the carbon number hydrocarbons which follow. A descending distribution can be observed for C_2 to C_4, but the decrease is slight, and possibly attributable to a limited extent by the reaction during the flushing. For the carbon number range above C_4, the amount of hydrocarbons started to increase exponentially with the increase of carbon number. The product distribution in the catalyst derived from the experiment is comparable with suggests the prediction that Zhan *et al.* [31] made on the basis of a simulation, except for the component CH_4. In their simulation, the concentration of CH_4 is the lowest in the liquid in the catalyst, while here in our experiment the result shows it is considerably higher when compared to the values of C_2–C_6. The distribution of

flushed-out hydrocarbons with carbon numbers is entirely different from the distribution of products from the reactor when the FT reaction takes place.

5.5 Conclusion

Flushing experiments in a stirred basket reactor were performed after the FTS reaction had reached steady state at 190 ^{o}C, and the FTS reaction was resumed once the flushing experiment had been completed. We compared the results of the reaction rate and product selectivity from FTS before and after flushing. We pointed out at the beginning that there were two apparent steady-states for the FT reaction, an initial one which spontaneously turned into a later one. Three different flushing temperatures (190 ^{o}C, 210 ^{o}C, and 230 ^{o}C) appeared to return the conversion and product selectivity in the reactor after flushing back to the initial levels before flushing to different extents. We surmised the flushing treatment by argon changed the amount and composition of a liquid phase that had formed during the reaction. This therefore suggested that the considerable changes in reaction rate and product selectivity we observed during the early stage of FT reaction were caused (either wholly or mainly) by liquid products deposited in the catalyst. We further surmised that the deposited liquid in the catalyst provided diffusional restrictions for the reactants and products so that the reaction rate was slowed down and the olefin/paraffin ratios were decreased owing to the enhancement of the secondary reaction of olefins.

The data for reactants and products in the flushed out stream during flushing were also collected and the results provided further interesting insights into FTS. The amount of H_2 driven out from the catalyst was around 4 times that of CO instead of 2 times, which was the ratio in the feed gas. We suggest that this is the reason that the selectivity towards CH_4 and paraffins increase dramatically when liquid is formed. The high H_2/CO ratio around the active sites of the catalyst also probably

made CO become the limiting reactant for reaction. The dynamic behaviour of the concentration of hydrocarbons in the flushed out stream suggested that stripping of the liquid by the flushing gas alone could not explain the slow rate of decrease of the lower hydrocarbons relative to the higher ones. This suggested that reactions among the products might take place under the moderate FT reaction conditions (such as the temperature and pressure applied for flushing) in the vessel.

The flushing experiments provided a new and unique way to examine the FTS reaction and enabled us to draw novel and interesting conclusions about the nature of the reaction and the liquid that was in the reactor.

5.6 Reference

1. Lu, X.; Hildebrandt, D.; Liu, X.; Glasser, D. Making Sense of the Fischer-Tropsch Synthesis Reaction: Start-up. *Industrial and Engineering Chemistry Research* **2010**, *49*, 9753.
2. Madon, R. J.; and Iglesia, E. Hydrogen and CO intrapellet diffusion effects in ruthenium-catalyzed hydrocarbon synthesis. *Journal of Catalysis*. **1994**, 149, 428.
3. Iglesia, E.; Reyes, S. C.; Soled, S. L. *Reaction-transport selectivity models and the design of Fischer-Tropsch catalysts,* in E.R. Becker; C.J. Pereira, eds., Computer-aided design of catalysts. Marcel Dekker: New York. 1993.
4. Anderson, R. B.; Seligman, B.; Schulz, J. F.; Kelly, R. E.; Elliot, M. A. Fischer-Tropsch Synthesis: Some Important Variables of the Synthesis on Iron Catalyst. *Industrial and Engineering Chemistry*. **1952**, *44*, 391.
5. Post, M. F. M.; van't Hoog, A. C.; Minderhoud, J. K.; Sie, S. T. Diffusion Limitations in Fischer-Tropsch Catalysts. *AIChE Journal.* **1989,** *35*, 1107.
6. Iglesia, E.; Reyes, S. C.; Madont, R. J. Transport-Enhanced α-Olefin Readsorption Pathways in Ru-Catalyzed Hydrocarbon Synthesis. Journal of Catalysis. **1991**, *129*, 238.
7. Schulz, H.; Nie, Z.; Ousmanov, F. Construction of the Fischer–Tropsch regime with cobalt catalysts. *Catalysis Today*. **2002**, *71*, 351.
8. Schulz, H., Major and Minor Reactions in Fischer–Tropsch Synthesis on Cobalt Catalysts. *Topics in Catalysis*. **2003**, *26*, 73.
9. Pichler, H.; Frankenburg, W. *Advances in Catalysis*. Academic Press: New York, 1952; Vol. IV
10. Wilson, J.; de Groot, C. Atomic-Scale Restructuring in High-pressure Catalysis. *The Journal of Physical Chemistry*. **1995**, *99*, 7860-7866.
11. Coulson, J. F.; Richardson, J. F. *Chemical Engineering, Vol. 2 (2nd edition)*. Pergamon Press: New York. 1993.

12. Himmelblau, D. M.; Riggs, J. B. *Basic Principles and Calculations in Chemical Engineering (7th edition)*. Peason Education: New Jersey. 2004
13. Albal, R. S.; Shah, Y. T.; Carr, N. L.; Bell, A. T. Mass Transfer Coefficient and Solubilities for Hydrogen and Carbon Monoxide under Fischer-Tropsch Conditions. *Chem. Eng. Sci.* **1984**, *39*, 905.
14. Masumoto, D. K.; Satterfield, C. N. Solubility of Hydrogen and Carbon Monoxide in Selected Non-aqueous Liquids. *Ind. Eng. Chem. Process Des. Dev.* **1985**, *24*, 1297.
15. Huang, S. H.; Lin, H. M.; Tsai, F. N.; Chao, K. C. Solubility of Synthesis Gases in Heavy n-Paraffins and Fischer-Tropsch wax. *Ind. Eng. Chem. Res.* **1988c**, *27*, 162.
16. Chou, J. S.; Chao, K. Solubility of Synthesis and Product Gases in a Fischer-Tropsch SASOL Wax. *Ind. Eng. Chem. Res.* **1992**, *31*, 621.
17. Satterfield, C. N.; Huff, G. A. Effects of mass transfer on Fischer-Tropsch synthesis in slurry reactors. *Chemical Engineering Science.* **1980**, *35*, 195.
18. Erkey, C.; Rodden, J. B.; Akgerman, A. Diffusivities of Synthesis Gas and n-Alkanes in Fischer-Tropsch Wax. *Energy & Fuels.* **1990**, *4*, 275.
19. Bartholomew, C. H.; Farrauto, R. J. Fundamentals of industrial catalytic processes. Wiley: New Jersey, 2006.
20. Yates, I. C.; Satterfield, C. N. Intrinsic Kinetics of the Fischer-Tropsch Synthesis on a Cobalt Catalyst. *Energy & Fuels.* **1991**, *5*, 168.
21. Maretto, C.; Krishna, R. Modelling of a bubble column slurry reactor for Fischer–Tropsch synthesis. *Catalysis Today*. **1999**, *52*, 279.
22. Hanlon, R.T.; Satterfield, C.N., Reactions of selected 1-olefins and ethanol added during the Fischer-Tropsch synthesis, *Energy Fuels* **1988**, *2*, 196–204.
23. Dwyer, D.J.; Somorjai, G.A., The role of readsorption in determining the product distribution during CO hydrogenation over Fe single crystals, *J.*

Catal. **1979**, *56*, 249–257.

24. Schulz, H.; Rao, B.R.; Elstner, M., 14C-Studien zum Reaktionsmechnanismus der Fischer-Tropsch-Synthese, *Erd¨ol Kohle* **1970**, *23*, 651–655.
25. Jordan, D.S.; Bell, A.T., Influence of ethene on the hydrogenation of CO over ruthenium, J. Phys. Chem. 1986, 90, 4797–4805.
26. Jordan, D.S.; Bell, A.T., The influence of butene on CO hydrogenation over ruthenium, *J. Catal.* **1987**, *108*, 63–76.
27. Jordan, D.S.; Bell, A.T., The influence of propylene on CO hydrogenation over silica-supported ruthenium, *J. Catal.* **1987**, *107*, 338–350.
28. Dry, M.E., The Fischer-Tropsch synthesis, in J.R. Anderson; M. Boudart, eds., *Catalysis-Science and technology*, vol. 1, Springer-Verlag, New York, 1981 pp. 160–255.
29. Dalla Betta, R.A.; Piken, A.G.; Shelef, M., Heterogeneous methanation: initial rate of CO hydrogenation on supported ruthenium and nickel, *J. Catal.* **1974**, *35*, 54.
30. Madon, R.J.; Reyes, S.C.; Iglesia, E., Primary and secondary reaction pathways in ruthenium-catalyzed hydrocarbon synthesis, *J. Phys. Chem.* **1991**, *95*, 7795– 7804.
31. Zhan, X.; Davis B. H. Assessment of internal diffusion limitation on Fischer–Tropsch product distribution. *Applied Catalysis A: General*. **2002**, *236*, 149.

Chapter 6

A STUDY OF FISCHER-TROPSCH SYNTHESIS IN A BATCH REACTOR ON A TIO_2 SUPPORTED COBALT CATALYST

The material in this chapter has been submitted for publication in Industrial and Engineering Chemistry Research. The current Reference is: Lu, X; Hildebrandt, D; Glasser, D. A Study of Fischer-Tropsch Synthesis in a Batch Reactor with a TiO_2 Supported Cobalt Catalyst. *Ind. Eng. Chem. Res.* **2011**, submitted for publication.

Abstract

We conducted a number of FT reaction experiments in a batch reactor on a TiO_2 supported cobalt catalyst. The batch experiment was started when the reactor was already being operated at steady state in CSTR mode. The reaction conditions applied were that of typical low temperature FTS for a cobalt catalyst, with a reaction temperature of 210^oC, a starting pressure of 20 bar(g), and $H_2/CO = 2$ in the feed. For the batch experiments we varied the duration of the batch reaction in a range lasting from 20 minutes to 22.5 hours. We tracked the conversion for each of the reaction durations, and compared the reaction rate with that obtained in the CSTR mode.

The reaction rate was shown to be first order reversible with respect to the H_2 concentration which never went to zero even after a very long time. We

investigated the CH_4 selectivity and compared the olefin to paraffin ratios for the light hydrocarbons at the different reaction durations with those recorded for the steady state in the CSTR mode. All of these, including the reaction rate, showed a sudden change when the reactor was switched from CSTR to batch mode. The product distribution for C_1–C_9, showed an ascending trend with the increase in carbon number, which is unusual and difficult to explain. The pressure in the reactor during the reaction was monitored, and a comparison of the pressure readings with the pressure predicted from the mass balance suggested that a considerable proportion of the water produced was in the liquid phase in the reactor.

6.1 Introduction

Fischer-Tropsch Synthesis (FTS) is a catalyzed chemical reaction in which synthesis gas (syngas), a mixture of carbon monoxide (CO) and hydrogen (H_2), is converted into paraffins, olefins and oxygenates [1-7]. The FT reaction, which can be written for the paraffins as:

$$nCO + (2n+1)H_2 \leftrightarrow C_nH_{2n+2} + nH_2O \qquad (6\text{-}1),$$

is generally assumed to be governed by kinetics but not thermodynamics in low-temperature (Co catalyst: 210-230 ^oC, Fe Catalyst: 230-250 ^oC) FTS, as the thermodynamic equilibrium constant is high (estimated from ΔG of reaction). Under suitable reaction conditions, the conversion extent of the reactant can be nearly complete. Since this type of synthesis was discovered by Franz Fischer and Hans Tropsch [16] in 1923, a great deal of research has been devoted to the kinetics of FTS in respect of the consumption rate of the reactants and the formation of products using cobalt and iron catalysts. [8-15] Researchers such as Hindermann *et al.*, [17] Dry, [6] Ribeiro *et al.*, [18], Van der Laan and Beenackers [19] and Bartholomew [20] have made significant contributions to the study of the kinetics of FTS. These scientists described the rate of reaction in terms of equations based on a power law or Langmuir–Hinshelwood Mechanism. Huff and Satterfield [21] published an overview of rate equations for iron catalysts, and Yates and Satterfield [22] did similar work for cobalt catalysts.

In practical terms, however, other aspects of FTS need to be taken into consideration when defining the reaction rate. An example is the pore diffusion when the particle size of a catalyst is larger than 0.2mm, [23] when an effective rather an intrinsic rate has to be used. The effect of mass transfer can be included in the reaction rate constant, when the pore diffusion is taken account of, in terms of the effectiveness factor, η_{pore}, [24] while the powers of the reactants do not

necessarily have to be modified. As an important by-product of the FT reaction, water, is thought to affect the synthesis and its partial pressure is included in some reaction rate expressions. However, the phase of the product water in the reactor remains unclear, although some researchers assume it is in the gas phase. This means that the expressions that include water are of questionable accuracy. The effect of the water on the performance of FTS (including the reaction rate and product selectivity) on cobalt catalysts has been studied through water co-feeding by various researchers. Dalai and Davis [25] reviewed the published work on this subject, and in their summary reported that adding water up to certain concentrations, to unsupported cobalt oxide catalysts has positive effects (in terms of higher CO conversion, C_5+ selectivity, olefin selectivity and lower methane and CO_2 selectivity). On the other hand, water has a positive effect for silica-supported catalysts, but is negative for alumina supports whereas for titania, its positive influence is small.

It has been generally agreed that a simple polymerization mechanism can be used to describe the distribution of FTS products. [26, 27] An FT chain growth intermediate can either propagate on a catalyst surface to form another intermediate of a higher carbon number or terminate to produce an oxygenate, paraffin, or olefin with the same carbon number. The path of termination to olefin is thought to be reversible, because of olefin adsorption/desorption and hydrogenation/dehydrogenation. [28]. The propagation probability (α value) of each surface intermediate has been assumed to be a constant that is independent of carbon number (single α distribution). This produces the so-called Anderson–Schulz–Flory distribution, [1, 29]

$$W_n / n = (1-\alpha)^2 \alpha^{n-1} \qquad (6\text{-}2).$$

There are three types of reactors used to carry out the FT process in the continuous commercial production of liquid fuels and chemicals. These are

tubular fixed bed, fluidized bed and slurry bed reactors. Laboratory-scale research for low-temperature FTS is normally carried out in a fixed bed or a slurry bed reactor. Researchers seldom use a batch reactor with a gas-solid reaction regime to evaluate a catalyst or study the mechanism of FTS, but we suggest it could be of value in investigating FTS. The reasons are that it can create an even reactant distribution environment for all the catalyst pellets in the reactor, and eliminate the effect of the medium (long chain) paraffins that are used in a slurry bed regime. Also, while the continuous mode reactors (PFR and CSTR) are operated at steady state in most cases, the batch reactor is operated at unsteady state, and the pressure of the reactor and partial pressure of the reactants and products change with the extent of the reaction. This provides extra information that may help us to understand the behaviour of the FT reaction.

6.2 Experimental Section

The FT experiments were carried out in a tank reactor in batch operation mode in a gas solid system with sufficient agitation. The batch experiments were performed with reaction durations ranging from 20 min to 22.5 h. Our purpose was to investigate the conversion and reaction rate of the reactants, the selectivity and the distribution of the products.

The experiments were carried out in a 100 ml CSTR (*Autoclave Engineers*) in a gas-solid system, without adding any solvent. Residence time distribution (RTD) experiments showed that the gaseous materials could be well mixed and the reactor could be regarded as an ideal CSTR when the SS was higher than around 65 rpm. The reactor was operated in CSTR mode and subsequently in batch mode. Premixed syngas (10% N_2/30% CO/60% H_2) was fed to the reactor at 20 bar(g), and the flow rate was controlled by a Brooks 5850 Mass Flow Controller. The product was drained from the bottom of the tank to ensure that the entire contents,

including liquid phase products, could be fully taken out of the reactor. To prevent product condensation in the outlet lines, these lines were heated at 180 ^oC down to the two product traps, which were kept at reactor pressure and at 150^oC and 30^oC, to collect wax and liquid products respectively. The gaseous stream was then reduced to atmospheric pressure and connected to an on-line GC (Agilent 6890A with a thermal conductivity detector—TCD and a flame ionization detector—FID).

A supported cobalt catalyst (BET area 28.6 m^2/g, average pore diameter 35.8 nm) with 10% Co/90% TiO_2 was used in the experiments. TiO_2 (Degussa P-25) was mixed with distilled water in a 1:1 ratio to prepare a paste, which was dried at 120 ^oC for two hours, calcined at 400 ^oC for six hours and then cooled overnight. The calcined paste was crushed and sieved to a particle size between 0.5–1 mm to serve as the support for the catalyst. An amount of $Co(NO_3)_3 \cdot 6H_2O$ (Sigma Aldrich), which had been calculated based on the mass of the support, was dissolved in distilled water to form a solution, which was then mixed with the support and allowed to absorb uniformly into it by impregnation. The wet catalyst pellets were dried at 120 ^oC for two hours and then calcined at 400 ^oC for six hours. Approximately 3g of prepared cobalt catalyst was loaded into a catalyst basket (provided with the reactor). The frame of the basket was fixed to the inner wall of the tank, but the basket itself did not extend over the whole diameter. A stirrer in the inner radius was used to mix the gas and force it through the catalyst held in the basket. The catalyst basket together with the catalyst inside was suspended in the tank throughout the experiment.

The catalyst was reduced with H_2 at 1.8 $NLh^{-1}(gcat)^{-1}$ at ambient pressure. The gas space velocity was based on the total mass of the unreduced catalyst. The temperature was increased from room temperature to 120 ^oC, first at a ramping rate of 60 $^oCh^{-1}$, and held for two hours before being raised to 280 ^oC at the same

ramping rate, and maintained at this temperature for 24 hours. After reduction, the reactor was cooled to below 100 ^oC.

The feed gas was switched from H_2, which had been used for the reduction, to syngas. The pressure of the reactor was stabilized at 20 bar(g) by a back pressure regulator (*Swagelok*), and the flow rate of the feed was kept at $1.2NLh^{-1}(gcat)^{-1}$ by a mass flow controller. The temperatures used in the experiments were 190 ^oC and 210 ^oC. The initial stirring speed inside the reactor was set at 100 rpm.

As suggested in chapter 4 [30], the performance of FTS with a fresh reduced catalyst and without liquid deposit differs from that of a catalyst with a deposit of, and coated by, liquid phase products. In order to establish the same starting point for the batch operations lasting for differing periods, we operated the reactor at CSTR mode until steady state was reached before beginning each batch operation. The procedure was carried out as a cyclical sequence: using CSTR operation mode until steady state, followed by a batch operation for a certain period of reaction and sampling, and then the resumption of CSTR operation until the achievement of steady state marked the start of the next batch operation timed for a different duration. We started the batch operation by isolating the reactor by closing the inlet and outlet valves, and starting the time record simultaneously. Once the designated duration (20min, 40 min, 1hr and so on) of the batch operation had been completed, a sample was taken and analyzed. During sampling, we flushed the sampling loop of the GC completely with the sample from the reactor to ensure the accuracy of the experiment. All the material in the reactor, including the light and heavy hydrocarbons, could be collected and injected into the GC. However, because the long chain hydrocarbons might be in liquid phase, we could not be sure that the online GC would analyze them effectively. Consequently, the data we give in this paper relate only to the short chain hydrocarbons.

Once the sample had been injected into the GC, we set the reactor into the original CSTR mode under the same operational conditions as previously. After around 24 hours the steady state had been achieved again and we started the next batch mode operation.

6.3 Results and Discussion

6.3.1 Conversion and Reaction Rate

Figures 6-1 and 6-2 illustrate the conversion of the reactants for the various reaction periods used in the batch experiments. Time 0 represents the end of the CSTR mode operation and the beginning of the batch mode operation for the reactor. The shape of the conversion curves is logarithmic, and the maximum conversion for CO and H_2 was found to be around 98.5%. None of the reactants achieved 100% conversion.

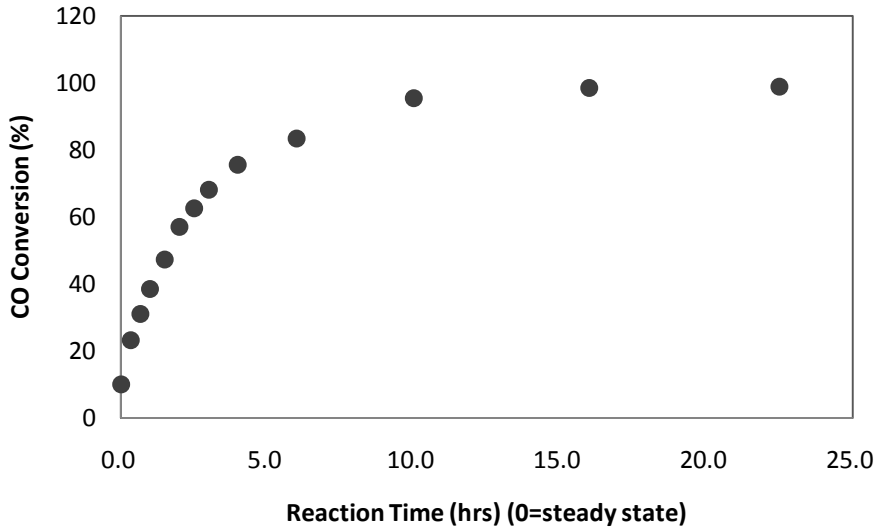

Fig. 6-1 CO conversion for various reaction durations

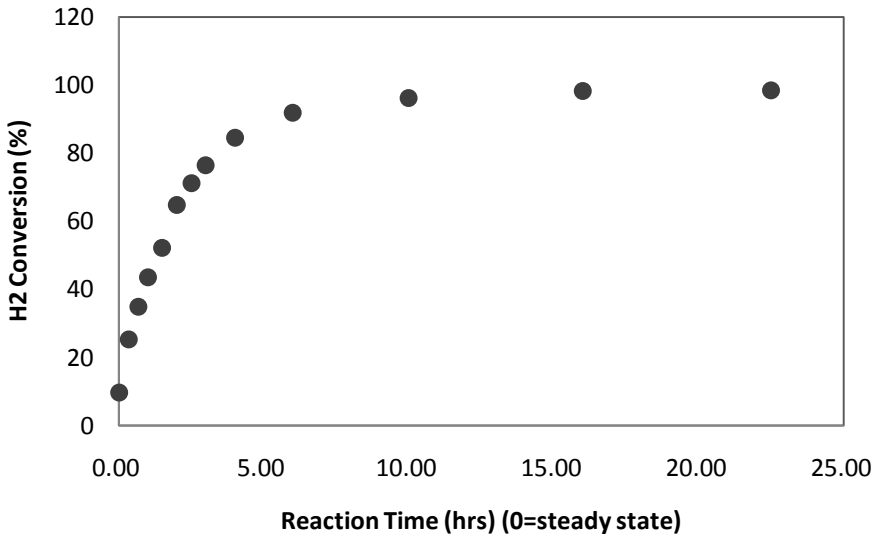

Fig. 6-2 H_2 conversion for various reaction durations

The reaction rates for the CSTR and batch modes are plotted in Figure 6-3. The reaction rate in batch operation mode is an average reaction rate during the time gap by counting the difference of reactants remained at two time points. The operational conditions for CSTR and batch experiments were identical in all but one respect: no feed and products were taken out during the batch operation. The change in the reaction rate with time in CSTR mode we believe was caused by the altered mass transfer caused by the build-up of the liquid product in the catalyst, as has already been discussed in Chapters 4 and 5. [30, 31] The reaction rate was around 2.0×10^{-5} mol CO/(g cat min) at the point when we switched the reactor from CSTR to batch, while the average CO reaction rate in the first 20 minutes of the batch operation jumped to around 3.4×10^{-5} mol CO/(g cat min). Then the reaction rate decreased as the duration lengthened (shown as the extent of the CO conversion in the Figure), as the reactants in the reactor diminished.

A decrease in the reaction rate commensurate with the reduced concentration of the reactants in the reactor is understandable from a kinetic point of view, as the reaction rate is likely to be a function of the concentrations of the reactants in the reactor. However, the jump in the reaction rate by around 70% when we switched

the operational mode from CSTR to batch is much more difficult to explain, as the average concentration of the reactants in the first 20 minutes of the reaction duration is only slightly lower than that of the CSTR mode. Remember that the catalyst had been conditioned, as the reactor had been operated at CSTR mode for more than a week before being switched to batch operations, and was at steady state. Thus no sudden change in the catalyst properties would be expected when the batch operation was started, so that the jump of the reaction rate was unlikely to be caused by property changes in the catalyst.

When the reactor is in CSTR mode, there are two processes occurring, namely reaction and flow. When we stop the flow we only have reaction occurring. Note however the effect is not caused by a change in mass transfer as we are still stirring vigorously, thus it must be because we have stopped the flow and the removal of products. We have suggested in previous publications that the apparent reaction rate is partly determined by stripping [31] and we see when we stop the stripping the reaction rate increases significantly.

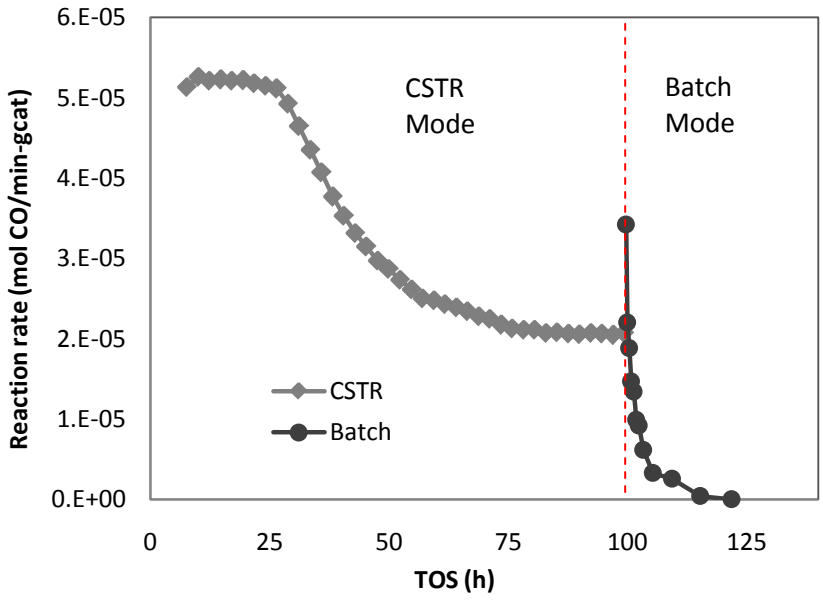

Fig. 6-3 The reaction rates in the CSTR and batch operation modes as a function of CO conversion and TOS (Time on Stream)

The concentrations of the reactants in the reactor is shown as a function of the reaction duration in Figure 6-4, and the ln ($C_{reactant}$-$C_{reactant,end}$) as a function of the reaction duration in Figures 6-5 and 6-6.

In Figure 6-4, we can see that the partial pressure of H_2 and CO in the reactor varied over a wide range, from 8.96–0.2 bar and 4.6–0.07 bar respectively, with a reaction duration that extended from 20 min–22.5 hours. In Figure 6-5, we observe that Ln(C_{H2}-$C_{H2,end}$) versus duration is an excellent straight line over the full range of the concentration of the H_2 (partial pressure of the H_2 in the reactor varied from 8.96–0.2 bar). This suggests the rate of the F-T reaction could be written as first order reversible in the concentration of H_2 (in gas phase). The results in Figure 6-6 show that a first-order reversible model in terms of the concentration of CO is not such a good model. This is perhaps not too surprising as with the feed of 2:1 hydrogen to carbon monoxide, the former is the limiting reagent as the reaction consumes hydrogen at a slightly higher ratio than the feed composition.

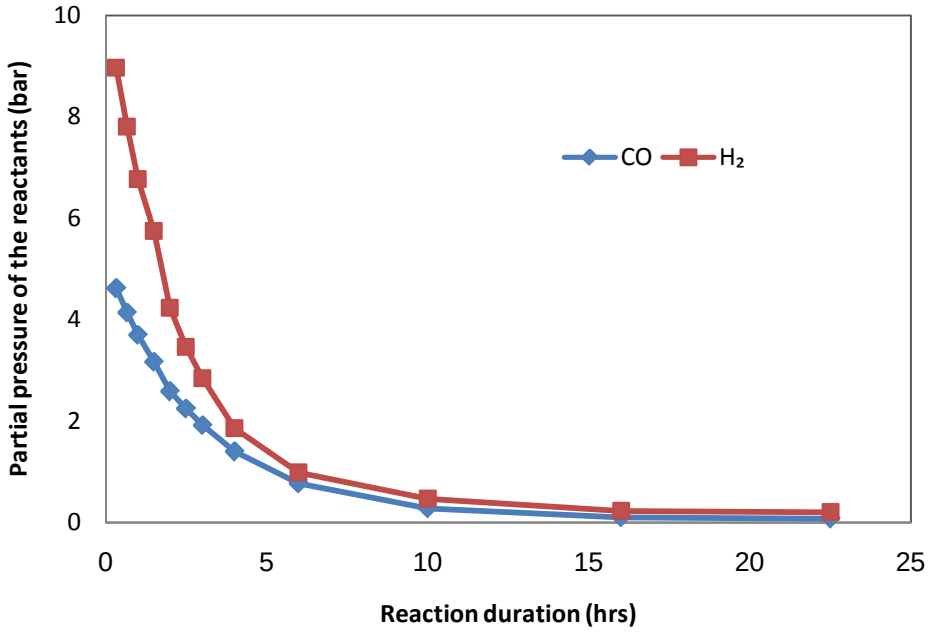

Fig. 6-4 Partial pressures of the reactants in the reactor for different reaction durations

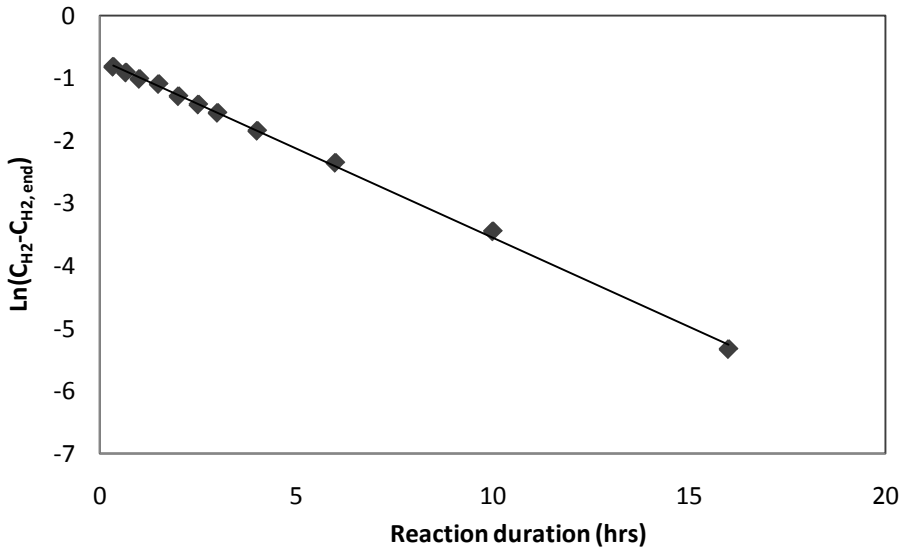

Fig. 6-5 Logarithmic plot of H_2 concentration as a function of the reaction duration

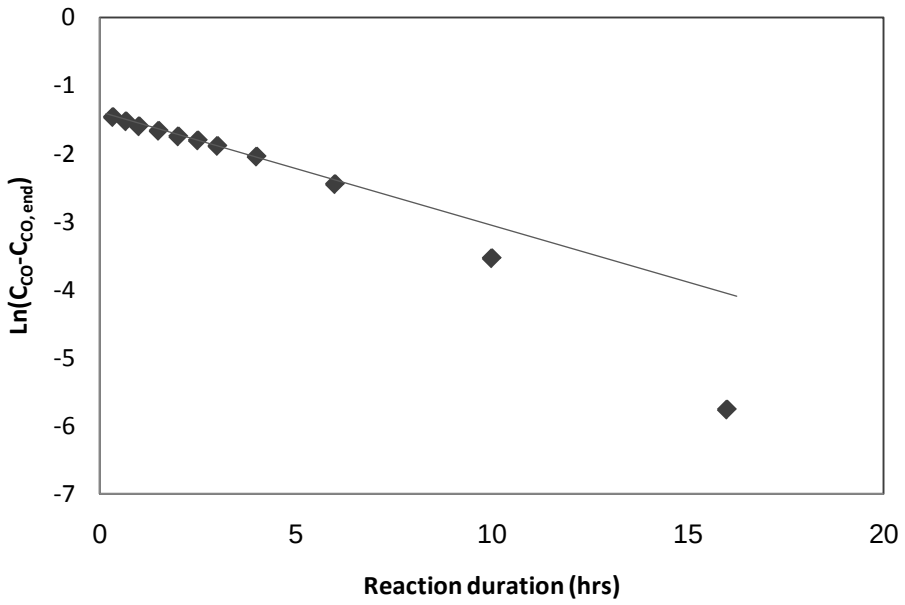

Fig. 6-6 Logarithmic plot of CO concentration as a function of the reaction duration

6.3.2 Product Selectivity and Distribution

CH_4 Selectivity

Methane selectivity, calculated on the basis of the reacted CO, at various reaction durations, is presented in Figure 6-7. We can see that the CH_4 selectivity at

different stages of the reaction duration is roughly the same, at a value of 22%, except one data point, at 10 hours, which is far lower than the others. This data point is believed to be an incorrect one, so it is not included in the discussion that follows.

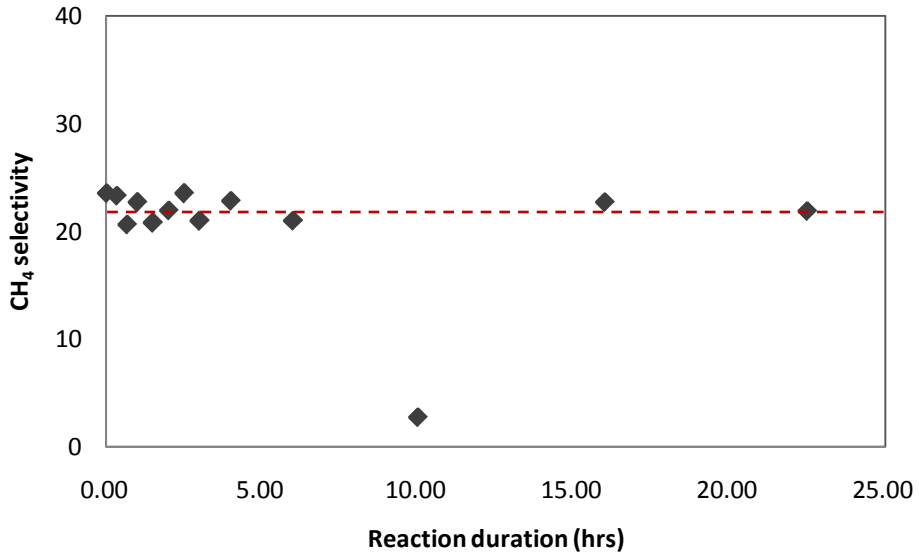

Fig. 6-7 CH_4 selectivity at different reaction durations

In the data presented in the Figure, the progressively longer reaction durations can be regarded as different residence times of the reactants and the H_2/CO ratio could be regarded as fairly constant, as the consumption of both was close to the feed ratio. One could therefore conclude that the residence time has no obvious influence on the CH_4 selectivity, which is mainly decided by the relative amount of H_2 to CO rather than the partial pressures of the reactants in the system. This result is not consistent with the reports of some researchers who have investigated the influence of residence time on CH_4 selectivity. For example, in the results given by Iglesia *et al.*, [32] they found that CH_4 selectivity increased with bed residence time on a supported Ru catalyst in a fixed bed reactor.

Olefin/Paraffin (O/P) Ratios

The O/P ratios at steady state in CSTR operation mode and at unsteady state in the batch operation mode are plotted in Figure 8. The data presented are the results

for C_2–C_5, as the olefin content for the longer chain hydrocarbons in the products was very limited in the CSTR mode and in the relatively longer durations in the batch mode. The data shown on the graph is only for reaction durations up to 10 hours, because in the longer reaction durations, the olefins are traces and nearly undetectable.

The O/P ratios for the short chain hydrocarbons (C_2–C_5) in the CSTR operation mode were at a very low level: 0.05, 0.16, 0.14, 0.11 for C_2–C_5 respectively. On the other hand, in batch operation mode the O/P ratios immediately jumped to much higher levels. As the duration of the reaction lengthened, these ratios gradually dropped, eventually reaching levels even lower than in CSTR mode. The obvious increment in O/P ratios for C_2–C_5 after the change-over from the CSTR mode to the batch mode suggests that the formation rate of the olefins is quicker than for the paraffins, and modified the previous low O/P ratios.

Again as above the only change in going from CSTR to batch operation is that the flow is stopped. As before the observed sudden change must be due to the stopping of the stripping. As the olefins and paraffins of the same chain length have very similar volatilities the effect must be associated with the decrease in removal rate of the species rather than their relative quantities. As the olefins are known to be more reactive it is probably associated with the olefins not being removed as rapidly. This ties in with the sudden increase in reaction rate when the batch operation is started. If the olefins are more reactive and stay behind when batch operation starts this would tie in with the sudden increase of reaction rate at the start of batch operation.

As the reaction duration extended, the O/P ratios diminished. The reason might be that the olefins formed in the reactor had re-entered the catalyst. The higher content of olefin in the reactor that formed during the previous batch duration

would cause the olefins to readsorb to the catalyst and initiate a further reaction (secondary reaction of olefins). The net rate of the formation of olefin in the system then became negative with the consumption of the olefins formed in the previous reaction period. Both the secondary hydrogenation and chain growth reactions will decrease the olefins content in the product and favour the formation of paraffins.

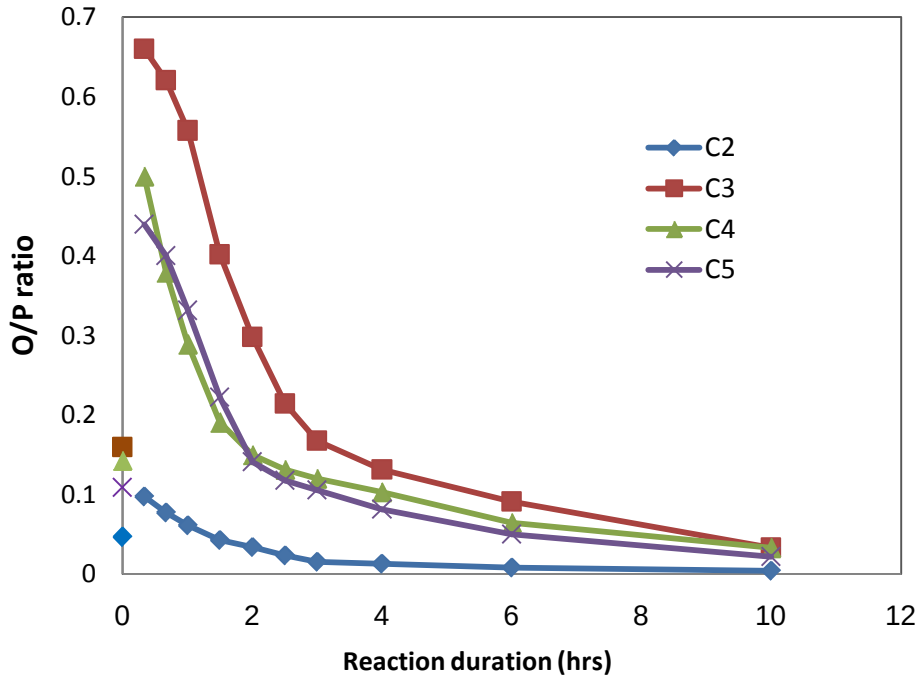

Fig. 6-8 The olefin/paraffin ratios starting at CSTR mode and with different subsequent durations of batch operation mode

Product Distribution

In an experiment carried out in continuous operation mode, analysis of the medium and long chain hydrocarbons is normally performed on the products collected in the product traps. This is a lengthy process in a mass balance run, as it takes time to collect enough product for the analysis. In the experiments we performed, the amount of liquid phase product formed in the batch mode was insufficient for collection and analysis, owing to the limited amount of reactant in the reactor. The sampling procedure we followed fed all the hydrocarbons to the

GC without any separation, to make sure that at least all the light hydrocarbons were made available to the analysis equipment. Therefore the product distribution presented below represents only the short chain hydrocarbons (C_1–C_9). Although the full spectrum of the product distribution is not available, the results for the light ones are clear enough to show the characteristics of the product distribution of FTS in a batch reactor.

The production distribution for 20 minutes of reaction under batch conditions is given in Figure 9, while that for the CSTR operation mode, which was the starting-point of the batch operation, is shown in Figure 10 for comparison. The distributions of the hydrocarbons at reaction durations from 20 minutes to 22.5 hours are illustrated in Figure 11. As we could not conduct a full product spectrum analysis in this experiment, the product distribution graph for the short chain hydrocarbons is a relative molar fraction rather than a standard ASF plot. But as the data shown were based on the molar amount, the relationship between C_n and C_{n+1} and the meaning of the slope in these Figures is the same as in a conventional ASF plot.

Figure 10 shows the product distribution when the CSTR was operated in a steady state, where the results followed those in the classic ASF model. In Figure 9, on the other hand, the results from the 20 minutes of batch operation, the product distribution differed from a normal FTS product distribution in that it showed an ascending trend from C_3 to C_7. All the results derived from different reaction durations show similar behaviour, as can be seen in Figure 11, although the ascending trend for the short reaction durations is slightly steeper than for the longer ones.

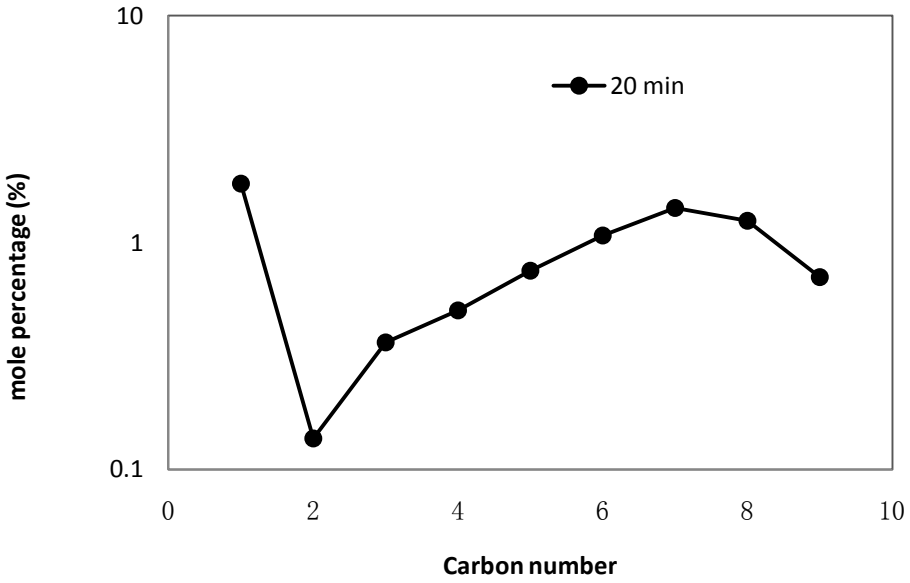

Fig. 6-9 The FT product distribution in the batch reactor
(reaction duration 20 min, T = 210 °C, H_2/CO = 2 in the feed)

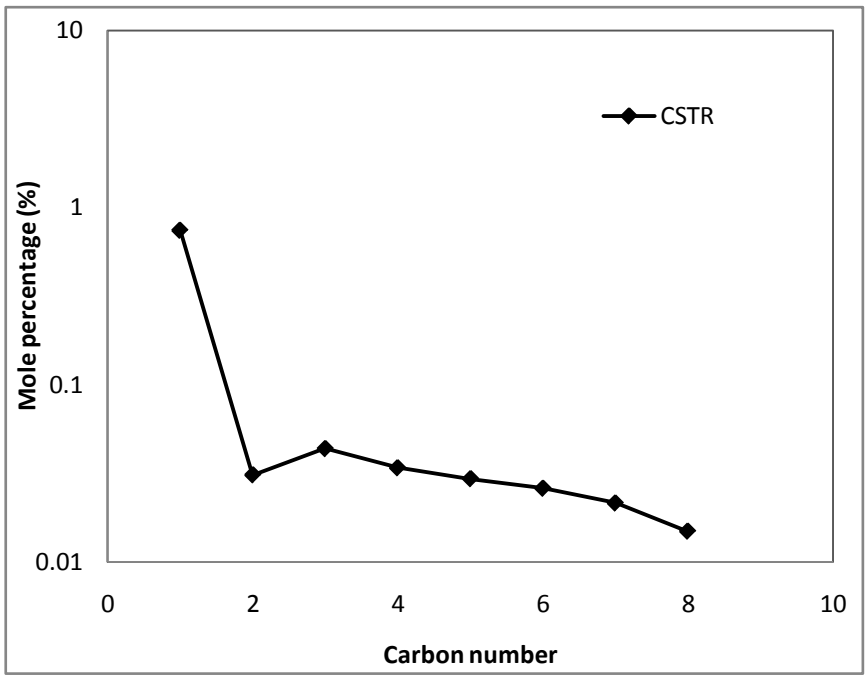

Fig. 6-10 The FT product distribution in the CSTR
(SV = 1.2 NL/(h gcat), T = 210 °C, H_2/CO = 2 in the feed)

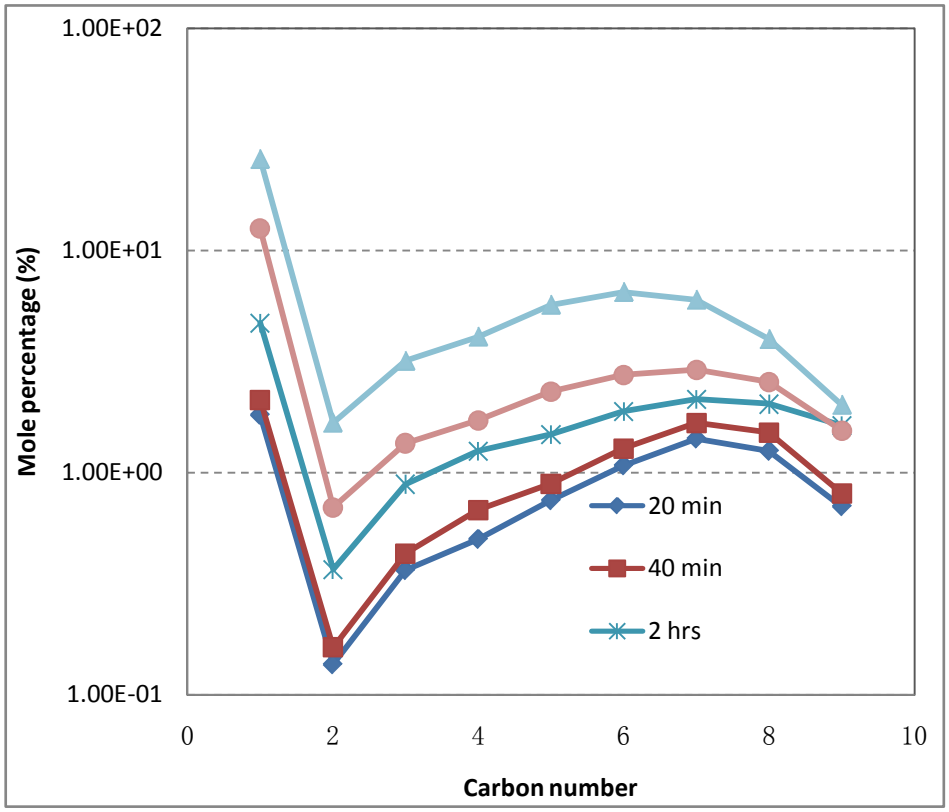

Fig. 6-11 The FT product distribution in the batch reactor for different reaction durations (T = 210 ^{o}C, H_2/CO = 2 in the feed)

We analyzed the reactor system and the experimental procedure very carefully to avoid that this unusual distribution was caused by the errors of the experiments. The first possibility was that this unusual product distribution was caused by the product condensed in the lines from the reactor to the GC in the previous sampling. However, the temperature of the line and the valves on it was kept at 180 ^{o}C and the pressure in the line before each sampling was atmospheric, so that the condensed material in the line, if there was any, was the boiling point above 180 ^{o}C at atmospheric pressure. Therefore, it is very unlikely that there were any C_1–C_6 hydrocarbons in the line that could alter the product distribution observed in the samples. The second possibility was that this distribution was altered by the products left in the reactor during the CSTR operation. However, the product distribution in the CSTR operation was entirely different from that in the batch mode. And also, if there was any effect from the products formed in the CSTR

mode, it will affect the distributions at different reaction durations in batch mode to different extents, but the distributions in Figure 6-11 show similar trend. Therefore, it is also very unlikely that this is the reason for the unusual distribution observed in the batch operation. Therefore, it seems that these results were the behaviour of FT reaction itself.

It is very interesting that as we move from the CSTR to the batch operation there is such a dramatic change in the operational parameters including a very unusual ASF distribution. To fully understand these results will clearly require further experimentation.

6. 3.3 The Phase of the Product Water

Water is the main product of FTS and its affect on the performance of the catalyst has been widely investigated by researchers. They have reported that water has both a positive and a negative influence on the reaction rate of FTS. The water produced can deactivate the catalyst by oxidizing the active sites, which are actually reduced metal. When a support is sensitive to high-temperature water, it can alter the stability of the support structure.

Besides its impact on the catalyst itself, the water also potentially has an effect on FTS from the reaction engineering point of view in that it influences the mass and heat transfer in the reaction system depending on whether it is in the liquid or gas phase. Under typical FTS reaction conditions, water is generally thought to be in the gas phase as its boiling point at the operational pressure is lower than the operational temperature.

For each duration of the batch operation, we were able to read the pressure of the reactor system by means of a pressure gauge mounted on top of the reactor. The pressures in the reactor at different durations are plotted in Figure 12. The

pressure readings for the reactor system and pressures derived for different scenarios for the reaction mass balances for the system are also given.

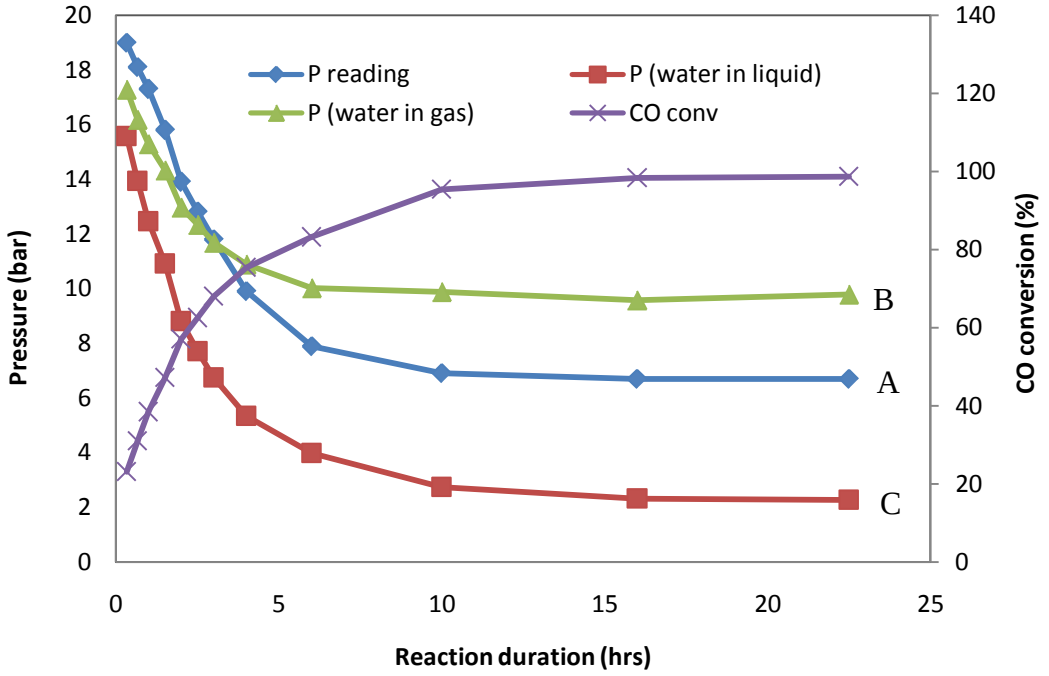

Fig. 6-12 The pressures in the reactor at different reaction times (CO conversion is plotted as a reference)

The Figure illustrates three total pressures in the reactor based on different assumptions. The CO conversions for the range of reaction durations are also given as a reference. Curve A is the experimental pressure reading of the reactor.

To be conservative we assumed all the hydrocarbons except the methane were in the liquid phase. If we assumed all the water was in the gas-phase $P_{system} = P_{CO}+P_{H2}+P_{N2}+P_{CH4}+P_{H2O}$ (Curve B) we obtained a pressure-time curve that was significantly higher than the measured curve. If we assumed all the water was in the liquid-phase, $P_{system} = P_{CO}+P_{H2}+P_{N2}+P_{CH4}$, we obtained Curve C which did give a graph much lower than the measured pressure curve. We therefore conclude at least some of the water must have been in the liquid-phase. We notice there is a crossing in curves A and B at around 3 hours. This could be corrected if we took the phase of C_2 and above hydrocarbons into consideration. The

information these results provide strongly suggest that a considerable proportion of the water formed by the reaction is in the liquid phase.

6.4 Conclusion

The FTS reaction was performed in a batch reactor with a TiO_2 supported cobalt catalyst. In order to prevent any interruption and depletion of the materials due to sampling from the reactor, we carried out a series of reaction duration batch operations separately; each starting once the reactor was at steady state in the CSTR operation mode. This ensured that the starting point for each batch operation was identical. The reaction durations varied from 20 minutes to 22.5 hours. During each of these we investigated the conversion, reaction rate, product selectivity and distribution, and the phase of the product water. When the reaction duration was sufficiently long, 98.5% but not complete conversion of the reactants was achieved, which suggests a thermodynamic limitation. A reaction rate jump with an increment of 70% was observed when the reactor was switched from CSTR mode to batch mode, with all other operation conditions remaining the same. Jumps in behaviour were also observed in the O/P ratios and the product distributions. We attributed this to the fact that when the change took place we had moved from a situation where reaction and stripping of the liquid were occurring simultaneously to one in which only reaction was occurring. We surmised that when stripping stopped that a reactive product was left behind.

The correlation between the reaction time and concentrations of the reactants suggest that the reaction rate could be expressed as first order reversible in the concentration of H_2. We also observed that CH_4 selectivity was unaffected by either the residence time or the partial pressure of the reactants but note that during these experiments the H_2/CO ratio remained roughly constant. A decrease in O/P ratios for light hydrocarbons as the reaction duration lengthened suggested

that the olefins could re-enter the catalyst and commence a secondary reaction. The product distribution for C_2–C_7 behaved entirely differently from that expected in a classic ASF distribution by showing an ascending instead of a descending trend with the increase of carbon number. This unusual behaviour is unlikely to be attributable to the sampling and/or the analysis, so we concluded that attention needs to be paid to this interesting result.

The batch operation also offered us a means to keep a continuous record of the pressure variations accompanying the extent of the reactants reacted. When product water was assumed in the gas phase, the pressure in the reactor derived from mass balance (even when all the C_2+ products were assumed in the liquid phase) was lower than predicted. Therefore we conclude a considerable proportion of the water produced by the reaction must have been in liquid phase.

6.5 References

1. Anderson, R. B. *The Fischer-Tropsch Synthesis*; Academic Press: New York, 1984.
2. Bond, G. C. *Catalysis by Metals*; Academic Press: London, 1962.
3. Storch, H. H.; Golumbic, N.; Anderson, R. B. *The Fischer-Tropsch and Related Syntheses;* John Wiley: New York, 1951.
4. Davis, B. H. *Technology Development for Iron Fischer-Tropsch Catalysis* (Final Report). Contract No. DE-AC22-94PC94055-13. 1999.
5. Dry, M. E. Practical and Theoretical Aspects of the Catalytic Fischer-Tropsch Process. *Appl. Catal.* **1996**, *138*, 319.
6. Steynberg, A.; Dry, M. Study in Surface Science and Catalysis, Vol. 152. *Fischer-Tropsch Technology*; Elsevier: Boston, 2004.
7. Iglesia, E. Fischer-Tropsch Synthesis on Cobalt Catalysts: Structural Requirements and Reaction Pathways. *Stud. Surf. Sci. Catal.* **1997**, *107*, 153.
8. Donnelly, T. J.; Satterfield, C. N. Product Distributions of the Fischer-Tropsch Synthesis on Precipitated Iron Catalysts. *Appl. Cat. A: Gen.* **1989**, *52*, 93.
9. Dry, M. E. Catalytic Aspects of Industrial Fischer-Tropsch Synthesis. *J. of Molecular Cat.* **1982**, *17*, 133.
10. Fernandes, F. A. N. Polymerization Kinetics of Fischer-Tropsch Reaction on Iron Based Catalysts and Product Grade Optimization. *Chem. Eng. Technol.* **2005**, *28*, 930.
11. Huff, G. A. Jr.; Satterfield, C. N. Evidence for Two Chain Growth Probabilities on Iron Catalysts in the Fischer-Tropsch Synthesis. *J. of Catalysis.* **1984**, *85*, 370.
12. Post, M. F. M.; Van't Hoog, J. K.; Minderhoud, J. K.; Sie, S. T. Diffusion Limitations in Fischer-Tropsch Catalysts. *AIChE J.* **1989**, *35*, 1107.
13. Schulz, H.; Claeys, M. Kinetic Modelling of Fischer–Tropsch Product

Distributions. *Appl. Cat. A: Gen.* **1999**, *186*, 91.

14. Schulz, H.; Schaub, G.; Claeys, M.; Riedel, T. Transient Initial Kinetic Regimes of Fischer–Tropsch Synthesis. *Appl. Cat. A: Gen.* **1999**, *186*, 215.
15. Van Steen, E.; Schulz, H. Polymerisation Kinetics of the Fischer–Tropsch CO Hydrogenation Using Iron and Cobalt Based Catalysts. *Appl. Cat.: A Gen.* **1999**, *186*, 309.
16. Fischer, F.; Tropsch, H. *Brennst. Chem.* **1923**, *18*, 274.
17. Hindermanm, J. P.; Hutchings, G. J.; Kiennemann, A. Mechanistic Aspect of the Formation of Hydrocarbons and Alcohols from CO Hydrogenation. *Catal. Reviews: Science & Engineering*. **1993**, *35*, 1-127
18. Ribeiro, F.; Wittenau, A.; Bartholomew, C. H.; Somorijai, G. Reproducibility of Turnover Rates in Heterogeneous Metal Catalysis: Compilation of Data and Guidelines for Data Analysis. *Catal. Rev. Sci. Eng.* **1997**, *39*, 49-76.
19. van de Laan, G. P.; Beenackers, A. A. C. M. Kinetics and Selectivity of the Fischer-Tropsch Synthesis: A literature Review. *Catal. Rev. Sci. Eng*. **1999**, *41*, 255.
20. Bartholomew, C. H.; Farrauto, R. J. *Fundamentals of industrial catalytic processes*; Wiley: New Jersey, 2006.
21. Huff, G. A. Jr.; Satterfield, C. N. Intrinsic Kinetics of the Fischer-Tropsch Synthesis on a Reduced Fused-Magnetite Catalyst. *Ind. Eng. Chem. Proc. Des. Dev.* **1984**, *23*, 696.
22. Yates, I. C.; Satterfield, C. N. Intrinsic Kinetics of the Fischer-Tropsch Synthesis on a Cobalt Catalyst. *Energy & Fuels* **1991**, *5*, 168.
23. Zimmerman, W. H.; Bukur, D. B. Effect of Particle Size on the Activity of a Fused Iron Fischer-Tropsch Catalyst. *Industrial & Engineering Chemistry Research* **1989**, *28*, 406.
24. Jess, A.; Kern, C. Modeling of Multi-Tubular Reactors for Fischer-Tropsch

Synthesis. *Chem. Eng. Technol.* **2009**, *32*, 1164.

25. Dalai, A. K.; Davis, B. H. Fischer–Tropsch synthesis: A Review of Water Effects on the Performances of Unsupported and Supported Co Catalysts. *Applied Catalysis A: General* **2008**, *348*, 1–15.
26. Madon, R. J.; Reyes, S. C.; Iglesia, E. Primary and Secondary Reaction Pathways in Ruthenium-Catalyzed Hydrocarbon Synthesis. *Journal of Physical Chemistry* **1991**, *95*, 7795.
27. Zhan, X.; Davis, B. H. Assessment of Internal Diffusion Limitation on Fischer–Tropsch Product Distribution. *Applied Catalysis A: General* **2002**, *236*, 149.
28. Gates, B. C.; Katzer, J. R.; Schmit, G. C. A. *Chemistry of Catalytic Processes*; McGraw-Hill: New York, 1979.
29. Friedel, R. A.; Anderson, R. B. Composition of Synthetic Liquid Fuels. I. Product Distribution and Analysis of C_5-C_8 Paraffin Isomers from Cobalt Catalyst. *Journal of the American Chemical Society* **1950**, *72*, 1212.
30. Lu, X.; Hildebrandt, D.; Liu, X.; Glasser, D. Making Sense of the Fischer-Tropsch Synthesis Reaction: Start-up. *Industrial and Engineering Chemistry Research* **2010**, *49*, 9753.
31. Lu, X.; Zhu, X.; Hildebrandt, D.; Liu, X.; Glasser, D. A new way to look at FTS using flushing experiments. *Industrial and Engineering Chemistry Research* **2011**. Accepted for publication.
32. Iglesia, E.; Reyes, S. C.; Madon, R. J. Transport-Enhanced α-Olefin Readsorption Pathways in Ru-Catalyzed Hydrocarbon Synthesis. *Journal of Catalysis* **1991**, *129*, 238.

CHAPTER 7

BEHAVIOUR OF LOWER HYDROCARBONS IN FISCHER-TROPSCH SYNTHESIS

The material in this chapter is to be submitted for publication in Industrial and Engineering Chemistry Research. The current Reference is: Lu, X; Hildebrandt, D; Liu, X; Glasser, D. Fischer-Tropsch Synthesis at Steady State in a Tubular Fixed Bed Reactor: Reaction rate and Product selectivity. *Ind. Eng. Chem. Res.* **2011**, submitted for publication.

Abstract

Steady state FTS experimental runs were conducted in a tubular fixed bed reactor on a TiO_2-supported cobalt catalyst. The reaction conditions were varied including the H_2/CO ratio in the feed, the reaction temperature, and space velocity (SV) of the feed gas.

The decrease of the reaction rate caused by a lack of H_2 when the H_2/CO ratio was low is discussed. The Olefin/Paraffin ratios we obtained at different temperatures and SVs are presented as they relate to the three H_2/CO ratios. We examine how the SV affected the O/P ratio, and how the low H_2/CO ratio inhibited the extent of hydrogenation. We also consider product selectivity in terms of the distribution of C_2 and C_3 in the product spectrum of FTS under varied reaction conditions and attempt to characterize the relationship between C_2 and C_3 in terms of both olefins and the total amounts of them.

The data derived from the experiments described in this chapter will also be used as a basis for the discussion of the pseudo olefin equilibrium in FT reaction in Chapter 8.

7.1 Introduction

A large number of researchers have investigated the influence of operational conditions on the performance of the FTS reaction, focusing on both the consumption of the reactants, which can be regarded as the reaction rate, and the product selectivity, which can be regarded as the product distribution. According to Anderson [1] the distribution for n-paraffins can be described by the Anderson-Schulz-Flory (ASF) equation:

$$W_n / n = (1-\alpha)^2 \alpha^{n-1} \qquad (7\text{-}1).$$

Where the growth probability factor α is independent of *n*. α is defined by:

$$\alpha = \frac{R_p}{R_p + R_t} \qquad (7\text{-}2),$$

in which R_p and R_t represent the rates of propagation and termination, which determine the carbon number distribution of the FT products. The range of α value is dependent on the reaction conditions and catalyst type. Dry [2] reported typical ranges of 0.85–0.95, 0.70–0.80, and 0.50–0.70 on Ru, Co, and Fe catalysts respectively. The chain growth probability decreases as the reactor temperature rises, [3–7] and wide variations are observed at temperatures higher than 280 °C. [4, 6, 7] It must be noted that the values reported by Lox and Froment [4] and Dictor and Bell [3] were obtained with a constant partial pressure of H_2 and a varying CO pressure. The data presented by Dictor and Bell [3] for experiments using a Fe_2O_3/K catalyst suggest that α depends very little on the H_2/CO ratio, in contrast to the findings of other investigations into Fe, Fe/Cu/K, and Ru catalysts. A decline in chain growth probability is observed at higher H_2/CO ratios. [4, 5, 8]

In general, the different types of catalyst used in FTS have varying hydrogenation abilities. This ability is in a sequence of Ni>Co>Fe>Ru. [9-11] Because of the relatively low tendency of Fe for secondary reactions, higher olefin yields can be

obtained with alkali-promoted iron catalysts. The extent of secondary reactions is also shown by the dependency of the O_n/P_n ratio or olefin content on the chain length. On Fe-, Ru-, and Co-based catalysts, an exponential decrease for the O_n/P_n ratio with chain length is observed (7-3): [12]

$$\frac{m_{O_n}}{m_{P_n}} = e^{Cn} \qquad (7\text{-}3),$$

where m_{On} and m_{Pn} are the production rates or mole fractions of olefins and paraffins with carbon number n, and C is a constant.

As Co is normally unable to catalyze the WGS, the H_2/CO ratio in the feed is always adjusted to correspond with the stoichiometry of the FT reaction. In the experiments described in this chapter we studied the performance of FTS on a cobalt catalyst with a H_2/CO ratio between 1:1 to 3:1, and compared the influence of each H_2/CO ratio in the feed on the reaction rate and the product selectivity. A low H_2 content in the feed gas caused a reduction of the reaction rate, and the effects of the variations in reaction temperature on the CH_4 selectivity at different H_2/CO ratios differed markedly. The chain growth probability α showed an increasing trend with extent of CO conversion at a low H_2/CO ratio.

The data provided by the experiments allowed us to examine O/P ratios in some detail. In the literature, FTS product distribution has been the subject of wide-ranging research, and a number of useful kinetic models for the distribution have been set. However, the role of C_2 (which always deviates from that expected in the distribution models) in the total product distribution has not been thoroughly investigated. This prompted the author to examine the distribution of C_2 and C_3 in the product spectrum of FTS under various reaction conditions.

7.2 Experimental

The experimental set-up has already been explained and illustrated (see Figure 3-1 in Chapter 3). The plug flow reactor experiments to which we refer in this chapter were carried out with a tubular fixed bed reactor (Autoclave Engineers, ID=8mm). A 1/8" OD thermocouple well, fitted with a 1/16" OD thermocouple to monitor the temperature of the centre of the catalyst bed, was placed in the centre of the reactor tube, along its axial direction. We loaded 1g of prepared supported cobalt catalyst into the mid-part of the reactor, which took up around 2cm of its full length of 25cm. The remaining space inside the reactor was loaded with stainless steel balls with a diameter range of 2.0–3.0 mm.

We reduced the catalyst with H_2 at a SV of 1.8NL/h/gcat at ambient pressure. The gas SV was calculated from the total mass of the unreduced catalyst. The temperature was first increased from room temperature to 120 ^oC at a ramping rate of 60^oC/h, held for two hours, and then raised to 300 ^oC at the same ramping rate and maintained at this temperature for 24 hours. After that, the reduction of the catalyst was completed, and the reactor was cooled to below 100 ^oC to prepare it for further experiments.

The feed gas was switched from H_2 (which was used for the reduction) to syngas. The pressure of the reactor was stabilized at 20 bar (g) by a back pressure regulator (Swagelok 0-34.4bar). The SV of the feed gas was held at 1.8 NL/h/gcat by a mass flow controller (Brooks 5850), and changed later according to the requirements of the experimental design.

The feed (whether for the catalyst reduction or for the FTS reaction) was introduced from the top of the reactor. The product was drained from the bottom of the reactor to ensure that all of it, including the condensed products, was

removed from the reactor. To prevent product condensation, we heated the product lines to 180 ^{o}C down to the two product traps at reactor pressure. These were kept at 150 ^{o}C and room temperature to collect wax and liquid products respectively. The gaseous stream was then reduced to atmospheric pressure and connected to an on-line GC (Agilent 6890A) for analysis.

The experiments were carried out under a variety of conditions. The parameters that we changed (all of them are essential elements of the FTS reaction) were gas composition, temperature, flow rate and pressure, to assess how different settings and combinations of these elements affected the experimental results. This was done to gain a clearer understanding of FTS. The H_2/CO ratio was varied from 1:1 to 3:1, as these are typical gas ratios used in mixing different feed stocks for synthesis gas-producing units. The syngas we used contained 10% of N_2 to act as a balance gas. We set the temperatures in a range from 190–250^{o}C. The flow rate was varied from 1.8 Nl/h/gm cat to 7.2 Nl/h/gm.

In the experiments, three different H_2 to CO syngas ratio was used to conduct the FTS runs. The catalysts remained the same.

- For H_2/CO=1:1, the syngas composition was 45% H_2, 45% CO, and 10% N_2 as balance gas.

- For H_2/CO=2:1, the syngas composition was 60% H_2, 30% CO, and 10% N_2 as balance gas.

- For H_2/CO=2, the syngas composition was 67.5% H_2, 22.5% CO, and 10% N_2 as balance gas.

For each ratio of syngas, we varied the reaction temperature in a reasonable range. At each temperature, we varied the SV from low to high and then back to low again. The SVs applied were 1.8, 3.6, 5.4, and 7.2NL/h/gcat.

7.3 Results and Discussion

The operation condition variables for the three different gas ratios were SV and temperature. We applied the same SVs for experimental runs with different gas ratios. This means that at each gas ratio all four SVs were used. Three to four temperatures were chosen for the runs at each gas ratio. However, the temperatures applied for different gas ratios were varied slightly, so as to avoid conversions that were too low (such as under 2%) or too high (for example 95%). The reason was that if the conversion is extreme (too low or too high), the margin of error in the data escalates, and furthermore the catalyst deactivates at high temperature and a high conversion. All the experimental results, including conversion and reaction rates and product selectivity under various conditions, are summarized in Appendix A. The results obtained for different gas ratios under common conditions are compared and discussed in the sections below.

7.3.1 Reactant conversions and reaction rates

Conversion of the reactants

At each reaction temperature and feed gas ratio, the SV was varied up and down, from 1.8 to 7.2 NL/h/gcat and then to 1.8 NL/h/gcat again. No CO_2 was detected in any of the operational conditions, so that the conversion and the reaction rate of the reactants are represented by CO conversion and CO consumption rate respectively. The CO conversions under each reaction condition are presented in Table 7-1.

Table 7-1 The CO conversion under different operation conditions with three feed gas compositions

Temperature [^oC]	Pressure [bar(g)]	SV [NL/h/gcat]	H_2/CO 1:1	H_2/CO 2:1	H_2/CO 3:1
210	20	1.8	6.30	20.11	42.95
		3.6	3.83	10.55	23.75
		5.4	2.46	7.31	16.95
		7.2	1.71	5.58	11.47
		5.4	3.01	7.31	NA
		3.6	4.15	10.15	NA
		1.8	7.47	19.49	NA
230	20	1.8	19.24	59.41	98.33
		3.6	10.32	35.57	70.43
		5.4	7.14	21.67	49.59
		7.2	5.86	17.45	37.10
		5.4	7.41	22.64	NA
		3.6	10.32	33.58	NA
		1.8	18.55	56.94	NA

Although the operational temperatures of the experiments carried out using the three gas ratios differed, two temperatures were applied in common to all of the gas ratios. The conversion figures for CO at these two temperatures, with the differentiated SVs and gas ratios, are given in Table 7-1. As the H_2/CO ratio was varied from 1:1 to 1:2 to 3:1, the H_2 partial pressure at the inlet of the reactor changed from 9 to 12 to 13.5 bar as the pressure of the reactor was held at 20bar. The SV of the feed was increased from a low value to a higher one, and then reduced to a low value again with the variation in a range of 1.8–7.2 NL/h/g cat in order to ascertain the reactor conditions between runs had not changed significantly..

For each set of operation conditions, the CO conversion proved to have a strong dependency on the H_2/CO ratio in the feed. The conversion increased dramatically with an increase of the H_2/CO ratio in the feed. If one takes the CO conversions at a 1:1 ratio of H_2/CO as a basis for comparison, the CO conversions when the H_2/CO ratio was around 2:1 were 2.8–3.2 times greater. When the H_2/CO ratio

was 3:1, the conversions were about 6.2–6.9 times the base value. In the mean time, when we look at the CO converted at these three gas ratios at different reaction conditions in Table 7-1, we can see the CO converted when the H_2/CO ratio was around 2:1 were 1.6–2.2 times greater when compared to the values at 1:1 ratio. When the H_2/CO ratio was 3:1, the CO converted were about 2.5-3.4 times the base value.

Reaction rate

The average reaction rates obtained in respect of the SV with three different H_2/CO ratios in the feed at two common temperatures are presented in Figures 7-1 and 7-2. For each gas ratio, raising the SV always resulted in a higher reaction rate. This might be attributable to an increase in average partial pressure of the reactants in the bed (lower conversion) when a higher SV was used.

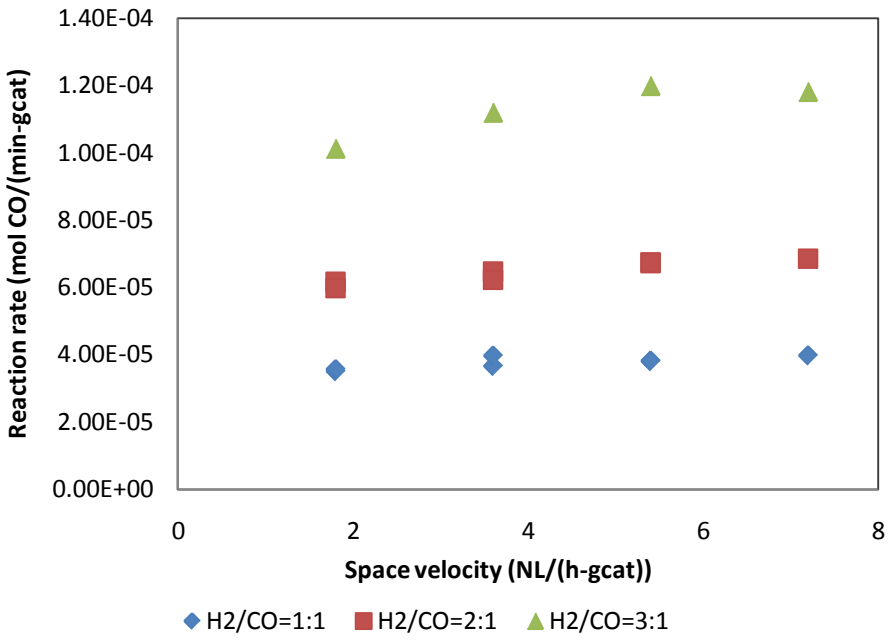

Fig. 7-1 The reaction rates with different space velocities and H_2/CO ratios when the temperature was at 210^{o}C and P at 20 bar(g)

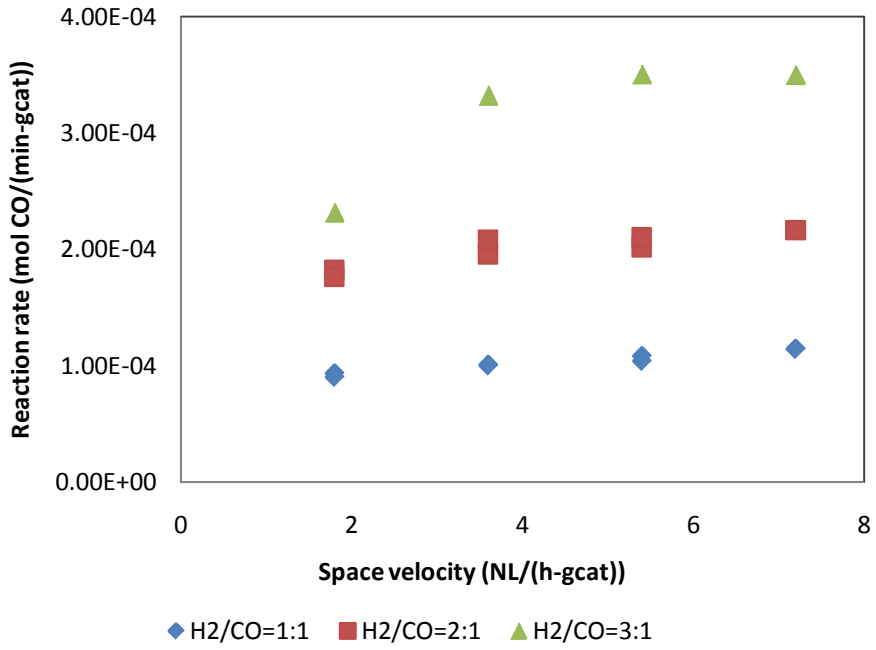

Fig. 7-2 The reaction rates with different space velocities and H_2/CO ratios when the temperature was at 230^{o}C and P at 20 bar(g)

7.3.2 Methane selectivity

The CH_4 selectivity at the three different H_2/CO ratios is given in Table 7-2. The data presented are those achieved at the common reaction temperatures. The other results are given in full detail in Appendix A.

In this table, there are three aspects that attract attention. The first is the obvious influence of the feed gas ratios on the CH_4 selectivity. As the data given in the Table show, this dependency occurred when the other operation conditions were the same. The higher H_2/CO ratio resulted in a raised CH_4 selectivity, although the extent of the increment varied at the two different temperatures. At a SV such as 1.8 NL/h/gcat and a change in the H_2/CO ratio in the feed gas from 1:1 to 3:1, the CH_4 selectivity at 210 ^{o}C rose from 8.25 to 13.77%, which is about a 60% increment. When 230 ^{o}C was used instead, the selectivity escalated from 8.29 to 24.64%, which increased almost two fold when the SV was 3.6 NL/h/gcat.

Table 7-2 The CH_4 selectivity under different operation conditions with three feed gas compositions

Temperature [^oC]	Pressure [bar(g)]	SV [NL/h/gcat]	H_2/CO		
			1:1	2:1	3:1
210	20	1.8	8.25	9.62	13.77
		3.6	7.71	9.42	14.01
		5.4	8.15	9.49	14.35
		7.2	9.38	9.55	14.61
		5.4	7.09	9.80	NA
		3.6	6.96	9.75	NA
		1.8	6.49	9.29	NA
230	20	1.8	7.22	12.96	27.52
		3.6	8.29	12.57	24.64
		5.4	8.57	14.41	23.95
		7.2	8.73	13.75	23.11
		5.4	8.80	13.77	NA
		3.6	8.62	12.17	NA
		1.8	7.94	10.88	NA

The second aspect concerns the influence of temperature on CH_4 selectivity, which produces different results with alterations in the feed gas ratios. We can see from the Table that when the reaction temperature was increased from 210 to 230^oC, the CH_4 selectivity in the column of 1:1 feed gas ratio stayed fairly constant, while the values in the column of 1:3 feed gas ratio lifted from an average value of about 14 to 24%. This shows that although the reaction temperature affects CH_4 selectivity, how far its influence extends depends on the H_2/CO ratio in the feed. A higher H_2/CO ratio will enable the reaction temperature to exert a stronger influence on the selectivity.

The third factor is the effect of SV on CH_4 selectivity, which proved to be very limited for all the three feed gas ratios. In the Table we can see that the CH_4 selective values at each reaction temperature and gas ratio were relatively unaffected by the SV (which can also be related to residence time). The CH_4 selectivity generally showed a slightly increasing trend with a higher SV. Although we found that SV had little effect on CH_4 selectivity, the case was

entirely different when we considered the O/P ratios at various SVs (which will be discussed in the section below). This discrepancy suggests that there is a significant difference between the effects of the operational conditions on CH_4 selectivity and on paraffins.

7.3.3 Olefin to paraffin ratios for light hydrocarbons

As the nature of our experimental set-up limited the data we could collect to olefins with low carbon numbers, the O/P ratios considered in this section apply to C_2-C_5 only. Even though we do not cover the full spectrum of the olefins, the effects of the reaction conditions on the behaviour of these O/P ratios were clearly demonstrated. If we assume that the product distribution of FTS follows certain kind of relationship which has already been widely researched and reported on, our summary of the O/P ratios for C_2–C_5 under a variety of operation conditions will serve to indicate a trend that the O/P ratios of higher hydrocarbons are likely to follow.

We investigated the influence of the operation conditions on O/P ratios based on the same carbon number for short chain hydrocarbons and we compared the experimental results and these are presented in Figures 7-3 to 7-5. In these three graphs, we grouped the O/P ratios for C_2–C_5 according to the variations in reaction temperature, plotted versus their CO conversion. The different CO conversions at each reaction temperature were caused by the variations of SV.

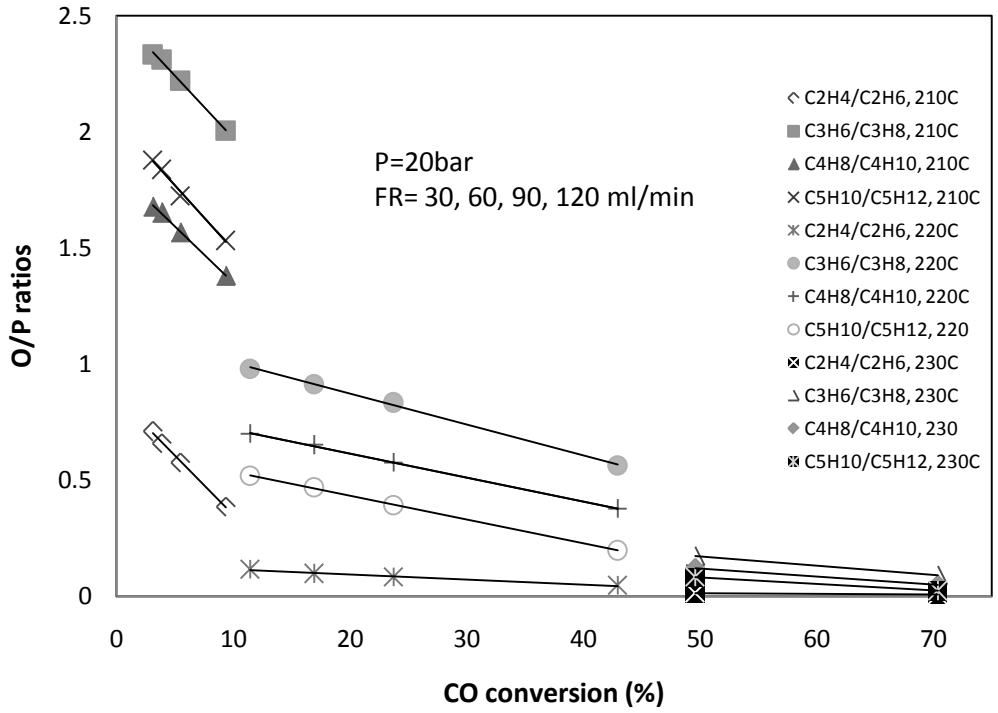

Fig. 7-3 The Olefin/Paraffin ratios for C_2–C_5 at their corresponding CO conversions when H_2/CO=3:1 (The change of CO conversion at each reaction temperature was caused by the variation of FR from 1.8 to 7.2 NL/h/gcat)

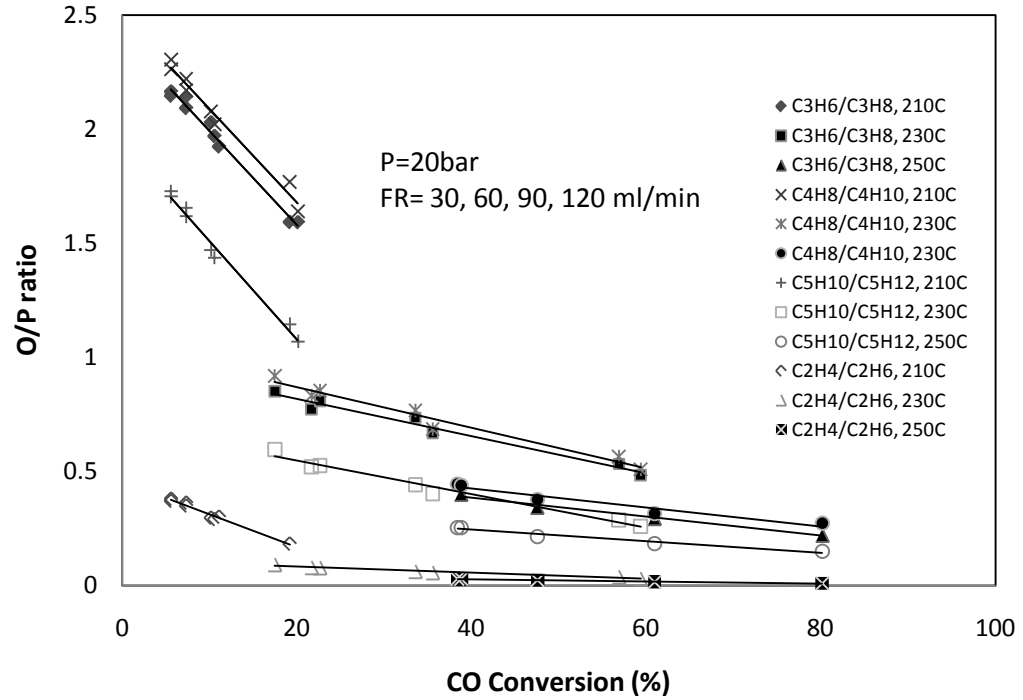

Fig. 7-4 The Olefin/Paraffin ratios for C_2–C_5 at their corresponding CO conversions when H_2/CO=2:1(The change of CO conversion at each reaction temperature was caused by the variation of FR from 1.8 to 7.2 NL/h/gcat)

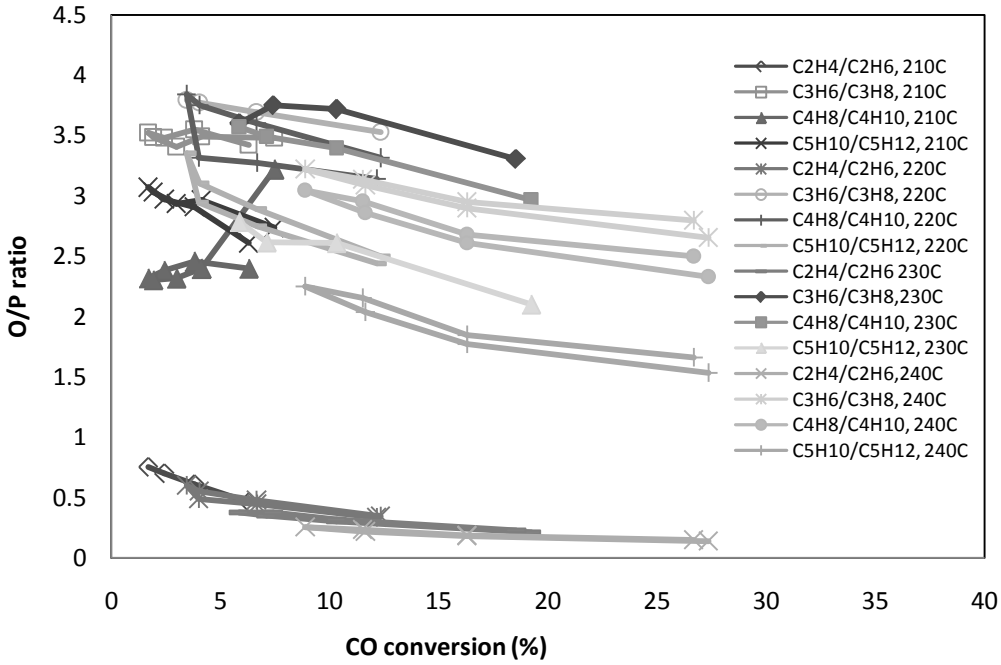

Fig. 7-5 The Olefin/Paraffin ratios for C_2–C_5 at their corresponding CO conversions when H_2/CO=1:1(The change of CO conversion at each reaction temperature was caused by the variation of FR from 1.8 to 7.2 NL/h/gcat)

In these three graphs, one can easily see that the variation in O/P ratios with the CO conversion is quite similar when the H_2/CO ratios in the feed were 2:1 and 3:1 (see Figures 7-3 and 7-4), and that a difference is manifest when the H_2/CO ratio in the feed became 1:1 (see Figure 7-5).

The O/P ratio for any same carbon number (such as C_3H_6 and C_3H_8) is strongly influenced by temperature, as can be seen in Figures 7-3 and 7-4. If we take the ratio of C_3H_6/C_3H_8 as an example, when the temperature increased from 210 to 230 ^oC while the other reaction conditions remained unchanged, the value dropped from 2.33 to 0.17 when the H_2/CO in the feed was 3:1. This means that the dominant product for carbon number 3 changed from olefin to paraffin when there was an increase of only 20 ^oC in the reaction temperature. The behaviour of the O/P ratios for the other carbon numbers investigated in this research study is similar to that of C_3. The dramatic turnaround from olefin to paraffin in response

to the reaction temperature means that temperature is key to FTS product distribution.

When we look at the data points in Figures 7-3 and 7-4, we can infer that the O/P ratio is also determined largely by the H_2/CO ratio in the feed gas. Continuing to use a C_3H_6/C_3H_8 ratio as our example, we find that with the temperature variation from 210 to 230 ^oC, the value changed from 2.14 to 0.85 when H_2/CO was 2:1, quite an obvious difference from the result we obtained when the H_2/CO was 3:1. However, when the H_2/CO in feed was varied to 1:1, with the same temperature increase as those for the other gas ratios, the value varied from 3.52 to 3.56. Both values were much higher than those achieved when the H_2/CO ratios were 2:1 and 3:1, and the temperature had a very limited influence on the O/P ratio. This suggests, first, that a higher H_2/CO ratio in the feed has a negative influence on the O/P ratios for the products, and second, that the higher the H_2/CO ratio, the more sensitive the O/P ratios are to temperature variations.

From the data presented in Figures 7-3 to 7-5, we can see that for each reaction temperature, a higher SV (lower conversion) always resulted in a higher O/P ratio, which also means that a longer residence time favoured the hydrogenation of olefins to paraffins through a secondary reaction of olefins. This phenomenon has been reported in the literature, for example by Iglesia *et al.*. [13] The explanation offered is that the primary products (olefins) formed in the upper layer of the catalyst bed will re-enter the next layer of catalyst to carry out the secondary reaction, but that a higher SV/shorter bed residence time will reduce the opportunity for re-entry, so that the secondary reaction of olefins is suppressed, making the O/P ratios higher.

However, when we performed FT reaction experiments in a CSTR (see Chapter 4), we found that even when there was no change in the reaction conditions, which

means that the SV or bed residence time was fixed, the O/P ratios were observed to vary dramatically, from more than 2.5 to less than 0.3. (See Figures 4-9 and 4-10.) And the later experiments carried out in the CSTR revealed that the large reduction in O/P ratio we observed was attributable to the liquid in the catalyst. This raised two matters for consideration: the influence of liquid in the catalyst on the O/P ratios, and the finding that its effect on the O/P ratios was greater than that of the SV, as shown in Figures 7-3 to 7-5 above. We suggest that the influence of the liquid in the catalyst plays a major role in slowing down the mass transfer of primary olefins from the catalyst pores to the stream that flows down the reactor, and increasing the opportunity for the olefins to carry on the secondary reaction.

7.3.4 Chain growth probability α

Figure 7-6 is an example of the ASF plot for the whole group of hydrocarbons produced at a set of operational conditions that have been specified above. As can be seen from the data points, except for the carbon number range from C_{11}–C_{15} and C_{34}+, the distribution of the hydrocarbons can be fitted by a single straight line, which means that single chain growth probability (α) can be assumed for the product distribution in the experiments. The deviation observed in the range of C_{11} to C_{15} is believed to have been the result of losses in the products through evaporation when the pressure dropped from 20bar (g) to atmospheric pressure during the draining of the liquid phase product from the bottom of the cool trap during the sampling. We believe that the deviation for C_{34}+ might be caused by inaccurate analysis of the wax sample by the offline GC.

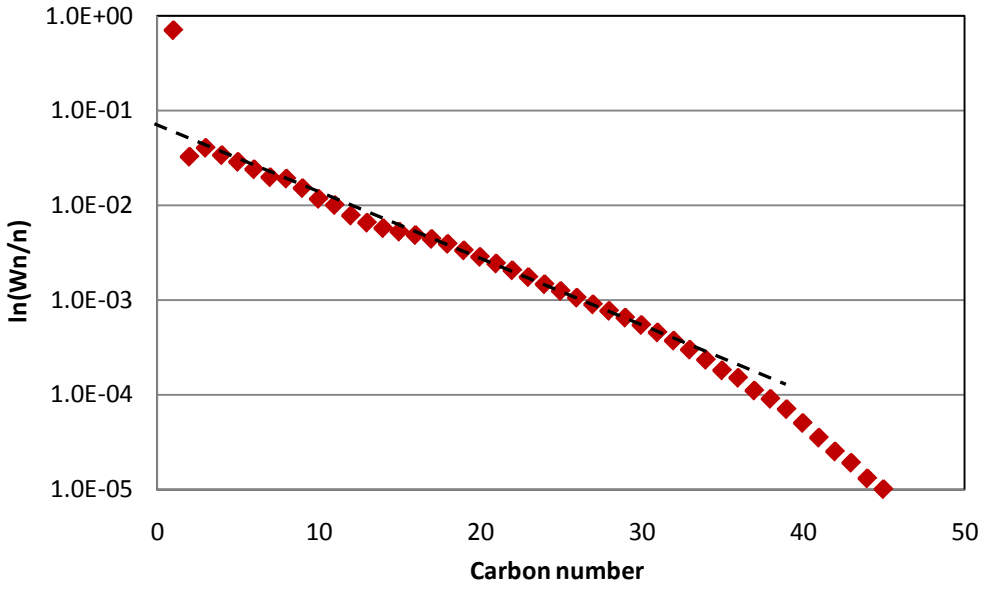

Fig. 7-6 Product distribution in a full mass balance run

The chain growth probabilities of the product under each set of operation conditions are given in the Appendix A. Here the manner in which the reaction conditions affect the chain growth probability will not be discussed in detail. Instead we focus on reporting and discussing the change in behaviour of α value when the ratio of H_2/CO in the feed is low. The chain growth probabilities under the various operational conditions when the H_2/CO ratio was 1:1 in the feed are given in Table 7-3. There we can see that α values increase when the reaction temperature was raised. This result differs from those reported in the literature, which state that a higher reaction temperature favours the formation of short chain hydrocarbons, and the chain growth probability becomes smaller. The different behaviour of the product distribution here we believe is because the chain growth reaction of olefin was favoured as the hydrogenation of olefins was suppressed due to insufficient H_2 in the system especially when the conversion of CO is higher at a higher reaction temperature.

Table 7-3 The chain growth probability under various operation conditions when the H_2/CO=1:1 in the feed

T	FR ml/min	CO conversion [%]	CH_4 Sel [%]	α
210	30	6.30	8.25	0.774
	60	3.83	7.71	0.800
	90	2.46	8.15	0.797
	120	1.71	9.38	0.803
	120	1.95	8.14	0.803
	90	3.01	7.09	0.868
	60	4.15	6.96	0.878
	30	7.47	6.49	0.871
220	30	12.18	6.67	0.868
	60	6.70	7.18	0.886
	90	4.02	8.59	
	120	3.46	8.77	0.901
	90	4.05	8.50	0.896
	60	6.68	7.11	0.888
	30	12.35	6.54	0.869
230	30	19.24	7.22	0.883
	60	10.32	8.29	0.901
	90	7.14	8.57	0.908
	120	5.86	8.73	0.907
	90	7.41	8.80	0.919
	60	10.32	8.62	0.918
	30	18.55	7.94	0.896
240	30	26.68	8.85	0.881
	60	16.32	10.27	0.911
	90	11.52	10.42	0.918
	120	8.90	10.44	0.923
	90	11.66	10.85	0.919
	60	16.32	10.66	0.909
	30	27.36	9.54	0.881

7.3.5 The distribution of C_2 and C_3

In general C_3+ products follow the description given in the classic ASF distribution model. However, C_2 is seen to have a relatively low molar content in the ASF diagram. Secondary reactions are often reported as the most plausible

reason for the anomalies in C_2 products, which various researchers have attributed to

i) incorporation of ethene in growing chains; [14, 15]

ii) rapid readsorption of ethane; [13, 16, 17]

iii) hydrogenolysis of ethane; [16] and

iv) hydrogenation of ethene to ethane. [17–19]

Komaya and Bell [16] modelled the elementary reactions in FTS over a Ru/TiO_2 catalyst, and found that ethene could form methyl and methylene (monomer), with the readsorption constant of ethene approximately four orders of magnitude larger than the higher olefins. Iglesia *et al.* [13] showed that ethene and propene have a higher reactivity and larger readsorption constant (factor 10) than other olefins.

In this section, the author tries to characterize the distribution relationship between C_2 and C_3 based upon the experimental data for both the relative amounts of the olefins (C_3H_6/C_2H_4) and the total product achieved for C_3/C_2. In the interests of comprehensiveness, we also present the relative molar amount of C_3H_6/C_2H_4 from the experimental data derived from the experiments in Chapters 4 and 6 using the other reactor type and varied operational modes. The relative amounts of C_3/C_2 (including olefins and paraffins) have been correlated in respect of the reaction temperature, and an empirical model based upon the results obtained from the experimental runs at steady states has been developed. No data from Chapters 4 and 6 are given for the model of C_3/C_2 ratio, as the range of the reaction temperature used in those experiments was limited.

C_3H_6/C_2H_4 olefin ratios

Before presenting the performance of C_3H_6/C_2H_4 ratio under various reaction conditions, we give the ratios of C_4H_8/C_3H_6 and C_5H_{10}/C_4H_8 that derived from the experiments performed in PFR and CSTR. Two examples are presented in Figures 7-7 and 7-8. These two Figures illustrate the ratio of C_4H_8/C_3H_6 and C_5H_{10}/C_4H_8 at different temperatures and SVs when the H_2/CO ratio was 2:1. These two examples demonstrate clearly that the relative amounts of neighbouring olefins (which were the focus of the investigation) were fairly constant during the changes in the reaction conditions. These results will be presented and discussed in detail in the next Chapter (Chapter 8).

When we look at the ratio of C_3H_6/C_2H_4 under the operational conditions, we found its behaviour entirely different but very interesting.

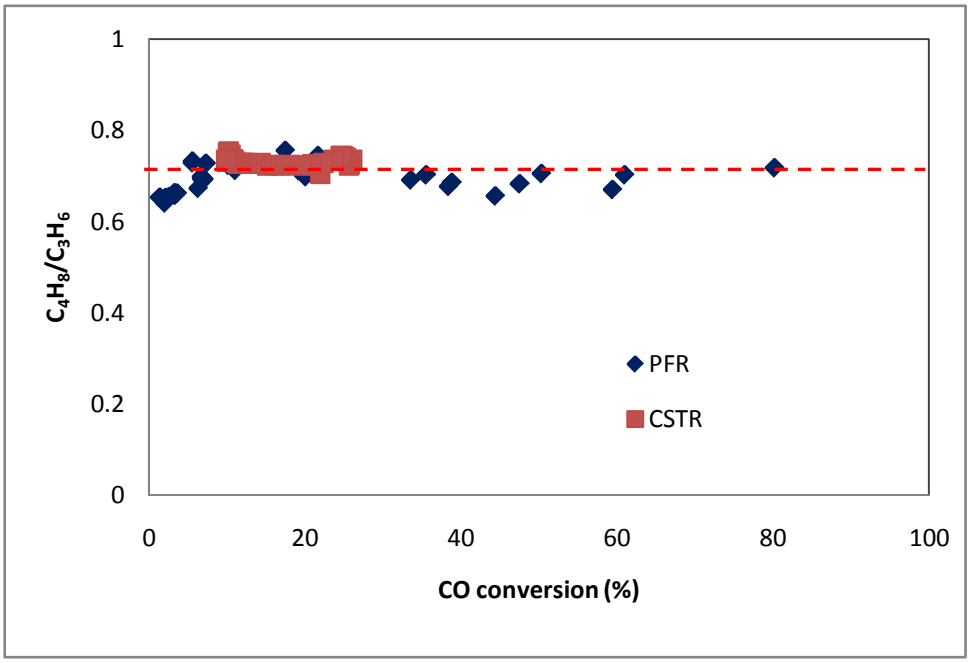

Fig. 7-7 C_4H_8/C_3H_6 as a function of CO conversion (PFR: H_2/CO = 2:1 T = 190-230 °C, FR=1.8-7.2 NL/(h-gcat); CSTR: H_2/CO = 2:1 T = 210 °C, FR=1.2 NL/(h-gcat))

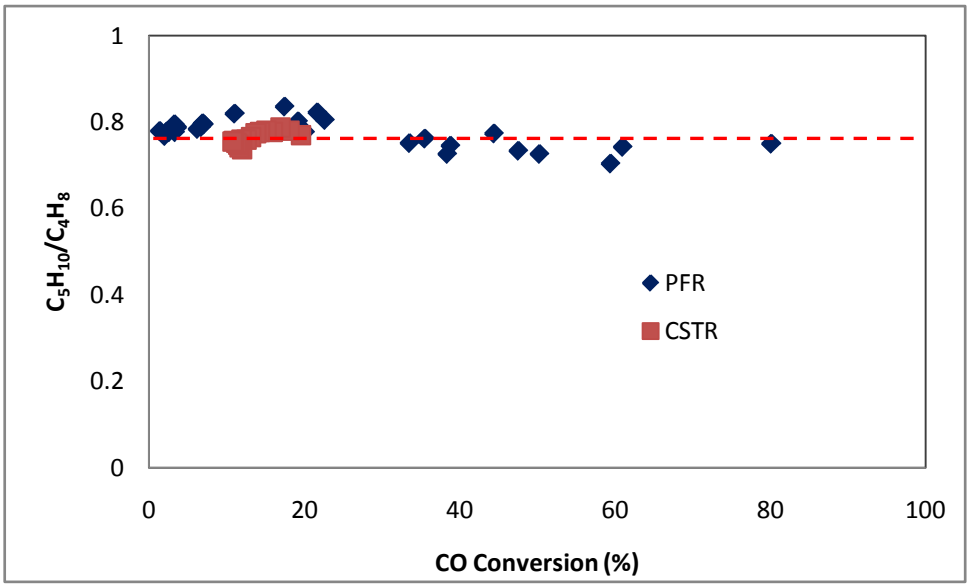

Fig. 7-8 C_5H_{10}/C_4H_8 as a function of CO conversion (PFR: H_2/CO = 2:1 T = 190-230 °C, FR=1.8-7.2 NL/(h-gcat); CSTR: H_2/CO = 2:1 T = 210 °C, FR=1.2 NL/(h-gcat))

C_3H_6/C_2H_4 olefin ratios at different reaction conditions at steady states

When an attempt was made to relate the C_3H_6/C_2H_4 ratio to various parameters, such as reaction temperature and conversion, it was found to have a promising correlation with the CO conversion regardless of the reason for the change in conversion. With each variation in feed gas ratio, we plotted the C_3H_6/C_2H_4 ratio versus its corresponding CO conversion. The results are given in Figures 7-9 to 7-11. In each Figure, the differences in CO conversion were caused by the alterations in both reaction temperature and feed gas SV.

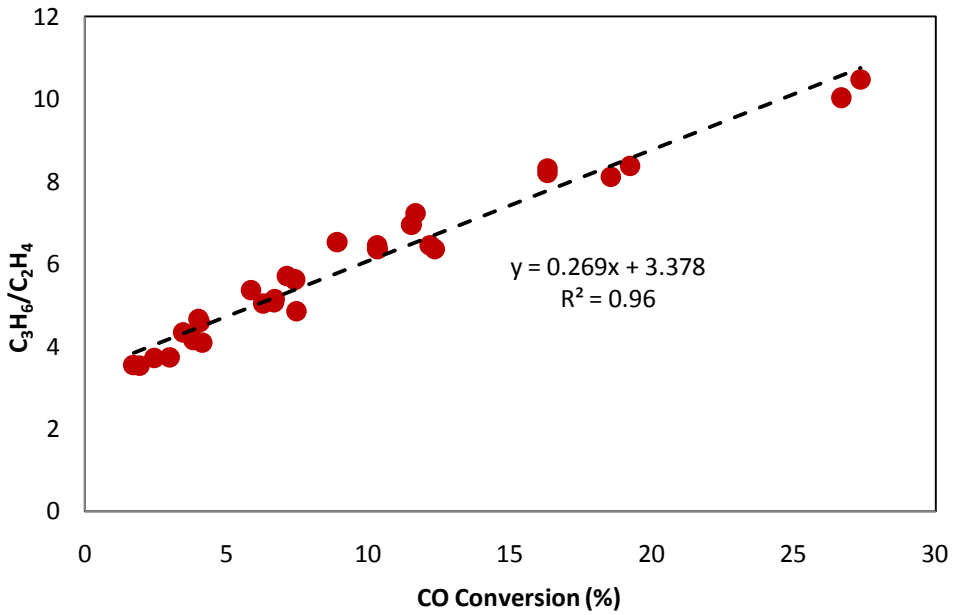

Fig. 7-9 The C_3H_6/C_2H_4 ratio versus CO conversion with H_2/CO=1:1 in the feed

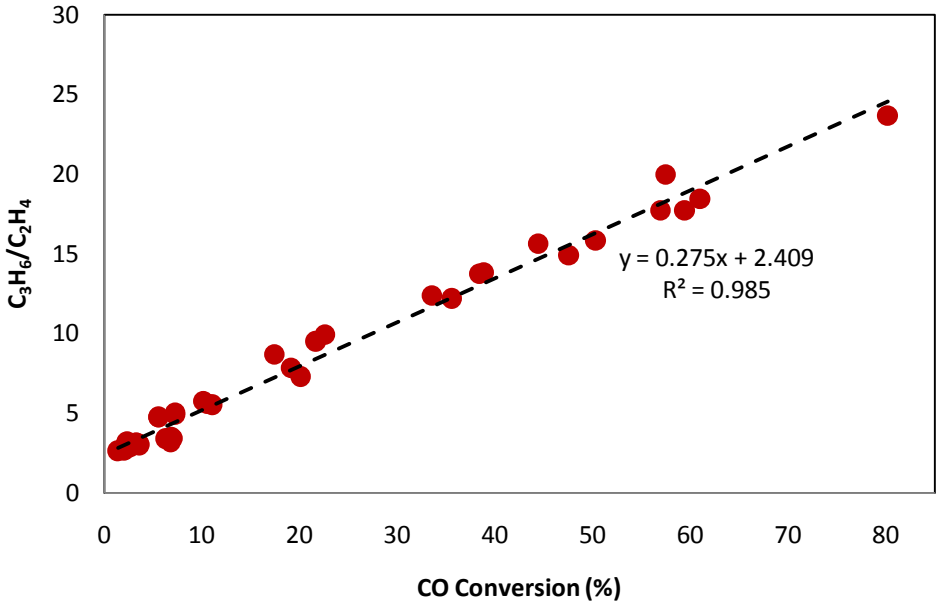

Fig. 7-10 The C_3H_6/C_2H_4 ratio versus CO conversion with H_2/CO=2:1 in the feed

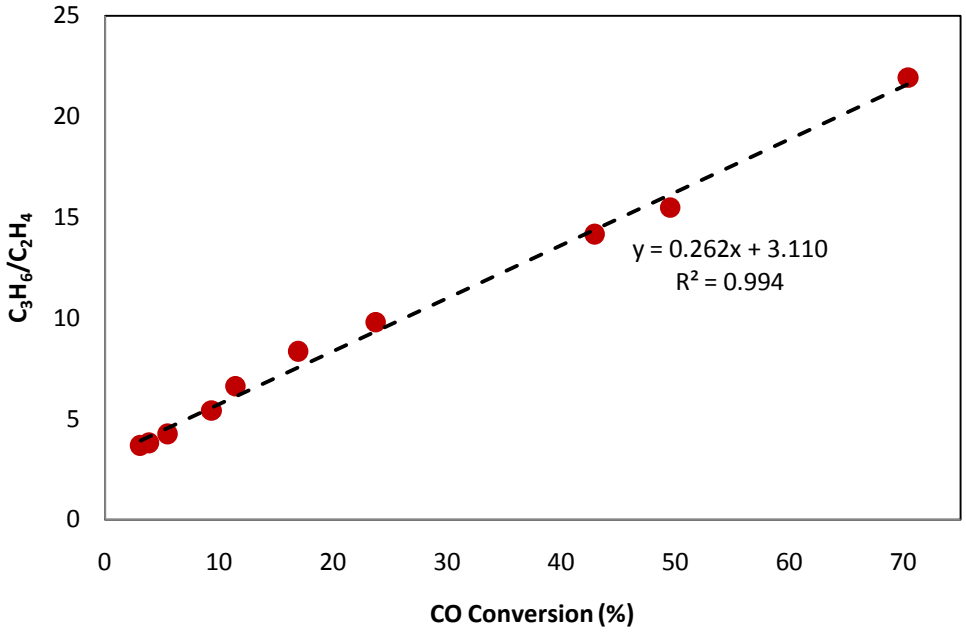

Fig. 7-11 The C_3H_6/C_2H_4 ratio versus CO conversion with H_2/CO=3:1 in the feed

In all three feed gas ratios, the C_3H_6/C_2H_4 ratio increases with the increase in CO conversion, and to a large extent. The ratio climbed from around 4 when the CO conversion was 2%, to around 22 when the CO conversion was 70%. The increase in the C_3H_6/C_2H_4 ratio was nearly linear with that of the CO conversion. The data points in each plot could be fitted by a straight line and the equations corresponding to the lines are given in the Figures as well. It is clear that the slopes of the fitting lines are very close to each other, although the H_2/CO ratio in the feed was varied from 1:1 to 3:1, and the change of the conversion was caused by variations in both reaction temperature and SV.

The C_3H_6/C_2H_4 olefin ratios at different reaction conditions at unsteady states

Since a very strong correlation can be observed in-between the ratio of C_3H_6/C_2H_4 and CO conversion from the experimental data obtained at steady state, it is valuable to verify whether the data from other runs with other type of reactor

could also follow this interesting correlation. Thus, the C_3H_6/C_2H_4 ratios from the data of the FTS runs in the CSTR (1 gas ratio feed and two different running temperatures) and the batch reactor (1 gas ratio and 1 temperature with different reaction durations) are illustrated in Figures 7-12 to 7-14.

The description of the CSTR runs is referred to the experimental sections in Chapter 4 and 5. We believe the CO conversion changes in Figures 7-12 and 7-13 were caused by the gradual liquid deposit in the catalyst. The detailed discussion about this has been presented in Chapter 4 and 5. The description of the batch run is referred to the experimental sections in Chapter 6. The changes of CO conversion in Figure 7-14 were caused by the different reaction durations.

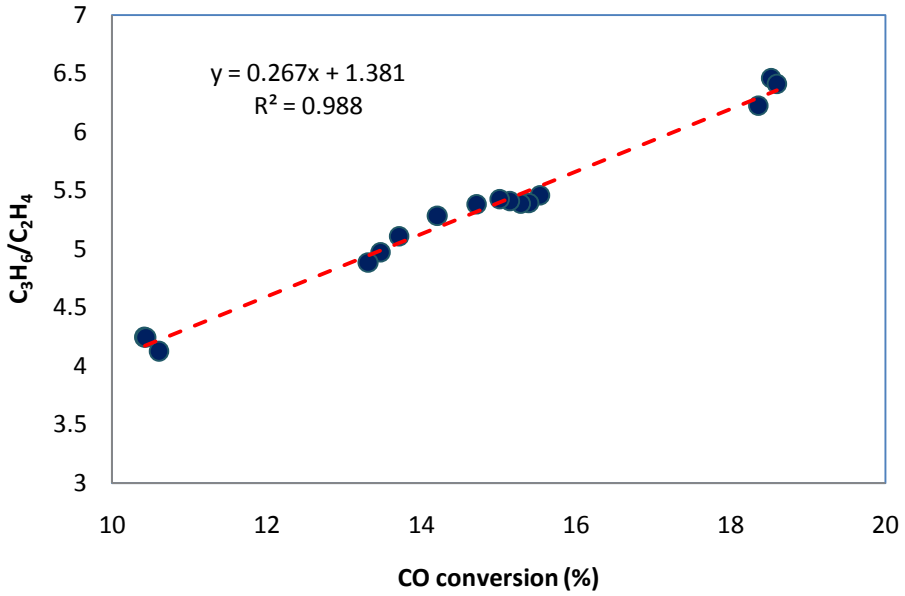

Fig. 7-12 The C_3H_6/C_2H_4 ratio versus CO conversion in a CSTR run (H_2/CO=2:1, T=190 ^oC)

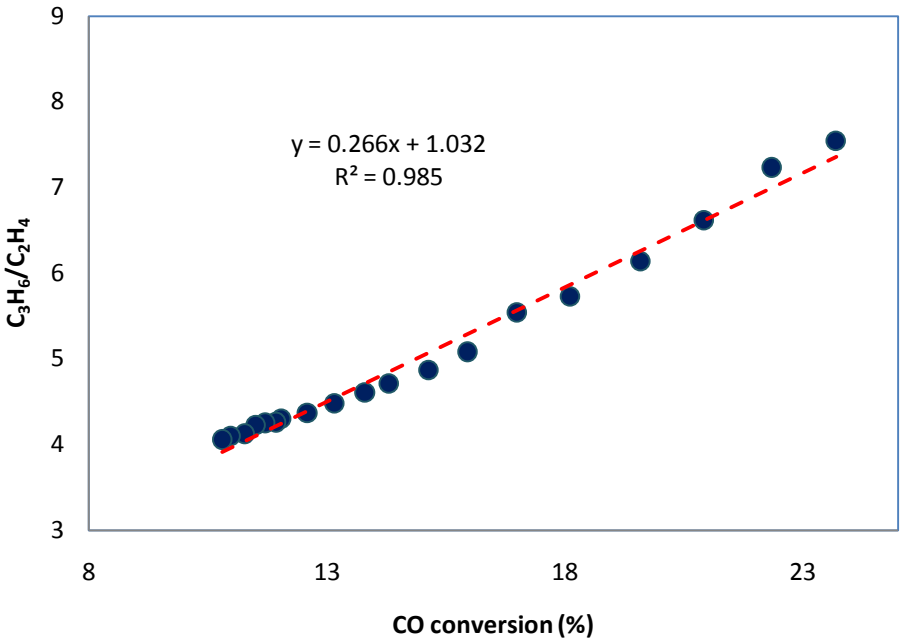

Fig. 7-13 The C_3H_6/C_2H_4 ratio versus CO conversion in a CSTR run (H_2/CO=2:1, T=210 ^oC)

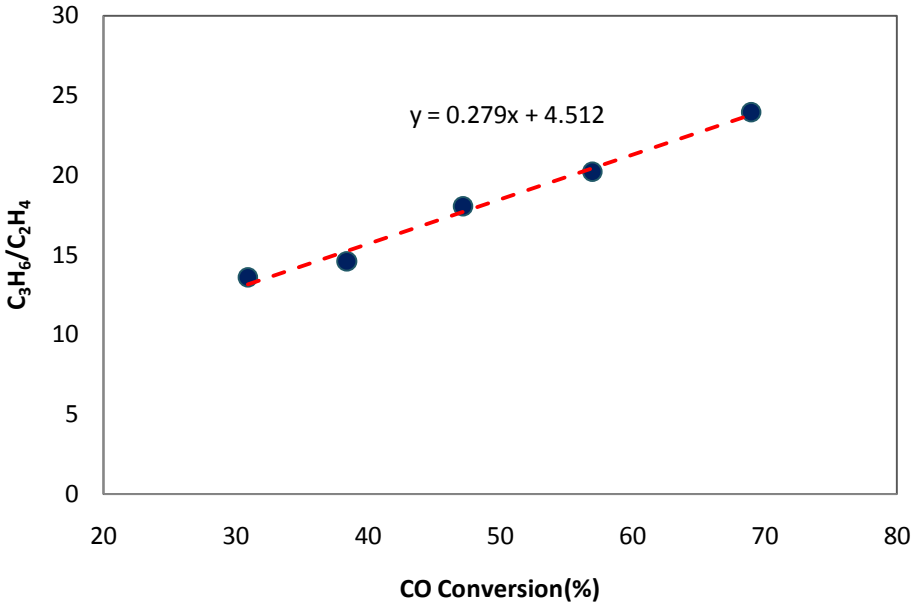

Fig. 7-14 The C_3H_6/C_2H_4 ratio versus CO conversion in a Batch run (H_2/CO=2:1, T=210 ^oC)

We can see that the data we got from CSTR and batch reactor could be fitted to the CO conversion with a straight line as well and the slopes of the fitting lines are very close regardless the reasons causing the CO conversions. We therefore plotted all the data points of C_3H_6/C_2H_4 at corresponding CO conversions in

Figure 7-15 below. The reasons causing different CO conversions for the data points in the Figure include the different H_2/CO ratios in the feeds, the different reaction temperatures, the different space velocities, the different amount of deposit of liquid in the catalyst (CSTR), a very wide range of partial pressures for H_2 and CO (batch reactor).

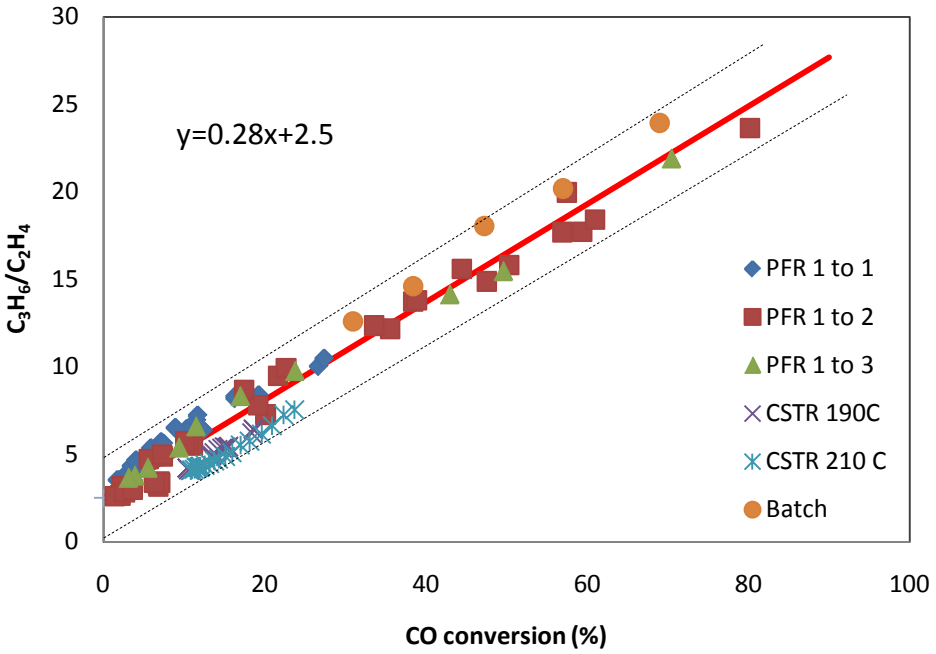

Fig. 7-15 The C_3H_6/C_2H_4 ratio as a function of CO conversion in all the experimental runs including PFR, CSTR, and BR

All the data points in the Figure show a linear ascending relationship in respect of the CO conversion, and the slop of the ascending trend are nearly identical as we expected from the observation for the Figures 7-9 to 7-14. The data are scattered as the intercepts for the fitting lines are slightly different for the data from different experiments, but all the data points fall into a relatively narrow linear zone which are demonstrated by the two dashed lines in the Figure. The two dashed lines have the same slope as those of the fitting line for the data points. The intercepts for them are around ± 2.5 relative to the intercept of the fitting line, which are not large values when the values of the C_3H_6/C_2H_4 ratio varied in a

range of more than 20 in the full range of CO conversion that we got in the experiments.

As has been described above, there were many reasons (temperature, type of reactor, H_2/CO ratio etc) causing the range of CO conversion and the extents of the secondary reactions for C_2H_4 to C_2H_6 and C_3H_6 to C_3H_8 are very different, so that the correlation of the C_3H_6/C_2H_4 ratio to the CO conversion is very powerful regardless the complex aspects that influences the CO conversion.

It is very difficult to think of a rational explanation for this phenomenon. It is however worth noting that the degree of CO conversion is closely related to the amount of water that is produced. Whether the explanation is associated with this is difficult to justify at this stage.

Overall C_3 to C_2 ratios

The ratio of total amount (olefin and paraffin) of C_{n+1}/C_n could reasonably be described by the chain growth probability, α, when $n \geq 3$. How the reaction conditions and the H_2/CO ratio affect α values have been discussed above in section 4.3.4. The values as a function of CO conversion at one H_2/CO ratio are illustrated in Figure 7-16. The different CO conversions presented in the Figure were due to the variation of both the reaction temperature and space velocity. Although the data points in the Figure show a decreasing trend when the CO conversion became higher at each reaction temperature, they were scattered and did not show a specific connection to either the temperature or the space velocity. This shows that the chain growth probability α is decided by the reaction conditions applied and no clear correlation could be made to a single parameter among the conditions.

The correlations of the relative amounts of C_3/C_2 to the reaction temperature and space velocity are different. The C_3/C_2 ratios at different reaction conditions are summarized in Figures 7-17 to 7-19 with the three H_2/CO ratios in the feeds. For each feed gas composition, the relative molar amounts of C_3 to C_2 at the operational temperatures applied at each gas composition are plotted with CO conversion, which, as mentioned in the previous parts, was caused by the various SVs of the feed gas when the operating temperature was fixed.

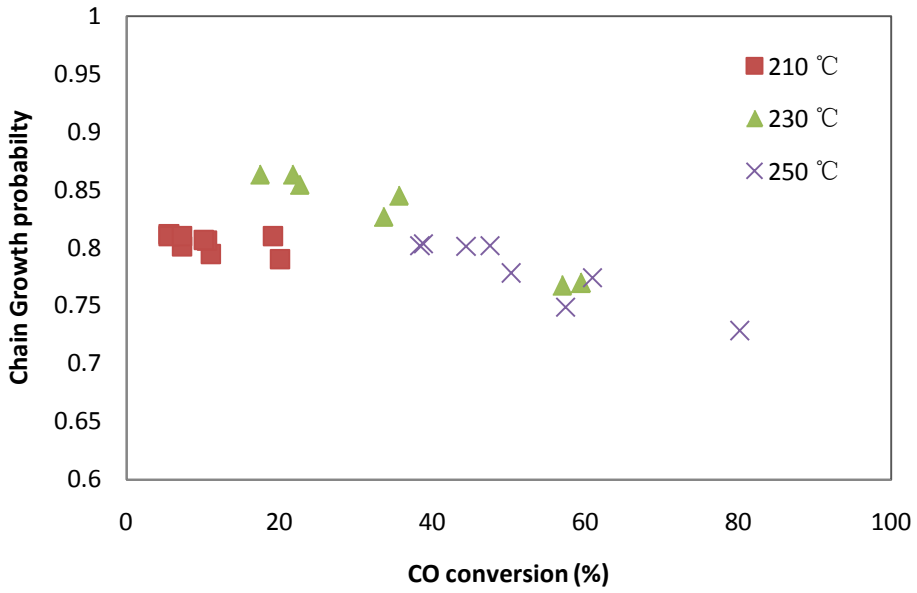

Fig. 7-16 The chain growth probabilities (α values) at various reaction conditions in respect of the CO conversion (T= 210, 230, and 250 ^{o}C; P = 20 bar; H_2/CO = 2:1)

In all these three graphs, at each operating temperature, the C_3/C_2 ratios are independent of the CO conversions. The data points, at any individual operating temperature, were fitted with a horizontal straight line. Although some few data points deviated from the fitting lines, especially when the CO conversion were extremely high (>80%) and low (<5%), most of the data points fell close to it. This kind of behaviour is quite different from that of C_3+ products which can be seen from the change of alpha values with both temperature and space velocity, and that of olefinic products of C_2 and C_3 which can clearly see in Figures 7-9 to 7-15. This suggests that the bulk C_3/C_2 molar ratio is independent of the space

velocity (or residence time) when the other reaction conditions were kept constant.

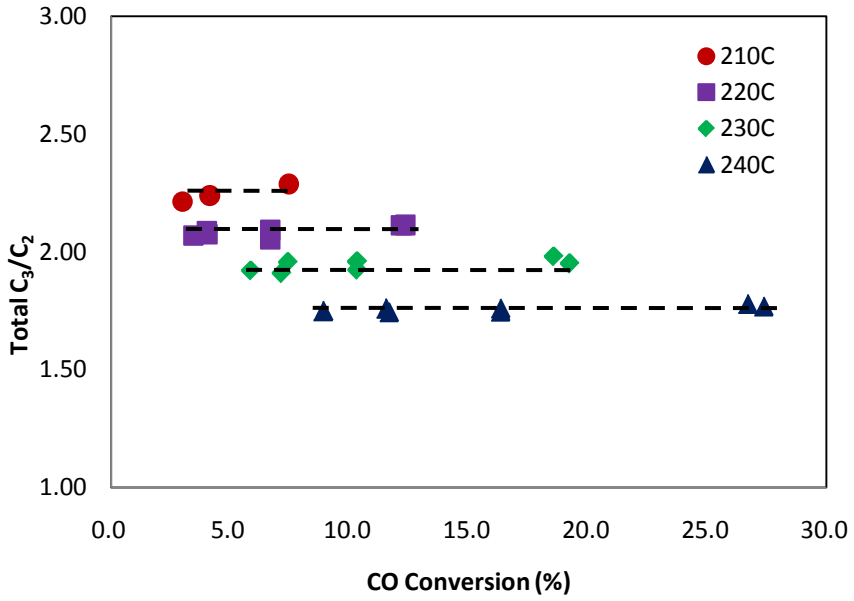

Fig. 7-17 The relative molar amount for C_3/C_2 versus CO conversion at different reaction temperatures (when H_2/CO=1:1 in the feed)

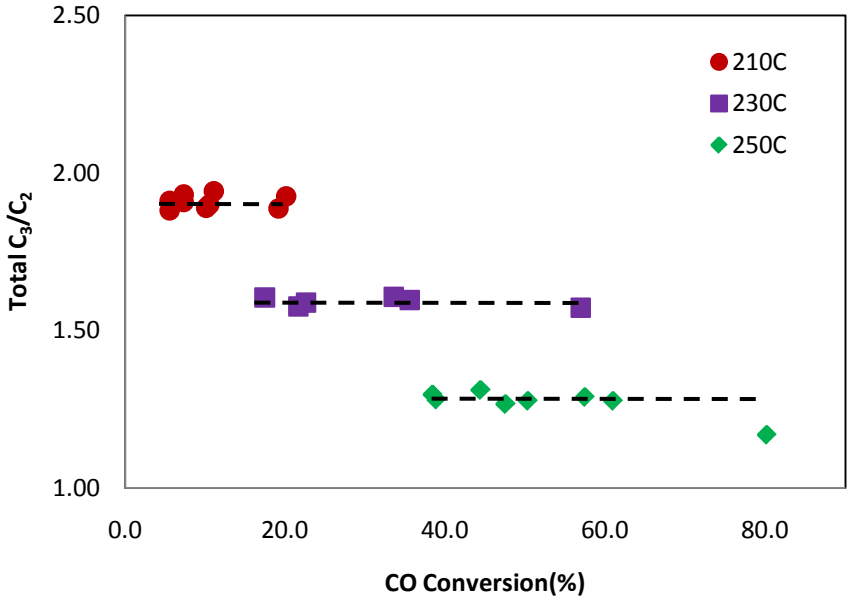

Fig. 7-18 The relative molar amount for C_3/C_2 versus CO conversion at different reaction temperatures (when H_2/CO=2:1 in the feed)

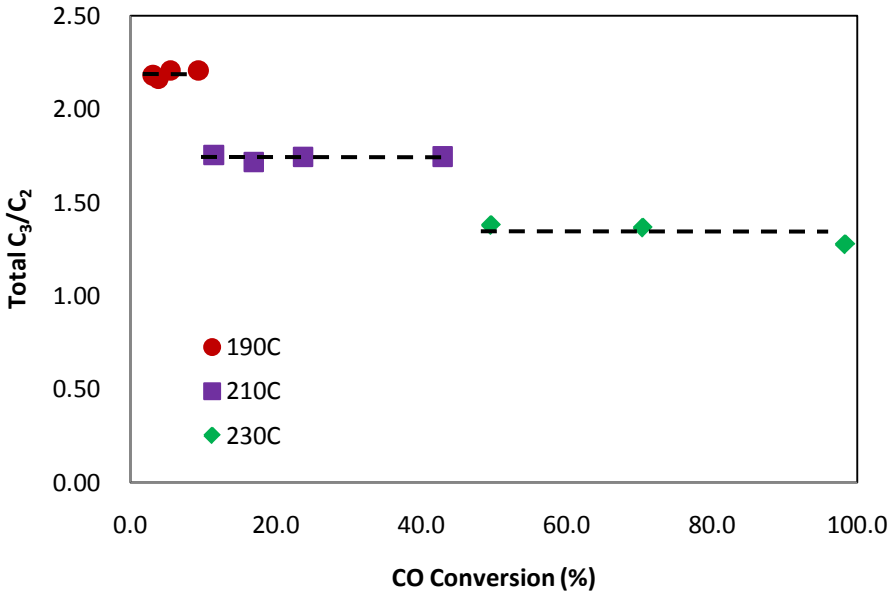

Fig. 7-19 The relative molar amount for C_3/C_2 versus CO conversion at different reaction temperatures (when H_2/CO=3:1 in the feed)

In the graphs, the C_3/C_2 ratio shows a decreasing trend with the increase of operating temperature. As an example, in Figure 7-17, once the reaction temperature varied from 210 to 240 ^oC the relative amount of C_3/C_2 dropped from around 2.26 to 1.74. On the other hand, the feed gas ratio also has an influence on the C_3/C_2. When the operational temperature was the same, such as 210^oC, the C_3/C_2 ratio decreased from 2.26 to 1.95 and then to 1.75 when the H_2/CO ratio in the feed was changed from 1:1 to 2:1 and then to 3:1.

The constant C_3/C_2 ratios with reaction temperatures grouped by the feed gas ratios are plotted in Figure 7-20.

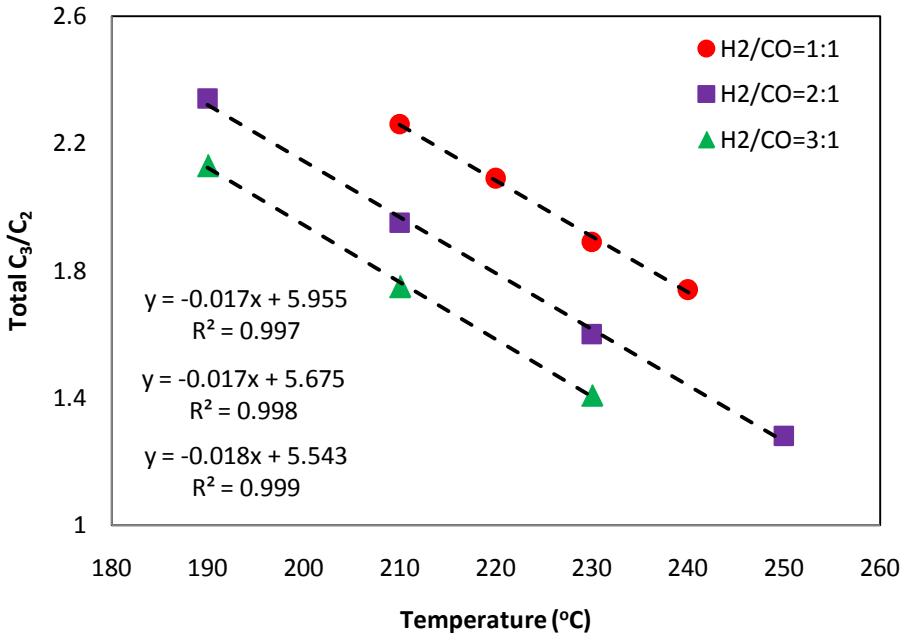

Fig. 7-20 The C_3/C_2 ratio at various H_2/CO ratios and operation temperatures (the equation for the fit lines follows the same sequence as the data groups from top to the bottom)

In this graph, the influence of reaction temperature on the C_3/C_2 ratio can be clearly seen. At all three gas ratios, the C_3/C_2 ratio shows a linear relationship to the temperature. The slopes of the fitting lines are almost the same and only their intercepts are different. These phenomena are also difficult to explain.

7.4 Conclusion

In this chapter, the author investigated the FT reaction at steady state with a wide range of operational parameters, including the H_2/CO ratio in the feed, the reaction temperature, the space velocity, in a tubular fixed bed reactor. The influence of these parameters on the reaction rate and the product selectivity were looked at. As the cobalt has no activity for the water gas shift reaction, the H_2/CO ratio in the feed becomes critical for the reaction rate. A low H_2/CO ratio decreases the reaction rate to a large extent. The CH_4 selectivity at a low H_2/CO ratio is very insensitive to the change of the reaction temperature with nearly no change at around 8.5% when reaction temperature increased from 210 to 230 ^oC.

This is in contrast to the case at a high H_2/CO ratio when the CH_4 selectivity increased from around 14% to 27.5%. At a low H_2/CO ratio, a higher reaction temperature favoured the increase of the chain growth probability which we interpreted as due to the chain growth reaction of the olefins as there was not sufficient H_2 for hydrogenation of them.

The author focused on the influence of reaction conditions on the lower hydrocarbon O/P ratios. The results from quite a number of experimental runs are summarized and the author suggested a way to describe how the space velocity of the feed affects the O/P ratio. Based upon the experimental data covering many types of reactors, SV, temperature and H_2/CO ratio the C_3H_6/C_2H_4 ratio was found to be a function of CO conversion only and the ratio follows a linear relationship with the CO conversion. When we look at the ratio of C_3/C_2 in total, it is a function of temperature and the space velocity of the feed had nearly no effect on it. The influence of reaction temperature to the C_3/C_2 is linear and the H_2/CO in the feed has an influence on the intercept of this straight line. Both these phenomena are very difficult to explain, but are likely to be important in understanding Fischer-Tropsch Synthesis reactions.

7.5 Reference

1. Anderson, R.B., Catalysts for the Fischer-Tropsch synthesis, vol. 4, Van Nostrand Reinhold, New York 1956.
2. Dry, M.E., Catalytic aspects of industrial Fischer-Tropsch synthesis, *J. Mol. Catal.* **1982**, *17*, 133–144.
3. Dictor, R.A.; Bell, A.T., Fischer-Tropsch synthesis over reduced and unreduced iron oxide catalysts, J. Catal. 1986, 97, 121–136.
4. Lox, E.S.; Froment, G.F., Kinetics of the Fischer-Tropsch reaction on a precipitated promoted iron catalyst. 1. Experimental procedure and results, *Ind. Eng. Chem. Res.* **1993**, *32*, 61–70.
5. Donnelly, T.J.; Satterfield, C.N., Product distributions of the Fischer-Tropsch synthesis on precipitated iron catalysts, *Appl. Catal. A* **1989**, *52*, 93–114.
6. Dry, M.E., Catalytic aspects of industrial Fischer-Tropsch synthesis, *J. Mol. Catal.* 1982, 17, 133–144.
7. Everson, R.C.; Woodburn, E.T.; Kirk, A.R.M., Fischer-Tropsch reaction studies with supported ruthenium catalysts I. product distributions at moderate pressures and catalyst deactivation, *J. Catal.* 1978, 53, 186–197.
8. Bell, A.T., Catalytic synthesis of hydrocarbons over group VIII metals. A discussion on the reaction mechanism, *Catal. Rev.-Sci. Eng.* **1981**, *23*, 203–232.
9. Iglesia, E.; Reyes, S.C.; Madon, R.J., Transport-enhanced E -olefin readsorption pathways Ru-catalyzed hydrocarbon synthesis, *J. Catal.* **1991**, *129*, 238–256.
10. Schulz, H.; Rao, B.R.; Elstner, M., 14C-Studien zum Reaktionsmechanismus der Fischer-Tropsch-Synthese, Erdöl Kohle 1970, 23, 651–655.
11. Schulz, H.; Gökcebay, H., Fischer-Tropsch CO-hydrogenation as a means for linear olefins production, in J.R. Kosak, ed., Catalysis of organic reactions,

Marcel Dekker, 1984 pp. 153–169.

12. Kuipers, E.W.; Vinkenburg, I.H.; Oosterbeek, H., Chain length dependence of α-olefin readsorption in Fischer-Tropsch synthesis, *J. Catal.* **1995**, *152*, 137–146.
13. Iglesia, E.; Reyes, S.C.; Madon, R.J., Transport-enhanced α-olefin readsorption pathways Ru-catalyzed hydrocarbon synthesis, *J. Catal.* **1991**, *129*, 238–256.
14. Novak, S.; Madon, R.J.; Suhl, H., Models of hydrocarbon product distributions in Fischer-Tropsch synthesis, *J. Chem. Phys.* **1981**, *74*, 6083–6091.
15. Novak, S.; Madon, R.J.; Suhl, H., Secondary effects in the Fischer-Tropsch synthesis, *J. Catal.* **1982**, *77*, 141–151.
16. Komaya, T.; Bell, A.T., Estimates of rate coefficients for elementary processes occurring during Fischer-Tropsch synthesis over Ru/TiO2, *J. Catal.* **1994**, *146*, 237–248.
17. Jordan, D.S.; Bell, A.T., Influence of ethene on the hydrogenation of CO over ruthenium, J. Phys. Chem. 1986, 90, 4797–4805.
18. Kuipers, E.W.; Scheper, C.; Wilson, J.H.; Oosterbeek, H., Non-ASF product distributions due to secondary reactions during Fischer-Tropsch synthesis, *J. Catal.* **1996**, *158*, 288–300.
19. Kuipers, E.W.; Vinkenburg, I.H.; Oosterbeek, H., Chain length dependence of α-olefin readsorption in Fischer-Tropsch synthesis, J. Catal. 1995, 152, 137– 146.

CHAPTER 8

A THERMODYNAMIC APPROACH TO OLEFIN PRODUCT DISTRIBUTION IN FISCHER-TROPSCH SYNTHESIS

The material in this chapter has been submitted for publication in Industrial and Engineering Chemistry Research. The current Reference is: Lu, X; Hildebrandt, D; Liu, X; Glasser, D. A Thermodynamic Approach to the Olefin Product Distribution in Fischer-Tropsch Synthesis. *Ind. Eng. Chem. Res.* **2011**, submitted for publication.

Abstract

Conventional FT experiments were performed in both a CSTR and a PFR on a TiO_2-supported cobalt catalyst. The O/P ratios for short chain hydrocarbons (C_2–C_5) were found to change when the reaction conditions were kept constant in a CSTR, while the ratio of neighbouring olefins (for example C_4H_8/C_3H_6) remained unchanged. In the PFR experiments, the temperature was varied from 210–250 ^oC and different flow rates ranging from 1.8–5.4 NL/h/gcat. The ratio of neighbouring olefins was found to be constant under these conditions as well. After proposing a thermodynamic model for olefin product distribution, we compared the results that the model predicted with those obtained in the experiments, and found that there is good agreement between the thermodynamic

predictions and the measured distributions. This supports the postulation that the olefin distribution in the FTS reaction might be determined by thermodynamics.

8.1 Introduction

It is generally agreed among scientists that a simple polymerization mechanism can be used to describe the distribution of FTS products. [1, 2] An FT chain growth intermediate on a catalyst surface can either propagate to form another intermediate one carbon number higher or terminate to produce an oxygenate, paraffin, or olefin with the same carbon number. The path of termination to olefin production is thought to be reversible, owing to the features of olefin adsorption/desorption and hydrogenation/dehydrogenation. [3] The propagation probability (α value) of each surface intermediate has been assumed to be a constant that is independent of carbon number (single α distribution), and this produces the so-called Anderson–Schulz–Flory (ASF) distribution equation: [4, 5]

$$W_n / n = (1-\alpha)^2 \alpha^{n-1}$$

However, various research studies published subsequently demonstrate that the measured product distribution resulting from FTS reactions often did not obey ASF kinetics, with a break being observed around a carbon number of the hydrocarbons of around 8-10, leading to negative [6–8] or positive [9–14] deviations from the ASF distribution model. Researchers developed explanations for the observed deviations from various points of view, such as proposing two chain growth active sites on the catalyst; an accumulation of the long chain products; an enhanced secondary reaction of the primary products (alkenes); and the VLE of the products under reaction conditions. Davis [15] wrote a review of work on the two alpha distribution model, and suggested that the observed deviation did not originate in the FTS reaction itself, but was caused by "conditions where experimental artifacts cannot be ruled out as causing the

experimental observations" or "experimental conditions that do not account accurately for the impact of accumulation of heavier products in the reactor".

Despite the attempts to go beyond the ASF model, its implications for the distribution of FTS products is widely accepted by researchers, as it provides an important means of understanding FTS. But even the theory itself, including its explanation of chain growth and termination, describes only the distribution of this particular product, but cannot explain why this occurs.

Various researchers have attempted to understand this distribution phenomenon from the catalytic point of view, focusing on the mechanism of FTS as a means to interpret the resultant product distribution. Almost all of the scientists undertaking this line of research initiated their investigations with the formation of surface monomers, introduced the ASF theory, and developed a mechanistic model. However, none of these has been able to offer a comprehensive explanation for the product distributions found in experiments.

Since Fischer and Tropsch [16] first reported that CO and H_2 could be converted into hydrocarbons by FTS, research into product distribution has focused mainly on a kinetic rather than a thermodynamic approach. The calculations made by Anderson [9] and Storch *et al.* [17] suggested that a global equilibrium is not achieved within the FT process when the free energy change for each reaction was considered, and each product was regarded as a different stoichiometric reaction derived from CO and H_2. In the mid-1970s, Tillmetz [18] investigated the equilibrium product as a function of the H_2/CO ratio. Various other researchers have considered an equilibrium explanation of FTS. Stenger and Askonas [19] used a free energy minimization technique to solve the equilibria for a family of chemical products, and Norval and Phillips [20] demonstrated that an equation relating equilibrium concentration and carbon number could be derived from

thermodynamics. More recently, Norval [21] has put forward a one-parameter equilibrium model for the product distributions for alkenes, alkanes and alcohols.

A great deal of research into FTS continues to be done, much of it directed towards the impact of changes in feed composition on the reaction rate and product distribution. However, the persistence of the search for a kinetic explanation ignores the issue that the FT process demonstrates many of the features an equilibrium-controlled system.

The work described in this chapter attempts to explore a small but very important part of the FTS reaction, the olefin distribution that was found in both a CSTR (Autoclave Engineers, 100ml in volume) and a PFR (Autoclave Engineers, 8mm in ID), and to suggest a thermodynamic approach that explains that distribution. The O/P ratios of the short chain hydrocarbons (C_2–C_5) produced in our experimental runs were found to change for different reasons in various cases, [22, 23] while the ratios of neighbouring olefins (for example C_4H_8/C_3H_6) remained unchanged. The ratios for $C_nH_{2n}/C_{n-1}H_{2(n-1)}$ under the reaction temperatures applied for the same carbon number n were found to be more or less the same. When we introduced an olefin pseudo equilibrium model, we found that the experimental equilibrium constant result obtained by both the CSTR and PFR matched the calculated equilibrium constant with the thermodynamic data in the handbook [24]. This suggests that a thermodynamic approach for the unique product distribution of FTS is not only practical but promising. We also investigated the thermodynamic approach for the case when C_2 was included. The result shows a trend approaching the equilibrium.

8.2 Experimental

8.2.1 Fischer-Tropsch experiments in a CSTR

The experiments were carried out in a 100 ml CSTR (Autoclave Engineers), having established previously through residence time distribution (RTD) experiments that this reactor can be regarded as an ideal mixed reactor and that the mean residence time (τ) showed a good match between the volume (Vr) and the volumetric flow rate of the feed gas when the stirring speed (SS) was higher than around 65 rpm. We used a supported cobalt catalyst with 10% Co/90% TiO_2. The experimental set-up and the details of the catalyst preparation have been described in detail in Chapter 3.

Approximately 3g of prepared cobalt catalyst was loaded into a catalyst cage (which was supplied with the reactor) that was suspended, without shaking, in the tank.

The catalyst was reduced with H_2 at a flow rate of 1.8$NLh^{-1}gcat^{-1}$ at ambient pressure. The gas SV was based on the total mass of the unreduced catalyst. The temperature was first increased from room temperature to 120 ^oC at a ramping rate of 60 $^oCh^{-1}$ and held for 2 hours. It was then raised to 280 ^oC at the same ramping rate, and maintained at this temperature for 24 hours. After reduction, the reactor was cooled to below 100 ^oC before starting the experiments.

The feed gas was switched from H_2, which had been used for the reduction, to syngas (H_2/CO = 2). The pressure of the reactor was stabilized at 2.0 MPa (g) by a back pressure regulator, and the SV of the reactants was maintained at 1.2lh-1(gcat)-1 by a mass flow controller (Brooks 5850). The temperatures used for the reaction in the experiments were 190 and 210 ^oC. The SS applied was

differentiated according to the requirements of individual experiments, but was kept above 100 rpm throughout to ensure that ideal mixing was achieved.

8.2.2 Fischer-Tropsch experiments in a PFR

An 8mm ID tubular reactor was used for these experimental runs, with the same supported catalyst as was used in the CSTR, but the catalyst loading amount for the PFR was 1g. We applied the same reduction procedure as in the CSTR, and stabilized the pressure in the PFR at 2.0 MPa (g) (as in the CSTR).

8.3 Results and Discussion

8.3.1 Olefin to paraffin ratio

In our analysis of the experimental results, the main focus was on the relative amounts of paraffins and olefins, because we believed this approach might offer more insight into FTS. We chose to work on light hydrocarbons because the product composition of the heavier hydrocarbon products changed continually in the period before the reaction had reached a final steady state (to be discussed below), and the system of analysis we were using was unable to monitor this continuously changing state. However, the information derived from the experimental use of light hydrocarbons proved to be very informative.

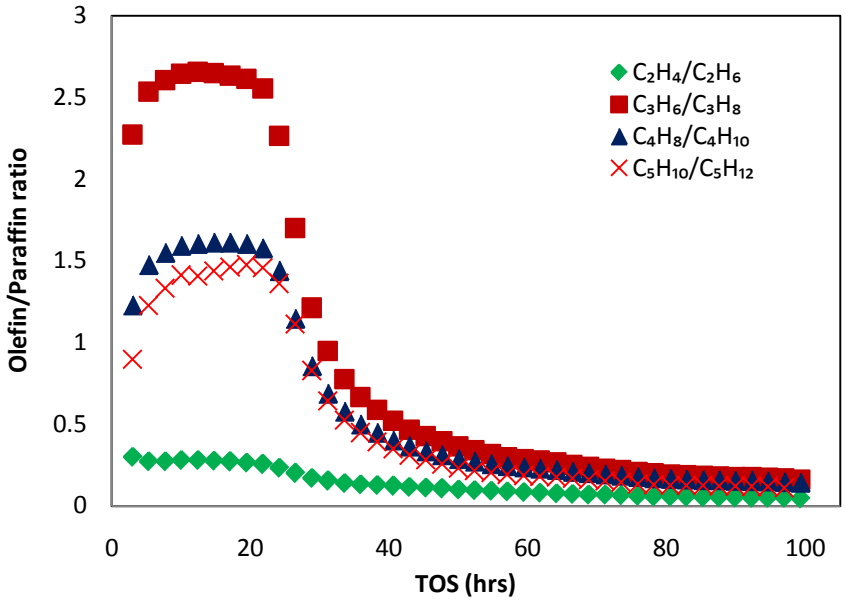

Fig. 8-1 Olefin/Paraffin ratios for C_2–C_5 at various TOS in a CSTR when all the conditions were fixed (P=20bar, T=210^{o}C, FR=1.2NL/h/gcat, SS=100rpm)

Figure 8-1 presents the behaviour of O/P ratios in FTS carried out in a CSTR when all the reaction conditions were kept constant. The data were recorded from the initiation of the experiment until a steady state was reached. The O/P ratios showed large variations, even when there was no change in the operational parameters. This phenomenon is believed to relate to the deposit of liquid phase products in the pores of the catalyst and has been discussed in Chapter 5. We believe that the factors that bring about the variations might be the change in the ratio of reactants (CO to H_2) in the liquid in the pores, and the strengthened secondary reaction opportunities for olefinic products caused by the slowing down of their mass transfer in the liquid-filled catalyst.

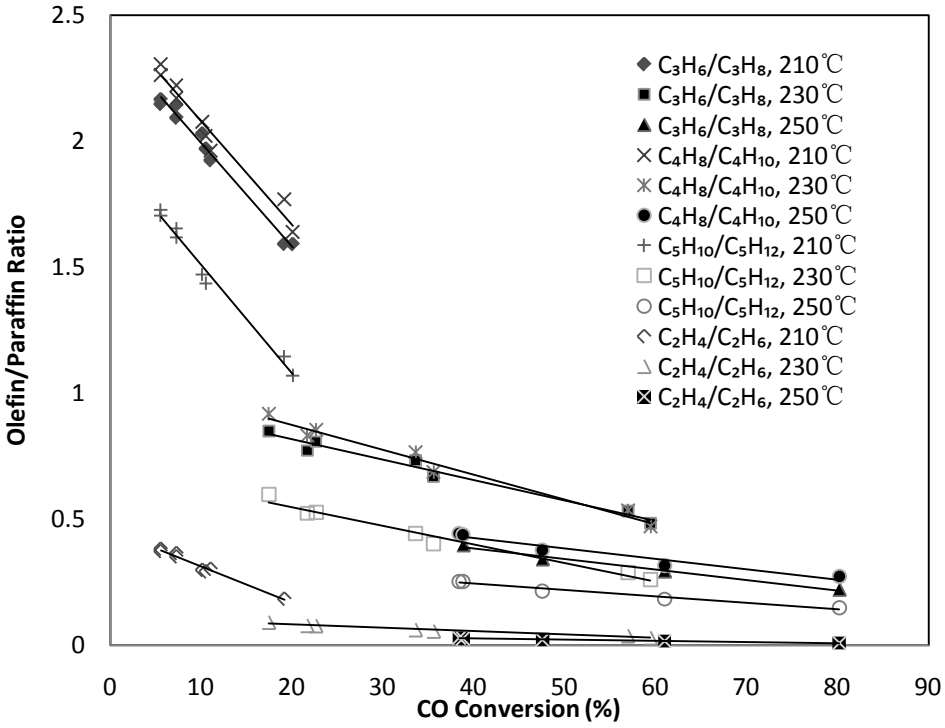

Fig. 8-2 Olefin/Paraffin ratios versus carbon monoxide conversion for C_2–C_5 at various conditions in a PFR (P=20bar, T=210-250^{o}C, FR=1.8-5.4NL/h/gcat H_2/CO=2)

Figure 8-2 illustrates the O/P ratios versus carbon dioxide conversion obtained in FTS with a supported cobalt catalyst in a fixed bed reactor (PFR). The pressure was maintained at 20 bar, while the reaction temperature was varied from 210 to 250 ^{o}C. The syngas flow rate was shifted up and down in a range of 1.8–5.4 NL/h/gcat and this resulted in the carbon monoxide conversion changing. All the data were collected when the FTS was being run at steady state. For each carbon number, the proportion of olefin to paraffin decreased when the FTS was run at the higher reaction temperature. This might be attributable to the increased extent of olefin hydrogenation at the higher temperature.

Figure 8-3 illustrates the O/P ratios with the TOS in FTS on a supported cobalt catalyst conducted in the CSTR before and after the reactor system had undergone flushing. [23] (Chapter 5) The O/P ratios for short chain hydrocarbons (C_2–C_4) showed a dramatic decrease as the Time on Stream (TOS) of the experiment proceeded. This is a result similar to those shown in Figure 8-1. Once the O/P

ratios had reached a steady state (at around 190 hours of TOS), the reactor system was flushed with an inert gas, argon, for 30 hours. Once the flushing had been completed the FTS operation resumed, under the same conditions as those used previously. After each flushing treatment, the reduced O/P ratios obtained at the end of the reaction period before the flushing started had been lifted to an extent that depended on the flushing temperature. The higher temperatures produced larger increases. Flushing at 230 ^{o}C raised the ratios to levels close to their original values at the beginning of the experiment, which is shown in the plot during the first 80 hours TOS.

In the three plots derived from three different cases that are shown above, we can observe a common characteristic, that the O/P ratio for the same carbon number altered considerably, regardless of whether the cause was the catalyst regime change (Figures 8-1 and 8-3) or the differences in the reaction conditions we set for the reactor (Figure 8-2). However, the relative molar amount of the neighbouring olefins is found to be fairly constant throughout, despite the large alteration in the O/P ratios. In the discussion below, we introduce a triangular plot that is commonly used in research on distillation to depict the relationship between the olefin and paraffin products. This technique allows the relative molar amounts of C_nH_{2n}, C_nH_{2n+2}, and $C_{n+1}H_{2(n+1)}$ to be shown in the same diagram. To simplify the presentation, we normalized the molar amounts so that the total mole fraction of these three components was one.

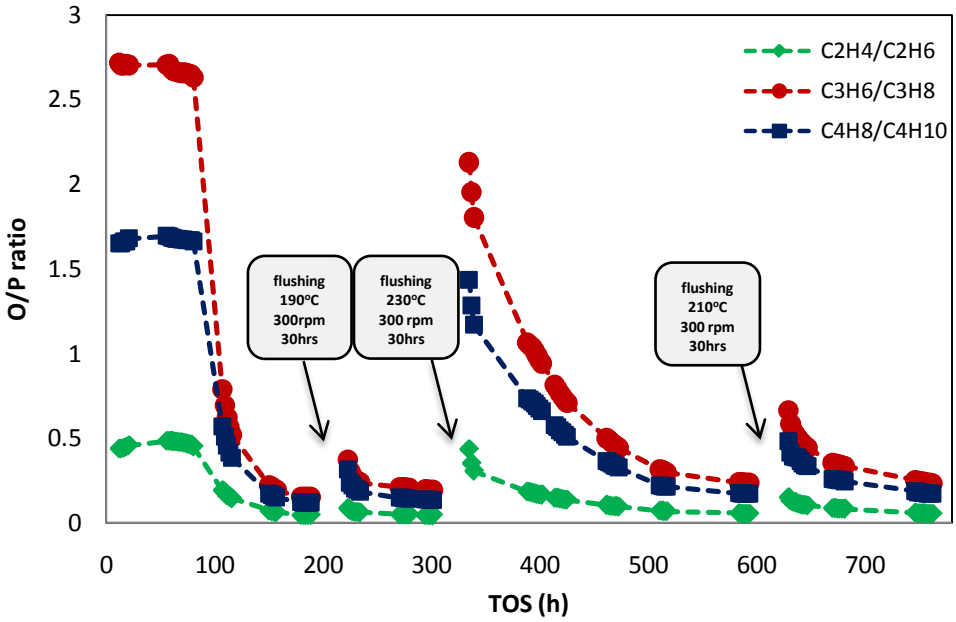

Fig. 8-3 Olefin to paraffin ratios for C_2–C_4 during reaction before and after flushing with different flushing temperatures

8.3.2 Normalized molar fraction for C_nH_{2n}, C_nH_{2n+2}, and $C_{n+1}H_{2(n+1)}$

Within all the reaction equations, the chain growth and hydrogenation from C_nH_{2n} can be simply written as follows:

$$C_nH_{2n} + CO + 2H_2 \rightarrow C_{(n+1)}H_{2(n+1)} + H_2O \quad (8\text{-}1)$$

$$C_nH_{2n} + H_2 \rightarrow C_nH_{2n+2} \quad (8\text{-}2).$$

Three kinds of hydrocarbons are contained in these two reaction equations. Their relative amounts can be normalized and plotted in a triangular diagram (Figure 8-4 below) in an order determined by their boiling points.

This triangular plot takes the idea of the residual curve used in distillation as its reference. In the triangular area, each of the three corners represents a pure component of the three hydrocarbons under consideration, and any data point inside the triangle gives the normalized mole fraction of these components, which

are arranged clockwise in a sequence following their boiling points from low to high.

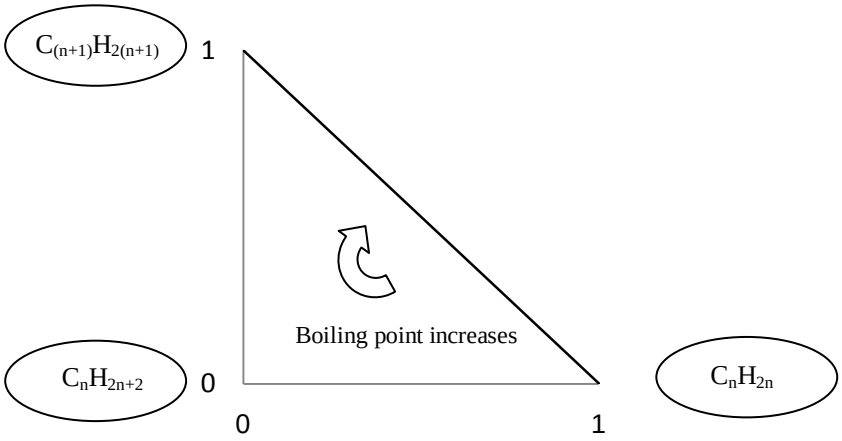

Fig. 8-4 Demonstration of triangular plot for normalized molar fractions of C_nH_{2n}, C_nH_{2n+2}, and $C_{n+1}H_{2(n+1)}$

The normalized mole fractions for C_nH_{2n}, C_nH_{2n+2}, and $C_{n+1}H_{2(n+1)}$ when n=3 and 4 are plotted in Figures 8-5 to 8-9 below, using the results from the FTS runs in the CSTR (before and after the reactor systems have been flushed) and the PFR.

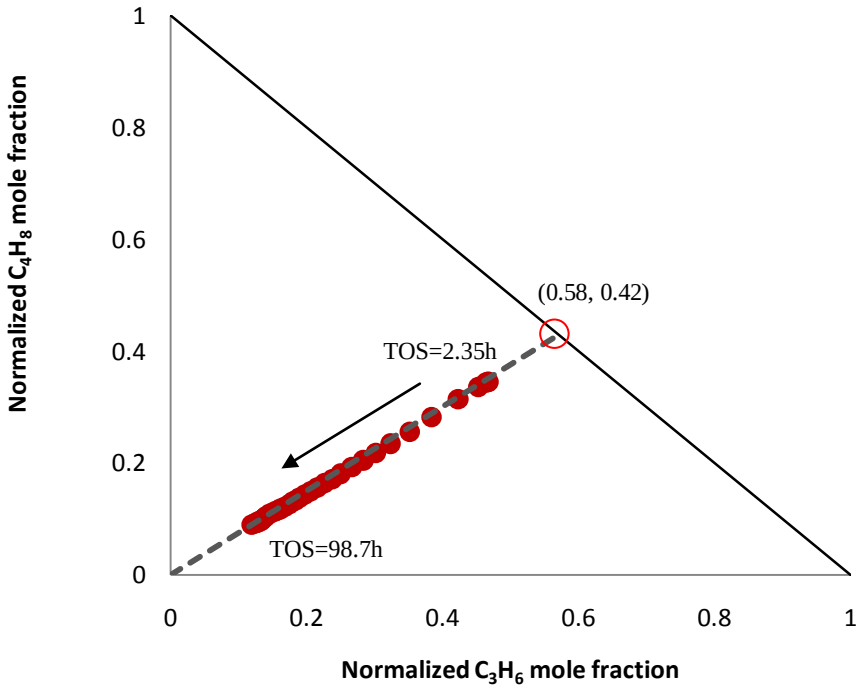

Fig. 8-5 The normalized mole fraction for C_3H_6, C_3H_8, and C_4H_8 from the experimental results in the CSTR

The plots in Figures 8-5 and 8-6 show the results of CSTR runs when all the reaction condition parameters were fixed. The changes in the normalized fraction that can be observed in the plots were caused by TOS only. As explained above, the origin (0, 0) denotes pure paraffin in the three components (C_nH_{2n}, C_nH_{2n+2}, and $C_{n+1}H_{2(n+1)}$) under consideration. The closer the data are to point (0, 0), the higher the paraffin fraction. In these two plots, at the beginning of the experimental run, the data point was situated far from the point (0, 0), which means the paraffin fractions were low and the olefins fractions high. As the TOS continued, the paraffin (C_3H_8, C_4H_{10}) fractions were increasing, as can be seen in the data points, which approach the pure paraffin point (0, 0) in both plots. With the increase of the paraffin fraction and decrease of that for olefins in each Figure, the changing data points show a very good linear trend passing through the origin (0, 0). This means the ratio of relative mole fractions of the neighbouring olefins was fixed, although the normalized mole fractions of C_nH_{2n}, C_nH_{2n+2}, and $C_{n+1}H_{2(n+1)}$ were not. Therefore, the molar ratios of C_4H_8/C_3H_6 and C_5H_{10}/C_4H_8 were all constant during the experimental run, although the O/P ratios were undergoing large-scale variations. In addition, the ratios for C_4H_8/C_3H_6 and C_5H_{10}/C_4H_8 had constant values both when the amounts of olefin were relatively large (TOS= 2.35 hrs) and much smaller (TOS= 98.7 hrs), when compared with the amount of paraffin.

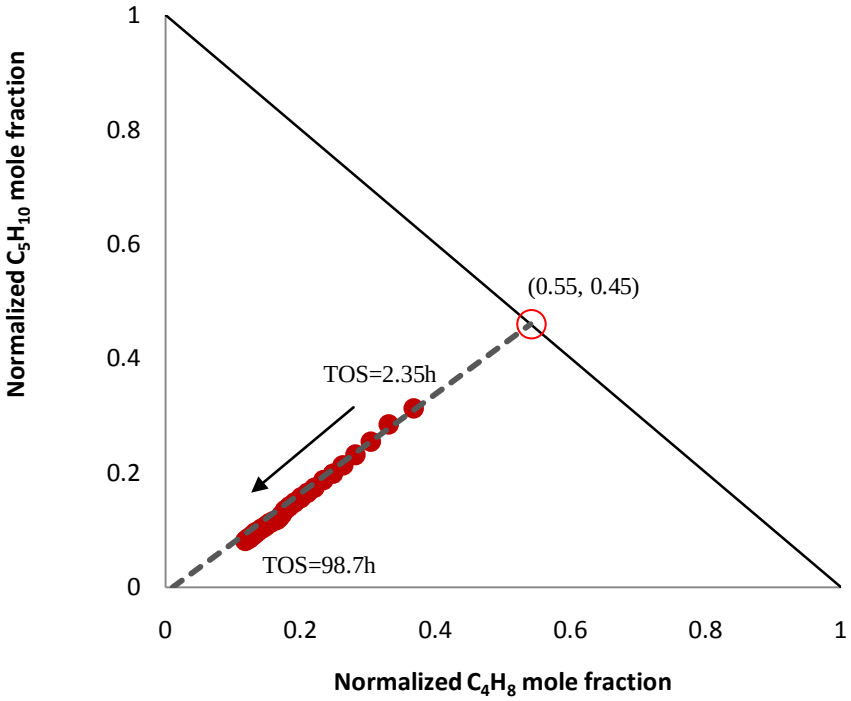

Fig. 8-6 The normalized mole fraction for C_4H_8, C_4H_{10}, and C_5H_{10} from the experimental results in the CSTR

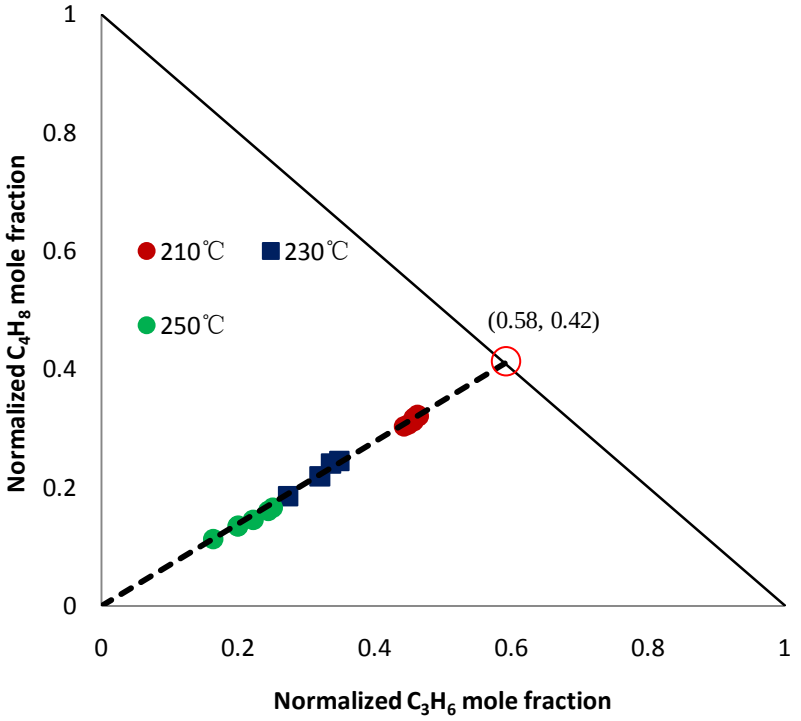

Fig. 8-7 The normalized mole fraction for C_3H_6, C_3H_8, and C_4H_8 from the experimental results in the PFR

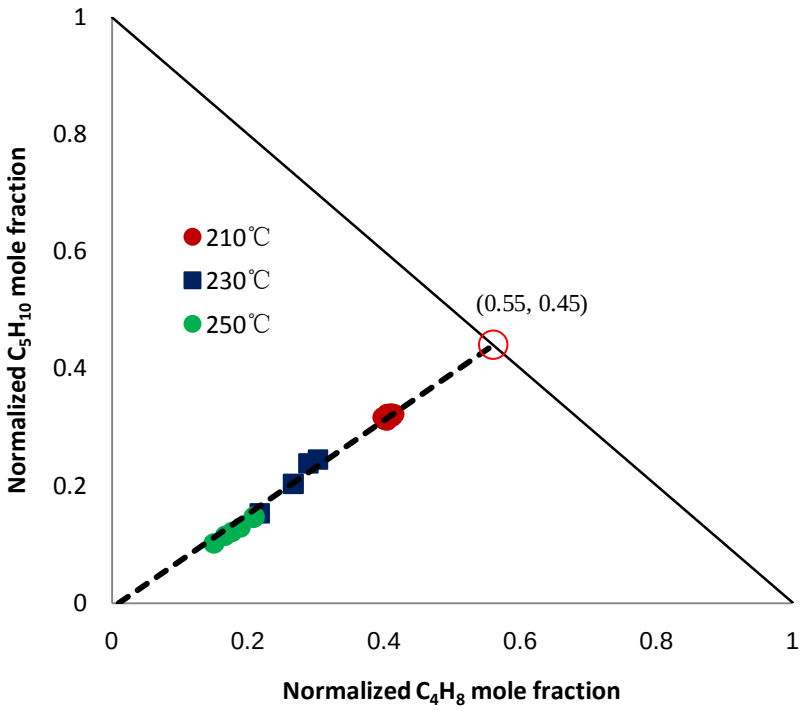

Fig. 8-8 The normalized mole fraction for C_4H_8, C_4H_{10}, and C_5H_{10} from the experimental results in the PFR

Figures 8-7 and 8-8 give the normalized mole fractions for C_3H_6, C_3H_8, C_4H_8 and C_4H_8, C_4H_{10}, C_5H_{10} in FTS runs in the PFR. The pressure in the reactor was fixed at 20bar, the reaction temperature was varied from 210 to 250 ^oC, and the flow rate was in the range of 1.8-5.4NL/h/gcat. The variations within any group of data points were caused by the changes in flow rate. As can be seen in these two graphs, the ratios of C_4H_8/C_3H_6 and C_5H_{10}/C_4H_8 also remain the same as the straight line fit for the data goes through the origin. The reaction temperature did not appear to affect the slope of the line, as it is the same for all three groups of data obtained at different temperatures. This suggests that the relative molar amount of neighbouring olefins is not sensitive to the reaction temperature that was considered.

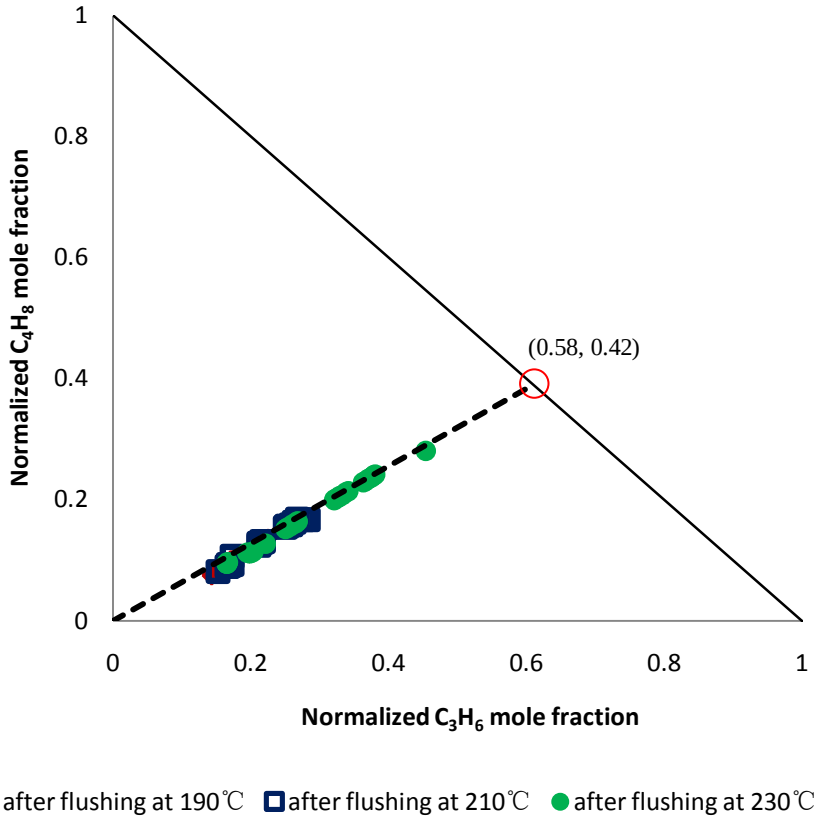

Fig. 8-9 The normalized mole fraction for C_3H_6, C_3H_8, and C_4H_8 from the experimental results of the CSTR during reaction before and after flushing with different flushing temperatures

The results shown in Figure 8-9 correspond to the results from Figure 8-3 in the case when FTS was carried out after flushing treatments at various temperatures. As can be seen, after the flushing at different temperatures, the initiating point of the normalized mole fraction is located in a different position; however, the variations follow the same direction and can be fitted with the same straight line, which again goes through the origin. This suggests that the neighbouring olefins always maintain a constant ratio, regardless of the level at which the O/P ratio initiates.

As discussed above, in a triangular plot the straight fitting line for the data points shows there is a constant ratios for $C_{n+1}H_{2(n+1)}/C_nH_{2n}$, and the intersection of the fitting line with the bevelled edge of the triangle (indicated by a red circle on the graph) gives the ratio value for $C_{n+1}H_{2(n+1)}/C_nH_{2n}$. In the three cases, all very different types of experiments and temperatures, the ratio of $C_{n+1}H_{2(n+1)}/C_nH_{2n}$, shows a constant value, as the intercepts are the same for the same carbon number n in the formula. (See Figures 8-5, 8-7 and 8-9 as examples.) This gives a fixed ratio for the $C_{n+1}H_{2(n+1)}/C_nH_{2n}$ in all the experiments carried out in this research.

8.3.3 Olefin equilibrium for C_3 and above

As shown and discussed above, all the results obtained from the FTS experiments in the CSTR before and after flushing, and the PFR yielded constant ratios for the neighbouring olefins for carbon numbers $n \geqslant 3$ (until C_5 in this study). This strongly suggested that there is some very strong reason for the olefin distribution in FTS. A possible explanation might be an equilibrium between olefin products in FTS.

Accordingly, we propose a thermodynamic model for olefin distribution, which can be simply illustrated by the following equation (Eq. 8-3). We have also

mentioned this in our previous work in a different research aspect [23] (Chapter 5).

$$C_{n-1}H_{2(n-1)} + C_{n+1}H_{2(n+1)} = 2C_nH_{2n} \quad (8\text{-}3).$$

In this olefin equilibrium model, we assume that the formation of alkenes follows a chain growth pathway, and that the formation of alkene n from alkene n-1 is reversible. For any olefins when n$\geqslant$2, Equation 3 describes an equilibrium for the neighbouring three olefins. The equilibrium constant for the three olefins is expressed in Equation 8-4.

$$K = \frac{[C_nH_{2n}]}{[C_{n-1}H_{2(n-1)}]}\frac{[C_nH_{2n}]}{[C_{n+1}H_{2(n+1)}]} \quad (8\text{-}4).$$

The value of the proposed thermodynamic equilibrium constant can be derived from the thermodynamic data by means of the following equations: [25]

$$K^{\theta} = \exp(\frac{-\Delta G_r^{\theta}}{RT}) \quad (8\text{-}5)$$

$$K = f(K^{\theta}, T, \Delta H_r) \quad (8\text{-}6).$$

The theoretical and experimental values of equilibrium constants for the proposed olefin equilibrium when carbon numbers are 3, 4, and 5 are given in Table 8-1.

Table 8-1 Thermodynamic equilibrium constants when n=3,4,5

Equilibrium constant	Temperature	
	190^{o}C	210^{o}C
Calculated	0.92	0.93
Experimental	0.92	0.92

When we look at the calculated equilibrium constants at these two temperatures, we can see the value of the constant increases only from 0.92–0.93 for an increment of 20^{o}C. This shows that the equilibrium constants are insensitive to the

change in temperature, a characteristic that matches the results shown in Figures 8-6 and 8-7. Also the constants we derived from the experimental results were almost the same as those derived from the thermodynamic data. This strengthens the suggestion that the distribution of olefins is thermodynamically determined.

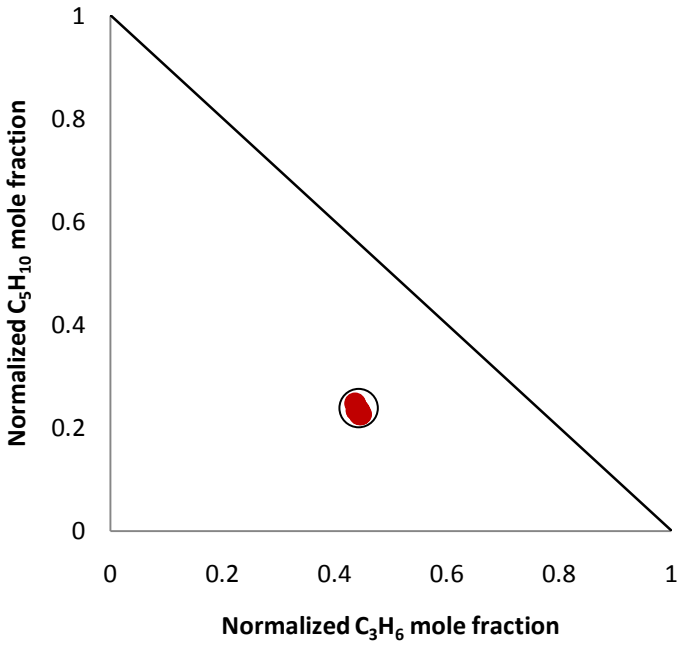

Fig. 8-10 The normalized mole fraction for C_3H_6, C_4H_8, and C_5H_{10} from the experimental results of the CSTR

To see this more clearly we can plot the normalized C_3H_6, C_4H_8, and C_5H_{10} mole fractions on a triangular diagram. If these three components are in equilibrium, their normalized measured mole fractions should be constant, so that the data points plotted in the triangle should coincide. Figure 8-10 presents the plot of the normalized mole fractions for C_3H_6, C_4H_8, and C_5H_{10} from one FTS run in the CSTR. All 40 data points fall within a very small region. This means that the relative molar amounts for C_3H_6, C_4H_8, and C_5H_{10} are constant, regardless of changes in other variables, and provides further proof of the proposed olefin equilibrium.

8.3.4 Olefin equilibrium when C_2 is included

Within the whole range of FTS products, C_2 has always been found by researchers to deviate from the classical ASF distribution pattern, but no satisfactory explanation for this phenomenon has yet been given. One possibility is that the ΔG of formation of C_2 deviates from the distribution of ΔG of formation of the C_3+ hydrocarbons. When we applied the methods introduced above, we found that when C_2 was included there was a clear difference from the situation described in 8.3.3. The normalized mole fractions for C_2H_4, C_2H_6, and C_3H_6 for the FTS runs in the CSTR and in the PFR are presented in Figures 8-11 and 8-12 respectively. In each diagram, the C_3H_6/C_2H_4 values no longer lie on a straight line through the origin. The range of values of the slopes is shown by the straight lines drawn from the origin to the intercept with the bevelled edge of the triangle.

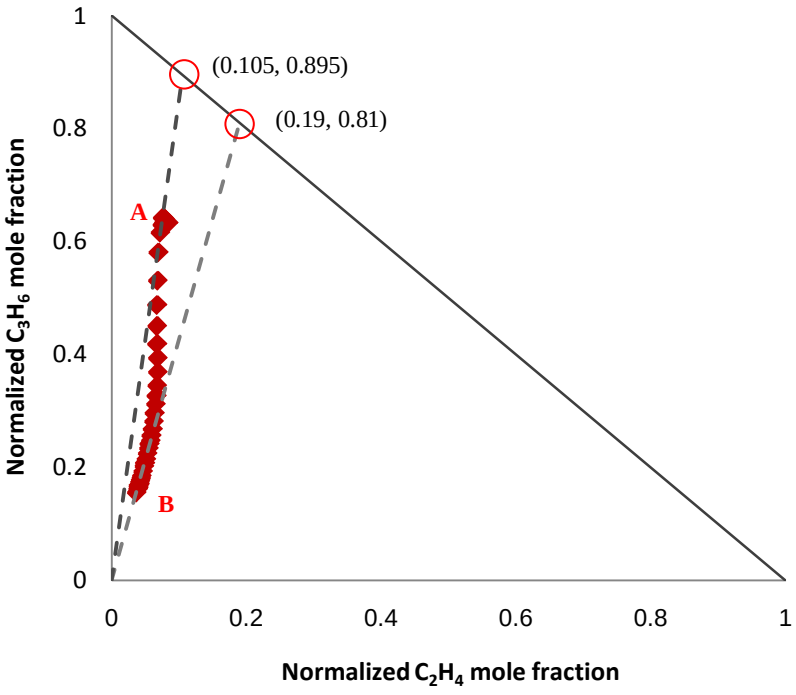

Fig. 8-11 The normalized mole fraction for C_2H_4, C_2H_6, and C_3H_6 from the experimental results in the CSTR

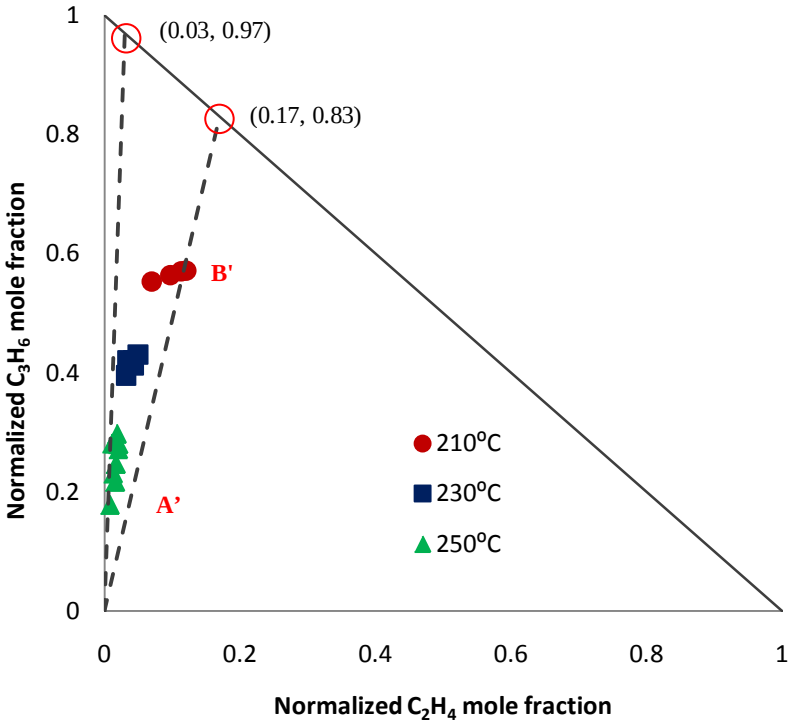

Fig. 8-12 The normalized mole fraction for C_2H_4, C_2H_6, and C_3H_6 from the experimental results in the PFR

In Figure 8-11, the reaction conditions were kept constant and the reaction temperature was set at 210 ^oC. Unlike the results presented in Figures 8-5 and 8-6 for the C_3+ hydrocarbons, the data points in this instance cannot be fitted to a straight line through the origin, so the ratio of C_3H_6/C_2H_4 is not fixed, but constantly altered during the experiment. Data point A, corresponding to the intercept (0.19, 0.81), represents the result obtained when the catalyst was fresh and the CO conversion was relatively high, while the results for data point B, which reflected the later stage when the CO conversion was consequently relatively low, corresponded with the intercept (0.105, 0.895).

Figure 8-12 illustrates the three groups of data points resulting from the use of three different temperatures. The variation within each group of data points was caused by different SVs. Unlike the results shown in Figures 8-7 and 8-8, the ratio of C_3H_6/C_2H_4 varies at different reaction conditions (temperature and SV in this

case). When we look at each group of data points at the same reaction temperature, we find that at a lower SV, which results a higher reactant conversion, the intercept is closer to the point (0, 1) than the others at higher SVs Also, if we look at the whole group of data points at three different reaction temperatures, and focus on the data points developed from B' to A', the reactant conversion shows a trend towards increase (the CO conversion varied from around 5% to around 85%). It follows that when the intercept is closer to point (0, 1) the reactant conversion has a higher value. This result matches the findings obtained in the FTS experiments run in the CSTR.

We proposed an olefin equilibrium model n=3, 4, and 5. We can do the same for n=2, 3, and 4. The equilibrium constants derived from the two sets of data are given in Table 8-2 below. As can be seen in the Table, the constants varied in ranges of 4.88–11.8 and 21.1–32.3 at reaction temperatures of 210 °C and 250 °C respectively. These are very different from the calculated values— 46.5 and 33.1—derived from the thermodynamic data at the corresponding temperatures. But when the CO conversion was at a high level, the reaction constant derived from the experimental result of the proposed equilibrium model was nearly the same as the calculated thermodynamic equilibrium constant. The results from both the CSTR and PFR suggest that the predicted equilibrium constants are closer to those of the thermodynamic equilibrium when the conversion of reactants is high and the temperature is higher.

Table 8-2 Thermodynamic equilibrium constants when n=3,4,5

Equilibrium constant	Temperature	
	210 ^{o}C	250 ^{o}C
Calculated	46.5	33.1
Experimental	4.88-11.8	21.1-32.3

8.4 Conclusion

The experiments were carried out in two kinds of reactors, A CSTR, a PFR and a CSTR, in which a cyclical sequence consisting of a normal FTS procedure alternated with a flushing treatment. The O/P ratios for short chain hydrocarbons were observed to either change during the reaction TOS in the CSTR or to remain constant at different levels in the PFR (because of variations in the reaction conditions). Despite the changes in, and different level of, the O/P ratios, those of neighbouring olefins for carbon number $n \geqslant 3$ (until C_5 considered in this work) were found to remain constant.

Based upon these results, we proposed an equilibrium model for distribution of olefin products. The equilibrium constants for the equilibrium model were derived from both thermodynamic and the experimental data. The constant values derived from the two different approaches were found to match when C_3 and above were considered. When C_2 was included in the analysis, experimental results did not agree with those equilibrium constants calculated from thermodynamic data. The results from both the CSTR and the PFR suggested that the experimentally estimated equilibrium constants were approaching those of the thermodynamic equilibrium when the conversion of reactants and the temperature were high.

It is suggested that a thermodynamic equilibrium approach to olefin distribution promises to provide a clearer understanding of the unique product distribution behaviour of FTS.

8.5 References

1. Madon, R. J.; Reyes, S. C.; Iglesia, E. Primary and secondary reaction pathways in ruthenium-catalyzed hydrocarbon synthesis. *Journal of Physical Chemistry* **1991**, *95*, 7795-7804.
2. Zhan, X.; Davis, B. H. Assessment of internal diffusion limitation on Fischer–Tropsch product distribution. *Applied Catalysis A: General* **2002**, *236*, 149–161.
3. Gates, B. C.; Katzer, J. R.; and Schuit, G. C. A. *Chemistry of Catalytic Processes*; McGraw-Hill: New York, 1979.
4. Friedel, R. A.; Anderson, R. B. Composition of Synthetic Liquid Fuels. I. Product Distribution and Analysis of C_5—C_8 Paraffin Isomers from Cobalt Catalyst. *Journal of the American Chemical Society* **1950**, *72*, 1212-1215.
5. Anderson, R. B. *The Fischer-Trospch Synthesis*; Academic Press: New York, 1984.
6. Satterfield, C. N.; Huff, G. A. Jr. Carbon number distribution of Fischer-Tropsch products formed on an iron catalyst in a slurry reactor. *Journal of Catalysis* **1982**, *73*, 187-197.
7. Satterfield, C. N.; Huff, G. A. Jr.; Longwell, J. P. Product distribution from iron catalysts in Fischer-Tropsch slurry reactors. *Industrial and Engineering Chemistry Process Design and Development* **1982**, 21, 465–470.
8. Dictor, R. A.; Bell, A. T. An explanation for deviations of Fischer-Tropsch products from a Schulz-Flory distribution. *Industrial and Engineering Chemistry Process Design and Development* **1983**, *22*, 678–681.
9. Anderson, R. B. *Catalysis*, Emmett, P. H. Editor. 1956, Reinhold: New York.
10. Atwood, H. E.; Bennett, C. O. Kinetics of the Fischer-Tropsch Reaction over Iron. *Industrial and Engineering Chemistry Process Design and Development* **1979**, *18*, 163–170.

11. Madon, R. J.; Taylor, W. F. Fischer-Tropsch synthesis on a precipitated iron catalyst. *Journal of Catalysis* **1981**, *69*, 32-43.
12. Huff, G. A. Jr.; Satterfield, C. N. Evidence for two chain growth probabilities on iron catalysts in the Fischer-Tropsch synthesis. *Journal of Catalysis* **1984**, *85*, 370-379.
13. Iglesia, E.; Reyes, S. C.; Madon, R. J. Transport-enhanced α-olefin readsorption pathways Ru-catalyzed hydrocarbon synthesis. *Journal of Catalysis* **1991**, *129*, 238-256.
14. Kuipers, E. W.; Scheper, C.; Wilson, J. H.; Vinkenburg, I. H.; Oosterbeek, H. Non-ASF product distributions due to secondary reactions during Fischer–Tropsch Synthesis. *Journal of Catalysis* **1996**, *158*, 288-300.
15. Davis, B. H. Anderson-Schulz-Flory Product Distribution – Can it be Avoided for Fischer-Tropsch Synthesis?
16. Fischer, F.; Tropsch, H. Die Erd¨ olsynthese bei Gew¨ohnlichen Druck aus den Vergasungsprodkten der Kohlen. *Brennst. Chem.* **1926**, *7*, 97–116.
17. Storch, H. H.; Golumbic, N.; Anderson, R. B. *The Fischer-Tropsch and Related Syntheses*; Wiley: New York, 1951.
18. Tillmetz, K. D. Uber Thermodynamische Simultangleichgewichte bei der Ficher-tropsch Synthese. *Chem. Ing. Tech.* **1975**, *48*, 1065.
19. Stenger, H. G.; Askonas, C. F. Thermodynamic Products Distributions for the Fischer-Tropsch Synthesis. *Ind. Eng. Chem. Fundam* **1986**, *25*, 410–413.
20. Norval, G. W.; Phillips, M. J. Application of Equilibrium Analysis to a Fischer-Tropsch Product. *J. Catal.* **1990**, *126*, 87–91.
21. Norval, G. W., Notes on issues of equilibrium in the FT synthesis. *The Canadian Journal of Chemical Engineering* **2008**, *86*, 1062-1069
22. Lu, X.; Hildebrandt, D.; Liu, X.; Glasser, D. Making Sense of the Fischer-Tropsch Synthesis Reaction: Start-up. *Industrial and Engineering Chemistry Research* **2010**, *49*, 9753.

23. Lu, X.; Zhu, X.; Hildebrandt, D.; Liu, X.; Glasser, D. A new way to look at FTS using flushing experiments. *Industrial and Engineering Chemistry Research* **2011**. Accepted for publication.
24. Perry, R. H.; Green, D. W. *Perry's Chemical Engineers' Handbook*; McGraw-Hill: New York, 1997.
25. Moran, M. J.; Shapiro, H. N. *Fundamentals of engineering thermodynamics*. Wiley: New Jersey, 2006.

CHAPTER 9

CONCLUSIVE REMARKS

The study carried out in this thesis mainly focused on understanding the phenomena related to the Fischer-Tropsch reaction. The experiments were performed in gas-solid reaction regime with three different types of reactors under typical low temperature Fischer-Tropsch Synthesis conditions.

The study of external mass transfer on a TiO_2-supported cobalt catalyst was carried out in a CSTR. The experimental results suggested that external mass transfer has an effect on the reaction rate and product selectivity for short TOSs, but very little after a certain longer TOSs. Therefore, the long term FTS is not an entirely external mass transfer controlled reaction system. The time on stream experiment showed dramatic changes in the reaction rate and product selectivity of FTS, which happened almost simultaneously. The TOS time at which these changes occurred depended on the reaction temperature and a higher temperature resulted in a shorter initiation time.

The flushing experiments with inert gas argon at different flushing temperatures were performed after the reaction reached steady state and FT reaction resumed after each flushing. Three different flushing temperatures (190, 210, and 230 ^{o}C) turned the conversion and product selectivity in the reaction after flushing back to the initial levels before flushing in different extents; and the higher the flushing temperature was, the closer the levels were. The flushing treatment by argon was believed to change the amount and composition of the liquid phase product that had formed during the reaction but not the surface properties of the catalyst. This therefore suggested that the considerable changes in reaction rate and product selectivity we observed during the early stage of FT reaction were caused (either

wholly or mainly) by liquid products deposited in the catalyst. The deposited liquid in the catalyst provided diffusional restrictions for the reactant so that the reaction rate was slowed down and the products so that the olefin/paraffin ratios were decreased owing to the enhancement of the secondary reaction of olefins.

The reactants and products information in the flushed out stream during flushing were also collected and results provided further interesting insights into FTS. The amount of H_2 driven out from the catalyst was around 4 times that of CO instead of 2 times, which was the ratio in the feed gas. This is a critical reason that made the selectivity of CH_4 and paraffins to increase dramatically. Considerable amounts of light hydrocarbons were driven off from the liquid in the catalyst pores. The dynamic behaviours of the content of hydrocarbons in the flushed out stream suggested that the reactions among the products might take place under moderate FT reaction conditions (such as the temperature and pressure applied for flushing). In the product distribution of C_1-C_8 in the liquid in the catalyst, CH_4 was outstanding; C_2-C_4 decreased slightly; and C_4 above started to increase.

In the experiments we performed in a batch reactor, the various reaction duration operations were carried out individually once the reactor was at steady state in the CSTR operation mode. When the given reaction duration was long enough, 98.5% but not complete conversions for the reactants were achieved, which matches the thermodynamic expectation for the FTS reaction. A reaction rate jump, with an increment of 70%, was observed when the reactor was switched from CSTR mode to batch mode while the other operation conditions remained the same. We attributed this to the fact that when the change took place we had moved from a situation where reaction and stripping of the liquid were occurring simultaneously to one in which only reaction was occurring. We surmised that when stripping stopped that a reactive product was left behind. CH_4 selectivity was observed to be affect by neither the residence time nor the partial pressure of the reactants as long as the H_2/CO ratio remained roughly constant. A decrease of olefin to

paraffin ratios for light hydrocarbons with extend of the reaction duration suggests that the formed olefins could re-enter the catalyst and commence the secondary reaction. The product distribution for C_2-C_7 behaved entirely different from a classic ASF distribution by showing an ascending trend instead of a descending trend with the increase of carbon number. The batch operation offered us a continuous track on the pressure variation with the extent of the FTS reaction. When product water was assumed in gas phase, the pressure derived by mass balance (even all the C_2+ products were assumed in liquid phase) could not explain why the pressure reading of the reactor was lower than it was supposed to be. Therefore a considerable proportion of the produced water by reaction should be in liquid phase.

In the experiments we conducted in a tubular fixed bed reactor, the FT reaction was investigated at steady state with wide range operation parameters, including the H_2/CO ratio in the feed, the reaction temperature, and the space velocity. A low H_2/CO ratio will inhibit the reaction rate in a big extent and the efficiency of the catalyst for converting the reactants is largely suppressed. When at a high H_2/CO ratio (3:1 in our case), the reaction rate at low space velocity was also inhibited due to insufficient CO in the system although in some case the CO conversion was less than 50%. The CH_4 selectivity at a low H_2/CO ratio is insensitive to the change of the reaction temperature with nearly no change at around 8.5% when reaction temperature increased from 210 to 230 ^oC, which in contrast to the case at high H_2/CO ratio, the CH_4 selectivity increased from around 14% to 27.5%. At low H_2/CO ratio, the increase of the reaction temperature favoured the increasing of the chain growth probability due to the chain growth reaction of the olefins as there was no sufficient H_2 for hydrogenation of them. The author focused on the influence of reaction conditions O/P ratios, the C_3H_6/C_2H_4 ratio and the C_3/C_2 ratio. The results from quite a number of experimental runs are summarized and the author suggested a way to describe how the space velocity of the feed affects the O/P ratio. Based upon the

experimental data covering many types of reactors, SV, temperature and H_2/CO ratio the C_3H_6/C_2H_4 ratio was found to be a function of CO conversion only and the ratio follows a linear relationship with the CO conversion. When we look at the ratio of C_3/C_2 in total, it is a function of temperature and the space velocity of the feed had nearly no effect on it. The influence of reaction temperature to the C_3/C_2 is linear and the H_2/CO in the feed has an influence on the intercept of this straight line. Both these phenomena are very difficult to explain, but are likely to be important in understanding Fischer-Tropsch Synthesis reactions

Despite the olefin/paraffin ratios for short chain hydrocarbons were observed to either be changing during the reaction TOS in the CSTR due to the catalyst regime change or sit at different levels because of various reaction conditions in the PFR, the ratio of neighbouring olefins was found to keep constant when carbon number $n \geqslant 3$. Based upon these results, we proposed an equilibrium model for distribution of olefin products. The equilibrium constants for the equilibrium model were derived from both thermodynamic and the experimental data. The constant values derived from the two different approaches were found to match when C_3 and above were considered. When C_2 was included in the analysis, experimental results did not agree with those equilibrium constants calculated from thermodynamic data. The results from both the CSTR and the PFR suggested that the experimentally estimated equilibrium constants were approaching those of the thermodynamic equilibrium when the conversion of reactants and the temperature were high. It is suggested that a thermodynamic equilibrium approach to olefin distribution promises to provide a clearer understanding of the unique product distribution behaviour of FTS.

.

Appendix A

This part presents the experimental results of Fischer-Tropsch Synthesis in a fixed bed reactor at various operating conditions, including the conversions of the reactants, average reaction rate through the catalyst bed, the CH_4 selectivity, and the product distribution (presented with α value).

T, P	SV [Nl/h/gcat]	CO Conversion [%]		
		1 to 1	1 to 2	1 to 3
190 °C 20bar	1.8		6.56	9.35
	3.6		3.35	5.49
	5.4		2.34	3.88
	7.2		2.06	3.11
	5.4		2.63	
	3.6		3.62	
	1.8		6.28	
210 °C 20bar	1.8	6.30	20.11	42.95
	3.6	3.83	10.55	23.75
	5.4	2.46	7.31	16.95
	7.2	1.71	5.58	11.47
	5.4	3.01	7.31	
	3.6	4.15	10.15	
	1.8	7.47	19.49	
220 °C 20bar	1.8	12.18		
	3.6	6.70		
	5.4	4.02		
	7.2	3.46		
	5.4	4.05		
	3.6	6.68		
	1.8	12.35		
230 °C 20bar	1.8	19.24	59.41	98.33
	3.6	10.32	35.57	70.43
	5.4	7.14	21.67	49.59
	7.2	5.86	17.45	37.10
	5.4	7.41	22.64	
	3.6	10.32	33.58	
	1.8	18.55	56.94	
240 °C 20bar	1.8	26.68		
	3.6	16.32		
	5.4	11.52		
	7.2	8.90		
	5.4	11.66		
	3.6	16.32		
	1.8	27.36		
250 °C 20bar	1.8		80.18	
	3.6		60.97	
	5.4		47.55	
	7.2		38.39	
	5.4		44.42	
	3.6		57.46	
	1.8		75.13	

T,P	SV [Nl/h/gcat]	CO rate [mol/g cat/min]		
		1 to 1	1 to 2	1 to 3
	1.8		2.03E-05	2.2061E-05
	3.6		2.08E-05	2.5904E-05
	5.4		2.18E-05	2.7439E-05
190°C 20bar	7.2		2.55E-05	2.9298E-05
	5.4		2.42E-05	
	3.6		2.22E-05	
	1.8		1.93E-05	
	1.8	3.52E-05	6.17E-05	1.01E-04
	3.6	3.67E-05	6.47E-05	1.12E-04
	5.4	3.82E-05	6.73E-05	1.20E-04
210°C 20bar	7.2	3.98E-05	6.85E-05	1.18E-04
	5.4	3.83E-05	6.73E-05	
	3.6	3.98E-05	6.23E-05	
	1.8	3.58E-05	5.98E-05	
	1.8	5.83E-05		
	3.6	6.42E-05		
	5.4	5.78E-05		
220°C 20bar	7.2	6.75E-05		
	5.4	5.93E-05		
	3.6	6.51E-05		
	1.8	6.02E-05		
	1.8	9.37E-05	1.82E-04	2.32E-04
	3.6	1.01E-04	1.95E-04	3.32E-04
	5.4	1.04E-04	2.02E-04	3.51E-04
230°C 20bar	7.2	1.14E-04	2.16E-04	3.50E-04
	5.4	1.08E-04	2.11E-04	
	3.6	1.01E-04	2.08E-04	
	1.8	9.04E-05	1.76E-04	
	1.8	1.30E-04		
	3.6	7.95E-05		
	5.4	1.68E-04		
240°C 20bar	7.2	1.74E-04		
	5.4	1.71E-04		
	3.6	1.59E-04		
	1.8	1.33E-04		
	1.8		2.49E-04	
	3.6		3.78E-04	
	5.4		4.42E-04	
250°C 20bar	7.2		4.76E-04	
	5.4		4.13E-04	
	3.6		3.56E-04	
	1.8		2.33E-04	

T,P	SV [Nl/h/gcat]	H_2 Conversion [%]		
		1 to 1	1 to 2	1 to 3
190°C 20bar	1.8		6.46	6.85
	3.6		3.55	4.05
	5.4		3.03	2.80
	7.2		2.28	2.46
	5.4		2.42	
	3.6		3.49	
	1.8		5.83	
210°C 20bar	1.8	14.56	20.76	31.67
	3.6	6.92	10.67	17.54
	5.4	5.07	7.35	12.59
	7.2	3.87	6.26	8.62
	5.4	6.20	7.61	
	3.6	8.54	10.35	
	1.8	15.56	20.14	
220°C 20bar	1.8	24.92		
	3.6	13.30		
	5.4	8.87		
	7.2	8.20		
	5.4	9.42		
	3.6	14.43		
	1.8	25.06		
230°C 20bar	1.8	39.36	62.44	76.30
	3.6	21.39	38.55	54.47
	5.4	14.67	23.96	38.17
	7.2	11.75	19.58	
	5.4	15.10	24.89	
	3.6	21.35	36.22	
	1.8	38.06	61.08	
240°C 20bar	1.8	54.75		
	3.6	33.55		
	5.4	23.59		
	7.2	18.26		
	5.4	23.77		
	3.6	33.84		
	1.8	56.23		
250°C 20bar	1.8		87.18	
	3.6		68.22	
	5.4		53.26	
	7.2		43.06	
	5.4		49.69	
	3.6		63.75	
	1.8		81.87	

T,P	SV [Nl/h/gcat]	H_2 rate [mol/g cat/min]		
		1 to 1	1 to 2	1 to 3
190°C 20bar	1.8		4.09E-05	4.81E-05
	3.6		4.49E-05	5.67E-05
	5.4		5.74E-05	5.90E-05
	7.2		5.77E-05	6.91E-05
	5.4		4.60E-05	
	3.6		4.43E-05	
	1.8		3.70E-05	
210°C 20bar	1.8	6.62E-05	1.32E-04	2.22E-04
	3.6	6.30E-05	1.35E-04	2.46E-04
	5.4	6.92E-05	1.40E-04	2.65E-04
	7.2	7.04E-05	1.59E-04	2.62E-04
	5.4	8.47E-05	1.45E-04	
	3.6	7.77E-05	1.31E-04	
	1.8	7.08E-05	1.28E-04	
220°C 20bar	1.8	1.13E-04		
	3.6	1.21E-04		
	5.4	1.21E-04		
	7.2	1.47E-04		
	5.4	1.27E-04		
	3.6	1.29E-04		
	1.8	1.12E-04		
230°C 20bar	1.8	1.76E-04	3.96E-04	5.35E-04
	3.6	1.92E-04	4.36E-04	7.64E-04
	5.4	1.97E-04	4.53E-04	8.03E-04
	7.2	2.10E-04	4.94E-04	8.11E-04
	5.4	2.03E-04	4.71E-04	
	3.6	1.91E-04	4.57E-04	
	1.8	1.70E-04	3.83E-04	
240°C 20bar	1.8	2.45E-04		
	3.6	1.50E-04		
	5.4	3.17E-04		
	7.2	3.27E-04		
	5.4	3.19E-04		
	3.6	3.03E-04		
	1.8	2.52E-04		
250°C 20bar	1.8		5.50E-04	
	3.6		8.60E-04	
	5.4		1.01E-03	
	7.2		1.09E-03	
	5.4		9.40E-04	
	3.6		8.04E-04	
	1.8		5.16E-04	

T,P	SV [Nl/h/gcat]	CH_4 sel [%]		
		1 to 1	1 to 2	1 to 3
190°C 20bar	1.8		7.45	9.54
	3.6		8.03	8.51
	5.4		8.10	8.53
	7.2		6.49	8.19
	5.4		7.51	
	3.6		7.81	
	1.8		7.96	
210°C 20bar	1.8	8.25	9.62	13.77
	3.6	7.71	9.42	14.01
	5.4	8.15	9.49	14.35
	7.2	8.78	9.55	14.61
	5.4	7.09	9.80	
	3.6	7.96	9.75	
	1.8	7.49	9.29	
220°C 20bar	1.8	6.67		
	3.6	7.18		
	5.4	8.59		
	7.2	8.77		
	5.4	8.50		
	3.6	7.11		
	1.8	6.54		
230°C 20bar	1.8	7.22	12.96	27.52
	3.6	8.29	12.57	24.64
	5.4	8.57	14.41	23.95
	7.2	8.73	13.75	
	5.4	8.80	13.77	
	3.6	8.62	12.17	
	1.8	7.94	10.88	
240°C 20bar	1.8	8.85		
	3.6	10.27		
	5.4	10.42		
	7.2	10.44		
	5.4	10.85		
	3.6	10.66		
	1.8	9.54		
250°C 20bar	1.8		20.87	
	3.6		20.37	
	5.4		20.45	
	7.2		20.50	
	5.4		19.96	
	3.6		18.86	
	1.8		18.59	

T,P	SV [Nl/h/gcat]	α		
		1 to 1	1 to 2	1 to 3
190°C 20bar	1.8		0.76	0.87
	3.6		0.74	0.84
	5.4		0.73	0.77
	7.2		0.72	0.80
	5.4		0.73	
	3.6		0.74	
	1.8		0.75	
210°C 20bar	1.8	0.77	0.79	0.70
	3.6	0.80	0.79	0.80
	5.4	0.80	0.80	0.80
	7.2	0.80	0.81	0.84
	5.4	0.87	0.81	
	3.6	0.88	0.81	
	1.8	0.87	0.81	
220°C 20bar	1.8	0.87		
	3.6	0.89		
	5.4			
	7.2	0.90		
	5.4	0.90		
	3.6	0.89		
	1.8	0.87		
230°C 20bar	1.8	0.88	0.77	0.60
	3.6	0.90	0.85	0.84
	5.4	0.91	0.86	0.84
	7.2	0.91	0.86	
	5.4	0.92	0.85	
	3.6	0.92	0.83	
	1.8	0.90	0.77	
240°C 20bar	1.8	0.88		
	3.6	0.91		
	5.4	0.92		
	7.2	0.92		
	5.4	0.92		
	3.6	0.91		
	1.8	0.88		
250°C 20bar	1.8		0.73	
	3.6		0.77	
	5.4		0.78	
	7.2		0.80	
	5.4		0.80	
	3.6		0.80	
	1.8		0.75	